DESIGN AND FABRICATION OF NO_2 GAS SENSOR USING NANOSTRUCTURED METAL OXIDES THIN FILM WITH POLYMERIC MATERIALS

THESIS SUBMITTED FOR THE AWARD OF THE DEGREE OF

Doctor of Philosophy

In

Applied Physics

BY

Rakesh Kumar Sonker

Enrollment No. 583/12

Under the Supervision of

Dr. Bal Chandra Yadav

DEPARTMENT OF APPLIED PHYSICS
SCHOOL FOR PHYSICAL SCIENCES
BABASAHEB BHIMRAO AMBEDKAR UNIVERSITY, LUCKNOW, (U.P.) INDIA – 226025

May, 2016

DECLARATION

I declare that the thesis entitled **"Design and Fabrication of NO_2 gas sensor using Nanostructured Metal Oxides Thin Film with Polymeric Materials"** has been prepared by me under the supervision of Dr. Bal Chandra Yadav, Associate Professor, Department of Applied Physics, School for Physical Sciences, Babasaheb Bhimrao Ambedkar University, Lucknow**.** No part of this thesis has formed the basis for the award of any degree, diploma or fellowship previously. Further, I declare that the material embodied in the present work is based on original research work and the indebtedness to others has been duly acknowledged at relevant places.

(Rakesh Kumar Sonker)

Department of Applied Physics, School for Physical Sciences,
Babasaheb Bhimrao Ambedkar University, Vidya Vihar,
Raebareli Road, Lucknow-226025, U.P., India.

Date: 5th May 2016
Place: Lucknow

Dedicated to My Teachers and Family

CERTIFICATE

This is to certify that the thesis titled **"Design and Fabrication of NO_2 gas sensor using Nanostructured Metal Oxides Thin Film with Polymeric Materials"** submitted by **Rakesh Kumar Sonker** is an original research work and has not been previously submitted in part or full for the award of any other degree or diploma to this or any other university or institutions.

The thesis submitted to the Babasaheb Bhimrao Ambedkar University, Lucknow satisfies all the requirements as stipulated in the *Doctor of Philosophy (Ph.D.) regulations -1999 as amended in 2010* and it is fit for submission and evaluation for the award of Doctor of Philosophy of the University.

Dr. B. C. Yadav
(Supervisor)

Dr. B. C. Yadav
(Head of the Department)

Date: 5th May 2016
Place: Lucknow

ACKNOWLEDGEMENT

It is my firm belief that any major research work to result in a positive outcome including a worthy thesis requires the culmination of several factors such as a meaningful subject which can motivate a determined researcher to take up the challenge, a learned and sincere guide in the form of friends, relatives and colleagues who selflessly encourage and help the researcher throughout the research. I had the honour and privilege to have **Dr. Bal Chandra Yadav** as excellent guide and head of department who meticulously guided and supervised throughout my research. I take this opportunity to place on record my heart-felt and sincere gratitude and deep indebtedness to him without whose guidance this work could not have been meaningfully concluded.

I am extremely thankful to my teachers **Dr. Devesh Kumar, Dr. Ramesh Chandra, Dr. A. K. Yadav, Dr. Khem Bhadur Thapa, Dr. Devendra Singh** and Lab Staff at Babasaheb Bhimrao Ambedkar University, for providing friendly and motivating environment during the course of this work.

I wish to express my reverence and sense of deep gratitude to **Prof. Vinay Gupta**, Department of Physics and Astrophysics, University of Delhi, for his invaluable, insightful comments and suggestions to improve the quality of this work. I am very grateful for showing keen interest in my work and constant support throughout the course of the work. I wish to express my reverence and sense of thankfulness to **Dr. Monika Tomar**, Miranda House, Department of Physics, University of Delhi, for her constant guidance, motivation and patience in my progress of academic learning and exploration.

I am deeply thankful to **Dr. Arijit Chowdhuri, Dr. Siddhartha, Dr. Md. Shahabuddin, Dr. Richa Shrivastava, Dr. Anjali Sharma** and **Dr. Satyendra Singh** for their help, support and patience in my progress of academic learning and exploration. I am grateful to them for providing useful suggestions at the hour of need.

I am obliged to **Mr. Amit Shrivastava** (Delhi Technical University, University of Delhi), **Mr. Rahul, Mr. Apoorva** (USIC, University of Delhi), **Mr. Borah** (Dept. of Physics

and Astrophysics, University of Delhi) and **Mr. Rahul** (Indian Institute of Technology, Kanpur, Uttar Pradesh) for technical help in XRD, SEM, FE-SEM, FTIR, TGA, AFM, TEM facilities.

I would like to acknowledge the contribution of my friends and colleagues, **Dr. V. Bhasker, Dr. Manish, Dr. Kajal, Dr. Surbhi, Dr. Neha, Dr. Ayushi, Dr. Savita, Dr. Akshta, Ms. Manveev, Ms. Reema, Ms. Shetal, Ms. Gurpreet, Mr. Avneet, Mr. Lokesh, Mr. Shaan, Mr. Ravindra, Mr. Praveen, Mr. Suresh, Ms. Monika, Ms. Samiksha, Mr. Utkarsh, Mr. Surya, Mr. Ratindra, Mr. Raj Kamal** and **Mrs. Shweta,** who helped me throughout this journey.

I am very thankful to my friends **Dr. Jitendra Kumar, Dr. Punit Tyagi and Mr. Radheshyam Saroj** for their continuous moral support and encouragement.

I owe this thesis to my parents for their love, support and sacrifice from the very first day of my journey of life. I also express my sincere thanks to all my **brothers** and **sister in laws** for providing me with every kind of support. I would acknowledge the sweet smile of my nephews **Mr. Kaushal, Mr. Asheesh, Mr. Kishan** and nieces **Ms. Rachana, Ms. Riya** and **Ms. Samiksha** which inspired and imparted happiness in my life and gave strength to overcome the failures and to start over again.

My final words of thanks will be for almighty God, for his constant support and companionship thorough all turmoil of my life.

Rakesh Kumar Sonker

(Ph.D. Scholar)

LIST OF PUBLICATIONS

Part of the thesis published and communicated in the refereed journals:

1. **Rakesh Kumar Sonker,** Anjali Sharma, Monika Tomar, Vinay Gupta, B. C. Yadav, "Low Temperature Operated NO_2 Gas Sensor Based on SnO_2-ZnO Nanocomposite Thin Film", Adv. Sci. Lett. 20 (2014) 911-916.

2. **Rakesh Kumar Sonker,** Anjali Sharma, Monika Tomar, Vinay Gupta, B. C. Yadav, "Nanocatalyst (Pt, Ag and CuO) Doped SnO_2 Thin Film Based Sensors for Low Temperature Detection of NO_2 Gas", Adv. Sci. Lett. 20 (2014) 1374-1377.

3. **Rakesh Kumar Sonker**, S. R. Sabhajeet, Satyendra Singh, B.C. Yadav, "Synthesis of ZnO nanopetals and its application as NO_2 gas sensor"**,** Materials Letters 152 (2015) 189-191.

4. **Rakesh Kumar Sonker**, B.C. Yadav, "Growth mechanism of hexagonal ZnO nanocrystals and their sensing application", Materials Letters, 160 (2015) 581-584.

5. **Rakesh Kumar Sonker**, B.C. Yadav, "Low temperature study of nanostructured Fe_2O_3 thin films as NO_2 sensor", Materials Today: Proceedings, (2016) (Accepted)

6. **Rakesh Kumar Sonker,** B.C. Yadav, Anjali Sharma, Monika Tomar, Vinay Gupta, Experimental investigations on NO_2 sensing of Pure ZnO and PANI-ZnO composite thin films, RSC Advances (Communicated).

7. **Rakesh Kumar Sonker**, B.C. Yadav, Preparation of nanostructured Fe_2O_3-PANI composite thin film and its application as NO_2 sensor, Materials Letters (Communicated).

8. **Rakesh Kumar Sonker,** B.C. Yadav, Anjali Sharma, Monika Tomar, Vinay Gupta, Design and fabrication of tin oxide-polyaniline nanocomposite thin films and their employment as nitrogen oxide gas sensor, Sens. Actuators B: Chemi., (Communicated).

9. **Rakesh Kumar Sonker,** B.C. Yadav, Fabrication of SnO_2-Polyaniline-ZnO (SPZ) multilayer nanocomposite thin film for improved NO_2 sensing at Room Temperature, Sens. Actuators B: Chemi., (Communicated).

10. **Rakesh Kumar Sonker,** B.C. Yadav, Synthesis of nanostructured PANI thin films prepare by sol-gel method as low temperature NO_2 sensor, Journal of Inorganic and Organometallic Polymers and Materials (Accepted).

11. **Rakesh Kumar Sonker,** Monika Singh, Utkarsh Kumar, B.C. Yadav, MWCNT doped ZnO nanocomposite thin film and its sensing, Journal of Inorganic and Organometallic Polymers and Materials (Accepted).

12. Utkarsh Kumar, Samiksha Sikarwar, **Rakesh Kumar Sonkar** and B.C. Yadav, Carbon Nanotube: Synthesis and application in solar cell, Journal of Inorganic and Organometallic Polymers and Materials (Accepted).

Work not included in Thesis

1. **Rakesh Kumar Sonker,** B. C. Yadav, Chemical Route Deposited SnO_2, SnO_2-Pt and SnO_2-Pd Thin Films for LPG Detection, Adv. Sci. Lett. 20 (2014) 1023-1027.

Papers in International Conferences/Proceedings

1. **Rakesh Kumar Sonker,** Anjali Sharma, Monika Tomar, Vinay Gupta, B. C. Yadav "Efficient room temperature detection of NO_2 gas using a novel sensor structure based on SnO_2-PANI composite", presented (oral talk) at **International Conference on Nanoscience and Nanotechnology** held on BBAU, Lucknow, **India** from 18-20 November 2013.

2. **Rakesh Kumar Sonker**, S. R. Sabhajeet, Ravindra Kumar, B.C. Yadav, "Study of NO_2 Sensing metal oxide (SnO_2) thin film" presented (poster) at "**International Symposium on Advances in Materials Characterization**" BBAU, Lucknow, **India** from 14 July 2014.

3. **Rakesh Kumar Sonker**, S. R. Sabhajeet, Ravindra Kumar, B.C. Yadav, "LPG detection for SnO_2, PANI-$SnO_2$and Ag-SnO_2 composite film fabricated by Chemical

route method", presented (poster) at **2nd International Conference, Kathmandu Symposia on Advanced Material**, **2014,** held on Tribhuvan University, Kathmandu, **NEPAL** from 7-10 September 2014.

4. **Rakesh Kumar Sonker,** Anjali Sharma, Monika Tomar, Vinay Gupta, B.C. Yadav, "NO_2 sensing Properties of PANI-ZnO hybrid composite thin film", presented (oral talk) at **3rd International Conference on Nanotechnology "NANOCON-2014",** held on Bharti Vidyapeeth University, Pune, **India** from 14-15 October 2014.

5. **Rakesh Kumar Sonker**, B.C. Yadav, "Fabrication of ZnO/MWCNTs nanocomposite thin film and its NO_2 sensing" presented (oral talk) at **International Conference on Euro Intelligent Materials, 2015**, held on Kiel University, **Germany** from 10-12 June 2015.

6. **Rakesh Kumar Sonker**, B.C. Yadav, "Low temperature study of nanostructured Fe_2O_3 thin films as NO_2 sensor" presented (oral talk) at **International Conference on Recent Advances in Nano Science and Technology "RAINSAT-2015"** held on Sathyabama University, Chennai, **India** from 8-10 July 2015.

7. **Rakesh Kumar Sonker,** B.C. Yadav, **"**Synthesis of ZnO/CNTs nanocomposite thin film and its sensing" presented (oral talk) at **International Conference on Recent Advances in Nano Science and Technology,** held on Sathyabama University, Chennai, **India, Young Research Award,** from 8-10 July 2015.
8. **Rakesh Kumar Sonker,** B.C. Yadav, "Nanostructure TiO_2 thin film prepared by sol-gel method as low temperature NO_2 sensor" presented (poster) at **International Conference on Plasma Science, Technology & Application,** held on Amity University, Lucknow**, India** from 20-21 January 2016.

9. **Rakesh Kumar Sonker,** B.C. Yadav, "Synthesis of CdS nanoparticle by sol-gel method as low temperature NO_2 sensor" presented (oral talk) at **International Conference on Energy Environment and Engineering "ICEEE-2016"** held on Coimbatore Institute of Technology, Tamilnadu, **India** from Feb. 29, March 1 and 2, 2016.

10. **Rakesh Kumar Sonker**, S. R. Sabhajeet, B.C. Yadav, "PANI doped TiO_2 composite nanoparticles employed as room temperature Liquefied Petroleum Gas sensor" presented (oral talk) at **International Conference on Energy Environment and Engineering "ICEEE-2016"** held on Coimbatore Institute of Technology, Tamilnadu, **India** from Feb. 29, March 1 and 2, 2016.

Papers in National Conferences/Proceedings

1. **Rakesh Kumar Sonker**, B.C. Yadav, "Synthesis of Nanocrystalline Tin oxide in Polyaniline Matrix and its Application as NO_2 Gas Sensor" presented (poster) at **2nd Lucknow Science Congress "LUSCON-2014"** held on BBAU, Lucknow, **India** from 27-28, March 2014.

2. **Rakesh Kumar Sonker**, S. R. Sabhajeet, Rahul, B.C. Yadav, "Effect of Polyaniline/ Titanium dioxide composite film for LPG sensing", presented (oral talk) at **"National Conference on Nanotechnology and Renewable Energy"**, held at Delhi, **India** from 28-29 April 2014 (ISBN-978-93-81212-65-3).

3. **Rakesh Kumar Sonker,** Anjali Sharma, Monika Tomar, Vinay Gupta, B. C. Yadav, "PANI/Ni doped SnO_2 thin film based novel NO_2 gas sensor" presented (poster) at **2nd National Conference on Multifunctional Advanced Materials,** held on Shoolini University**,** Solan, H. P., **India** from 11-13 June 2014.

4. **Rakesh Kumar Sonker**, B.C. Yadav, **"Chemical route synthesis of ZnO nanoflower and its application as NO_2 sensor"** presented (oral talk) at **National conference on Emerging Trends In Nanoscience and Nanotechnology**, held on MVP Samaj's Arts, Science and Commerce College, Ozar, Nashik, **India** from 23-24 December 2014.

5. **Rakesh Kumar Sonker**, B.C. Yadav, "Enhanced response for NO_2 Gas Sensor mode of WO_3 Doped SnO_2 Nanostructured thin film" presented (oral talk) at **3rd Lucknow Science Congress and National Conference on "Science For Society: An Interdisciplinary Approach"** held on BBAU, Lucknow, **India** from 31st October-2nd November 2015.

ABSTRACT

Over the past two decades, a great deal of research efforts has been made towards the development of gas sensing devices for practical applications ranging from toxic/inflammable gas detection to continuous environmental monitoring. Air pollution is one of the major consequences which continuously causing increasing threats to living beings and vegetation. Air pollution may be defined as any atmospheric condition in which certain substances are present in such concentrations that may produce undesirable effects on human beings and ecosystem. These substances include gases (sulphur dioxide, nitrogen oxides, carbon monoxide, hydrocarbons, etc.), particulate matters (smoke, dust, fumes, aerosols, etc), radioactive materials and many others. Amongst various air pollutants, nitrogen oxide (NO_2) is an important pollutant. It contributes to the formation of photochemical smog, which can have significant impacts on human health.

Gas sensors play a pivotal role in domestic and industrial fields and also help to keep a cleaner environment by giving an early warning of leakage of toxic gases. Nitrogen oxides (NO_x), a mixture of nitric oxide (NO) and nitrogen dioxide (NO_2), are produced from natural sources, motor vehicles and other fuel combustion processes. Nitrogen dioxide (NO_2) is an intermediate product in the industrial synthesis of nitric acid, millions of tons which are produced every year. Nitrogen dioxide is harmful to vegetation, can fade and discolor fabrics, reduce visibility, and react with surfaces and furnishings. Vegetation exposure to high levels of nitrogen dioxide can be identified by damage to greenery, decreased growth or reduced crop yield. This reddish-brown toxic gas has a characteristic sharp and pungent odor. NO_2 is the main air pollutant in the combustion exhaust gases of automobiles, industrial, combustion of fossil fuels or domestic heater/burners. As a matter of fact, NO_2 associated with other pollutants like volatile organic compounds (VOCs) are responsible for the formation of ozone in lower atmosphere (troposphere) when interacts directly with sun rays and smog in urban areas. Ground level ozone is severe irritant, responsible for the choking, coughing and burning eyes. Also chemical reaction of NO_2 gas with water vapour in atmosphere causes acid rain. NO_2 is also a precursor to nitrates, which contribute to increase the irrespirable particle levels in the environment. Constantly increasing level of NO_2 gas is harmful to living

beings as it is irritating to the upper respiratory tract and lungs even at low concentrations. Immediately dangerous to life or health Concentrations (IDLHs) of NO_2 gas has been declared to be 20 ppm by Occupational Safety and Health Administration, USA. Thus it is very important to accurately monitor and control the increasing level of NO_2 gas using efficient sensors.

Semiconducting metal oxides are best suited for fabrication of gas sensors. However, obtaining high response for low concentration of target gas, good selectivity with fast response and recovery time and low operating temperature simultaneously are the major concern which are not yet reported in literature. The modulation of electronic properties of sensing layer with suitable catalyst/modifier or development of novel sensor design such as n-n or p-n heterojunctions are expected to improve the response characteristics to a great extent, which can be easily attained using thin film technology. Metal oxide semiconductors SnO_2, ZnO, Fe_2O_3 and PANI are extensively utilized for the detection of various gases due to their high chemical stability. Thus in the present work, an effort has been made to develop an efficient sensor based on SnO_2, ZnO, Fe_2O_3 and PANI thin film for detecting trace level of NO_2 gas with enhanced response. The SnO_2, ZnO, Fe_2O_3 and PANI thin films are prepared by sol-gel method. Structural and optical properties of SnO_2, ZnO, Fe_2O_3 and PANI thin films are found to be highly dependent on the film thickness. NO_2 gas sensing properties of SnO_2, ZnO, Fe_2O_3 and PANI doped nanocomposite thin films are studied.

In present investigations synthesis and characterization of n and p-type semiconducting metal oxides like Tin oxide (SnO_2), Zinc Oxide (ZnO), Ferric Oxide (Fe_2O_3) and Polyaniline (PANI) have been carried out. Thin films of various thickness and on various substrates have been fabricated using sol-gel method. For the purpose of gas sensing thick as well as thin films were fabricated.

Nitrogen Dioxide (NO_2) is a reddish-brown toxic gas with a sharp characteristic, biting odor and is a prominent air pollutant. Present paper reports the synthesis of α-Fe_2O_3-PANI and its application as NO_2 gas sensor operable at low temperature. For this purpose the iron oxide-polyaniline (α-Fe_2O_3-PANI) films were prepared by spin coating method on various corning glass substrates over Pt inter digital electrodes (IDEs) and characterized for

structural and morphological properties by means of X-ray diffraction (XRD), Fourier transform infrared (FTIR) spectroscopy, and scanning electron microscopy (SEM). The sensing mechanism pertains to a change in the depletion region of the p-n junction formed between PANI and α-Fe_2O_3 as a result of electronic charge transfer between the gas molecules and the sensor. The sensing mechanism of α-Fe_2O_3 materials to NO_2 was presumed to be the synergism of α-Fe_2O_3 with NO_2 gas molecules. The prepared nanostructured α-Fe_2O_3-PANI film showed a high sensing response ~2.29×10^2 towards 20 ppm of NO_2 gas. Besides giving the higher sensing response towards NO_2 gas, α-Fe_2O_3-PANI sensor structure was found to be highly selective and exhibited the poor gas sensing response towards other interfering gases including 2000 ppm of Acetone, IPA, NH_3, LPG and CO_2 gases ranged from 0.98 to 1.29.

In the present chapter zinc oxide has been prepared by using two different methods and their characterizations were carried out using SEM, AFM, XRD, UV and FTIR. Sensing performances of each samples were investigated and found that hexagonal ZnO nanocrystals were mere sensitive responsive than ZnO nanopetal structures.

In the present work, the comparative investigations on NO_2 gas sensing properties of the hybrid nanocomposite thin films of Polyaniline (PANI), ZnO and PANI-ZnO towards NO_2 gas at room temperature have been reported. Effect of concentrations of PANI in the composite thin films on the NO_2 gas sensing has been investigated. Structural and surface morphological characterizations have been carried out by using X-ray diffraction (XRD) and scanning electron microscope (SEM) respectively. The presence of 5% PANI in composite film was found to give maximum sensing response of ~ 6.11×10^2 towards to 20 ppm NO_2 gas having fast response and recovery time of about 2.16 min and 3.5 min respectively.

The highly sensitive low temperature operated nitrogen dioxide (NO_2) gas sensor has been fabricated using SnO_2 thin film doped with different catalysts (Pt, Ag and CuO) using chemical route. Amongst all the prepared sensor structures, Pt-doped SnO_2 thin film based sensor (SnO_2-Pt) was found to give maximum sensing response of about 1.83×10^2 towards low concentration of (20 ppm) of NO_2 gas at a lower operating temperature of 90˚C with very fast response (~ 6 sec) and recovery (~ 13 sec) time. The structural, microstructural and

optical properties of the prepared sensor have been studied using X-ray diffraction (XRD), Scanning electron microscope (SEM) and UV-Visible spectroscopy and the results have also been correlated with the observed gas sensing properties.

A novel sensor structure has been fabricated by incorporating polyaniline (PANI) into SnO_2 sensing film using chemical route and exploited for room temperature detection of NO_2 gas. Amongst different concentration of PANI incorporated into SnO_2 thin film, 1% PANI was found to give maximum sensing response (~ 2.58×10^2) at room temperature towards 20 ppm of NO_2 gas with modulated response and recovery time of about 5.8 min and 4.55 min respectively. The structural, morphological and optical properties of the prepared sensor structures have been revealed by X-ray diffraction (XRD), Scanning Electron Microscope (SEM), Transmission Electron Microscope (TEM), Fourier transform infrared spectroscopy (FTIR) and UV-Visible spectroscopy.

Nitrogen dioxide (NO_2) is a typical automotive air pollutant that causes many environmental and health problems. Detection of low concentrations of NO_2 is becoming very important now a day and various approaches have been used for the same. SnO_2 and ZnO are the two widely explored semiconductor materials for the detection of a number of toxic and harmful gases. Thus, in the present work an effort has been made to synthesize nanocrystalline composite thin films of Zinc oxide and Tin oxide (ZSO) using chemical route for the efficient trace level detection of NO_2 gas at lower operating temperature. Thin film of SnO_2-ZnO (ZSO) composite was prepared onto the surface of Pt IDEs/corning glass and has been exploited for studying the gas sensing response characteristics towards NO_2 gas. The prepared ZSO sensor structure showed a high sensing response of about 3×10^2 towards 20 ppm of NO_2 gas at operable room temperature with an average response and recovery time of 10.23 and 11.75 min. respectively. The structural, optical and surface morphology properties of the ZSO composite thin film have been studied by X-ray diffraction (XRD), Fourier transform infrared spectroscopy (FTIR), UV-Visible spectroscopy, Scanning electron microscope (SEM) and have also been correlated with the observed enhancement in gas sensing properties of prepared sensor structure.

We report the synthesis of SnO_2-polyaniline (PANI)-ZnO composite thin film for NO_2 sensor was fabricated from SnO_2-ZnO porous nanostructure and PANI by a predictable spin coating method. The SnO_2-ZnO composite porous nanostructure was prepared by a sol-gel method. It was found that the composite sensor has high selectivity and response to low concentration NO_2 gas. Furthermore, the composite sensor also showed high stability to NO_2 over a long period at operable at room temperature (30 ºC). As experiment results show that both the pore structures of SnO_2 and porous nanostructure of ZnO had effects on the sensor response of SnO_2-PANI-ZnO (SPZ) nanocomposites sensor response calculate 995 at 20 ppm NO_2 operable at room temperature. The response and recovery times of SnO_2-PANI-ZnO composite sensor (SPZ) were calculated as about 3.8 and 2.2 min to 20 ppm NO_2 at room temperature, respectively.

PREFACE

Over the past two decades, a great deal of research efforts has been made towards the development of gas sensing devices for practical applications ranging from toxic/inflammable gas detection to continuous environmental monitoring. Gas sensors play a pivotal role in domestic and industrial fields and also help to keep a cleaner environment by giving an early warning of leakage of toxic gases. Nitrogen oxides (NO_x), a mixture of nitric oxide (NO) and nitrogen dioxide (NO_2), are produced from natural sources, motor vehicles and other fuel combustion processes. Nitrogen dioxide (NO_2) is an intermediate product in the industrial synthesis of nitric acid, millions of tons which are produced every year. NO_2 is the main air pollutant in the combustion exhaust gases of automobiles, industrial, combustion of fossil fuels or domestic heater/burners. As a matter of fact, NO_2 associated with other pollutants like volatile organic compounds (VOCs) are responsible for the formation of ozone in lower atmosphere (troposphere) when interacts directly with sun rays and smog in urban areas. Ground level ozone is severe irritant, responsible for the choking, coughing and burning eyes. Also chemical reaction of NO_2 gas with water vapour in atmosphere causes acid rain. NO_2 is also a precursor to nitrates, which contribute to increase the respirable particle levels in the environment. Constantly increasing level of NO_2 gas is harmful to living beings as it is irritating to the upper respiratory tract and lungs even at low concentrations. Immediately dangerous to life or health Concentrations (IDLHs) of NO_2 gas has been declared to be 20 ppm by Occupational Safety and Health Administration, USA. Thus it is very important to accurately monitor and control the increasing level of NO_2 gas using efficient sensors. Metal oxide semiconductors SnO_2, ZnO, Fe_2O_3 and PANI are extensively utilized for the detection of various gases due to their high chemical stability. Thus in the present work, an effort has been made to develop an efficient sensor based on SnO_2, ZnO, Fe_2O_3 and PANI thin film for detecting trace level of NO_2 gas with enhanced response. The SnO_2, ZnO, Fe_2O_3 and PANI thin films are prepared by sol-gel method. Structural and optical properties of SnO_2, ZnO, Fe_2O_3 and PANI thin films are found to

be highly dependent on the film thickness. NO_2 gas sensing properties of SnO_2, ZnO, Fe_2O_3 and PANI doped nanocomposite thin films are studied.

The present thesis is divided in to nine chapters. Chapter 1 introduces the materials, methods, characterization tools and describes the object of the present investigation. Detailed investigation on nanostructured polyaniline (PANI) doped ferric oxide thin film synthesis, characterization and application as NO_2 sensor is depicted in Chapter 2. In chapter 3, the synthesis, characterization and NO_2 sensing properties of zinc oxide is reported. Chapter 4 describes the fabrication of PANI doped zinc oxide thin film using sol-gel method and its application as NO_2 sensor at room temperature. In chapter 5 describes the synthesis of Pt, Cu and Ag nanoparticle doped SnO_2 thin film using chemical route and its application as NO_2 sensor at room temperature. In chapter 6 describes the synthesis of PANI doped with SnO_2 thin film has been used for NO_2 sensing material and has been demonstrated as an evidence of circular structure effects on the sensing characteristics. Chapter 7 deals with the NO_2 sensing properties of thin film of ZnO and SnO_2 fabricated by sol-gel spin coating technique. In chapter 8 describes the synthesis of PANI doped with ZnO/SnO_2 thin film has been used for NO_2 sensing properties. A study of synthesis, characterization and NO_2 sensing properties of ferric oxides (Fe_2O_3), Fe_2O_3-PANI, Zinc Oxide (ZnO), ZnO-PANI, Pt, Cu and Ag doped SnO_2, SnO_2-ZnO and SnO_2-PANI-ZnO is summarized in chapter 9. This chapter also gives the guidelines for further research work in the field of nanosized materials and their composites as NO_2 sensor.

LIST OF ABBREVIATIONS

S. No.	Name Compound	Full Name
1.	SnO_2	Stannic Oxide
2.	ZnO	Zinc Oxide
3.	Fe_2O_3	Ferric Oxide
4.	PANI	Polyaniline
5.	NO_2	Nitrogen Dioxide
6.	TiO_2	Titanium Oxide
7.	CVD	Chemical Vapour Deposition
8.	XRD	X-ray diffraction
9.	SEM	Scanning Electron Microscope
10.	FE-SEM	Field Emission of Scanning Electron Microscope
11.	UV-vis	Ultra Violet-Visible spectroscopy
12.	TEM	Transmission Electron Microscope
13.	AFM	Atomic Force Microscope
14.	IDLHs	Immediately dangerous to life or health Concentrations
15.	OSHA	Occupational Safety and Health Administration
16.	VOCs	Volatile Organic Compounds
17.	IDE	Inter Digital Electrode
18.	LE, EB, ES	Leucoemeraldine, Emeraldine Base, Emeraldine Salt
19.	NPs	Nanoparticles

20.	IPA	Isopropyl alcohol
21.	SZO	SnO_2(Tin oxide)-Zinc oxide
22.	SPZ	SnO_2(Tin oxide)-polyaniline-Zinc oxide
23.	HA	Hydrogen Acid (e.g. HCl)

LIST OF TABLES

LIST OF FIGURES

LIST OF APPENDICES

TABLE OF CONTENTS

Chapter 1

Introduction and Aim of Present Work

This chapter presents a view on different type of polymers, metal oxides and their applications in day to day life. Significant developments of gas sensors based on polymers are critically reviewed and the advantages of thin film nanostructures have been discussed in detail. The main objectives and a brief outline of the present investigations carried out in this thesis are presented in brief.

1.1 Introduction

In this era of technology driven society, sensors are essentially required in all aspects of life. Sensor is a measuring device that senses a stimulus and converts them into measurable output directly or in a tandem way [1]. The increasing needs of mankind have led to the technological advancements, and efforts are increasing now-a-days for building smart and intelligent systems which combine sensors with electronics [2]. Experimental material science research is usually motivated by industrial and commercial requirements. This is particularly valid in the field of gas sensing, finding wide range of applications in domestic gas alarms, medical diagnostics, apparatus ensuring safety, environmental and chemical monitoring. Worldwide gas sensing technology is playing a major role in protecting the environment and improving home-land security. Sensors are also critical in improving the reliability and efficiency of manufacturing operations by providing faster and more accurate feedback regarding product quality [3]. Keeping in view the ever increasing vehicular density in both rural and urban sectors, detection of gas emission from automotive exhaust becomes an inescapable need. The alarming increase in the usage of various gases in day-to-day life, either in a domestic kitchen or workplaces or industries especially of explosive or toxic nature has immensely increased the need for reliable gas sensors in the commercial market [3]. In the area of environmental health and safety, lowering the limits of detection can improve the quality of life through precise information regarding the pollutants in air, water and soil. High performance sensors and systems are required to monitor various kinds and quantities of analysts.

Amongst various air pollutants like SO_2, CO, CO_2, O_3, NO_x etc., Nitrogen oxide (NO_x) is very harmful because it contributes to the formation of photochemical smog, which can have significant impact on human health [4]. The two most predominant oxides of nitrogen are nitrogen dioxide (NO_2) and nitric oxide (NO), which are significant pollutants at lower atmosphere. Both are toxic and harmful gases with NO_2 acting as a highly reactive oxidant and possessing exceedingly corrosive nature. Thus trace-level detection of NO_2 assumes importance and hence is the focus of present work.

A brief discussion on NO_2 gas, sources of its emission and detection techniques followed by are view on NO_2 gas sensors has been presented in the following sections [5].

1.2 Introduction to Gas Sensor

A gas sensor is a type of transducer which converts a physical or chemical quantity into an equivalent electrical for the purpose of measurement. It is used to detect the presence of moderate to very low concentrations of toxic or harmful target gases of importance, such as NH_3, H_2, CO, CO_2, NO_X, SO_X, C_3H_8, LPG, H_2S, volatile organic compounds etc. and also it quantifies their concentration.

In the present world of industrialization, because of the production of harmful gases as a by-product of the factories and automobiles, sensors are essentially required in all aspects of life. In case of accidental leakage, these gases can be life threatening also and hence it has become very important to develop highly sensitive gas sensors. Such sensors should have the capability of continuous monitoring of the threshold level of concentration of particular gases in a quantitative and selective way that might be present due to leakage/accident in the environment. The sensors so developed should detect the harmful and explosive gases at levels below their prescribed/allowed limits, so that the condition could be controlled well ahead of any catastrophe due to any leakage. Furthermore, automobile by-products from exhaust like NO_x, SO_x etc. contribute to air pollution and in extreme cases can be very harmful to mankind as well.

Accidents could have been prevented by installation of on-site sensors, to alarm the presence of toxic and explosive gases before reaching dangerous high level. As a result, a lot of basic research is going worldwide for designing efficient and selective gas sensors for a detection of number of gases. From the last few decades research on development of gas sensors is taking place at a very high pace [5]. Some gas sensors have also been commercialized but still lack the important characteristics like poor sensitivity and high power consumption, and hence demand further research for attaining the improved sensing characteristics.

Typically gas sensors are described using the main characteristics such as sensing response, stability, repeatability, reproducibility, linearity, response time, and recovery time. An efficient gas sensor,

- Should have high sensing response towards a very low concentration of target gas (high response).
- Should give the same sensing characteristics after repeated usage (stability) and for different sensors of the same kind (reproducibility).
- Should be capable of responding fast towards a target gas (fast response time).
- Should regain initial characteristics as soon as the target gas is flushed out (fast recovery time).
- Sensing response should increase linearly with increasing the concentration of target gas (linearity).

Gas sensors are used for both the identification and quantification of gases, and hence must be both selective and sensitive to a desired target gas in a mixture of gases. Selectivity describes the degree to which a sensor responds to only the desired target gas, with little or ideally no interference from non-target gases present in the surrounding atmosphere. Sensitivity describes the minimum concentration of gas/vapour that can be successfully and repeatedly sensed by a sensor. Conventionally, a number of sensing techniques are employed to detect toxic/harmful gases some of which are discussed in the subsequent text.

1.2.1 Gas sensing methods

Besides the classification discussed above, the electrical method can further be divided in to two categories based on their operating modes: (a) based on direct contact in which both sensing unit & monitoring station are integrated with wire or wireless method to transfer the signals and (b) based on wireless transducers using the variation of electrical signals which indicate the change in physical parameters like gas concentration.

Now-a-days, the most frequently used method is the type discussed in point (a). On the other hand, the developments of wireless transducer, particularly at high frequency need further deep research.

1.2.2 Classification of Gas Sensing Methods

There are several methods for gas sensing. In this section the sensors are classified on two basic methods based on variation of electrical properties and other based on calorimetric optical methods, as shown in Fig. 1.1.

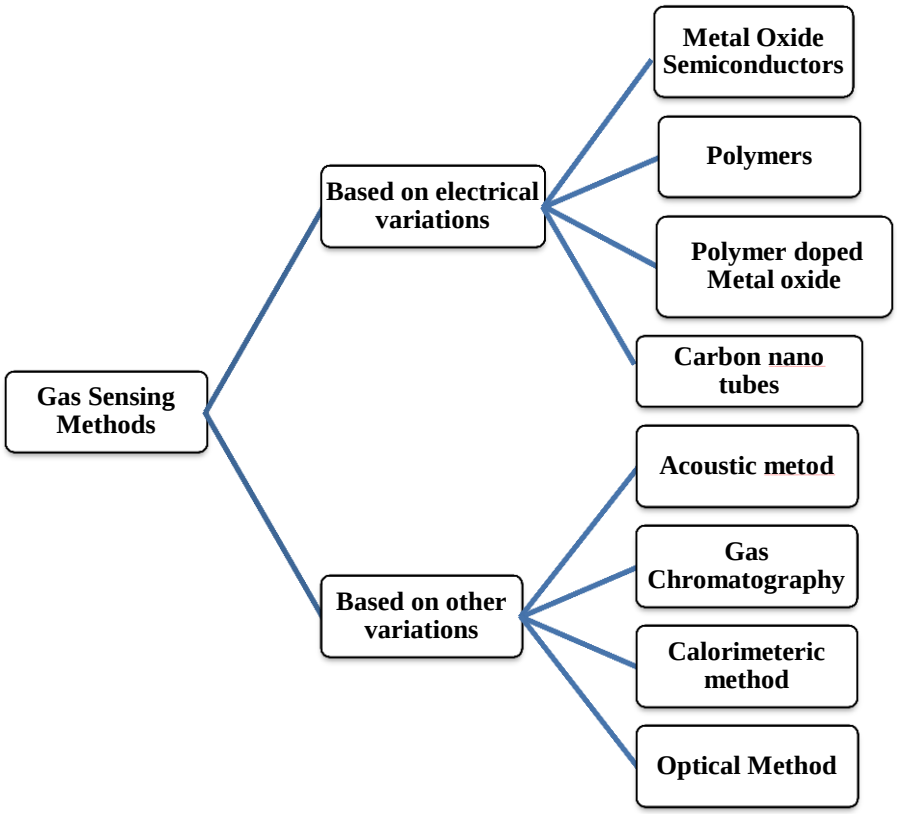

Fig. 1.1: Classification of gas sensing methods

1.3 Gas Sensing Methods (Electrical Properties)

1.3.1 Metal Oxide Semiconductor Sensor

Metal oxide semiconductors are commonly used materials as gas sensing application. This is because of it versatile advantages like high sensitivity and low manufacturing is Al_2O_3 which contain the elements having one oxidation state because it require more

energy to form more than one oxidation states. On the other hand, the transition type processes occur in more than one oxidation state [6] like in the case of Fe_2O_3. Thus, due to more than one transition state in transition-metal oxides it can form several oxidation states on the surface. These are further used by metal oxide semiconductors as sensing materials in compared to the non-transitions. Moreover, the d0 and d10 electronic configurations can be utilized for gas sensing applications [7]. There are some example in which d0 configuration can be found such as in TiO_2, V_2O_5, WO_3 where d10 can be found in post-transition-metal oxides such as SnO_2 and ZnO.

As we know, the commonly utilized gas sensors are metal oxide semiconductors which are n-type. But p-type semiconductors can also be used. The example of such type is NiO_x which could be used for sensing applications. These are generally doped with n-type semiconductor as TiO_2. This has been shown that ~10% wt. NiO_x content is required for the conversion from n type to p-type [8]. The major difference between n-type and p-type NiO_x doped TiO_2 film is that as the temperature increases, the sensitivity of n-type material increase towards reducing gases but in case of the p-type it decreases [8]. Thus p-type semiconductors work at lower temperature a n-type.

The basic concept of metal oxide semiconductors is the redox reactions between the target gases and oxide surface [9]. Further, this can be divided in to two steps: (a) occurrence of redox reactions, in which oxygen is distributed over the surface that react with molecules of target gases which makes an electronic change in the oxide surface; after this (b) these changes in the surface properties lead to the change in the sensors. These changes can be the monitored by the change in capacitance, work function, optical characteristics or reaction energy [6].

There are few examples like CuO, WO_3, SnO_2, V_2O_5, Cr_2O_3 and TiO_2which can be used to monitor oxidizing, reducing, combustible gases [10]. However TiO_2 is frequently utilized as gas sensing material. This is an n-type granular material in which electrical conductivity depends on the density of pre-adsorbed oxygen ions on its surface. Change in gas concentration like liquefied petroleum gas (LPG), carbon monoxide (CO), methane (CH_4) and other reducing gases leads to the change in resistance of TiO_2 surface [11]. The relation between the concentration and resistance variation is purely nonlinear

[12]. On the other hand tungsten trioxide (WO_3) semiconductors is also used for gas sensing purpose in which anodic tungsten gives good sensing responses to hydrogen (H_2) and nitrous oxide $(NO)_x$ [4]. In case of NH_3 gas sensing by WO_3, the gas sensing selectivity is very poor due to the interference from NO_x. In order to apply WO_3 as gas sensing purpose, it need to be coated with vanadium and copper which could act as a catalyst and selectivity of sensors could be maintained [1]. Titanium dioxides (TiO_2) can also be utilized as a gas sensing layer which could monitor the target gas in term of dielectric permittivity to gas adsorption [2].

There are many important factors like characteristics and structure of the sensing layer which could affect the redox reaction and can decide the selectivity and sensitivity of sensing layer. On comparing the sensitivity of other sensors the selectivity of SnO_2 is very high, which is the reason for its popularity. But this sensitivity is achieved at high working temperature which is obtained by heating the filament. In many case the high working temperature is due to the occurrence of proper reaction temperature of O^- with sensing layer [6]. In order to increase the sensitivity, the sensing layer need to be pre heated to an elevated temperature so that the probability of target gas molecule, adsorption could be increased. The layer uses the ions of gas molecules due to which the conductivity of the film increases and enhances the sensitivity. There are some devices as filament and micro hot plate which maintains the working temperature of the sensor [13]. Besides the heated method, the other technique is pre concentration technology which can also be utilized to increase the sensitivity of a gas sensor [14]. In these techniques the characteristics of sensing materials is not affected during sensing processes. But for methods, in which the characterization properties of materials get changed, the materials like SnO_2-ZnO or FeO_3-ZnO can be utilized for enhancing the sensitivity of target gas. The material offers the synergetic effect between the two components of the same composite [6]. However, the sensitivity could be adjusted by changing the proposition of each material in the composites.

The operating temperature of SnO_2 sensor lies between 25 to 500 ^oC. In such sensors the sensitivity of different gases lies at different temperatures due to which selective problem at a single temperature occurs and hence avoids its particle utility [15].

This can be understood if the diversion of temperature from the appropriate value is too much than other gases which may react with SnO_2 which lead to a poor sensitivity. Now, if the difference between two working temperature is larger than one sensor could be used to detect two gases at time as an example the working temperature of SnO_2 for CH_4 is 400 ^oC and for CO_2 it is 90 ^oC. In order to detect the gases, a thermostatic cycle layer (Fig. 1.2) is required so that both the gases may be monitored by noting its sensing resistance during that temperature range [16]. For this sensing material, the working temperature of gas like HF is 380 ^oC separate from above gases [15].

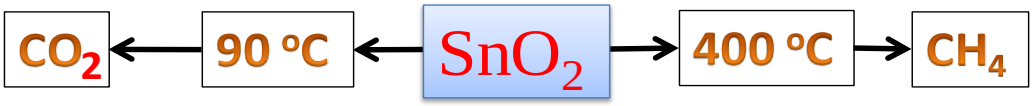

Fig. 1.2: A thermostatic cycle of a sensitive element (SnO_2) for CO_2 and CH_4

In another method of improving sensitivity of SnO_2 based sensor, the suitable catalyst material could be doped in SnO_2 film [3]. Further, the selectivity can be enhanced by using sensor array based on various sensing elements [17]. The composition of a sensor array is made up to multi sensing elements for the detection of several of gases.

In the case of many elements, it is accomplished by an electronic circuit for sensor array which enhance the selectivity [18]. There is another technique for improving selectivity. This is called catalytic filtering technology [19]. This includes the compositional control of sensing materials as TiO_2-SnO_2 composites that represents good sensitivity [20]. The widely used sensors are metal oxide semiconductors but for some of the sensors they require high operating temperatures, complex configuration and high manufacturing cost. These conditions restrict their further development. Keeping them in mind, same techniques have been developed for example use of micro sized sensor element along with micro sized heating elements designed on silicon IC [21] and temperature pulse operating mode small heating intervals [22]. This is providing the minimum power consumption. There is a problem of large recovery period which is required after each gas exposure. This might not be a practical technique for some devices as e-noses. This restricts its utilization for sudden change in gas concentration.

Their field of practical applications is limited due to structural instability and defect of other indicators. Consequently, these sensors are facing serious challenges of their own nature. It is suggested that field of metal oxide gas sensors should go for deep research work. It has been proposed in literature that the nanostructure metal oxide could improve gas sensors sensitivity and response time [23].

1.3.2 Polymer Sensors

Normally, metal oxide semiconductors exhibit good sensitivity towards different organic gases such as ammonia and other volatile organic compound (VOCs). However their high operating temperatures and cumbersome electronics makes them expensive and complicated. Therefore there is a need to explore some new sensing materials. Conducting polymers have good chemical stability of to develop room temperature sensors and also facilitate for creating new functionalities owing to their organic nature. Although, many studies have been carried out on polymer based gas sensing material for the detection of inorganic gases[24]. In polymer sensing mechanism, there are various interactions like induced dipole/induced dipole, dipole-dipole interactions and hydrogen bonds (Lewis acidity/basicity concept) [25]. Moreover, the dynamics of the change in properties are different from those of metal oxide semiconductors. This process can be expected to take place at room temperature. Therefore the sensing can occur at room temperature.

1.3.2.1 Non-Conducting polymer sensors

The applications of non-conducting polymers have been used as sorption layer for various sensor devices. It is applied only when the coating and device are considered as a common transducer. Various transducers are coated with polymer having concerning properties or physiosorption mechanism. The layer of this polymer can change the intrinsic properties like resonance frequency dielectric constant and enthalpy when the target gas is incident on it. The devices in which non conducting polymer layer can be useful for sensing purpose are quartz crystal microbalance (QCM), surface acoustic wave and surface transverse wave (STW), capacitive and calorimetric sensor devices. The

variation produced in the properties of polymer after sensing can be converted in to electrical signal output [25].

However, the mechanism of non-conducting polymer in gas sensing application is comprehensible. The performance of devices based on these polymers is rather poor. As an example, STW in a resonant device coated with thin film of non-conducting polymer layers shows some advantage such as better electrical response and low noise of gas sensor oscillator over SAW [26]. Moreover, the polyimide can be coated on metal oxide semiconductor gas sensor as molecular sieve in order to improve the sensitivity due to additional sensitivity of polymer layer [27].

Polymer coated gas sensors are advantageous due to their high sensitivity and fast response (i.e. short response time). Another important advantage of polymer sensor is that they can work at room temperature unlike metal oxide semiconductor based sensors whose working temperature is high. Thus, they consume less energy when enable for sensing and can be operated by a battery driven unit. Also, they can be fabricated at low cost with simple and portable structures. They show good reproducibility [28].

However, there are some disadvantages of polymer gas sensor such as long time instability, reversibility, and poor stability. Also, the response of such sensors can be affected by working environment. The dynamics of sensing principle need further attention. As future device, the conducting polymer is the promising candidate.

1.3.2.2 Conducting polymer sensors

This is a well-known fact that electrical conductivity of the conducting polymer changes when exposed to organic and inorganic gases. This variation in conducting and other properties has been considered as the investigation parameters of sensing layer by many groups [29]. There are some example of conducting polymer which has been studied as a sensing layer such as poly PPy, PTh, PANI, and their derivatives [30]. In case of pure PANI, the conductivity is too low and is hard to be used for sensing application.

So in order to make them applicable for gas sensing, one need to improve the conductivity of polymer by redox reaction or protonation. This can be accomplished by doping the conducting polymer. One can change the level of doping by chemical reaction between polymer chain and target gas which makes the analyte detection possible. Many polymers are doped using redox reaction technique. As an example, the redox reaction of CO is not possible at room temperature but the PANI can respond to CO at room temperature [30]. The doped PANI can be directly considered as transducer to show the changes in electrical properties.

1.3.3 Polymer doped Metal oxide sensor

There is a growing interest to combine both organic and inorganic materials for applications in electronics and optics [31]. The combination of nanosized metal oxides and polyaniline has the potential to increase the sensitivity of the conducting polymer. Such composites can operate at room temperature and the sensitivity towards different gas species can be optimized by the volume ratio of nanosized metal oxides. In addition, the composite may have better long term stability. The nanocomposite organic/inorganic materials are considered as bi-phase materials where the organic and inorganic phases are mixed at the nanometer scale. The properties of nanocomposite materials depend not only on the properties of their constituents but also on their combined morphology and interfacial characteristics [32].

A number of researchers have already developed polyaniline/inorganic nanocomposite sensors. Conn et al. [33] developed a polyaniline/PtO_2 based selective H_2 sensor and reported that the conductivity of polyaniline increases with H_2 exposure, due to the formation of water. It is known that water present in the polymer takes part in charge transfer leading to an increase in the conductivity of polyaniline which is reversible [34-35]. Wang et al. [36] developed polyaniline intercalated MoO_3 thin film sensors and reported that the conductivity change is due to the reversible absorption of analyte. Parvatikar et al. [37] developed polyaniline/WO_3 composite based sensors and reported that conductivity of the film increases with increasing humidity. Ram et al. [38] developed conducting polymer/SnO_2 and TiO_2nanocomposite thin film based sensors and found that conductivity of the film increases with NO_2 exposure. Geng et al.

[39] synthesized polyaniline/SnO_2 hybrid materials by a hydrothermal process for gas sensing applications. They found that hybrid materials are sensitive to ethanol and acetone vapor at 60 to 90 °C.

1.3.4 Carbon nanotubes sensors

In the field of sensing research, carbon nanotubes (CNTs) have shown their potential due to their unique properties. Now-a- days, CNTs are emerging as a promising material for their better sensitivity over the existing one. The potentiality of CNTs lies in their sensitive electrical properties towards the gases like alcohol, CO_2, NO, and NH_3 at room temperature. The high sensitivity avoids the need of existing technologies such as pre-concentration that can contribute toward the fabrication of low cost and simple configuration. On the other hand, CNTs offer a great adsorptive capability, large surface to volume ratio and short response time and thus a great change in electrical properties like capacitance and resistance is observed [40]. CNTs offer corrosion resistance and better band width as compared to the metal oxide semiconductors which require adhoc electronic, power supply and microfabrication [41].

In literature, CNTs have been classified on the basis of layer, so called the single walled CNT (SWCNT) and multiwalled CNT (MWCNT). There are few examples given for the sensing capabilities: SWCNTs are used in RFID tag antenna for the detection of toxic gases [42].

In another application of MWCNTs, the remote monitoring of several gases like CO_2, O_2, and NH_3 have been carried out using MWCNTs. The sensing parameter of MWCNTs is the variation in the permittivity and its conductivity [43]. The different target gas shows dissimilar response time and properties of CNTs, as in case of metal oxide semiconductors. As an example, the response of MWCNT based sensors towards CO_2 and O_2 is linear and reversible. This shows that the dynamics detecting process is only due to the physiosorption. On the other hand, the detecting response to NH_3 is reversible and irreversible as well which means the process involved is both physiosorption and chemisorption. Also, different gases show different response time [43].

For the purpose of sensing, CNTs are decorated with some other material to obtain the increment in the sensitivity and selectivity. Further, the enhancement of the selectivity can be achieved by mixing CNTs in-to silane. Also this provides also the adhesion to the substrate [44]. Oligonucleotides (DNA and RNA) can be employed to enhance the sensitivity. Also, the response time can be affected by the length of DNA sequence [45].

Other than the above mentioned applications of CNTs, they can also be incorporated in to other sensing material to improve sensitivity for example metal oxide semiconductors [46]. CNTs offer the field of further research for gas sensors.

1.4 Sensor based on other variables

1.4.1 Acoustic method

The acoustic based gas sensors have their own weaknesses that seems hard to overcome, particularly when they installed in wireless networks (WSNs). The main problems are short life time and secondary pollution. Such problems can be overcome by adopting the concept of ultrasonic (acoustic) method [47]. The sensing parameters based on ultrasonic methods lie into three types: (a) speed of sound, (b) attenuation and (c) acoustic impedance. The most commonly studied parameter is the measurement of sound velocity. The time of flight is one of the measured parameter to detect the sound velocity. In this concept, the travel time of ultrasonic waves for a given distance is used to calculate the propagation velocity of ultrasonic wave. In this process, there are two similar channels for measuring ultrasonic parameters in the target gas and the mixture of gases, as shown in Fig. 1.3 [48]. The measurement of gas concentration is carried out by different techniques [49].

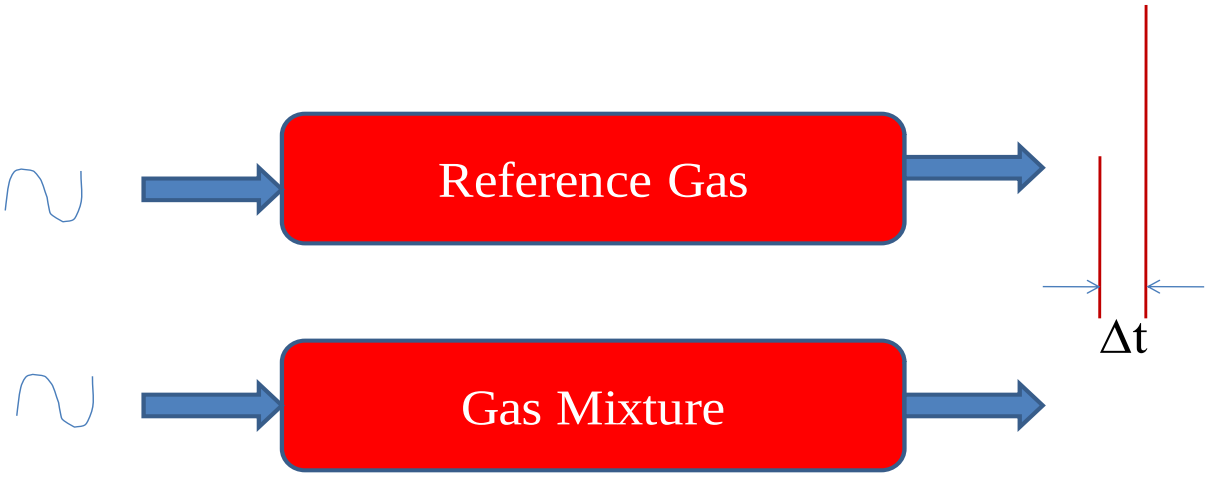

Fig. 1.3: Schematic of the method of ultrasonic detection

This method of ultrasonic detection has large precision but the effect of environment on the two channels may not affect them equally and hence the reliability of device may be lost with time. Due to large consumption of power, the construction of nodes for ultrasonic gas concentration is very difficult. So a device is fabricated with improved time of flight for binary mixture. In such a case, the single channel is used for the mixture of gases. There is a use of relationship between sound speed in air and the temperature of air in order to know the reference sound speed.

Hence, the difference in time between air transmitting target gases can be obtained [48]. The acoustic impedance is one of the important parameter to find out the density of gas. Acoustic impedance has the relation with the gas density and speed of sound as $z = \rho c$, where ρ is density of gas and c is speed of sound [50].

However, the practical application of this concept is very hard to implement due to the difficulty in the measurement of speed of sound in the processing environment. Thus, its commercialization seems very difficult.

1.4.2 Calorimetric method

A category of electrical gas sensor controlled by Pellistors is calorimetric in nature. These come in the category of solid state devices that can monitor combustible gases or to these gases which have observable difference in thermal conductivity as compared to air [51]. Small pallets of crystal loaded ceramic have been used as gas sensing elements. In this case a specific name '*pellister*' is given to the device. The name combines the word pellet and resistor.

The resistance of pellet varies when the gas is exposed to it and hence the name emerges. The calorimetric sensor has limitation of detection which lies in the range of part per thousand [51]. The range can suit industrial application but not applicable for laboratories.

Further, the pellistors can have two categories: catalytic and thermal conductivity. Catalytic sensors work on the heat detection from catalytic oxidation of analyte. They are commercially available. The target is burned and generates a specific enthalpy. This allows the detection of low concentration analyses in the short time [52]. But still some serious problems are there due to pre poisoning of sensor in the electric field. The process of sensitivity in poisoning environment is slower than conventional catalytic sensor [53].

1.4.3 Optical method

Optical method of gas sensing is more sensitive, more selectivity and stable than non-optical methods. This method shows longer life time and short response time which can give real time detection. The environment does not affect the performance of sensors based on optical method. The spectroscopy is the base of this technique. But this technique is restricted to be implemented due to miniaturization and high manufacturing cost. Therefore, some selected models are available in markets which are based on this principal.

Gas sensing by optical methods is usually straightforward and could achieve higher sensitivity, selectivity and stability than non-optical methods with much longer lifetime. Their response time is relatively short, which enables on-line real time detection.

The performance will not be deteriorated by the changing environment or catalyst poisoning caused by specific gases, etc. Optical methods for gas sensing are mostly based on spectroscopy. However, their applications on gas sensors are seriously restricted due to miniaturization and relatively high cost. Only a few commercial gas sensors are based on optical principles.

Besides this, there are several other methods like differential optical absorption spectroscopy [54], Raman like detection and ranging [55] etc. The schematic diagram of IR-source gas sensor is shown in Fig. 1.4. It contains four important parts: gas chamber, IR-source, IR detector and optical filter which is shown in Fig. 1.4 (a). Fig. 1.4 (b) shows a different technique for the same purpose. In this set up, the same source is used by two gas cells which receive the IR signls reflected from the some suitable concave mirror. The selection of mid IR range is suitable for the sensing due to its molecular absorption in comparison to near IR radiations. But the major drawback of mid IR laser source is lack of continuous tenability, heating of lead salt diode laser which has cooling problem and low out power.

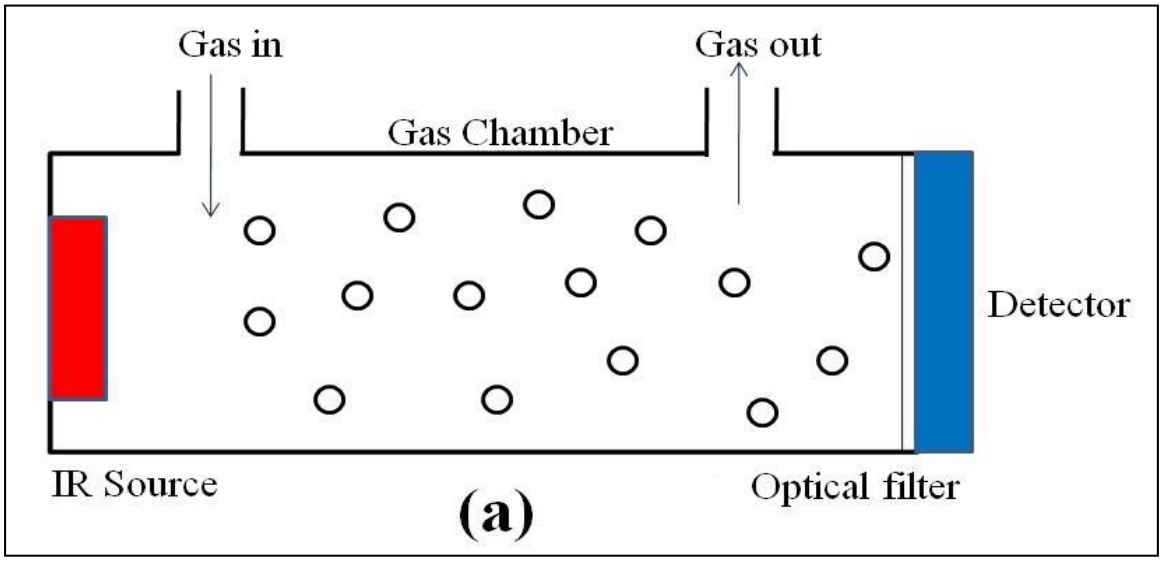

Fig. 1.4 (a): IR-source gas sensors based on the basic absorption spectroscopy.

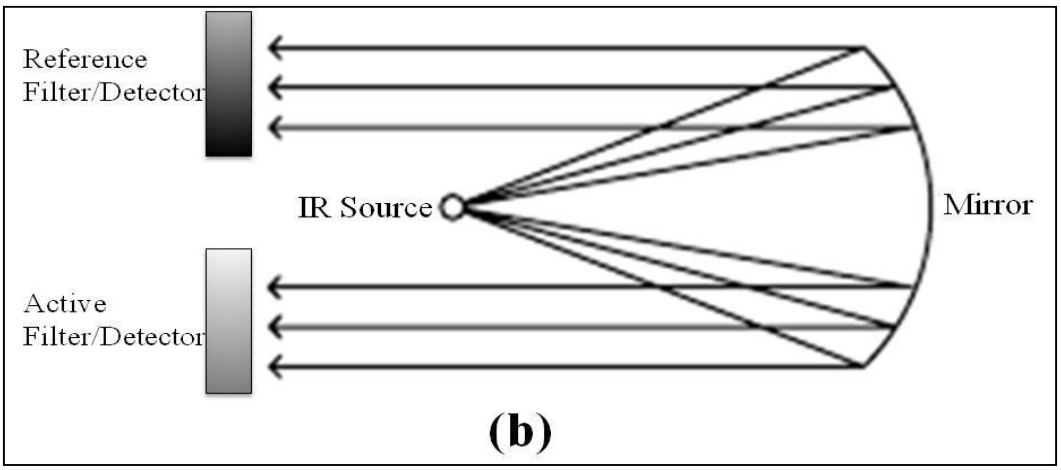

Fig. 1.4 (b): IR-source gas sensors with reference filter/detector.

1.5 Nitrogen Dioxide (NO_2) gas

NO_2 gas is known to exhibit paramagnetic properties with bent molecule having C2v point group symmetry [56]. The typical bond length between the nitrogen and the oxygen atoms is 119.7 picometer while molecular weight of NO_2 gas is 46.01 gm mol^{-1} (heavier than air). Nitrogen dioxide is reddish-brown gas with a pungent, irritating odour, and is known to be a strong oxidant.

1.5.1 Sources of emission

Group of nitrogen oxide gases possess simple chemical composition and are usually formed by reaction between nitrogen (N_2) and oxygen (O_2) which occur abundantly in nature, which however do not react which each other under normal conditions. For the reaction between N_2 and O_2 gases to take place, extremely hot environment is required. Nitrogen oxides are naturally formed in flashes during thunderstorms, where temperature of about 30000 ºC is achieved. Natural sources include intrusion of stratospheric oxides, bacterial and volcanic action, and lightening. Anthropogenic sources of emission of NO_2 gas has been categorized into indoor and outdoor sources. Indoor emission sources of NO_2 gas include gas-boiled fired appliances (stoves, ovens, etc.), unvented gas space heaters, unvented kerosene heaters, wood stoves, environmental tobacco smoke etc. In ambient air, the primary nitrogen oxide emitted by indoor sources is nitric oxide (NO), which easily reacts with atmospheric air and gets

converted into NO_2 gas. Outdoor sources contributing NO_2 gas to the atmosphere are specific non-combustion industrial processes, such as the manufacture of nitric acid (HNO_3), the use of explosives and welding, combustion of fossil fuels in stationary sources (heating, power generation) and in motor vehicles (internal combustion engines) [57].

Fig. 1.5 shows the common zones of emission of NO_2 gas reported by Ministry of Environment (Ontario, Canada) where NO_2 emitted from other transportations, road vehicles and industrial process cover a major portion of the total emitted NO_2 [58].

According to a survey by World Resources Institute, annual emissions of anthropogenic NO_2 gas are estimated to be 20-90 micrograms per cubic meter ($\mu g/m^3$) (0.01-0.05 ppm) in urban areas [5]. Maximum 30-minute or 1-hour average and maximum 24-hour average outdoor emission of nitrogen dioxide concentrations of up to 400 $\mu g/m^3$ (0.5 ppm) and 940 $\mu g/m^3$ (0.21 ppm), respectively, have been reported [59].

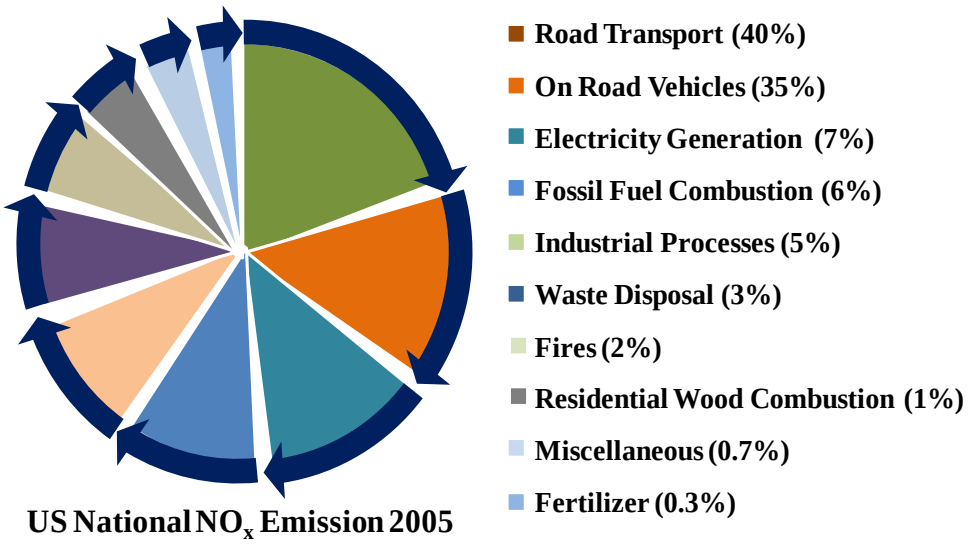

Fig. 1.5: The chart presents US national NO_x emission (in tons) in the year 2005 by source sector. (Data obtained from EPA website: http://www.epa.gov/air/emissions/nox.htm)

1.5.2 Effects of NO_2 gas on ecosystems

NO_2 gas is precursor for both ozone at ground level and acid precipitation, each of which are blamed for injury to plants. Ozone being a secondary pollutant is not emittedas such by any specific source, whereas it is formed due to the atmospheric photo chemical reaction of NO_2 gas emitted from automobiles and other sources explained above in presence of sunlight as shown in equations 1.1 (a) and (b) [60].

$$NO_2 \xrightarrow{h\nu} NO + O \qquad 1.1\ (a)$$

$$O_2 + O \xrightarrow{electric\ spark} O_3 \qquad 1.1\ (b)$$

The increasing emissions of NO_2 in the urban areas have significantly increased the concentration of O_3 at ground level or lower atmosphere (troposphere) causing global warming all over the world [61], NO_2 gas also reacts with water vapours in atmosphere to form nitric acid precipitate leading to acid rain [62].

$$NO_2 + H_2O \rightarrow HNO_3 \qquad (1.2)$$

Nitric acid precipitates are the reason for the growth of natural vegetation with nitrogen deficient soil and also hamper the agricultural crops. Acid precipitation is major cause for the lowering of pH level of fresh water bodies, potentially causing harm to aquatic living species [1] constantly increasing level of NO_2 gas is harmful to living beings, as it is irritates the upper respiratory tract and lungs even at low concentrations. Continuous exposure of 380- 560 $\mu g/m^3$ (0.2 - 0.3 ppm) NO_2 gas for 30 minutes to human beings may lead to mild asthma attack and prolonged exposure of slightly higher concentration of 560 - 940 $\mu g/m^3$ (0.3 ppm to 0.5 ppm) NO_2 gas has reported to produce changes in lung structure, lung metabolism and lung defenses against bacterial infection [63-66]. Continuous emission of NO_2 gas lower atmosphere is also causing to the formation of smog and leading to poor visibility.

1.5.3 Need for the detection of NO_2 gas

According to the statement “Nitrogen dioxide levels have risen dramatically over India and China, according to experts at the University of Bremen” given by RTCC

(Respond to climate changes) which is a Non-Governmental Organization and an official observer to the United Nations climate change negotiations, there is an increase in NO_2 gas level in the atmosphere in Asian countries [67]. According to a survey conducted by RTCC, level of NO_2 has dropped in Europe and North America [http://www.rtcc.org]. Occupational Safety and Health Administration (OSHA, United States Department of Labour), declares the Permissible Exposure Limit (PEL) of NO_2 gas as 5 ppm for general industries and 20 ppm as Immediately Dangerous to Life or Health Concentrations (IDLHs) [68]. Thus it is very important to accurately monitor and control the increasing level of NO_2 gas in India as well. Only one or two breaths of a very high concentration (> 20 ppm) of NO_2 gas can cause severe toxicity. Since, NO_2 is heavier than air; its exposure in poorly ventilated, enclosed, or low-lying areas can cause asphyxiation [69]. Therefore, the development of an efficient gas sensor having capability to precisely detect very low concentration of NO_2 gas for environmental monitoring has become a necessary task. It is envisioned that in the next few years, an automatic damper (ventilation) system will be introduced in all vehicles. These dampers will keep a constant monitoring on theNO_2 gas inside and outside the vehicles in a rather wide concentration range (from ppb to several ppm). Thus, these systems require a compact sensor that can monitor NO_2 gas accurately with low power consumption.

1.6 Literature Survey

The literature surveys of metal oxides represent an interesting, and a varied class of materials that are suited for gas sensor applications for various gases. For more than five decades it is well known that electrical resistance of semiconducting metal oxides shows a change with varying the concentration of gas in their immediate neighborhood [70]. Since the literature on the metal oxides for gas sensing application is vast, a brief review on the important materials used extensively for detection of various gases is presented in Table 1.1 Worldwide researchers are actively working on various semiconducting metal oxide materials for gas sensing applications (Table 1.1) and developed a variety of sensor structures but mostly through empirical approach is used to resolve the core issues of sensitivity, selectivity and stability.

Table 1.1: Different metal oxide materials investigated for semiconductor sensor for detection of various gases.

Sensing material	Fabrication technique	Target gas	Gas Conc. (ppm)	Response	Temp (°C)	Authors Name	Ref.
CuO-ZnO-SnO_2 Pellets	Ball mill + Pechini method	CO	200	16	300	Moon et al. (2002)	[71]
Cu- SnO_2-ZnO thick Film	Screen Printing	H_2S	50	6×10^6	150	Wagh et al. (2004)	[72]
Zn_2SnO_4 SnO_2 nanocomposites	Hydrothermal Synthesis	Ethanol	200	0.85	250	Lu et al. (2005)	[73]
Polypyrrole/WO_3	Emulsion Method	H_2S	1000	60.65	90	Geng et al. (2006)	[74]
Fe_2O_3-ZnO nanocomposites	Hydrothermal Synthesis	NH_3	0.4	10^5	RT	Tang et al. (2006)	[75]
SnO_2-ZnO	Drop Coating	C_2H_5OH	200	4.69	300	Kim et al. (2007)	[76]
SnO_2-ZnO nanoroad	MBE+PLD	H_2	5000	70	400	Tien et al. (2007)	[77]
PPy/sulfonated polyaniline	Electrochemical Polymerization	NH_3	80	4×10^4	RT	Bai et.al (2007)	[78]
In_2O_3:Ag	Dip coating	C_2H_5OH	1000	436	400	Singh et al. (2007)	[79]
MWCNTs:PMMA	Chemical route	CH_3OH	-	428	30	Li et al. (2007)	[80]
Poly (o-anisidine)/WO_3	Mechanical Mixing	Humidity	85% RH	353	RT	Patil et al. (2008)	[81]
Sr(II)- $CuAl_2O_4$ Composites	Sol-gel	CH_3COOH	1000	150	175	Vijaya et al. (2008)	[82]
SnO_2-In_2O_3 NCs incorporating TiO_2	Co-precipitation	CH4	850	48	325	Aifan et al. (2006)	[83]
ZnO-SnO_2	Reverse Micro emulsion	NO_2	500	34.5	250	Liangyuan et al. (2008)	[84]
ZnO-SnO_2	Paste coating	Trimethy	50	156	240	Zhang et al.	[85]

		l Amine				(2008)	
WO_3-SnO_2	Co-precipitation	NO_2	200	1.8×10^2	100	Shouli et al. (2010)	[86]
PTP(5%)/SnO_2	Chemical Oxidative Polymerization	NO_x	150	45%	RT	Kong et al. (2008)	[87]
Poly(methyl methacrylate)/PANI	Electrospinning + Polymerization	Triethylamine (TEA) vapours	500	77	RT	Jia et al. (2008)	[88]
TiO_2‑KCl nanocomposite	Sol-gel	Humidity	-	2.56	RT	Qi. et al. (2009)	[89]
PANI/Inorganic Oxides Nanocomposite	Chemical route	NH_3	1	141×10^{-6}	RT	Tai et al. (2009)	[90]
MWNT doped PANI	Chemical Oxidative Polymerization	H_2	1	1.25	RT	Srivastava et al. (2009)	[91]
Nanotube MWCNT/PANI	LPCVD	NH_3	90	1.16	RT	Yoo et al. (2009)	[92]
Cu‑Zn/ZnO	Surface precipitation process	CO	100	6.3	240	Zeng et al. (2009)	[93]
ZnO-SnO_2	Paste coating	Toluene	100	9.8	360	Song et al. (2009)	[94]
SnO_x- SWNT	RGTO	NO_x	60	2300%	200	Hoa et al. (2009)	[95]
CuO/Cu_xFe_3−xO	RF Sputtering	CO_2	5000	50%	250	Chapelle et al. (2010)	[96]
SnO_2-CuO	Chemical route	H_2S	20	8×10^2	150	Arijit et al. (2010)	[97]
SnO_2/ZnO	Hydrothermal Method	C_2H_5OH	100	50	300	Jia et al. (2010)	[98]
SnO_2−ZnO	Electrospinning + PLD	NO_2	4	105	200	Park et al. (2010)	[99]

ZnO-SnO_2	Vapour growth	NO_2	10	66.3	200	Hwang et al. (2010)	[100]
Polypyrrole (PPy)/$ZnSnO_3$	In situ Chemical Polymerization	NH_3	200	82%	RT	Song et al. (2011)	[101]
PANI/TiO_2	Chemical Oxidation Polymerization	H_2	-	1.75	RT	Srivastava et al. (2011)	[102]
Au/SnO_2	Successive ionic layer deposition (SILD)	H_2	2000	25	240	Korotcenkov et al. (2011)	[103]
Ag/ZnO	PE-CVD	H_2	5000	960	200	Simon et al. (2011)	[104]
SnO_2/ZnO	Electrospinning	C_2H_5OH	5000	250(V)	300	Khorami et al. (2011)	[105]
Pd/CNT/Ni	Nanocomposite Plating and Firing	H_2	200	3.96%	RT	Huang et al. (2011)	[106]
Polyaniline‑Ag	Spin Coating	Ethanol	100	3.3	RT	Barkade et al. (2011)	[107]
WO3/MWCNTs	Chemical vapor deposition (CVD)	NO_2	200 ppb	1.4	500	Su et al. (2011)	[108]
PANI/MWCNT	In-Situ chemical Polymerization	H_2	1%	20	RT	Shin et al. (2011)	[109]
SnO_2-Pt	Spettering	LPG	200	5×10^3	250	Haridas et al. (2011)	[110]
PANI/TiO_2	Electrospinning and chemical oxidation polymerization	NH_3	25 ppb	420(I)	RT	Li et al. (2011)	[111]
TiO_2-ZrO_2	Chemical route	NO_2	2	5.1	150	Mohammadi et al. (2011)	[112]
CNT	Chemical	H_2	1000	3.7	100	Huang et al.	[113]

	oxidative polymerization					(2011)	
Doped CNT-SnO_2	CVD/ Drop Coating	NO_2	50 ppb	0.59	RT	Leghrib et al. (2011)	[114]
Ni, Sm doped $CoFe_2O_4$	Sol-gel	H_2S	800	0.79	200	Bodade et al. (2012)	[115]
Au-NiO & Au-ZnO	Sol-gel	H_2, CO, NO_2	300, 500,6	1.3,1,1 1,1,12	200	Gaspera et al. (2012)	[116]
CSA doped polyaniline-ZnO	Spin coating	NH_3	100	28.11%	RT	Patil et al. (2012)	[117]
Cellulose-TiO_2-MWCNT	Hydrothermal	NH_3	500	50%	RT	Mun et al. (2012)	[118]
SnO_2-CuO	Sputtering	H_2S	20	2.7×10^4	270	Verma et al. (2012)	[119]
Pd NPs/CNT	Facile solutionprocessed	H_2	100	1.1	RT	Huang et al. (2012)	[120]
Polypyrrole-ZnO	Spin-coating	NO_2	100	38%	RT	Chougule et al. (2012)	[121]
Si/SnO_x	Magnetron Sputtering	NO_2	6	0.42	200	Bolotov et al. (2012)	[122]
Alpha-Fe_2O_3 Nanotubes	Hydrothermal	Acetone	100	32	360	Wang et al. (2012)	[123]
SnO_2/CNT	Hydrothermal	NH_3	30	1	RT	Ghaddab et al. (2012)	[124]
SnO_2/Graphene	Hydrothermal	NH_3	50	15.9%	RT	Lin et al. (2012)	[125]
αMoO_3/ZnO	Hydrothermal	H_2S	100	30	270	Yu et al. (2012)	[126]
Metal oxide/MWCNT	Catalytic Pyrolysis	C_2H_5OH	100	16%	-	Liu et al. (2012)	[127]
Graphene-WO_3	Oxidative Polymerization	NO_2	5	130	250	Srivastava et al. (2012)	[128]
Ag-In_2O_3	Nanocasting Route	HCHO	85	152	300	Lai et al. (2012)	[129]

Graphene-WO_3	Drop coating	NO_2	5	133	250	Srivastava et al. (2012)	[130]
A-MnO_2/ZnO	Sol gel	H_2S	100	27	270	Yu et al. (2012)	[131]
ZnO-Graphene oxide	Chemical route	CO	22	24.3	RT	Singh et al. (2012)	[132]
Al-SnO_2	RGTO	NO_2	80	85%	160	Ammar et al. (2013)	[133]
MWCNT-poly(1,5-DAN)	Chemical route	NO_2	10	20%	RT	Nguyen et al. (2013)	[134]
Au-ZnO Nanosheets	Hydrothermal method	NO_2	5	450 %	RT	Mun et al. (2013)	[135]
RuO_x-SnO_2 Thin Film	Chemical Route	NH_3	50	120	200	Marikutsa et al. (2013)	[136]
PPy-TiO_2 Heterojunction	Chemical Route	LPG	1040	55%	RT	Bulakhe et al. (2013)	[137]
CSA doped ZnO-PANI	Chemical Route	NH_3	100	28.11%	RT	Patil et al. (2014)	[138]
Pt-loadedWO_3 thick films	Sputtering	NO_2	20	327	150	Samerjai et al. (2014)	[139]
$K_2W_4O_{13}$ nanowire	Hydrothermal	H_2S	10	48	300	Supothina et al. (2014)	[140]
Ce-ZnO nanoroad	Chemical Route	NO_2	5	500%	100	Chang et al. (2014)	[141]
In-ZnO thin film	Chemical Route	H_2	1666	2	300	Pati et al. (2014)	[142]
CSA-polypyrrole thin film	Chemical Route	NO_2	100	46	RT	Navale et al. (2014)	[143]
CuO-ZnO thin film	Chemical Route	NO_2	30	10	350	Yang et al. (2014)	[144]

It may be seen from Table 1.1 that a wide variety of metal oxides (compoundor ternary) are being used for fabrication of semiconductor sensors for detection of various explosive, toxic and harmful gases. Fig. 1.6 shows a relative comparison of different oxide materials used for gas-sensing application.

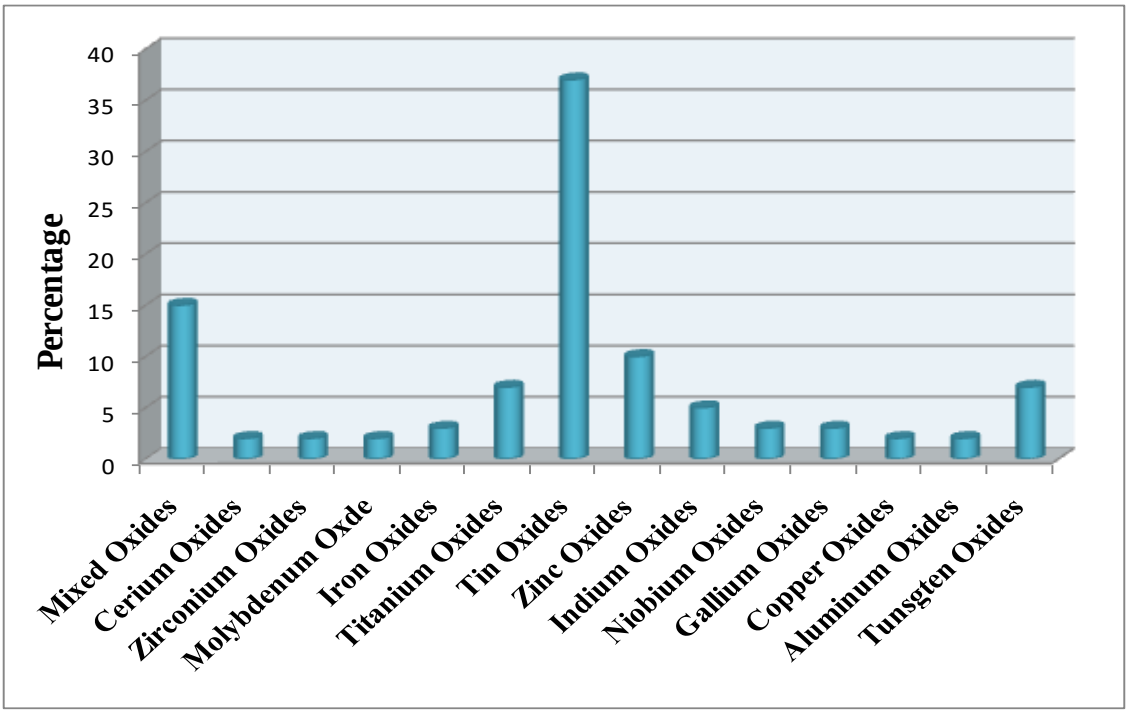

Fig. 1.6: Relative comparison of different oxides used for gas-sensing application

It may be clearly seen from the Pi-chart (Fig.1.6) that amongst all oxide materials [145] tin oxide is the most widely investigated material (37%) for detection of various gases, indicating that SnO_2 is very sensitive to most of the gases. SnO_2 is extensively used in the form of porous ceramics, thick films or thin films because of several advantages over other materials including low cost, ease processing and high sensitivity for different gas species. Zinc oxide (ZnO) has also attracted the attention of research community (10%) for gas sensing applications apart from tin oxide and both (SnO_2 and ZnO) are sharing jointly about half of the research activities related to semiconductor metal oxide gas sensors [Fig. 1.6]. Oxides of tungsten, titanium, and indium besides mixed or multi-component oxides have drawn considerable attention. However, other oxide materials are used towards the realization of semiconductor sensors for the sensing

of specific gases. Each oxide material has its own advantages and must be carefully selected according to their applicability for the sensing of specific target gas. In the present work, focus is on the utilization of SnO_2 material for the development of semiconductor sensor because of its excellent gas sensing properties and widespread usage. A brief review on the SnO_2 material and its properties desired for gas sensing application is presented in following section.

1.7 Tin oxide (SnO_2)

SnO_2 or stannic oxide is a wide band gap compound semiconductor with good chemical and mechanical stability. It has one stable phase in the form of rutile structure. Are presentation of the SnO_2 unit cell is given in Fig. 1.7, where big sphere (red color)represent oxygen atoms and smaller sphere (blue color) represents Sn atoms.

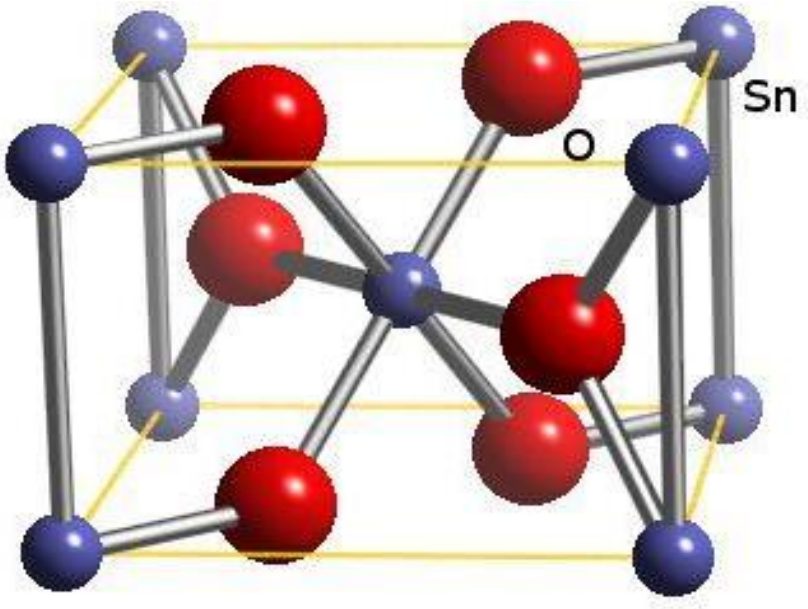

Fig.1.7: Unit cell of the crystalline structure of SnO_2 (http://www.tcd.ie/Chemistry)

The rutile structure has a tetragonal unit cell with a space-group symmetry of P42/mnm. The crystalline structure contains Sn atoms in octahedral coordination and oxygen atom in planar three coordination (Fig. 1.7). Table 1.2 gives a brief summary of the physical properties of SnO_2.

Table 1.2: Physical properties of SnO_2 [146]

Stable phase	**Tetragonal, rutile**
Space Group	**P42/mnm**
Lattice parameters	**a = 4.737Å, c = 3.186 Å**
O-O distance	**4.6646 Å**
O-Sn distance	**3.7662 Å**
c/a	**0.673**
Density at 300K	**6.90-7.00 g/cm^3**
Melting Point	**1630 ℃**
Energy band gap	**3.6eV**

It is reported that (110) and (101) planes of SnO_2 crystal are F (plane) faces while the(111) plane is K (kinked) i.e. (110) and (101) are smoother than (111) plane [146]. According to periodic bond chain (PBC) theory (110) plane is the most stable face of SnO_2 because of the fact that F faces are strongly bound to each other indirection parallel to the face.

In an ionic form, Sn^{2+} has a $5s^2$ electron configuration. The surface energies of the low index surfaces of SnO_2 with bulk composition termination are calculated theoretically by Density Functional Theory (DFT) [146]. For these surfaces with surface-tin atoms in their Sn^{4+} oxidation state, the (110) surface exhibits the lowest energy surface followed by the (100), (101), and (001) surfaces. It is reported that the Sn ions on the perfect surface of SnO_2 are all in the nominal Sn^{4+} state, as in the bulk [146]. The conduction and valence bands do not appear to be bent at this surface, i.e., surface is in a flat-band state. For this reason, the surface and the bulk exhibit same resistivity values. The surface (110) is thermodynamically the most stable one [146]. The interesting defect properties of this surface arise because of the bridging of oxygen ions, lying above the main surface plane. These oxygen ions can be removed easily either by heating or by particle bombardment. When oxygen ions are removed, the two electrons left behind

occupy orbitals, a mixture of *5s* and *5p*, on surface Sn^{4+} ions, converting them to Sn^{2+}. The dual valency of Sn facilitates reversible transformation composition of the surface from stoichiometric surface (Sn^{4+} surface cations) into a reduced surface with Sn^{2+} surface cations depending on the oxygen chemical potential of the system [146]. Reduction of the surface influences the surface electronic structure by formation of Sn 5s derived surface states that lie deep within the band gap and also may cause a lowering of the work function.

On the other hand stoichiometric (101) surface is known to exhibit higher surface energy as compared to the (110) surface [146]. The reduced surface (101) shows a surface termination with a perfect $Sn^{2+}O^{2-}$ stoichiometry which satisfies the valency of Sn. Whereas, for a reduced (110) surface, no analogous arrangement of atoms exists that can readily satisfy the Sn^{2+} oxidation state [146]. This explains the stability of the (101) surface, while the (110) surface forms complex reconstructions despite the fact that the surface energy of the stoichiometric (110) is lower than that of (101). Thus, (110) surface adsorbs more oxygen from the atmosphere as compared to (101) surface due to which when reducing gas comes into contact of (110) surface, it interacts with adsorbed oxygen species and releases electrons to the SnO_2 surface, thereby reducing the resistance of SnO_2 surface [110,119].However, (101) surface adsorbs comparatively lesser oxygen from atmosphere, thus more Sn^{2+} sites are available for oxidizing gases to interact from SnO_2 surface.

1.8 Zinc Oxide (ZnO)

Zinc oxide (ZnO), another direct wide band gap semiconductor, belongs to the II-VI compound family. Depending on the growth conditions it crystallizes either in hexagonal wurtzite (B4 type), zinc blende (B3 type) or rock salt lattice (B1 type) forms [147]. Wurtzite phase of ZnO is the thermodynamically stable phase under ambient temperature and pressure conditions. Zinc blende structure can be stabilized by growth on cubic substrates, whereas the rock salt (NaCl) structure may be obtained at relatively high pressures [147]. In hexagonal wurtzite lattice of ZnO, Zn and O planes are alternately stacked along the c-axis direction such that each anion is surrounded by four cations at the corner of a tetrahedron and vice versa as shown in Fig. 1.8.

Physical properties of ZnO are summarized in Table 1.3. In wurtzite structure, oxygen ions are arranged in a hexagonal closed packed lattice and the zinc ions occupy half of the tetrahedral positions and have the same relative arrangement as oxygen ions (Fig. 1.8). Therefore, ZnO wurtzite structure is relatively open with all the octahedral and half the tetrahedral sites empty which assist in incorporating any external dopant to tailor its specific property [147]. Each ion does not have exact tetrahedral symmetry because spacing between nearest neighbors along the c-axis is somewhat smaller than the other three neighbors. This tetrahedral coordination gives rise to polar symmetry along the c-axis which is responsible for the observed piezoelectricity, pyroelectricity and spontaneous polarization in ZnO [147]. The tetrahedral coordination in ZnO indicates the sp^3 covalent bonding due to hybridization of Zn *d*-electrons and *p*-electrons of O atoms. Zn-O bond also possesses very strong ionic character, and therefore ZnO lies on the borderline of covalent and ionic compounds.

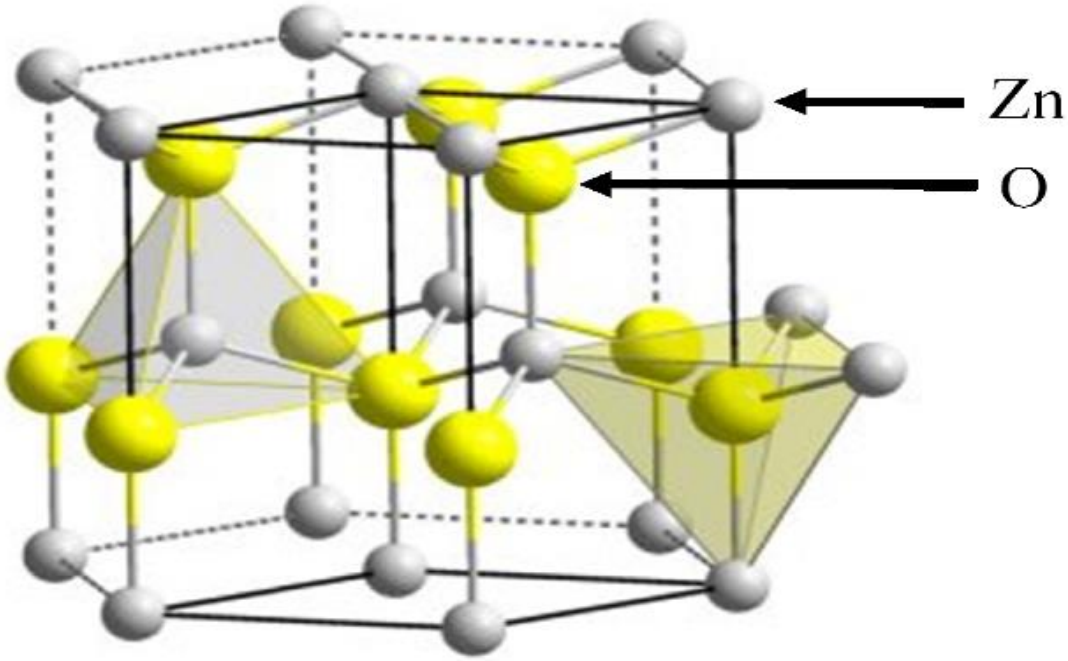

Fig. 1.8: Wurtzite structure of ZnO unit cell [147]

Table 1.3: Physical properties of ZnO [147]

Crystallite Structure	Hexagonal, Wurtzite
Space Group	P63 mc
Lattice parameters	a = 3.249Å, c = 5.206Å
Dielectric constant	9.6 (∥ c), 3.6 (⊥c)
Density at 300K	5.605 g/cm^3
Melting Point	>1900 ^{o}C
Energy band gap	3.3 eV

ZnO exhibits multifunctional properties and has been exploited for a wide range of applications including transparent electronics, surface acoustic wave (SAW) devices, piezoelectric transducers, spintronics devices, gas/chemical/biosensors, varistors and optoelectronic devices such as UV laser, ultraviolet detectors etc. [148]. ZnO was the first oxide semiconducting thin film to be used as a semiconductor gas sensor [149].

1.9 Iron Oxide

The most common iron oxides in nature and sensing applications are magnetite (Fe_3O_4) and maghemite (Fe_2O_3). The physical propertied of them are listed in Table 1.4.

Table 1.4: Physical Properties of Iron Oxides [150]

Properties	**Magnetite (Fe_3O_4)**	**Maghemite (Fe_2O_3)**
Density (g/cm^3)	5.18	4.87
Melting point (°C)	1583-1597	-
Type of magnetism	Ferromagnetic	Ferromagnetic
Curie temperature (K)	850	820-986
Crystallographic system	Cubic	Cubic or tetrahedral
Structural type	Inverse spinel	Defect spinel
Space group	Fd_3m	$P4_332$ (cubic); $P4_12_12$ (tetragonal)
Lattice parameter (nm)	a = 0.8396	a = 0.83474 (cubic); a =0.8347, c =2.501 (tetragonal)

Magnetite is a black magnetic mineral and also called iron(II,III) oxide or ferrous ferrite. The molecular formula, Fe_3O_4, can also be written as FeO, Fe_2O_3, which consists of wüstite (FeO) and hematite (Fe_2O_3). Maghemite is a brown magnetic mineral, which occurs in soils. It exhibits strong magnetism and it is metastable with respect to hematite and forms a continuous metastable solid solution with magnetite. In its mineralogical form, hematite is steel-gray, white to gray-white, with a bluish tint, in reflected light, with characteristic deep blood-red internal reflections. The α-Fe_2O_3 crystal structure is a rhombohedrally centered hexagonal cell of the corundum type. α-Fe_2O_3 belongs to the space group R3c [151]. Hematite has been widely used since antiquity as a red pigment and as jewelry material. Hematite is the most stable of all the iron oxides and behaves as an n-type semiconductor at ambient conditions [152]. In the last few decades, hematite has been investigated for novel applications such as detection of gas sensor [152-153] and other volatile organic compounds [152]. α-Fe_2O_3 has some significant advantages as a photoelectrode for solar cells: for example hematite has a band gap of 2.10 eV for bulk form α-Fe_2O_3 and 2.2 eV for the nanocrystalline form [153]; hematite is also highly resistant to corrosion, and commercially available at a relatively low cost. The iron and

oxygen ions form a face-centered cubic crystal system, and the oxygen ions are in the cubic close-packed arrangement (Fig. 1.9).

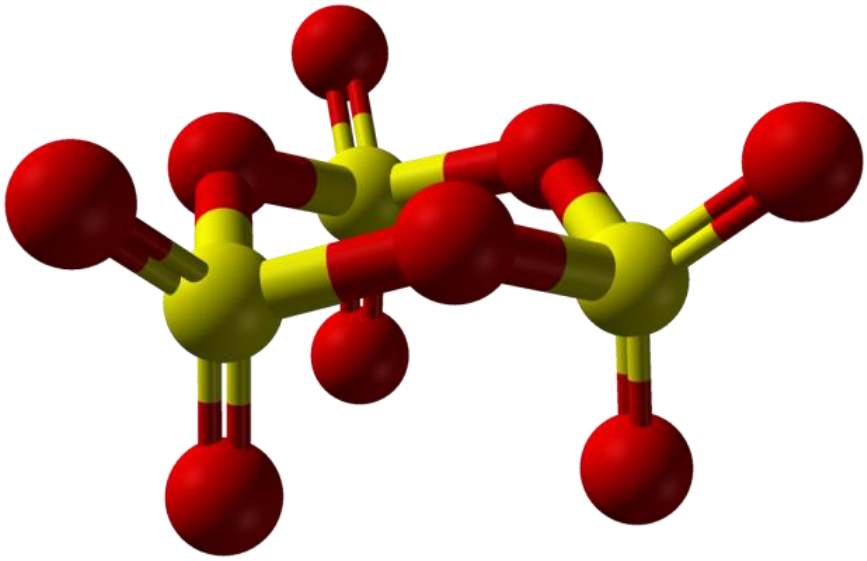

Fig. 1.9: Crystal structure of iron oxide [152]

Similar to Fe_2O_3, SnO_2, ZnO is also a stable semiconducting oxide, where adsorption/desorption of oxygen species on its surface plays a crucial role in changing electrical conductivity and hence suited for gas sensing phenomena. Both ZnO and SnO_2 have been exploited for the sensing of various toxic and harmful gases in the form of ceramics, thick films, thin films or nanostructures. Sensors based on ceramics have shown advantages in terms of their mechanical strength, large resistance to chemical attack and good thermal and physical stability [154] and most of the available commercial sensors are based on ceramics only. However, thin film and nanostructure based sensors score over the ceramic based sensors due to certain advantages offered bythem including high sensor response, low operating temperature and fast sensor response and recovery. Recently efforts are being made to commercialize the thin film based gas sensors. Different forms of sensing materials for gas sensors have their own advantages and disadvantages. In the subsequent section, a brief review on SnO_2, Fe_2O_3 and ZnO based thick and thin film, and nanostructure room temperature NO_2 gas sensors is summarized in Table1.5.

Table 1.5: SnO_2, Fe_2O_3 and ZnO based thin film for NO_2 gas sensors operable at room temperature.

Sensing material	Fabrication technique	Gas Conc. (ppm)	Response	Authors Name	Ref.
ZnO Nanowire	CVD	10	0.46	Verma et al. (2010)	155
ZnO Nanorods	Chemical Route	1000	43	Quy et al. (2011)	156
CNTs/SnO_2	CVD	50	0.59	Leghrib et al. (2011)	157
ZnO thin film	PLD	200	0.52	Rueda et al. (2012)	158
ZnO/SnO_2 nanoroad	Hydrothermal	50	1066	Lu et al. (2012)	159
ZnO-SnO_2 (NNH)	VLS growth	70	8	Choi et al. (2013)	160
Pt-SnO_2 thin film	Sputtering	4	80	Kodu et al. (2013)	161
PPy/α-Fe_2O_3	Sol-gel	10	0.56	Navale et al. (2014)	162
ZnO-rGO	Chemical Route	25	0.45	Liu et al. (2014)	163
rGO-CNT-SnO_2 Film	Hydrothermal	5	2	Liu et al. (2015)	164
ZnO	Chemical Route	20	150	Sonker et al. (2015)	165
SnO_2-Polyaniline	Sol-gel	20	12	Betty et al. (2015)	166
Graphene aero gel-ZnO	Sol-gel	200	0.30	Liu et al. (2015)	167
Graphene/SnO_2	Chemical Route	100	4	Srivastava et al. (2016)	168
SnO_2-Pd Film	Chemical Route	50	1650	Saboor et al. (2016)	169
AgNPs-SnO_2-rGO	Chemical Route	200	7	Wang et al. (2016)	170

1.10 Polyaniline

In the present work we have focused on developing conducting polymer based resistive gas sensor. We have considered polyaniline as the candidate material due to its superior electrical properties and stability.

Polyaniline has been discovered by Runge (1834) and he named it as aniline black [171]. Green and Woodhead (1912) discovered PANI Chain has a mixed oxidation state polymer composed of reduced benzonoid and oxidized quinoid units [172]. Epstein et al. discovered that the characteristic of PANI switches between conductor and an insulator [173]. Further to this work the research on polyaniline attracted much attention from material scientist and engineering community. Conductive polymers such as PANI remain of widespread interest [174] providing an opportunity to address fundamental issues of importance to condensed matter physics, including, for example, the metal-insulator transition [175], the Peierls instability and quantum de-coherence [176]. The unique property of polyaniline to alter its electrical properties on exposure to acidic and basic environment by forming lewis acid-base complex which is explained in preceding section.

1.10.1 Mechanism of polymerization

The polymerization of aniline proceeds via radical propagation mechanism as shown in Fig. 1.10. The initial steps (1 and 2) are common to both methods, but slight differences appear in the initial product of the chain propagation step and product formation steps (3 and 4) [177].

Step 1: Monomer oxidation

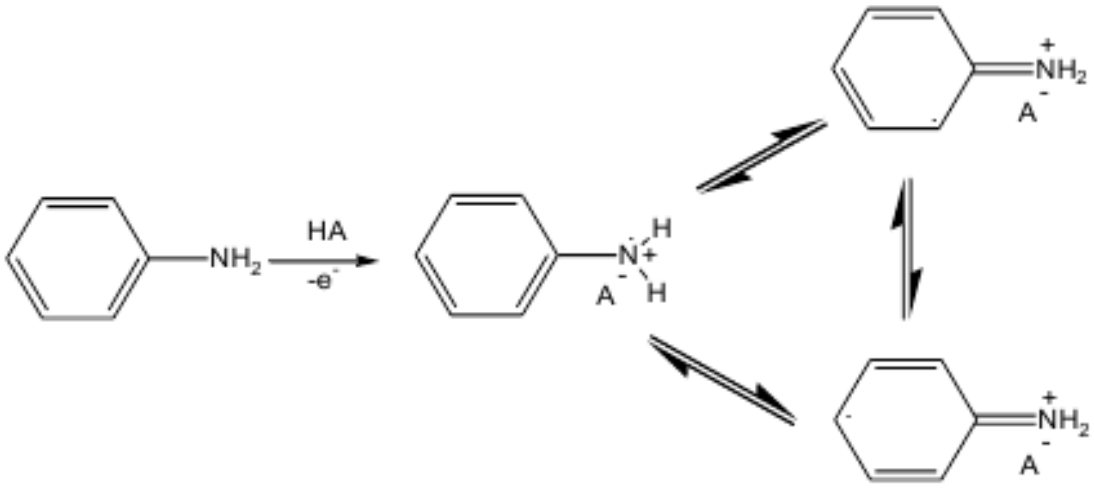

Fig. 1.10(a): Oxidation of monomer during polymerization of aniline

Step 2: Radical coupling and re-aromatization

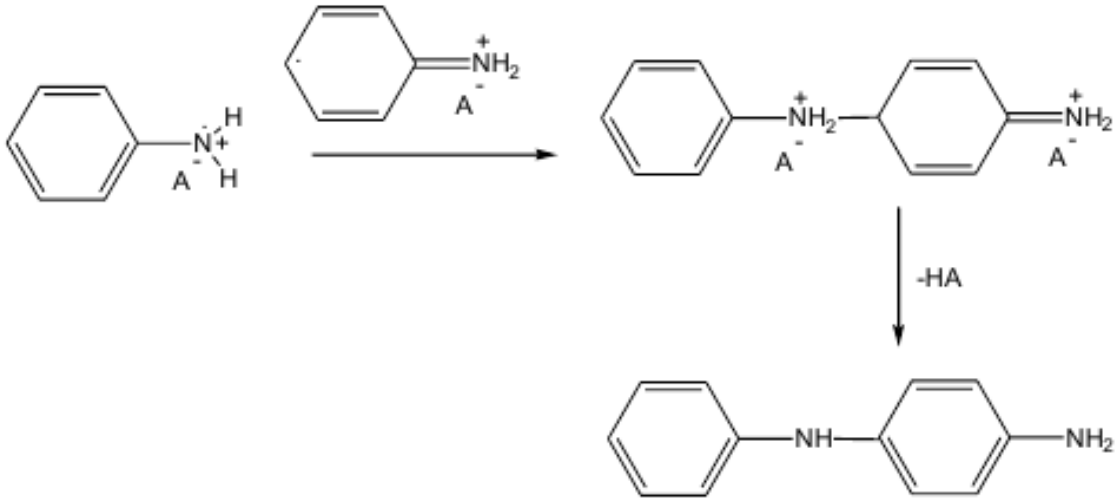

Fig. 1.10(b): Radical coupling and re-aromatization during polymerization of aniline

Step 3: Chain propagation for polymer synthesis

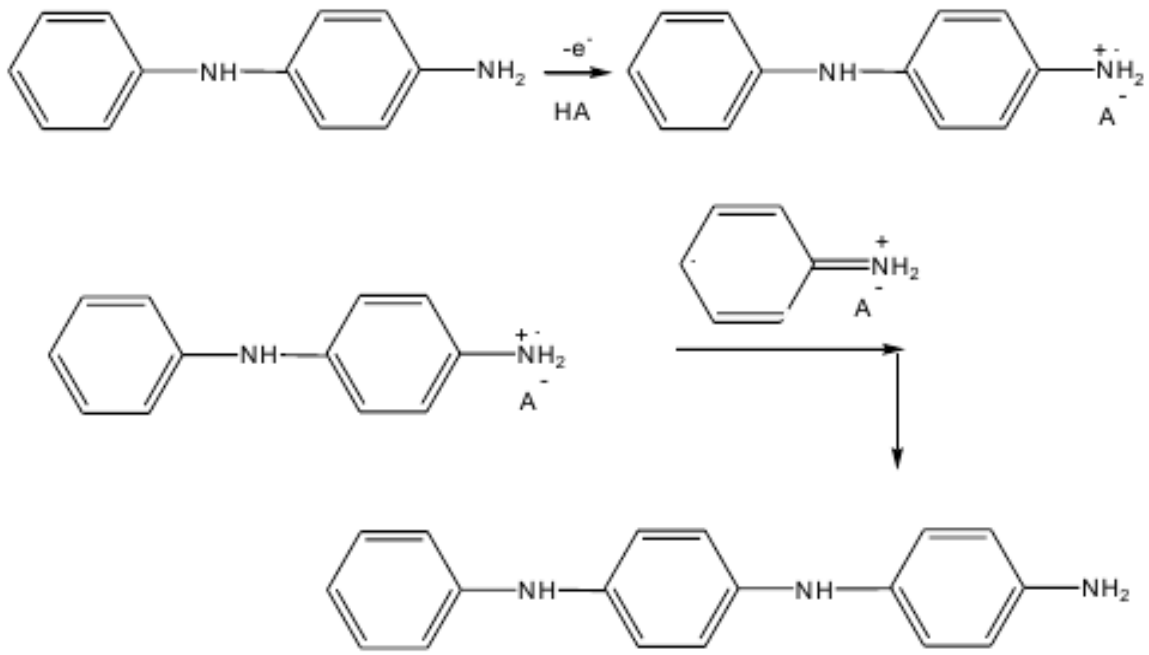

Fig. 1.10(c): Chain propagation during polymerization of aniline

Step 4: Oxidation and doping of the polymer for polymer synthesis

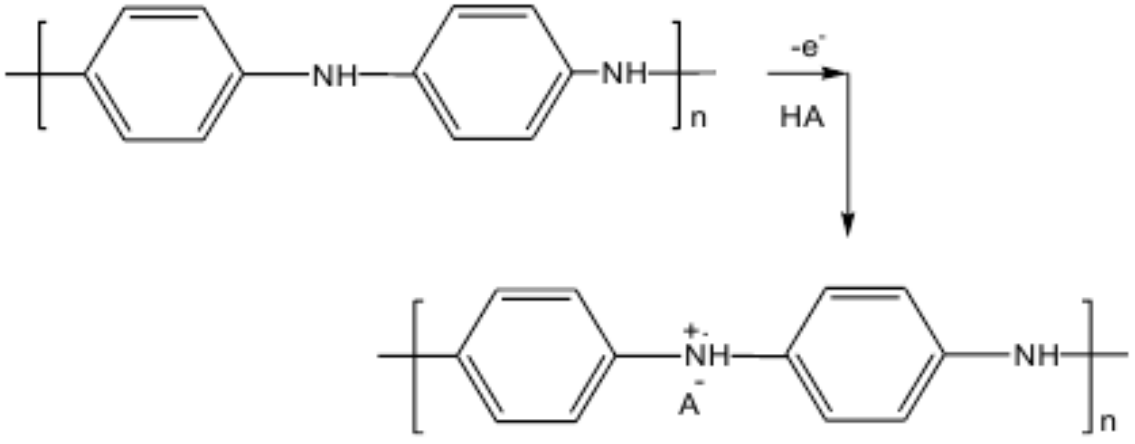

Fig. 1.10(d): Oxidation and doping of the polymer during polymerization of aniline monomer

1.10.2 Structure of Polyaniline

PANI have mixed oxidation state of benzenoid and oxidized quinoid units [178], PANI's average oxidation state is denoted as 1y whereby the value of y determines the existence of each of the three distinct PANI oxidation states [178] as shown in Fig. 1.11. Thus PANI exists as fully reduced leucoemeraldine (LE) where 1-y = 0, half oxidized emeraldine base (EB) where 1-y= 0.5 and fully oxidized pernigraniline (PE) where 1-y =1[178]. The EB is most useful form of PANI due to its high stability at room temperature for long time; it is composed of three benzenoid units and one quinoid unit. Furthermore, EB can be doped in a non-redox reaction in acidic medium which results in an emaraldine salt (ES). On the other hand LE is easily oxidized while the PE is easily degraded [179].

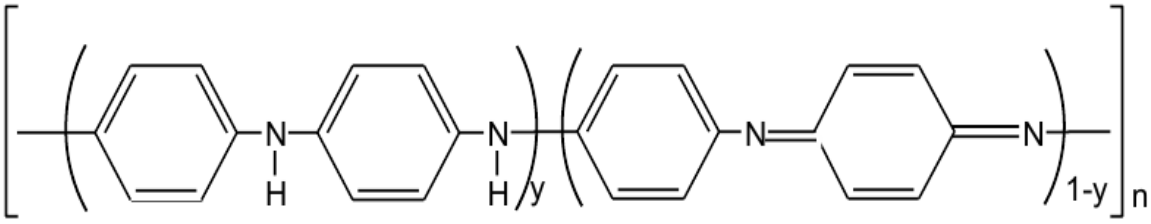

Fig. 1.11: Different oxidation states of polyaniline (y = 1: leucoemeraldine, y = 0.5: emeraldine and y= 0: pernigraniline

1.10.3 Conductivity properties of PANI

The polyaniline chain can be formed by various combinations of the two repeating units known as the X and Y components of polyaniline as shown in above figure [180]. Due to this, PANI has many unique properties and electronic conduction mechanisms that distinguish it from the rest of the conducting polymers.

Among the various oxidation states that PANI can exist in, the one that can be doped to a highly conductive state is the moderately oxidized EB [181]. This form of PANI has a structure which consists of equal proportions of imine (=N–) and amines (–NH–) sites. Through protonic acid doping, imine sites are protonated by acids HA to the bipolaron (dication salt) form [182].The bipolaron then undergoes a further

rearrangement to form the delocalized polaron lattice which is a polysemiquinone radical-cation salt as shown in Fig. 1.12 below.

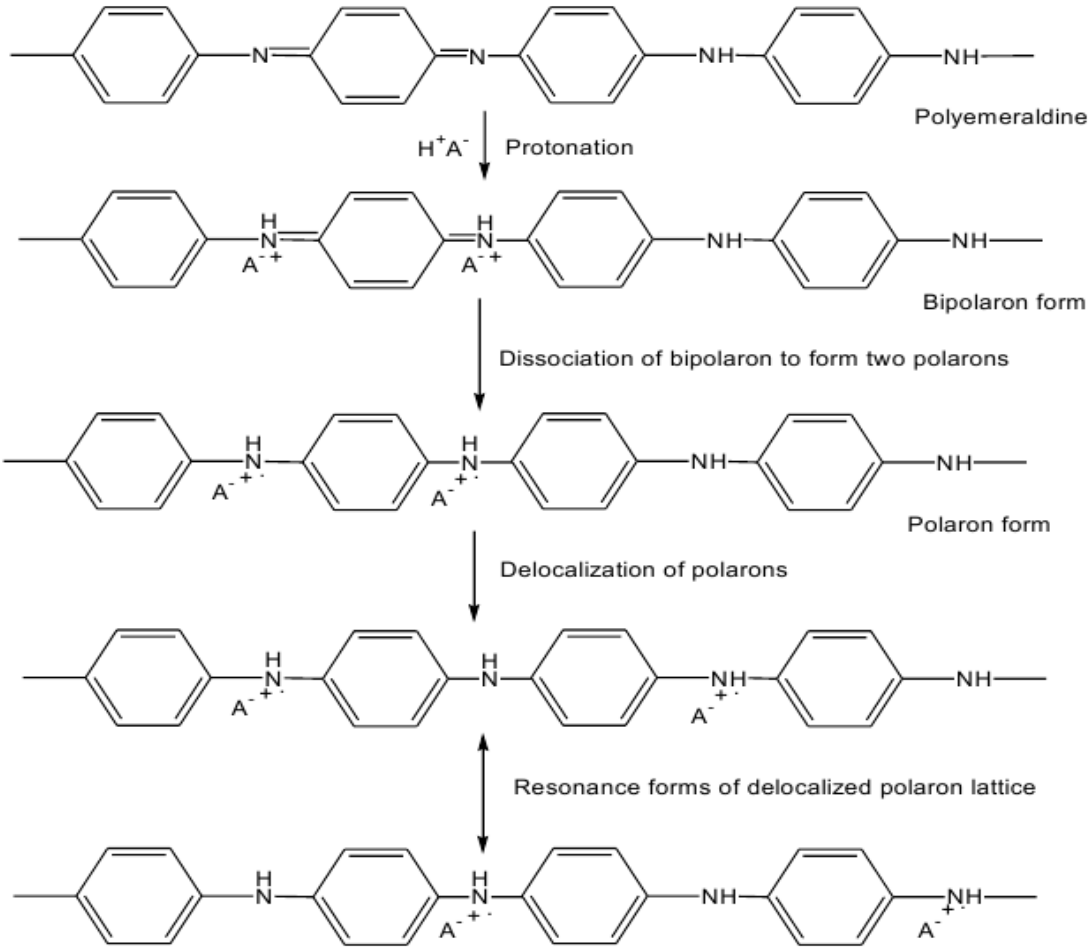

Fig. 1.12: Doping of EB with protons to form the conducting emeraldine salt (PANI/HA) form of polyaniline (a polaron lattice).

The resulting emeraldine salt has conductivity on a semiconductor level of the order of 100 S/cm, which is many orders of magnitude higher than that of common polymers ($<10^{-9}$ S/cm) but lower than that of typical metals ($>10^{4}$ S/cm) [183]. Only 1% of the charge carriers which are available in the ES salt actually contribute to its observed conductivity. If all the available charge carriers were to contribute, the resulting conductivity at room temperature would be ~ 10^{5} S/cm, which is comparable to that of copper [184]. Owing to its excellent electrical properties PANI has many technological promises which are summarized in following schematics.

Application of PANI is summarized in Fig. 1.13.

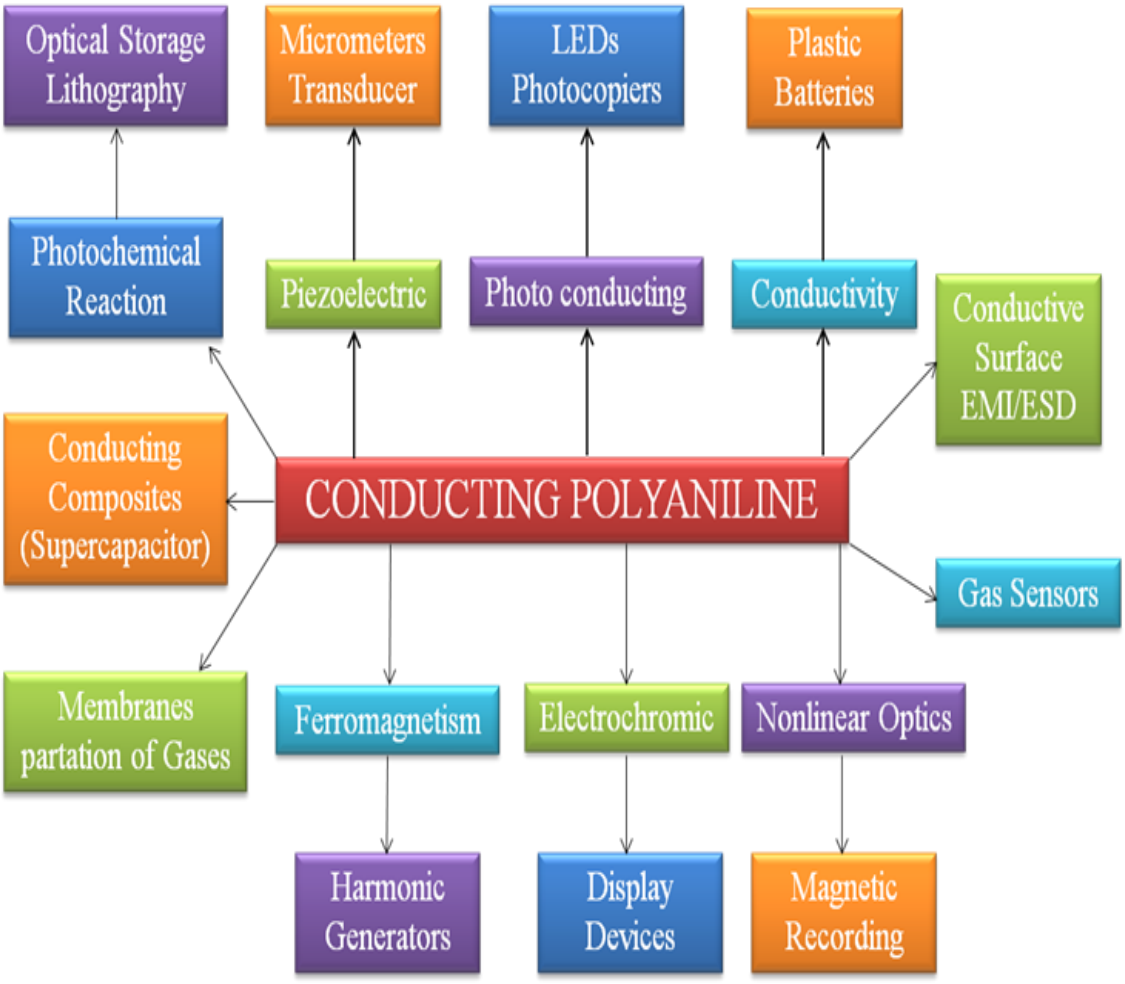

Fig. 1.13: Various applications of conducting PANI

1.10.4 Polyaniline (PANI) doped Metal oxide

The study of conducting polymers has become a major part of modern material science and many institutes, laboratories and commercial establishments involves multidisciplinary research in to chemical synthesis, polymer preparation, electronics, physics, chemistry and applied physics. Fig. 1.13 shows the various field of application of conducting PANI.

Table 1.6: Conducting PANI with different component used for gas sensors

Materials	**Gases**	**Authors (Years)**	**Ref.**
PVP	Humidity,CO_2	K. Ogura et. al. (1999)	[185-187]
PMMA	NH_3,	M. Mastuguchi et.al. (2003)	[188-189]
PS	NH_3, Aliphatic alcohol	E. Segal et. al. (2005)	[190-191]
PVDF	VOCs	J.S. Kim et. al. (2005)	[192]
Poly(butyl acrylate-co-vinyl acetate) (PBuA-V Ac)	Humidity	G.W. Lu et. al. (2005)	[193]
PS+Carbonblack+Thermoplastic PU	Alcohol	E. Segal et. al. (2005)	[194]
Ethylene vinyl acetate copolymer (EVA)/ copolymer	Alcohol	H. Copper et. al. (2006)	[195]
Nylon 6	NH_3	K.H. Hong et. al.(2004)	[196]
Polyimide(PI)	CO	S. Watcharaphalakorn et. al. (2005)	[197]
PEDOT	HCl	Q.L. Hao et. al. (2005)	[198]
Carbon Black	Biogenic amine	G.A. Sotzinget al.(2000)	[199]
SWNT	NH_3	T. Zhang et. al. (2006)	[200]
MWNT	Chemical vapors	X.F. Ma et. al. (2006)	[201]
Cu(II)-exchanged hectorite	Ethanol and hexane	T. L. Porter et. al.(1997)	[202]
PtO_2	H_2	C. Conn et. al. (1998)	[203]
TiO_2	CO	M.K. Ram et. al. (2005)	[204]
MoO_3	VOCs	J.Z. Wang et. al. (2006)	[205]
$CuCl_2$	H_2S	S. Viraj et. al. (2005)	[206]
CeO_2	Humidity	N. Parvatikar et.al.(2006)	[207]
In_2O_3	H_2,NO_2,CO	A.Z. Sadek et.al.(2006)	[208]
Zeolite and Cu^{2+}	CO	N. Densakulprasert et.al.(2006)	[209]
Nafion/metal	NO_2	J.S. Do et.al.(2004)	[210-211]
Cu	Chloroform	K. Suri et.al.(2002)	[212]

The concept of developing new sensors is accomplished by adding new components into conducting polymer. The complicated chemical synthesis can be avoided by following the concept of adding external component. There are some frequently added materials like insulating polymer, carbon nanotube (CNTs), metal oxides and nanoparticles to prepare conducting polymers. The summary of some literature survey is listed above in Table 1.4. The adding second component is very important in sensing process. They can increase the sensing properties of the film of sensing materials [213], helping in electron or proton transfer [196] or interacting directly with analytes by swelling [190].

On the other hand, the role of second component is to induce the effects of enhanced device configuration i.e. change in morphology of the film, increment in mechanical property or protecting sensing film. In this process of adding external component, the performances of sensor are influenced for sensing various gases [214].

1.11 Objective of the present work

The thesis focuses on the fabrication of various sensing elements for the efficient detection of NO_2 gases. Polyaniline (PANI), Fe_2O_3, ZnO and SnO_2 have been chosen as the basic sensing materials. A hybrid composite of PANI doped SnO_2 thin film has been exploited for the possible low temperature detection of NO_2 gas.

An attempt has been made to reduce the operating temperature of the Fe_2O_3, Fe_2O_3-PANI, ZnO, ZnO-PANI, SnO_2-PANI, SnO_2-ZnO and SnO_2-PANI-ZnO composite thin film sensor structures to low operating temperature. The present thesis consists of nine chapters, which are briefly described below:

Chapter 1:

This chapter introduces about the basics of π-conjugated polymers, conductivity process in conducting polymers and different metal oxide doped polymer. A brief review about the doping, conducting mechanism and various routes for the synthesis of metal oxide and conducting polymers has been presented. The literature survey of the various types of gas sensors including PANI and metal oxide has been depicted in this chapter.

Chapter 2:

Present chapter reports the synthesis of α-Fe_2O_3-PANI and its application as NO_2 gas sensor operable at low temperature. For this purpose, the iron oxide-polyaniline (α-Fe_2O_3-PANI) films were prepared by spin coating method on various corning glass substrates over Pt inter digital electrodes (IDEs) and characterized for structural and morphological properties by means of X-ray diffraction (XRD), Fourier transform infrared (FTIR) spectroscopy, and scanning electron microscopy (SEM). The sensing mechanism pertains to a change in the depletion region of the p-n junction formed between PANI and α-Fe_2O_3 as a result of electronic charge transfer between the gas molecules and the sensor. The sensing mechanism of α-Fe_2O_3 materials to NO_2 was presumed to be the synergism of α-Fe_2O_3 with NO_2 gas molecules. The sensitivity in relative response of the sensor was measured at room temperature as function of time with varying concentration of NO_2 gas. The prepared gas sensor exhibited the enhanced sensitivity even at room temperature.

Chapter 3:

In this chapter zinc oxide has been prepared by using two different methods and their characterizations were carried out using SEM, AFM, XRD, UV and FTIR. Sensing performances of each samples were investigated and found that hexagonal ZnO nanocrystals were more sensitive than ZnO nanopetal structures.

Chapter 4:

In the present work, the comparative investigations on NO_2 gas sensing properties of the hybrid nanocomposite thin films of Polyaniline (PANI), ZnO and PANI-ZnO towards NO_2 gas at room temperature have been reported. Effect of concentrations of PANI in the composite thin films on the NO_2 gas sensing has been investigated. Structural and surface morphological characterizations have been carried out by using X-ray diffraction (XRD) and scanning electron microscope (SEM) respectively. The prepared gas sensor exhibited enhanced sensitivity in relative response even at room temperature. The presence of 5% PANI in composite film was found to give maximum sensing response of ~ 6.11×10^2

towards to 20 ppm NO_2 gas having fast response and recovery time of about 2.16 min and 3.5 min respectively.

Chapter 5:

Chapter describes the highly sensitive low temperature operated nitrogen dioxide (NO_2) gas sensor fabricated by using SnO_2 thin film doped with catalysts e.g. Pt, Ag and CuO. Amongst all the prepared sensor structures, Pt-doped SnO_2 thin film based sensor (SnO_2-Pt) was found to give maximum sensing response of about 1.83 $\times 10^2$ towards low concentration (20 ppm) of NO_2 gas at a operating temperature of 90 °C with quick response (~ 6 sec) and recovery (~ 13 sec) time. The structural, microstructural and optical properties of the prepared sensor have been studied using X-ray diffraction (XRD), Scanning electron microscope (SEM) and UV-Visible spectroscopy and the results have also been correlated with the observed gas sensing properties.

Chapter 6:

A novel sensor structure has been fabricated by incorporating polyaniline (PANI) into SnO_2 sensing film using chemical route and exploited for room temperature detection of NO_2 gas. Amongst different concentration of PANI incorporated into SnO_2 thin film, 1% PANI was found to give maximum sensing response (~ 2.58×10^2) at room temperature towards 20 ppm of NO_2 gas with modulated response and recovery time of about 5.8 min and 4.55 min respectively. The structural, morphological and optical properties of the prepared sensor structures have been investigated by X-ray diffraction (XRD), Scanning electron microscope (SEM), Transmission electron microscope (TEM), Fourier transform infrared spectroscopy (FTIR) and UV-Visible spectroscopy.

Chapter 7:

Nitrogen dioxide (NO_2) is a typical automotive air pollutant that causes many environmental and health problems. Detection of low concentrations of NO_2 is becoming very important now a day and various approaches have been used for the same. SnO_2 and ZnO are the two widely explored semiconductor materials for the detection of a number of toxic and harmful gases. Thus, in the present work an effort has been made to

synthesize nanocrystalline composite thin films of Tin-Zinc oxide (SZO) using chemical route for the efficient trace level detection of NO_2 gas at lower operating temperature. Thin film of SnO_2-ZnO (SZO) composite was prepared onto the surface of Pt IDEs/corning glass and has been exploited for studying the gas sensing response characteristics towards NO_2 gas. The prepared ZSO sensor structure showed a high sensing response of about 1.578×10^3 towards 20 ppm of NO_2 gas at a lower operating temperature of 70 °C with an average response and recovery time of 3.91 min. and 6.91 min. respectively. The structural, optical and surface morphological properties of the SZO composite thin film have been studied by X-ray diffraction (XRD), Fourier transform infrared spectroscopy (FTIR), UV-Visible spectroscopy, Scanning electron microscope (SEM) and have also been correlated with the observed enhancement in gas sensing properties of prepared sensor structure.

Chapter 8:

In this chapter the synthesis of SnO_2-PANI-ZnO composite thin film for NO_2 sensor has been described. The SnO_2-ZnO composite porous nanostructure was prepared by a sol-gel method. It was found that the composite sensor has high selectivity and response to low concentration NO_2 gas with the long period stability operable at room temperature (30 ºC). The response and recovery times of SnO_2-PANI-ZnO composite sensor (SPZ) were calculated as about 3.8 and 2.2 min to 20 ppm NO_2 at room temperature, respectively.

Chapter 9:

The results and discussion given in various chapters and concluding remarks have been discussed in brief with further scope of the present work.

References:

[1] H. Thomann, L. R. Dalton, Y. Tomkiewicz, N. S. Shiren, T. C. Clarke, Electron nuclear double resonance determination of the ^{13}C and ^{1}H hyperfine tensor for polyacetylene, Phys. Rev. Lett. 50 (1983) 533-536.

[2] J.L. Bredas, R. R. Chance, R. Silbey, Comparative theoretical study of the doping of conjugated polymers: Polarons in polyacetylene and polyparaphenylene, Phys. Rev., B 26 (1982) 5843.

[3] A. Sharma, M. Tomar, V. Gupta, Low temperature operating SnO_2 thin film sensor loaded with WO_3 micro-discs with enhanced response for NO_2 gas, Sens. Actuators B: Chem., 161 (2012) 1114-1118

[4] D.S. Boudreaux, R. R. Chance, J.L. Bredas, R. Silbey, Solitons and polarons in polyacetylene: Self-consistent-field calculations of the effect of neutral and charged defects on molecular geometry, Phys. Rev. B 28 (1983), 6927.

[5] World Bank Group, (1998) Nitrogen oxides, Pollution Prevention and Abatement Handbook World Bank Group Effective July 1998

[6] W.J. Moore, Seven Solid States: An Introduction to the Chemistry and Physics of Solids, Benjamin, New York (1967).

[7] W.P. Su, J.R. Schrieffer, A.J. Heeger, Solitons in Polyacetylene, Phys. Rev. Lett. 42 (1979) 1698.

[8] W.P. Su, J.R. Schrieffer, A.J. Heeger, Soliton excitations in polyacetylene, Condens. Matter Mater. Phys. 22 (1980) 2099-2111.

[9] W.P. Su, J.R. Schrieffer, Soliton dynamics in polyacetylene, Proc. National Academy Sci. USA 77 (1980) 5626-5629.

[10] A.R. Bishop, D.K. Campbell, K. Fesser, Polyacetylene and Relativistic Field Theory. Models, Mol. Cryts. Liq. Cryst. 77 (1981), 253.

[11] J.L. Bredas, R.R. Chance, R. Silbey, Theoretical Studies of Charged Defect States in Doped Polyacetylene and Polyparaphenylene, Mol. Cryst. Liq. Cryst. 77 (1981) 319.

[12] J.L. Bredas, G.B. Street, Polarons ,Bipolarons and Solution in Conducting Polymers, Accounts Chem. Res. 18 (1985) 309.

[13] J.L. Bredas, J.C. Scott, K. Yakushi, G.B. Street,Polarons and bipolarons in polypyrrole: Evolution of the band structure and optical spectrum upon doing, Phys Rev. B 30 (1984) 1023.

[14] J.L. Bredas, B. Themans, J. M. Andre, R.R. Chance, R. Silbey, The Role of mobile organic radicals and ions (Solitons, Polarons and Bipolarons) in the transport properties of doped conjugated polymers, Synth. Met. 9 (1984) 265-274.

[15] J.H. Kaufman, N.Colanari, J.C. Scott, K.K. Kanazawa, G. B. Street, Evolution of Polaron States Into Bipolarons In Polypyrrole, Mol. Cryst Liq. Cryst. 118 (1985) 171-177.

[16] H. Segawa, T. Shimadzu, M. Honda, A novel photo-sensitized polymerization of pyrrole, J. Chem. Soc. Chem. Commun. 66 (1989) 132-133.

[17] M.M. Coleman, R.J. Petanck, Fourier transform infrared studies on the thermal degradation of polyacrylonitrile, J. Polym. Sci. 16 (1978) 821-832.

[18] C.K. Chen, R. Liepins, Electrical Properties of Polymers, Hanser Publisher Munich, (1987) 274.

[19] G. Natta, G. Mazzanti, P. Corradini, Atti Accad. NazLinceicl. Sci. Fis. Mat. Nat Rend 2 (1958) 25.

[20] A.M. Saxman, R. Liepins, M. Aldissi, Polyacetylene: Its synthesis, doping and structure, Polyacetylene: Its synthesis, doping and structure, Prog. Polym. Sci. 11 (1985) 57-89.

[21] P. Kovacic, A. Kyriakis, Polymerization of benzene to p-polyphenyl, Tetrahedron Lett. (1962) 467-469.

[22] G.M. Carter, M. K. Thakur, Y. J. Chen, J. V. Hryniewicz, Time and wavelength resolved nonlinear optical spectroscopy of a polydiacetylene in the solid state using picosecond dye laser pulses, Appl. Phys. Lett. 47 (1985) 457.

[23] B. Thomas, M.G.K. Pillai, S. Jayalakshmi, On the mechanism of electrical conduction in plasma-polymerised thiophene thin films, J. Phys. D: Appl. Phys. 21 (1988) 503.

[24] A.W. Snow, Vapour deposition polymerization of butadiyne, Nature 292 (1981) 40-41.

[25] T. Yamamoto, Y. Hayashi, A. Yamamoto, A novel type of polycondensation utilizing transition metal-catalyzed CC coupling. I. Preparation of thermostable polyphenylene type polymers, Bull. Chem. Soc. Japan 51 (1978) 2091-2097.

[26] Md. S. Rahman, M. Mahapatra, M.M. Maiti, S. Maiti,New conducting polymers for synthesis of poly(ethynyl sulfide) J. Polym. Mater. 6 (1989) 213.

[27] K. Soga, M. Nakamura, Y. Kobayashi, S. Ikeda, Electrical and physical properties of a polyene arising from dehydrochlorination of poly(vinyl chloride), Synth. Met. 6 (1983) 275-283.

[28] F.E. Karasz, J.D. Capistran, D.R. Gagnon, R.W. Lenz, High molecular-weight polyphenylene vinylene, Mol. Cryst. Liq. Cryst. 118 (1985) 327-332.

[29] M. Sato, S. Tanaka, K. Kaeriyama, Electrochemical preparation of conducting poly(3-methylthiophene): comparison with polythiophene and poly(3-ethylthiophene), Synth. Met. 14 (1986) 279-288.

[30] R. Sugimoto, S. Takeda, H.B. Gu, K. Yoshino, Preparation of soluble polythiophene derivatives utilizing transition metal halides as catalysts and their property, Chem. Express 1 (1986) 635-638.

[31] S.J. Su and N. Kuramoto, Process-able polyaniline-titanium dioxide nanocomposites: effect of titanium dioxide on the conductivity, Synth. Met., 114 (2000) 147-153.

[32] P. Judeinstein and C. Sanchez, Hybrid organic-inorganic materials: a land for multidisciplinarity, J. Mater. Chem., 6 (1996) 511-525.

[33] C. Conn, S. Sestak, A.T. Baker, and J. Unsworth, A polyaniline-based selective hydrogen sensor, Electroanal., 10 (1998) 1137-1141.

[34] T. Taka, Humidity dependency of electrical conductivity of doped polyaniline, Synth. Met., 57 (1993) 5014-501.

[35] S. Jain, S. Chakane, A.B. Samui, V.N. Krishnamurthy and S. V. Bhoraskar, Humidity sensing with weak acid-doped polyaniline and its composites, Sens. Actuators B: Chem., 96 (2003) 124-129.

[36] J. Wang, I. Matsubara, N. Murayama, S. Woosuck and N. Izu, The preparation of polyaniline intercalated MoO_3 thin film and its sensitivity to volatile organic compounds, Thin Solid Films, 514 (2006) 329-333.

[37] N. Parvatikar, S. Jain, S. Khasim, M. Revansiddappa, S.V. Bhoraskar, and M.A. Prasad, Electrical and humidity sensing properties of polyaniline/WO_3 composites, Sens. Actuators B: Chem., 114 (2006) 599-603.

[38] M.K. Ram, O. Yavuz and M. Aldissi, NO_2 gas sensing based on ordered ultra-thin films of conducting polymer and its nanocomposite, Synth. Met., 151 (2005) 77-84.

[39] L. Geng, Y. Zhao, X. Huang, S. Wang, S. Zhang, and S. Wu, Characterization and gas sensitivity study of polyaniline/SnO_2 hybrid material prepared by hydrothermal route, Sens. Actuators B: Chem., 120 (2007) 568-572.

[40] J. Roncali, Conjugated Poly(thiophenes): Synthesis, Functionalizatlon, and Applications, Chem. Rev. 92 (1992) 711-738.

[41] Y. Cao, A. Andreatta, A.J. Heeger, P. Smith, Influence of chemical polymerization conditions on the properties of polyaniline, Polymer 30 (1989) 2305-2311.

[42] J.C. Chiang, A.G. MacDiarmid, Polyaniline': Protonic acid doping of the emeraldine form to the metallic regime, Synth. Met. 13 (1986) 193-205.

[43] A. Yasuda, T. Shimidzu, Aliphatic polyesters as models for relaxation processes in crystalline polymers: 2. Dielectric relaxation in copolymers of adipic acid with 1,6 and 2,5-hexanediols, Polym. J. 25 (1993) 330-390.

[44] H. Meng, Z.K. Chen, W.L. Yu, J. Pei, X.L. Liu, Y.H. Lai, W. Huang, Synthesis and electrochemical characterization of a new polymer constituted of alternating carbazole and oxadiazole moieties, Synth. Met. 100 (1999) 297-301.

[45] S. Palaniappan, Benzoyl peroxide oxidation route to polyaniline salts, Polym. Adv. Technol. 15 (2004) 111-117.

[46] Y. Wang, Z. Liu, B. Han, Z. Sun, Y. Huang, G. Yang, Facile Synthesis of Polyaniline Nanofibers Using Chloroaurate Acid as the Oxidant**,** Langmuir 21 (2005) 833-836.

[47] B.K. Kim, Y.H. Kim, K. Won, H. Chang, Y. Choi, K. Kong, B.W. Rhyu, J.J. Kim, J.O. Lee, Electrical properties of polyaniline nanofibre synthesized with biocatalyst, Nanotechnology 16 (2005) 1177-1181.

[48] A.F. Diaz, K.K. Kanazawa, G.P. Gardini, Electrochemical polymerization of pyrrole, Chem. Comm. 14 (1979) 635-636.

[49] A.F. Diaz, J.C. Bargon, Handbook of Conducting Polymers, Marcel Dekker, New York T. A. Skotheim, (ed.) 1 (1986) 81.

[50] G.B. Street, Handbook of Conducting Polymers, Marcel Dekker, New York, T. A Skotheim, (ed.) 1 (1986) 265.

[51] Y. Wei, Y. Sun, X. Tang, Auto-acceleration and kinetics of electrochemical polymerization of aniline, J. Phys. Chem., 93 (1989) 4878-4881.

[52] G. Zotti, S. Cattarin, N. Comisso. Cyclic potential sweep electro polymerization of aniline: The role of anions in the polymerization mechanism, J. Electroanal. Chem. and interfacial electrochemistry, 239 (1988) 387-396.

[53] K. Sasaki, M. Kaya, J. Yano, A. Kitani, A. Kunai, Conducting Polymers with Micro or Nanometer Structure, J. Elecrroanal. Chem. 215 (1986) 401.

[54] D. Nicolas-Debarnot, F. Poncin-Epaillard, Polyaniline as a new sensitive layer for gas sensor, Anal. Chim. Acta 475, (2003) 1-15.

[55] G.W. Lu, L.T. Qu, G.Q. Shi, Electrochemical Fabrication of Neuron-type Networks Based on Crystalline Oligopyrene Nanosheets, Electrochim. Acta 51 (2005) 340-346.

[56] K. Aoki, K. Hoshina, K. Shibuya, Vibronic analysis of fluorescence spectrum of NO_2 $\tilde{D}^2$ B_2(0,0,0) in the region of 250-550 nm, J. Chem. Phys, 105 (1996) 2228-2235.

[57] EPA Report (1993), Air quality criteria for oxides of nitrogen. Research Triangle Park, NC, US Environmental Protection Agency (EPA Report No. EPA/600/8-91/049aF-cF. 3v).

[58] A. Afzal, N. Cioffi, L. Sabbatini, L. Torsi, NO_x sensors based on semiconducting metal oxide nanostructures: Progress and perspectives, Sens. Actuators B: Chem., 171-172 (2012) 25-42.

[59] M. Berglund, C.E. Bostrom, G. Bylin, L. Ewetz, L. Gustafsson, P. Moldeus, S. Norberg, G. Pershagen, K. Victorin, J. Scand, Absorption and metabolic fate of nitrogen oxides, Work Envirn Heal. 19 (1993) 21-27.

[60] S.V. Krupa, W.J. Manning, Atmospheric ozone: formation and effects on vegetation, Envirn. Pol. 50 (1988) 101-137.

[61] M. Prather, M. Gauss,T. Berntsen, I. Isaksen, J. Sundet, I. Bey, Fresh air in the 21st century?, Geophysical Research Letters, 30 (2003) 1100, doi:10.1029/2002GL016285

[62] P. Ramge, F.W. Badeck, M. Plochl, G.H. Kohlmaier, Apoplastic antioxidants as decisive elimination factors within the uptake process of nitrogen dioxide into leaf tissues, New Phytologist 125 (1993) 771-785.

[63] V. Strand, S. Rak, M. Svartengren, G. Bylin, Americ. Nitrogen dioxide exposure enhances asthmatic reaction to inhaled allergen in subjects with asthma, J. Resp. Crit. Care Med. 155 (1997) 881-887.

[64] V. Strand, M. Svartengren, S. Rak, C. Barck, G. Bylin, Repeated exposure to an ambient level of NO_2 enhances asthmatic response to a nonsymptomatic allergen dose, Euro. Resp. J. 12 (1998) 6-12.

[65] H. S. Jenkins, J. L. Devalia, R.L. Mister, A.M. Bevan, C. Rusznak, R.J. Davies, The effect of exposure to ozone and nitrogen dioxide on the airway response of atopic asthmatics to inhaled allergen: dose- and time-dependent effects, Amer. J. Resp. Criti. Care Med., 160 (1999) 33-39.

[66] R. Jorres, D. Nowak, F. Grimminge, W. Seeger, M. Oldigs, H. Magnussen, The effect of 1 ppm nitrogen dioxide on bronchoalveolar lavage cells and inflammatory mediators in normal and asthmatic subjects, Euro. Resp. J. 8 (1995) 416-424

[67] http://www.rtcc.org

[68] http://www.osha.gov

[69] B.T. Marquis, J.F. Vetelino, A semiconducting metal oxide sensor array for the detection of NO_x and NH_3, Sens. Actuators B: Chem., 77 (2001) 100-110.

[70] Walter H. Brattain and John Bardeen, American Telephone and Telegraph company xxxII (1953)

[71] W. J. Moon, J. H.Yu, G. M. Choi, The CO and H_2 gas selectivity of CuO-doped SnO_2-ZnO composite gas sensor, Sens. Actuators B: Chem., 87 (2002) 464-470.

[72] M.S. Wagh, L.A. Patil, T. Seth, D.P Amalnerkar, Surface cupricated SnO_2-ZnO thick films as a H_2S gas sensor, Sens. Actuators B: Chem., 222 (2016) 78–86.

[73] Z. Lu, Y. Tang, Two-step synthesis and ethanol sensing properties of Zn_2SnO_4-SnO_2 nanocomposites, Matr. Chem. Phys. 92, (2005) 5-9.

[74] L. Geng, X. Huang, Y. Zhao, P. Li, S. Wang, S. Zhang, S. Wu, H_2S sensitivity study of polypyrrole/WO_3 materials**,** Solid-State Electro. 50 (2006) 723-726.

[75] H. Tang, M. Yan, H. Zhang, S. Li, X. Ma, M. Wang, D. Yang, A selective NH_3 gas sensor based on Fe_2O_3-ZnO nanocomposites at room temperature, Sens. Actuators B: Chem., 114 (2006) 910-915.

[76] I.J. Kim, S.D. Han, C.H. Han, J. Gwak, D.U. Hong, D. Jakhar., K.C. Sing, J.S. Wang, Development of micro hydrogen gas sensor with SnO_2–Ag_2O–PtO_x composite using MEMS process, Sens. Actuators B: Chem., 127 (2007) 441-446.

[77] L.C. Tien, D.P. Norton, B.P. Gilaa, S.J. Pearton, H.T. Wang, B.S. Kang, F. Ren, Detection of hydrogen with SnO2-coated ZnO nanorods, Appl. Surf. Sci. 253 (2007) 4748-4852.

[78] H. Bai, Q. Chen, C. Li, C. Lu, G. Shi, Electrosynthesis of polypyrrole/sulfonated polyaniline composite films and their applications for ammonia gas sensing, Polymer 48 (2007) 4015-4020.

[79] V.N. Singh, B. Rajmehta, R.K. Joshi, F.E. Kruis, Effect of silver addition on the ethanol-sensing properties of indium oxide nanoparticle layers: optical absorption study, J. Nanomaterials 2007 (2007) 28031

[80] Y. Li, H.C. Wang, M.J. Yang, n-Type gas sensing characteristics of chemically modified multi-walled carbon nanotubes and PMMA composite, Sens. Actuators B: Chem., 121 (2007) 496-500.

[81] D. Patil, Y.K. Seo, Y.K. Hwang, J.S. Chang, P. Patil, Humidity sensing properties of poly(o-anisidine)/WO_3 composites, Sens. Actuators B: Chem., 128 (2008) 374-382.

[82] A. Vergara, J.L. Ramrez, E. Llobet, Reducing power consumption via a discontinuous operation of temperature-modulated micro-hotplate gas sensors:

Application to the logistics chain of fruit, Sens. Actuators B: Chem., 129 (2008) 311-318.

[83] C. Aifan, H. Xiaodong, T. Zhangfa, B. Shouli, L. Ruixian, L.C. Chiun, Preparation, characterization and gas-sensing properties of SnO_2-In_2O_3 nanocomposite oxides, Sens. Actuators B: Chem., 115 (2006) 316-321.

[84] C. Liangyuan, B. Shouli, Z. Guojun, L. Dianqing, C. Aifan, C.C. Liu, Synthesis of ZnO-SnO_2 nanocomposites by microemulsion and sensing properties for NO_2, Sens. Actuators B: Chem., 134 (2008) 360-366.

[85] W.H. Zhang, W.D. Zhang, Fabrication of SnO_2-ZnO nanocomposite sensor for selective sensing of trimethylamine and the freshness of fishes, Sens. Actuators B: Chem., 134 (2008) 403-408.

[86] B. Shouli, L. Dianqing, H. Dongmei, L. Ruixian, C. Aifan, C.C. Liu, Preparation, characterization of WO_3–SnO_2 nanocomposites and their sensing properties for NO_2, Sens. Actuators B: Chem., 150 (2010) 749-755.

[87] F. Kong, Y. Wang, J. Zhang, H. Xia, B. Zhu, Y. Wang, S. Wang, S. Wu, The preparation and gas sensitivity study of polythiophene/SnO_2 composites, Matr. Sci. Engg. B 150 (2008) 6-11.

[88] S. Jia, Y. Lia, M. Yang, Gas sensing properties of a composite composed of electrospun poly(methyl methacrylate) nanofibers and in situ polymerized polyaniline, Sens. Actuators B: Chem., 133 (2008) 644-649.

[89] Q. Qi. Y. Feng, T. Zhang, X. Zheng, G. Lu, Influence of crystallographic structure on the humidity sensing properties of KCl-doped TiO_2 nanofibers, Sens. Actuators B: Chem., 139 (2010) 611-617.

[90] H.L. Tai, Y.D. Jiang, G,Z. Xie, International Conference on Apperceiving Computing and Intelligence Analysis, ICACIA 531166 (2009) 5

[91] S. Srivastava, S.S. Sharma, S. Kumar, S. Agrawal, M. Singh, Y.K. Vijay, Characterization of gas sensing behavior of multi walled carbon nanotube polyaniline composite films**,** Int. J. Hydro. Ener, 34 (2009) 8444-8450.

[92] K.P. Yoo, K.H. Kwon, N.K. Min, M.J. Lee, C.J. Lee, Effects of O_2 plasma treatment on NH_3 sensing characteristics of multiwall carbon

nanotube/polyaniline composite films, Sens. Actuators B: Chem., 143 (2009) 333-340.

[93] Y. Zeng, T. Zhang, H. Yang, L. Qiao, Q. Qi, F. Cao, Y. Zhang, R. Wang, Preparation of Cu–Zn/ZnO core-shell nanocomposite by wire electrical explosion and precipitation process in aqueous solution and CO sensing properties, Appl. Surf. Sci. 255 (2009) 4045-4049.

[94] X. Songa, D. Zhang, M. Fan, A novel toluene sensor based on ZnO-SnO_2 nanofiber web, Appl. Surf. Sci. 255 (2009) 7343-7347.

[95] N.D. Hoa, N.V. Quy, D. Kim, Nanowire structured SnO_x-SWNT composites: High performance sensor for NO_x detection, Sens. Actuators B: Chem., 142 (2009) 253-259.

[96] A. Chapelle, F.O. Hassani, L. Presmanes, A. Barnabe, P. Tailhades, CO_2 sensing properties of semiconducting copper oxide and spinel ferrite nanocomposite thin film, Appl. Surf. Sci. 256 (2010) 4715-4719.

[97] A. Chowdhuri, S.K. Singh, K. Sreenivas, V. Gupta, Contribution of adsorbed oxygen and interfacial space charge for enhanced response of SnO_2 sensors having CuO catalyst for H_2S gas, Sens. Actuators B: Chem., 145 (2010) 155-166.

[98] X. Jia, H. Fan, L. Qin, C. Yang, Hierarchically Structure SnO_2/ZnO Nanocomposites: Preparation, Growth Mechanism and Gas Sensing Property**,** J. Dispersion Sci. Tech. 31 (2010) 1405-1408.

[99] J.A. Park, J. Moon, S.J. Lee, S.H. Kim, H.Y. Chu, T. Zyung, SnO_2-ZnO hybrid nanofibers-based highly sensitive nitrogen dioxides sensor, Sens. Actuators B: Chem., 145 (2010) 592-595.

[100] I.S. Hwang, S.J. Kim, J.K. Choi, J. Choi, H. Ji, G.T. Kim, G. Cao, J.H. Lee, Synthesis and gas sensing characteristics of highly crystalline ZnO-SnO_2 core-shell nanowires, Sens. Actuators B: Chem., 148 (2010) 595-600.

[101] P. Song, Q. Wang, Z. Yang, Ammonia gas sensor based on PPy/$ZnSnO_3$ nanocomposites, Matr. Letts. 65 (2011) 430-432.

[102] S. Srivastava, S. Kumar, V.N. Singh, M. Singh, Y.K. Vijay, Synthesis and characterization of TiO_2 doped polyaniline composites for hydrogen gas sensing, Int. J. Hydro. Ener.36 (2011) 6343-6355.

[103] G. Korotcenkov, L.B. Gulina, B.K. Cho, S.H. Han, V.P. Tolstoy, SnO_2-Au nanocomposite synthesized by Successive Ionic Layer Deposition (SILD) method: characterization and application in gas sensors, Matr. Chem. Phys. 128 (2011) 433-441.

[104] Q. Simon, D. Barreca, D. Bekermann, A. Gasparotto, C. MacCato, E. Comini, V. Gombac, P. Fornasiero, O.I. Lebedev, S. Turner, A. Devi, R.A. Fischer, G.V. Tendeloo, Plasma-assisted synthesis of Ag/ZnO nanocomposites: First example of photo-induced H_2 production and sensing, Int. J. Hydro. Ener. 36 (2011) 15527-15537.

[105] H.A. Khorami, M. Keyanpour, M.R. Vaezi, Synthesis of SnO_2/ZnO composite nanofibers by electrospinning method and study of its ethanol sensing properties, Appl. Surf. Sci. 257 (2011) 7988-7992.

[106] T.C. Lin, B.R. Huang, Palladium nanoparticles modified carbon nanotube/nickel composite rods (Pd/CNT/Ni) for hydrogen sensing, Sens. Actuators B: Chem., 162 (2012) 108-113.

[107] S.S. Barkade, J.B. Naik, S.H. Sonawane, Colloids and Surfaces A: Physicochemical and Engineering Aspects, Colloids and Surfaces A: Physicochemical and Engineering Aspects 378 (2011) 94-98.

[108] P.G. Su, T.T. Pan, Fabrication of a room-temperature NO_2 gas sensor based on WO_3 films and WO_3/MWCNT nanocomposite films by combining polyol process with metal organic decomposition method, Mater. Chem. Phys. 125 (2011) 351-357.

[109] K. Shin, L.A. Mashat, J.S. Song, S.H. Han, D.S. Ann, B.Y. Yoo, K.Z. Kalantar, W. Wlodarski, Polyaniline/MWCNT Nanocomposite Based Hydrogen Sensor Operating at Room Temperature, Sens. Letts. 9 (2011) 69-72.

[110] D. Haridas, A. Chowdhuri, K. Sreenivas, V. Gupta, Enhanced room temperature response of SnO_2 thin film sensor loaded with Pt catalyst clusters under UV radiation for LPG, Sens. Actuators B: Chem., 153(2011) 152-157.

[111] Y. Li, J. Gong, G. He, Deng, Fabrication of polyaniline/titanium dioxide composite nanofibers for gas sensing application, Matr. Chem. Phys. 129 (2011) 477-480.

[112] M.R. Mohammadi, D.I. Fray, Synthesis and characterisation of nanosized TiO_2-ZrO_2 binary system prepared by an aqueous sol-gel process: Physical and sensing properties, Sens. Actuators B: Chem., 155 (2011) 568-576.

[113] B.R. Huang, T.C. Lin, A novel technique to fabricate horizontally aligned CNT nanostructure film for hydrogen gas sensing, Int. J. Hydro. Ener. 36 (2011) 15919-15926.

[114] Leghrib R., Felten A., Pireaux J. J., Llobet E., Gas sensors based on doped-CNT/SnO_2 composites for NO_2 detection at room temperature, Thin Solid Films 520 (2011) 966-970.

[115] A.B. Bodade, A.B. Bodade, H.G. Wankhade, G.N. Chaudhari, D.C. Kothari, Conduction mechanism and gas sensing properties of $CoFe_2O_4$ nanocomposite thick films for H_2S gas, Talanta 89 (2012) 183-188.

[116] Y. Gonullu, G.C.M. Rodriguez, B. Saruhan, M. Urgen, Improvement of gas sensing performance of TiO_2 towards NO_2 by nano-tubular structuring, Sens. Act. B 169 (2012) 151-160.

[117] S.L. Patil, M.A. Chougule, S. Sen, V.B. Patil, Measurements on room temperature gas sensing properties of CSA doped polyaniline-ZnO nanocomposites, Measurement 45 (2012) 243-249.

[118] S. Mun, Y. Chen, J. Kim, Cellulose‐titanium dioxide‐multiwalled carbon nanotube hybrid nanocomposite and its ammonia gas sensing properties at room temperature, Sens. Actuators B: Chem., 171 (2012) 1186-1191.

[119] M.K. Verma, V. Gupta, A highly sensitive SnO_2-CuO multilayered sensor structure for detection of H_2S gas, Sens. Actuators B: Chem., 166-167 (2012) 378-385.

[120] B.R. Huang, T.C. Lin, Palladium nanoparticles modified carbon nanotube/nickel composite rods (Pd/CNT/Ni) for hydrogen sensing, Sens. Actuators B: Chem., 162 (2012) 108-113.

[121] M.A. Chougule, D.S. Dalavi, S. Mali, P.S. Patil, A.V. Moholkar, G.L. Agawane, J.H. Kim, S. Sen, V.B. Patil, Novel method for fabrication of room temperature polypyrrole-ZnO nanocomposite NO_2 sensor, Measurement 45 (2012) 1989-1996.

[122] V.V. Bolotov, V.E. Roslikov, E.A. Kurdyukova, O.V. Krivozubov, S.A. Sten'kin, D.V. Cheredov, Electrical and gas sensing properties of *por*-Si/SnO_x nanocomposite layers, Semiconductors 46 (2012) 105-108.

[123] Y. Wang, Y. Chen, J. Shi, J. Cao, G. Sun, B. Hari, Z. Zhang, Ethanol Sensor Based on Hydrothermal Method Prepared Porous α-Fe_2O_3 Nanorods, Adv. Mat. Res. 476-478 (2012) 1075-1078.

[124] B. Ghaddab, J.B. Sanchez, C. Mavon, M. Paillet, R. Parret, A.A. Zahab, J.-L. Bantignies, V. Flaud, E. Beche, F. Berger, Detection of O_3 and NH_3 using hybrid tin dioxide/carbon nanotubes sensors: Influence of materials and processing onsensor's sensitivity, Sens. Actuators B: Chem., 170(2012) 67-74.

[125] Q. Lin, Y. Li, M. Yang, Tin oxide/graphene composite fabricated via a hydrothermal method for gas sensors working at room temperature, Sens. Actuators B: Chem., 173 (2012) 139-147.

[126] H.L. Yu, L. Li, X.M. Gao, Y. Zhang, F. Meng, T.S. Wang, G. Xiao, Y.J. Chen, C.L, Zhu, Synthesis and H_2S gas sensing properties of cage-like-MoO_3/ZnO composite, Sens. Actuators B: Chem., 171 (2012) 679-685.

[127] H. Liu, H. Ma, W. Zhou, W. Liu, Z. Jie, X. Li, Synthesis and gas sensing characteristic based on metal oxide modification multi wall carbon nanotube composites, Appl. Surf. Sci. 258 (2012) 1991-1994.

[128] S. Srivastava, K. Jain, V.N. ingh, S. Singh, N. Vijayan, N. Dilawar, Gupta G., Senguttuvan T. D., Faster response of NO_2 sensing in grapheme-WO_3 nanocomposites, Nanotechn. 23 (2012) 205501

[129] X. Lai, P. Li, T. Yang, J. Tu, P. Xue, Ordered array of Ag-In_2O_3 composite nanorods with enhanced gas-sensing properties, Scripta Materialia 67 (2012) 293-296.

[130] S. Srivastava, S. Kumar, Y.K. Vijay, Preparation and characterization of tantalum/polyaniline composite based chemiresistor type sensor for hydrogen gas sensing application, Int. J. Hydro. Ener. 37 (2012) 3825-3832.

[131] H.L. Yu, L. Li, X.M. Gao, Y. Zhang, F. Meng, T.S. Wang, G. Xiao, Y.J. Chen, C.L. Zhu, Synthesis and H_2S gas sensing properties of cage-like α-MoO_3/ZnO composite, Sens. Actuators B: Chem., 171 (2012) 679-685.

[132] G. Singh, A. Choudhary, D. Haranath, A.G. Joshi, N. Singh, S. Singh, R. Pasricha, ZnO decorated luminescent graphene as a potential gas sensor at room temperature, Carbon 50 (2012) 385-394.

[133] A.H. Ammar, M.S. Abo-Ghazala, A.A.M. Farag, N.M. Abdel-Moniem, El-Sayed M. Farag, Effect of gas type, pressure and temperature on the electrical characteristics of Al-doped SnO_2 thin films deposited by RGTO method for gas sensor application, Vacuum 94 (2013) 30-40.

[134] D.T. Nguyen, M.T. Nguyen, G.T. Ho, T.N. Nguyen, S. Reisberg, B. Piro, M. C. Pham, Design of interpenetrated network MWCNT/poly(1,5-DAN) on interdigital electrode: Toward NO_2 gas sensing, Talanta 115 (2013)713-717.

[135] Y. Mun, S. Park, S. An, C. Lee, H. Woo Kim, NO_2 gas sensing properties of Au-functionalized porous ZnO nanosheets enhanced by UV irradiation, Ceramics International 39 (2013) 8615-8622.

[136] A. Marikutsa, V. Krivetskiy, L. Yashina, M. Rumyantseva, E. Konstantinova, A. Ponzoni, E. Cominic, A. Abakumov, A. Gaskov, Catalytic impact of RuO_x clusters to high ammonia sensitivity of tin dioxide, Sens. Actuators B: Chem., 175 (2013) 186-193.

[137] R.N. Bulakhe, S.V. Patil, P.R. Deshmukh, N.M. Shinde, C.D. Lokhande, Fabrication and performance of polypyrrole (Ppy)/TiO_2 heterojunction for room temperature operated LPG sensor, Sens. Actuators B: Chem., 181 (2013) 417-423.

[138] S.L. Patil, M.A. Chougule, S. Sen , V.B. Patil, Measurements on room temperature gas sensing properties of CSA doped polyaniline-ZnO nanocomposites, Measurement 45 (2012) 243-249.

[139] T. Samerjai, N. Tamaekong, C. Liewhiran, A. Wisitsoraat, S. Phanichphant, NO_2 gas sensing of flame-made Pt-loaded WO_3 thick films, Journal of Solid State Chemistry, 214 (2014) 47-52.

[140] S. Supothina, M. Suwan, A. Wisitsoraat, Hydrothermal synthesis of $K_2W_4O_{13}$ nanowire with high H_2S gas sensitivity, Microelectronic Engineering 126 (2014) 88-92.

[141] Chi-J.Chang, C. YiLin, J.K. Chen, Mu-H. Hsu, Ce-doped ZnO nanorods based low operation temperature NO_2 gas sensors, Ceramics International 40 (2014) 10867-10875

[142] S. Pati, P. Banerji, S.B. Majumder, n- to p- type carrier reversal in nanocrystalline indium doped ZnO thin film gas sensors, International Journal of Hydrogen Energy 39 (2014) 15134-15141

[143] S.T. Navale, M.A. Chougule, V.B. Patil, A.T. Mane, Highly sensitive, reproducible, selective and stable CSA-polypyrrole NO_2 sensor, Synthetic Metals 189 (2014) 111-118.

[144] Li. Yang, C. Xie, G. Zhang, J. Zhaoa, X. Yua, D. Zeng, S. Zhang, Enhanced response to NO_2 with CuO/ZnO laminated heterostructured configuration, Sens. Actuators B: Chem., 195 (2014) 500-508.

[145] G. Eranna, B.C. Joshi, D.P. Runthala, R.P. Gupta, Oxide Materials for Development of Integrated Gas Sensors-A Comprehensive Review, Crit. Rev. Solid State Mater. Sci. 29 (2004) 111-188.

[146] M. Batzill, U. Diebold, The surface and materials science of tin oxide, Prog. Surf. Sci. 79 (2005) 47-154.

[147] H. Markoc, U. Ozgur, ZnO Fundamentals, Materials and Device Technology, Wiley-VCH (2009) 488.

[148] R. Menon, V. Gupta, H.H. Tan, K. Sreenivas, C. Jagadish, Origin of stress in radio frequency magnetron sputtered zinc oxide thin films, J. Appl. Phys. 109 (2011) 064905.

[149] T. Seiyama, A. Kato, K. Fujiishi, M. Nagatani, A New Detector for Gaseous Components Using Semiconductive Thin Films, Anal. Chem. 34 (1962) 1502-1503.

[150] R.M. Cornell, U. Schwertmann, The Iron Oxides: Structure, Properties, Reactions, Occurrences and Uses, second ed. Wiley-VCH, Weinheim, German, 2003.

[151] U. Schwertmann, R. M. C. U. Cornell, The Iron Oxides, Structure, Properties, Reactions, Occurences and Uses; Wiley: Weinheim, 2003 (http://trove.nla.gov.au/version/36973177).

[152] P.Y.C. Wu, X. Zhu, C. OuYang, Y. Xie, Synthesis of Hematite (α-Fe_2O_3) Nanorods: Diameter-Size and Shape Effects on Their Applications in Magnetism, Lithium Ion Battery, and Gas Sensors, J. Phys. Chem., B 110 (2006) 17806-17812.

[153] L. Huo, Q. Li, H. Zhao, L. Yu, S. Gao, J. Zhao, Sol-gel route to pseudocubic shaped α-Fe_2O_3 alcohol sensor: preparation and characterization, Sens. Actuators B: Chem., 107 (2005) 915-920.

[154] M. Nitta, S. Kanefusa, M. Haradome, H_2S gas detection by ZrO-doped SnO_2, IEEE Trans. Elec. Dev. 35 (1988) 65-69.

[155] V.P. Verma, S. Das, S. Hwang, H. Choi, M. Jeon, W. Choi, Nitric oxide gas sensing at room temperature by functionalized single zinc oxide nanowire, Materials Science and Engineering: B, 171 (2010) 45-9.

[156] N. Van Quy, V.A. Minh, N. Van Luan, V.N. Hung, N. Van Hieu, Gas sensing properties at room temperature of a quartz crystal microbalance coated with ZnO nanorods, Sens. Actuators B: Chemi., 153 (2011) 188-193.

[157] R. Leghrib, A. Felten, J.J. Pireaux, E. Llobet, Gas sensors based on doped-CNT/SnO_2 composites for NO_2 detection at room temperature, Thin Solid Films, 520(2011) 966-970.

[158] D. Padilla-Rueda, J.M. Vadillo, J.J. Laserna, Room temperature pulsed laser deposited ZnO thin films as photoluminiscence gas sensors, Applied Surface Science, 259 (2012) 806-810.

[159] G. Lu, J. Xu, J. Sun, Y. Yu, Y. Zhang, F. Liu, UV-enhanced room temperature NO_2 sensor using ZnO nanorods modified with SnO_2 nanoparticles, Sens. Actuators B: Chem., 162 (2012) 82-88.

[160] S.W. Choi, A. Katoch, G.-J. Sun, S.S. Kim, Synthesis and gas sensing performance of ZnO–SnO_2 nanofiber–nanowire stem-branch heterostructure, Sens. Actuators B: Chem., 181 (2013) 787-794.

[161] M. Kodu, T. Avarmaa, A. Floren, R. Jaaniso, Bias dependent NO_2 sensitivity of SnO_2 thin films at room temperature, Journal of the European Ceramic Society, 33 (2013) 2335-2340.

[162] S.T. Navale, G.D. Khuspe, M.A. Chougule, V.B. Patil, Room temperature NO_2 gas sensor based on PPy/α-Fe_2O_3 hybrid nanocomposites, Ceramics International, 40 (2014) 8013-8020.

[163] S. Liu, B. Yu, H. Zhang, T. Fei, T. Zhang, Enhancing NO2 gas sensing performances at room temperature based on reduced graphene oxide-ZnO nanoparticles hybrids, Sens. Actuators B: Chem., 202 (2014) 272-278.

[164] S. Liu, Z. Wang, Y. Zhang, C. Zhang, T. Zhang, High performance room temperature NO_2 sensors based on reduced graphene oxide-multiwalled carbon nanotubes-tin oxide nanoparticles hybrids, Sens. Actuators B: Chem., 211 (2015) 318-324.

[165] R.K. Sonker, B.C. Yadav, Growth mechanism of hexagonal ZnO nanocrystals and their sensing application, Materials Letters, 160 (2015) 581-584.

[166] C.A. Betty, S. Choudhury, S. Arora, Tin oxide-polyaniline heterostructure sensors for highly sensitive and selective detection of toxic gases at room temperature, Sens. Actuators B: Chem., 220 (2015) 288-294.

[167] X. Liu, J. Sun, X. Zhang, Novel 3D graphene aerogel-ZnO composites as efficient detection for NO_2 at room temperature, Sens. Actuators B: Chem., 21 (2015) 220-226.

[168] V. Srivastava, K. Jain, At room temperature graphene/SnO_2 is better than MWCNT/SnO_2 as NO_2 gas sensor, Materials Letters, 169 (2016) 28-32.

[169] F.H. Saboor, T. Ueda, K. Kamada, T. Hyodo, Y. Mortazavi, A.A. Khodadadi, et al., Enhanced NO_2 gas sensing performance of bare and Pd-loaded SnO_2 thick film sensors under UV-light irradiation at room temperature, Sens. Actuators B: Chem., 223 (2016) 429-439.

[170] Z. Wang, Y. Zhang, S. Liu, T. Zhang, Preparation of Ag nanoparticles-SnO_2 nanoparticles-reduced graphene oxide hybrids and their application for detection of NO_2 at room temperature, Sens. Actuators B: Chem., 222 (2016) 893-903.

[171] H. Letheby, On the production of a blue substance by the electrolysis of sulphate of aniline, J. Chem. Soc. 15 (1862) 161-163.

[172] A.G. Green and A.E. Woodhead, J. Chem. Soc. Trans 101 (1912) 1-18.

[173] A.J. Epstein, J.M. Ginder, F. Zuo, R.W. Bigelow, H. Woo, D.B. Tanner, A.F. Richter, W. Huang and G.A. MacDiarmid, Insulator-to-metal transition in polyaniline, Synth. Met. 18 (1987) 303-309.

[174] A.J. Heeger, The fourth generation of polymeric materials Semiconducting and metallic polymers: Nobel Lecture, Reviews of Modern Physics 73 (2001) 681-700.

[175] G. Tzamalis, N. Zaidi, A. Monkman, Applicability of the localization-interaction model to magnetoconductivity studies of polyaniline films at the metal-insulator boundary, Physical Review B 68 (2003) 245106.

[176] C.J. Carlos, R. A. Bustos-Marún, H.M. Pastawski, Crucial role of decoherence for electronic transport in molecular wires: Polyaniline as a case study, Physical Review B 82 (2010) 144201.

[177] N. Gospodinova and L. Terlemezyan, Conducting polymers prepared by oxidative polymerization: polyaniline, Progress Polym. Sci. 23 (1998) 1443-1484.

[178] J.Y. Shimano and A.G. MacDiarmid, Polyaniline, a dynamic block copolymer: key to attaining its intrinsic conductivity?, Synth. Met. 123 (2001) 251-262.

[179] G.G. Wallace, G.M. Spinks, L.A.P. Kane-Maguire and P.R. Teasdale, Intelligent Polymer Systems, CRC Press, London (2009).

[180] W.S. Huang and A.G. MacDiarmid, Optical properties of polyaniline Polymer, 34 (1993) 1833-1845.

[181] J. E. de Albuquerque, L.H.C. Mattoso, R.M. Faria, J.G. Masters and A.G. MacDiarmid, Study of the interconversion of polyaniline oxidation states by optical absorption spectroscopy, Synth. Met. 146 (2004) 1-10.

[182] S. Stafström, J.L. Brédas, A.J. Epstein, H.S. Woo, D.B. Tanner, W.S. Huang and A.G.MacDiarmid, Polaron lattice in highly conducting polyaniline: Theoretical and optical studies, Phys. Rev. Lett., 59 (1987) 1464-1467.

[183] S. Bhadra, D. Khastgir, N.K. Singha, J. H. Lee, Progress in preparation, processing and applications of polyaniline, Prog. Polym. Sci. 34 (2009) 783-810.

[184] R. Kohlman, S.A. Zibold, D.B. Tanner, C.G. Ihas, T. Ishiguro, Y.G. Min, A.G MacDiarmid and A. Epstein, Limits for Metallic Conductivity in Conducting Polymers, Phys. Rev. Lett., 78 (1997) 3915-3918.

[185] K. Ogura, H. Shiigi, M. Nakayama, A. Ogawa, Thermal Properties of Poly(anthranilic acid) (PANA) and Humidity-Sensitive Composites Derived from Heat-Treated PANA and Poly(vinyl alcohol), J. Polym. Sci. A 37 (1999) 4458-4465.

[186] K. Ogura, T. Saino, M. Nakayama, H. Shiigi, Room temperature synthesis of zinc pyrovanadate $Zn_3(OH)_2V_2O_7 \cdot 2H_2O$, J. Mater. Chem. 9 (1999) 1543-1545.

[187] K. Ogura, H. Shiigi, Electrochem. A CO_2 Sensing Composite Film Consisting of Base-Type Polyaniline and Poly(vinyl alcohol), Solid State Lett. 2 (1999) 478-480.

[188] M. Matsuguchi, J. Io, G. Sugiyama, Y. Sakai, Effect of NH_3 gas on the electrical conductivity of polyaniline blend films**,** Synth. Met. 128 (2002) 15-19.

[189] M. Matsuguchi, A. Okamoto, Y. Sakai, Effect of humidity on NH_3 gas sensitivity of polyaniline blend films, Sens. Actuators B: Chem., 94 (2003) 46-52.

[190] E. Segal, R. Tchoudakov, M. Narkis, A. Siegmann, Y. Wei, Polystyrene/polyaniline nanoblends for sensing of aliphatic alcohols, Sens. Actuators B: Chem., 104 (2005) 140-150.

[191] M.S. Silverstein, H.W. Tai, A. Sergienko, Y.L. Lumelsky, S. Pavlovsky, PolyHIPE: IPNs, hybrids, nanoscale porosity, silica monoliths and ICP-based sensors, Polymer 46 (2005) 6682-6694.

[192] J.S. Kim, S.O. Sohn, J.S. Huh, Fabrication and sensing behavior of PVF_2 coated-polyaniline sensor for volatile organic compounds, Sens. Actuators B: Chem., 108 (2005) 409-413.

[193] S.T. McGovern, G.M. Spinks, G.G. Wallace, Micro-humidity sensors based on a processable polyaniline blend, Sens. Actuators B: Chem., 107 (2005) 657-665.

[194] E. Segal, R. Tchoudakov, I. Mironi-Harpaz, M. Narkis, A. Siegmann, Chemical sensing materials based on electrically-conductive immiscible polymer blends, Polym. Int. 54 (2005) 1065-1075.

[195] H. Cooper, E. Segal, S. Srebnik, R. Tchoudakov, M. Narkis, A. Siegmann, Electrically Conductive Sensors for Liquids Based on Quaternary Ethylene Vinyl Acetate (EVA)/Copolyamide/ Maleated-EVA/Polyaniline Blends, J. Appl. Polym. Sci. 101 (2006) 110-117.

[196] K.H. Hong, K.W. Oh, T.J. Kang, Polyaniline–nylon 6 composite fabric for ammonia gas sensor J. Appl. Polym. Sci. 92 (2004) 37-42.

[197] S. Watcharaphalakorn, L. Ruangchuay, D. Chotpattahanont, A. Sirivat, J. Schwank, Polyaniline/polyimide blends as gas sensors and electrical conductivity response to CO–N_2 mixtures, Polym. Int. 54 (2005) 1126-1133.

[198] Q. Hao, X. Wang, L. Lu, X. Yang, V.M. Mirsky, Electropolymerized Multilayer Conducting Polymers with Response to Gaseous Hydrogen Chloride, Macromolecular Rapid Commun. 26 (2005) 1099-1103.

[199] G.A. Sotzing, J.N. Phend, R.H. Grubbs, N.S. Lewis, High selective and discrimination of Biogenic Amine Utilizing Array of Polyaniline/Carbon Black Composite Vapor Detectors, Chem. Mater. 12 (2000) 593-595.

[200] T. Zhang, M.B. Nix, B.Y. Yoo, M.A. Deshusses, N.V. Myung, Electrochemically Functionalized Single-Walled Carbon Nanotube Gas Sensor, Electroanalysis 18 (2006) 1153-1158.

[201] X. Ma, G. Li, M. Wang, Y. Cheng, R. Bai, H. Chen, Preparation of a Nanowire-Structured Polyaniline Composite and Gas Sensitivity Studies, Chem. Eur. J. 12 (2006) 3254-3260.

[202] T.L. Porter, D. Thompson, M. Bradley, M.P. Eastman, M.E. Hagerman, J.L. Attuso, A.E. Votava, E.D. Bain, Nanometer-scale Structure of Hectorite-Aniline Intercalates**,** Journal of Vacuum Science & Technology: A Vacuum Surfaces and Films 15 (1997) 500-504.

[203] C. Conn, S. Sestak, A.T. Baker, J. Unsworth, A Polyaniline-Based Selective Hydrogen Sensor, Electroanalysis 10 (1998) 1137-1141.

[204] M.K. Ram, O. Yavuz, V. Lahsangah, M. Aldissi, CO gas sensing from ultrathin nano-composite conducting polymer film, Sens. Actuators B: Chem., 106 (2005) 750-757.

[205] J.Z. Wang, I. Matsubara, N. Murayama, S. Woosuck, N. Izu, The preparation of polyaniline intercalated MoO_3 thin film and its sensitivity to volatile organic compounds, Thin Solid Films 514 (2006) 329-333.

[206] S. Virji, J.D. Fowler, C.O. Baker, J.X. Huang, R.B. Kaner, B.H. Weiller, Polyaniline Nanofiber Composites with Metal Salts: Chemical Sensors for Hydrogen Sulfide, Small 1 (2005) 624-627.

[207] N. Parvatikar, S. Jain, S.V. Bhoraskar, M. Prasad, Spectroscopic and electrical properties of polyaniline/CeO_2 composites and their application as humidity sensor, J. Appl. Polym. Sci. 102 (2006) 5533-5537.

[208] A.Z. Sadek, W. Wlodarski, K. Shin, R.B. Kaner, K. Kalantar-zadeh, A layered surface acoustic wave gas sensor based on a polyaniline/In_2O_3 nanofibre composite, Nanotechnology 17 (2006) 4488-4492.

[209] N. Densakulprasert, L. Wannatong, D. Chotpattananont, P. Hiamtup, A. Sirivat, J. Schwank, Electrical conductivity of polyaniline/zeolite composites and synergetic interaction with CO, Mater. Sci. Eng. B 117 (2005) 276-282.

[210] J.S. Do, W.B. Chang, Amperometric nitrogen dioxide gas sensor: preparation of PAn/Au/SPE and sensing behavior, Sens. Actuators B: Chem., 72 (2001) 101-107.

[211] J.S. Do, W.B. Chang, Amperometric nitrogen dioxide gas sensor based on PAn/Au/Nafion prepared by constant current and cyclic voltammetry methods, Sens. Actuators B: Chem., 101 (2004) 97-106.

[212] S. Sharma, C. Nirkhe, S. Pethkar, A.A. Athawale, Chloroform vapour sensor based on copper/polyaniline nanocomposite, Sens. Actuators B: Chem., 85 (2002) 131-136.

[213] B.J. Hwang, J.Y. Yang, C.W. Lin, A microscopic gas sensing Model for Ethanol Sensor Based conductive polymer composite from polypyrrole and poly (Ethylene Oxide), J. Electrochem. Soc. 146 (1999) 1231-1236.

[214] K. Suri, S. Annapoorni, A.K. Sarkar, R.P. Tandon, Gas and humidity sensors based on iron oxide-polypyrrole nanocomposites, Sens. Actuators B: Chem., 81 (2002) 277-282.

Chapter 2

Low temperature study of nanostructured Fe_2O_3 and Fe_2O_3-PANI thin films as NO_2 sensor

Nitrogen dioxide (NO_2) is a reddish-brown toxic gas with a sharp characteristic, biting odor and is a prominent air pollutant. Present chapter reports the synthesis of α-Fe_2O_3-PANI and its application as NO_2 gas sensor operable at low temperature. For this purpose the iron oxide-polyaniline (α-Fe_2O_3-PANI) films were prepared by spin coating method on various corning glass substrates over Pt inter digital electrodes (IDEs) and characterized for structural and morphological properties by means of X-ray diffraction (XRD), Fourier transform infrared (FTIR) spectroscopy, and Scanning electron microscopy (SEM). The sensing mechanism pertains to a change in the depletion region of the p-n junction formed between PANI and α-Fe_2O_3 as a result of electronic charge transfer between the gas molecules and the sensor. The sensing mechanism of α-Fe_2O_3 materials to NO_2 was presumed to be the synergism of α-Fe_2O_3 with NO_2 gas molecules. The prepared nanostructured α-Fe_2O_3-PANI film showed a high sensing response ~2.29×10^2 towards 20 ppm of NO_2 gas. Besides giving the higher sensing response towards NO_2 gas, α-Fe_2O_3-PANI sensor structure was found to be highly selective and exhibited the poor gas sensing response towards other interfering gases including 2000 ppm of Acetone, IPA, NH_3, LPG and CO_2 gases ranged from 0.98 to 1.29.

2.1 Introduction:

The organic and inorganic materials are used to improve the various properties of polymers like thermal [1], mechanical [2], chemical [3], electrical [4], etc. Polyaniline (PANI) is one of the conducting polymers in which nonmaterials are used for their synergism effect to improve electronic properties [5]. Among the nanosized metal oxides that have been the focus of research due to their potential application in electronic devices, maghemite (α-Fe_2O_3) has attained prominence due to its magnetic, photocatalytic and electrochemical properties [6-9]. In order to monitor the air pollution on a large scale, inexpensive, reliable and easy to use gas sensors are needed. The electrical resistance of semiconductor oxides, such as SnO_2, ZnO, TeO_2 and Fe_2O_3, has a strong dependence on the concentration of surrounding gases. According to this principle, these oxides are commercially designed as chemical sensors to detect toxic gases such as LPG, and NO_2 [10-11]. With this intention, several methods of preparation of ferric oxides are known as co-precipitation, micro emulsion, pulsed wire discharge and hydrothermal processes are employed in order to obtain nanostructured powder [12-14]. The sol-gel process has a unique advantage of producing large-surface-area films at low cost, which is useful to enhance the gas sensitivity [15-16].

Polyaniline (PANI) as a typical conducting polymer has received a great deal of attention recently. As is known that PANI has a variety of oxidation states and three different states of them are usually referred to in the literature [17–19]: leucoemeraldine base (LEB, fully reduced), emeraldine base (EB, half-oxidized) and pernigraniline base (PNB, fully oxidized). Therein, EB is the most attractive one, because it can be doped with protonic acid to become emeraldine salt (ES) and the DC conductivity of the ES is increased due to the charge delocalization on the polymer backbone created by doping H^+. Thus, a suitable combination of conducting polymers and metal oxide (Fe_2O_3) nanoparticles could generate enhanced catalytical/electrocatalytical activities. With regard to the background, using a composite carrier composed of PANI and ferric oxide nanoparticles could combine the excellent properties of ferric oxide and polyaniline, in addition, a synergistic effect might play a role in enhancing the properties of composite catalysts. They have unique electronic properties due to the π-conjugation present in their

backbones, and display improved characteristics over conventional sensors based on nanometal oxides. PANI, in particular, has been extensively used due to its ease of fabrication, high stability and electrical conductivity.

In the present investigation, we have prepared PANI/α-Fe_2O_3 nanocomposite thin film on corning glass substrate via chemical polymerization method, and tested the electrical response of the thin film to NO_2 gas at room temperature.

2.2 Experimental

2.2.1 Materials

Ferric nitrate ($Fe(NO_3)_3.9H_2O$ Aldrich 98% purity), citric acid, ammonium hydroxide, monohydrate citric acid, lithium hydroxide, ethanol and n-butyl acetate used for the sensor preparation were purchased from Sigma Aldrich Chemical Co.

2.2.2 Synthesis of nanostructures

In this experiment, 0.1M of iron nitrate ($Fe(NO_3)_3.9H_2O$) was used as a precursor solution with 0.1M of monohydrate citric acid solution as legend molecules and 100 ml distilled water as the solvent. The prepared ferric nitrate solution was added to the citric acid solution drop wise with vigorous stirring. The obtained solution was then heated to a temperature from 70 ºC to 120 ºC, with vigorous stirring until the gel was formed. Such prepared precursor was used to fabricate the thin films on various corning glass substrates over Pt inter digital electrodes (IDEs) using spin coating process.

For the formation of the powder, the gel was precipitated by NH_4OH added drop by drop to the prepared gel. The powder was then dried at 60 ºC for 4 h and grinded using mortar and pestle. The grinded powder was annealed at 500 ºC for 2 h.

50 ml of conc. HCl was added to 500 ml of distilled water in a beaker marked as A. 331ml of distilled water was taken and to it 18.924 g of ammonium persulphate was added and stirred in beaker B. To beaker A, 8.33 ml of aniline was added and stirred for 20 min in ice bath. Ammonium persulphate solution was then added drop wise (15 s between 2 drops) to the above solution with continuous stirring. After complete addition,

the solution was left overnight and then filtered. The precipitate was washed with water repeatedly till the filtrate became colorless and after washing, it was left overnight. The precipitate was then dried at 40-50 ºC and made into fine powder. The fine powder was then washed with methanol, refluxed for 4-5 h at 40-50 ºC. It was again dried at 40-50 ºC to obtain emeraldine salt of PANI. To un-doped emeraldine salt, it was washed with ammonium hydroxide solution, filtered and dried to obtain emeraldine base of PANI [20].

All the prepared films and powder samples were characterized using SEM, XRD, FTIR and UV-vis. Spectroscopy. Thickness of each prepared film was measured using a surface profiler (Veeco dektak 150) and found as 400 nm. Crystalline structure and surface morphology of the sensing layer were studied using Bragg–Brentano (θ-2θ) scan of X-ray Diffractometer (X-Pert PRO PANalytical) using the CuKα_1 source (λ = 0.154 nm) and Scanning electron microscope (SEM, JEOL, JSM-6490LV) respectively.

Optical characterization was carried out by the UV-vis Spectrophotometer (Thermo, Evolution 200). For studying the gas sensing properties, the home-made gas dilution system was utilized [11]. The total amount of gas flow rate of the diluted NO_2 gas by dry air is 5000 ml/min and the volume of chamber is 5000 ml. The α-Fe_2O_3 array sensor was inserted between the two electrodes and the diluted NO_2 gas was injected into the test chamber. Variations in the electrical resistance with the exposure of NO_2 gas to the sensor were measured through a Keithley (6517B) electrometer interfaced with a personal computer. The sensing response of prepared sensor structure towards oxidizing NO_2 gas is given as under [21]:

$$S = \frac{R_g - R_a}{R_a} \quad (1)$$

where, R_a and R_g are the values of resistance of the sensor in the presence of atmospheric air and target gas respectively.

2.3 Results and Discussion

As prepared thin film was investigated through UV-visible absorption spectroscopy, a record of the amount of light absorbed by the ferric oxide thin film

deposited on corning glass substrate, as a function of the wavelength of light in the range 190-1100 nm was observed. Optical band gap was calculated from the intercept on energy axis obtained by extrapolating the linear portion of the Tauc plot $(\alpha h\nu)^2$ *vs* photon energy ($h\nu$) as shown in inset of Fig. 2.1. Error in the determination of band gap value was less than 5%. Estimated value of band gap for as-grown ferric oxide thin film was found to be 2.78 eV which is close to the actual reported value for ferric oxide thin films (2.40 eV) grown by other techniques. Similarly the UV visible spectra of the as deposited Fe_2O_3-PANI nanocomposite thin film is shown in Fig. 2.1 (b) having high absorption spectra in the visible region. The value of band gap increases slightly for Fe_2O_3-PANI composite thin film with the incorporation of PANI nanoparticles to 3.04 eV.

The FTIR spectra of ferric oxide thin film are shown in Fig. 2.2. The sharp peak corresponding to Fe–O stretching mode was observed at 530 cm^{-1} wavenumber. Results also show absorption bands at 3748 cm^{-1} which correspond to Fe–OH bending and stretching vibrations. The peaks observed at around 1137, 1220, and 1632 cm^{-1} corresponded to C–N bond, N–H bond and CH_2 group, respectively. The absorption band observed at around 1632 cm^{-1} corresponds to N–H bending vibration and a broad peak observed at around 2371 cm^{-1} attributed to Fe–OH stretching vibration which overlapped the N–H stretching vibrations.

The SEM micrographs of α-Fe_2O_3 and α-Fe_2O_3/PANI composite film were shown in Fig. 2.3. Fig. 2.3 (a) and (b) shows the irregular and spherical shaped α-Fe_2O_3 nanoparticles. The average diameter of α-Fe_2O_3 was absorbed 136 nm. Fig. 2.3 (c) and (d) shows the SEM image of α-Fe_2O_3/PANI film at different magnifications. Average diameter of α-Fe_2O_3/PANI nanocomposite was 258 nm from Fig. 2.3 (d). Over all the film is meso porous. During polymerization, the aniline monomer is absorbed onto the surface of Fe_2O_3 through electrostatic attraction via the formation of weak charge transfer complexes between the aniline monomer and the spherical Fe_2O_3 structure. The average pore size of α-Fe_2O_3 film and α-Fe_2O_3/PANI composite film were found 125 and 258 nm. These active sites (pores) are significant factors for improving the NO_2 sensing properties and hence are responsible for enhancing the response of the fabricated sensor.

The XRD pattern of the as-grown thin film is found to be crystalline, which become polycrystalline after a post deposition annealing treatment at 100 and 500 ^{o}C for 2 h in air. The annealed thin films were found to be more porous and strongly adherent to the substrate. Fig. 2.4 (a) and (b) shows the XRD pattern of PANI and ferric oxide thin film. The XRD pattern of pure PANI shown by Fig. 2.4 (a), reveals the reflection peaks occur at 2θ = 24.77° and 20.57º which corresponds to (110) and (100) plane of PANI respectively [22]. An additional peak at 2θ ≈ 15.73º is also observed and is in agreement with the reported value [22]. Broad and well defined reflections corresponding to (012), (104), (110), (113), (024), (116) and (018) planes of ferric oxide were observed at 24.23^{o}, 33.28º, 35.79^{o}, 40.98^{o}, 49.61º, 54.21º and 57.82º respectively for the deposited ferric oxide thin film shown by Fig. 2.4 (b) and are in good agreement to the corresponding values reported for the rhombohedral crystal structure of ferric oxide [23]. The values of lattice constants ('a' and 'c') estimated from XRD data for the ferric oxide thin films were found to be about 5.03 Å and 13.74 Å (JCPDS card No. 89-596) respectively. The crystallite size (*D*) of the sensing material was calculated by the Debye-Scherrer's formula [24], given by

$$D = \frac{K\lambda}{\beta \cos\theta} \quad (2)$$

where K= 0.94 is Scherrer's coefficient, which depends on the shape of the crystallite and the type of defects present, λ is the wavelength of X-ray radiation, β is the full width at half maximum (FWHM) of the diffraction peak and θ is the angle of diffraction. The average crystallite size of ferric oxide was calculated as ~ 27 nm.

Fig. 2.5 shows the dynamic sensing response curve of ferric oxide thin film annealed at different temperature towards 20 ppm of NO_2 gas. It was observed that the sensing response of all sensors structures increases with increase in annealing temperature. As prepared ferric oxide thin film sensor showed the sensing response of 2.07 and it was annealed at 200 ºC and 500 ºC sensing responses ware found as 9 and 114 towards 20 ppm of NO_2 gas. When NO_2 gas interacts with the ferric oxide thin films, it traps free electrons from the sensor surface and decreases the conductivity. As film was annealed, it becomes more porous and sensitive towards NO_2 gas resulting the enhancement in sensitivity of sensor.

Fig. 2.6 shows the dynamic response of α-Fe_2O_3/PANI thin film sensor at room temperature towards 20 ppm NO_2 gas. It is evident from Fig. 2.6 (a) that the exposure of NO_2 gas to the sensing film surface, results in the increase of resistance from 72.89 to 16693.98 kΩ (S = 229). The response and recovery times of the sensor were observed to be 2.35 and 3.8 min, respectively at room temperature. Fig. 2.6 (b) shows the variation in sensing response of thin film sensors of pristine α-Fe_2O_3 and α-Fe_2O_3 with different concentrations of PANI as 1%, 3%, 5% and 10% as a function of temperature towards 20 ppm of NO_2 gas. The pristine α-Fe_2O_3 thin film sensor shows the sensing response of 10 at room temperature towards 20 ppm of NO_2 gas. The Fe_2O_3-PANI (1%), Fe_2O_3-PANI (3%) and Fe_2O_3-PANI (10%) doped based sensors show the sensing response of 70, 150 and 100 at room temperature respectively. The enhancement in sensing response of order of 229 has been observed for Fe_2O_3-PANI (5%) sensor structure at room temperature. It was supposed that because of maximum adsorption sites developed and the electrons coming out from valance band to conduction band were trapped and no electrons were found in conduction band. As a result maximum increase in the resistance was observed on increasing the concentration of PANI beyond this limit and sensitivity goes down for Fe_2O_3-PANI (10%) it becomes minimum."

It may be clearly seen from Pi-chat Fig. 2.6 (c) that almost all pristine Fe_2O_3 and Fe_2O_3-PANI composite thin film, the Fe_2O_3-PANI (5%) is the most widely investigated (40.97%) and pristine Fe_2O_3 (1.79%) for detection of 20 ppm NO_2 gas sensor.

The variation of response and recovery time of Fe_2O_3/PANI thin film as a function of temperature towards 20 ppm of NO_2 gas is represented in Fig. 2.6 (d) which shows that the response and recovery times vary inversely with respect to the increase in temperature. The response time decreases from 2.35 to 1.39 min while the recovery time decreases from 3.80 min to 2.33 min with increasing of temperature in the range 30-200 °C towards 20 ppm of NO_2 gas. The decrease in response time is due to the large availability of vacant sites on the thin film for adsorption of the gas as evident from SEM images.

Thus the resistance R_g for all the sensors increases on exposure to NO_2 gas. At increasing annealing temperatures, the predominant oxygen species on the ferric oxide

surface are still O_2^- but NO_2 gas molecules interact directly with Fe ionic sites instead of reacting with O_2^- species.

$$O_2^- \rightarrow 2O^- + e^-$$

Physisorbed nitrogen dioxide molecules forms new surface acceptor levels deeper than surface oxygen ions. Therefore, bound electron is transferred from O_2^- ion to physisorbed NO_2 molecule.

$$NO_2 + e^- \rightarrow NO_2^- \text{ (ad)}$$

$$NO_2 + Fe^{3+} \xrightarrow{\text{adsorption}} (Fe^{4+} - NO_2^-) \xrightarrow{\text{desorption}} (Fe^{4+} - O^-) + NO$$

$$3(Fe^{4+} - O^-) \xrightarrow{\text{desorption}} 4Fe^{3+} + \frac{3}{2}O_2$$

During adsorption, NO_2 gas molecules attack the available free Fe sites on the sensor surface and take away electrons from the conduction band of Fe_2O_3 forming NO_2^- species.

2.4 Selectivity

The experiment on the selectivity of ferric oxide-polyaniline composite thin film deposited by spin coater was carried out by monitoring the change in electrical resistance towards different interfering gases (concentration = 2000 ppm) including Acetone, IPA, NH_3, LPG and CO_2 at room temperature. The prepared sensor was found to be highly selective towards NO_2 gas (Fig. 2.7) and exhibits higher increase in the sensor resistance after interaction with NO_2 gas molecules at room temperature. However, a small decrease in the sensor resistance was observed when exposed to other interfering gases (Fig. 2.7) indicating the development of highly selective ferric oxide thin film based sensor for detection of NO_2 gas.

2.5 Conclusion:

Ferric oxide-polyaniline composite thin film sensor structure has been designed for the trace level (20 ppm) detection of NO_2 gas at room temperature with sensor

response ~2.29 $\times 10^2$, moderate response time ~2.35 min and recovery time as 3.80 min. Nanoporous spherical surface morphology having nanocrystalline grains were found of much importance for obtaining the enhanced response characteristics.

References:

[1] V.K. Rana, A.K. Pandey, R.P. Singh, B. Kumar, S. Mishra, C.S. Ha, Enhancement of thermal stability and phase relaxation behavior of chitosan dissolved in aqueous L-lactic acid: using 'silver nanoparticles' as nano filler, Macromol. Res. 18 (2010) 713-720.

[2] S. Mishra, N.G. Shimpi, A.D. Mali, Influence of nano inorganic particles on properties of epoxy nanocomposites, Polym. Plast. Technol. Eng. 50 (2011) 758-761.

[3] S. Mishra, N.G. Shimpi, A.D. Mali, Investigation of photo-oxidative effect on morphology and degradation of mechanical and physical properties of nano $CaCO_3$ silicone rubber composites, Polym. Adv. Technol. 23 (2012) 236-246.

[4] S. Jing, S. Xing, L. Yu, Y. Wu, C. Zhao, Synthesis and characterization of Ag/polyaniline core-shell nanocomposites based on silver nanoparticles colloid, Mater. Lett. 61 (2007) 2794-2797.

[5] S. Mishra, N.G. Shimpi, T. Sen, The effect of PEG encapsulated silver nanoparticles on the thermal and electrical property of sonochemically synthesized polyaniline/silver nanocomposite, J. Polym. Res. 20 (2013) 49-58.

[6] B. David, O. Schneeweiss, E. Santava, O. Jasek, Magnetic properties of γ-Fe_2O_3 nanopowder synthesized by atmospheric microwave torch discharge, Acta Phys. Polon. A. 122 (2012) 9-11.

[7] S.K. Apte, S.D. Naik, R.S. Sonawane, B.B. Kale, J.O. Baeg, Synthesis of nanosize necked structure α- and γ-Fe_2O_3 and its photocatalytic activity, J. Am. Ceram. Soc. 90 (2007) 412-414.

[8] B.B. Li, M.R. Ji, X.M. Ni, F. Zhou, D.E. Zhang, J. Cheng, Convenient approach to γ-Fe_2O_3 nanoparticles: magnetic and electrochemical properties, Chin. J. Chem. Phys. 20 (2007) 203.

[9] B.C. Yadav, S. Singh and A. Yadav, Nanonails structured ferric oxide thick film as room temperature liquefied petroleum gas (LPG) sensor, App. Surf. Sci., 257 (2011) 1960-1966.

[10] R.K. Sonker, B. C. Yadav, Chemical Route Deposited SnO_2, SnO_2-Pt and SnO_2-Pd Thin Films for LPG Detection, Adv. Sci. Lett., 20 (2014) 1023-1027.

[11] R.K. Sonker, S. R. Sabhajeet, S. Singh, B.C. Yadav, Synthesis of ZnO nanopetals and its application as NO_2 gas sensor, Materials Letters, 152 (2015) 189-191.

[12] N.K. Chaudhari, J.S. Yu, Size control synthesis of uniform β-FeOOH to high coercive field porous magnetic α-Fe_2O_3 nanorods, J. Phys. Chemistry C, 112 (2008) 19957-19962.

[13] S. Shi, J.Y. Hwang, Microwave-assisted wet chemical synthesis: advantages, significance and steps to industrialization, J. Minerals and Materials Characterization and Engineering 2 (2003) 101-110.

[14] J.H. Bang, K.S. Suslick, Sonochemical synthesis of nanosized hollow hematite, Journal of the American Chemical Society 129 (2007) 2242-2243.

[15] R.K. Sonker, A. Sharma, M. Tomar, V. Gupta, B.C. Yadav, Low Temperature Operated NO_2 Gas Sensor Based on SnO_2-ZnO Nanocomposite Thin Film, Adv. Sci. Lett. 20 (2014) 911-916.

[16] S. Singh, A. Singh, M. Wan, R.R. Yadav, P. Tandon, S.S.A. Rasool, B.C. Yadav, Fabrication of self-assembled hierarchical flowerlike zinc stannatethin film and its application as liquefied petroleum gas sensor, Sensors and Actuators B, 205 (2014) 102-110

[17] J. Stejskal, R.G. Gilbert, Polyaniline. Preparation of a conducting polymer(IUPAC Technical Report), Pure Appl. Chem. 74 (2002) 857-867.

[18] J.E. Albuquerque, L.H.C. Mattoso, D.T. Balogh, R.M. Faria, J.G. Masters, A.G. Mac Diarmid, A simple method to estimate the oxidation state of polyanilines, Synth. Met. 113 (2000) 19-22.

[19] B. Lesiak, A. Jablonski, J. Zemek, M. Trchova, J. Stejskal, Determination of the Inelastic Mean Free Path of Electrons in Different Polyaniline Samples**,** Langmuir 16 (2000) 1415-1423.

[20] J. Stejskal, R.G. Gilbert, Preparation of a conducting polymer, Pure Appl. Chem. 74 (2002) 857-867.

[21] R.K. Sonker, A. Sharma, M. Tomar, V. Gupta, B.C. Yadav, Nanocatalyst (Pt, Ag and CuO) Doped SnO_2 Thin Film Based Sensors for Low Temperature Detection of NO_2 Gas, Adv. Sci. Lett. 20 (2014) 1374-1377.

[22] H. Xu, X. Chen, J. Zhang, J. Wang, B. Cao, D. Cui; NO_2 gas sensing with SnO_2-ZnO/PANI composite thick film fabricated from porous nanosolid; Sens. Actuators B:Chem., 176 (2013) 166-173.

[23] S. Singh, N. Verma, B.C. Yadav, R. Prakash, A comparative study on surface morphological investigations of ferric oxide for LPG and opto-electronic humidity sensors, Applied Surface Science 258 (2012) 8780-8789.

[24] S. Singh, A. Singh, B.C. Yadav, P.K. Dwivedi, Fabrication of nanobeads structured perovskite type neodymium iron oxide film: Its structural, optical, electrical and LPG sensing investigations, Sens. Actuator B: Chem., 177 (2013) 730-739.

Figures:

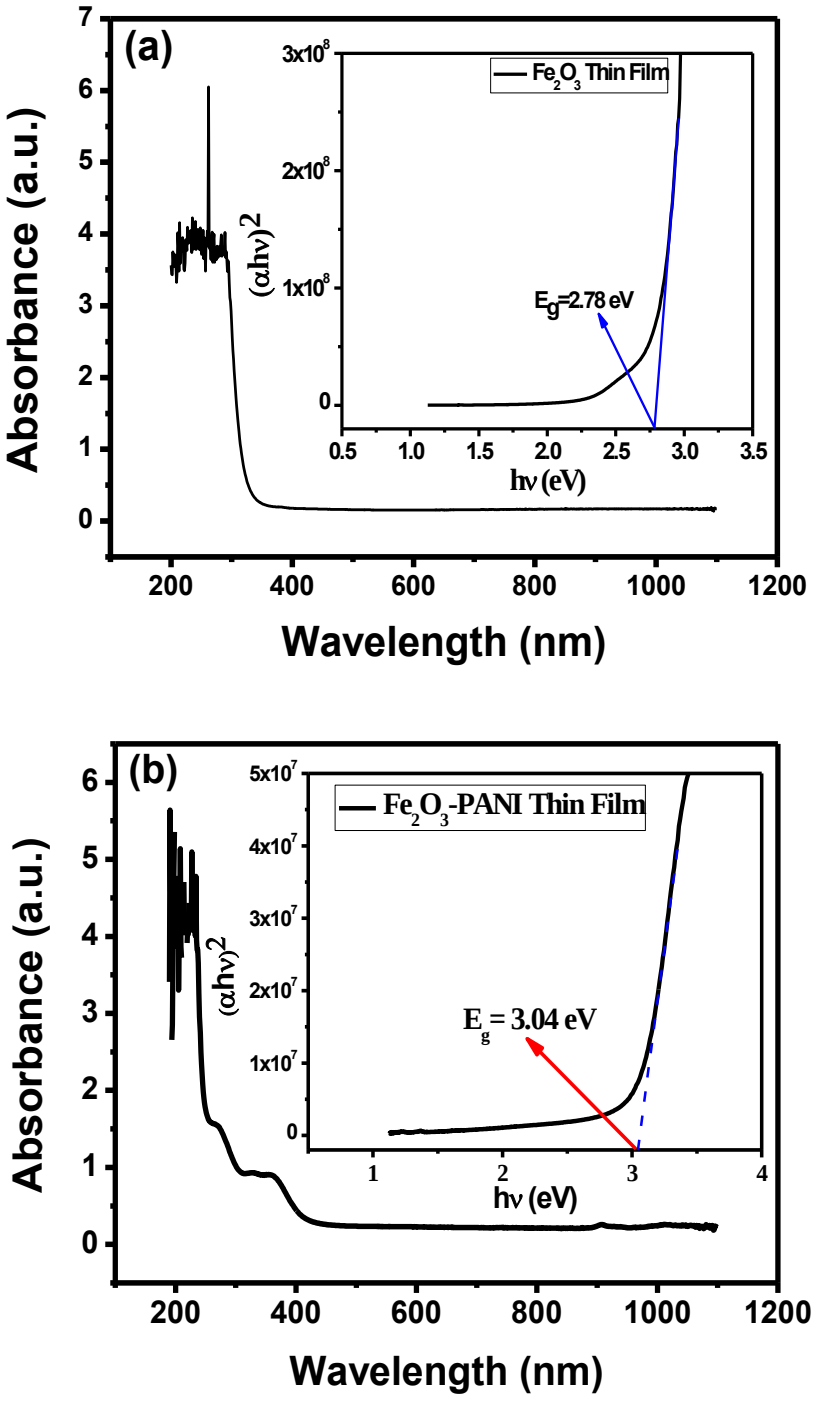

Fig. 2.1: UV-visible absorbance spectra of (a) ferric oxide (Fe_2O_3) and (b) Fe_2O_3-PANI composite thin film and inset Tauc plot [$(\alpha h\upsilon)^2$ vs. $h\upsilon$]

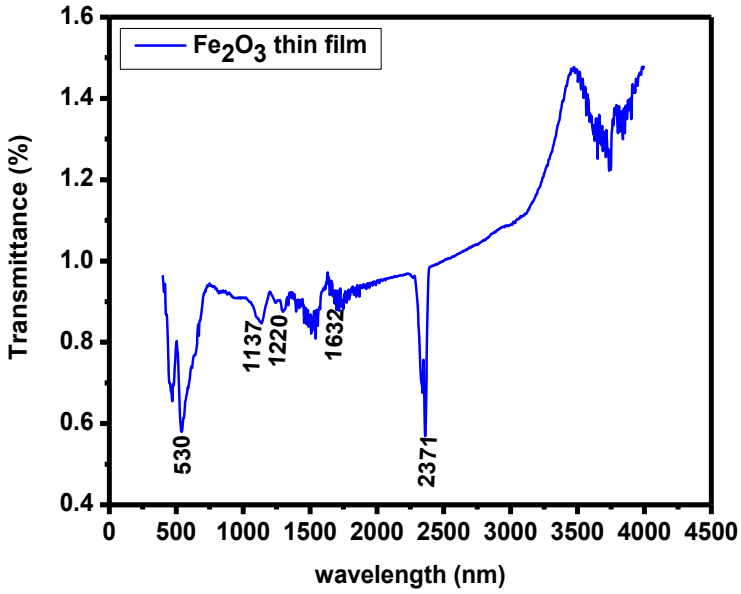

Fig. 2.2: FTIR spectra of Fe_2O_3 thin film

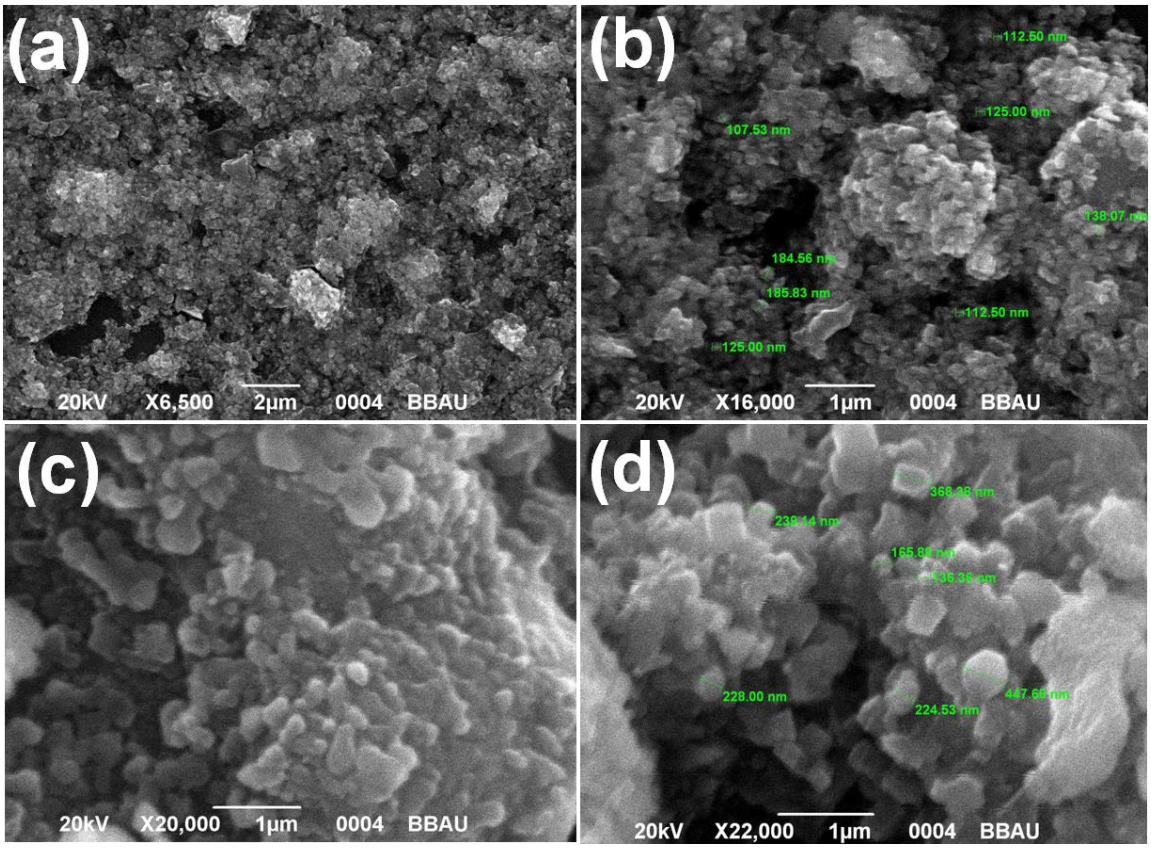

Fig. 2.3: SEM image of (a) and (b) α-Fe_2O_3; (c) and (d) α-Fe_2O_3/PANI film

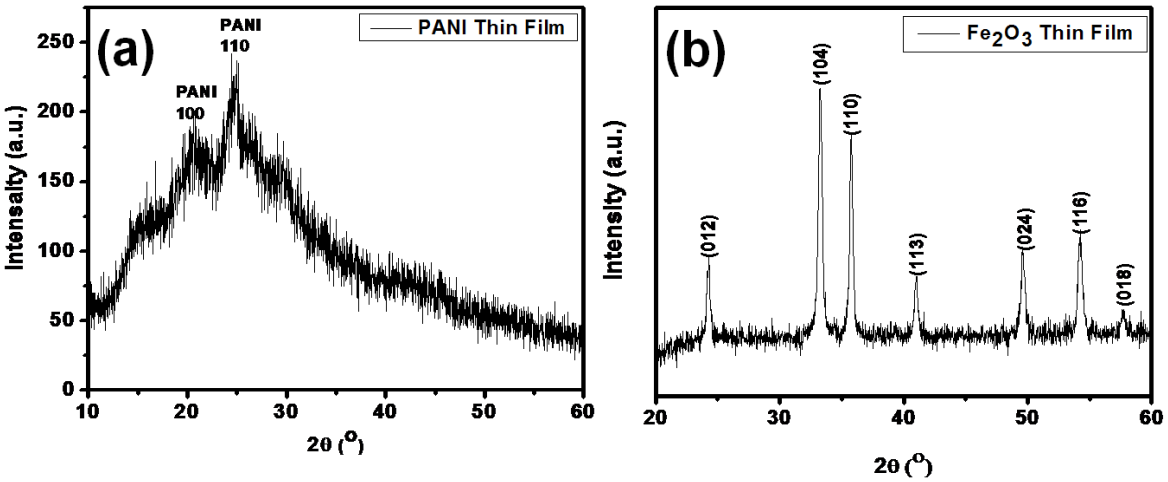

Fig.2.4: XRD Pattern of (a) PANI and (b) Ferric Oxide thin film

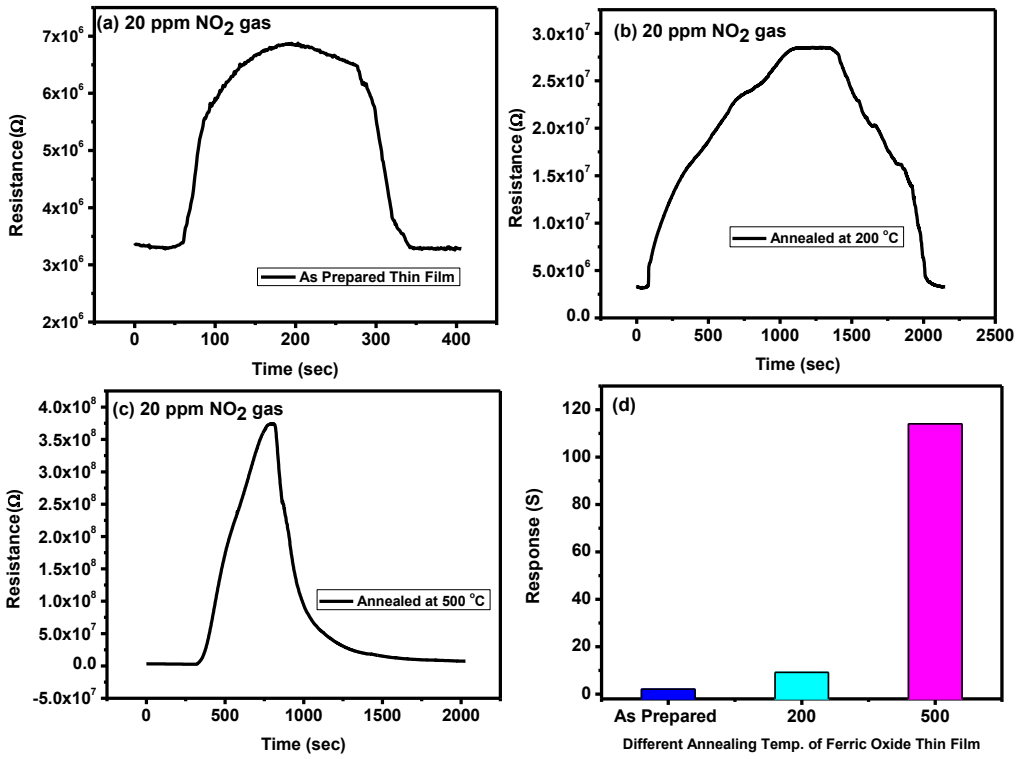

Fig. 2.5: Dynamic response curve Ferric Oxide film (a) as prepared (b) annealed at 200 ^{o}C (c) annealed at 500 ^{o}C and (d) Sensor Response of various sensing elements

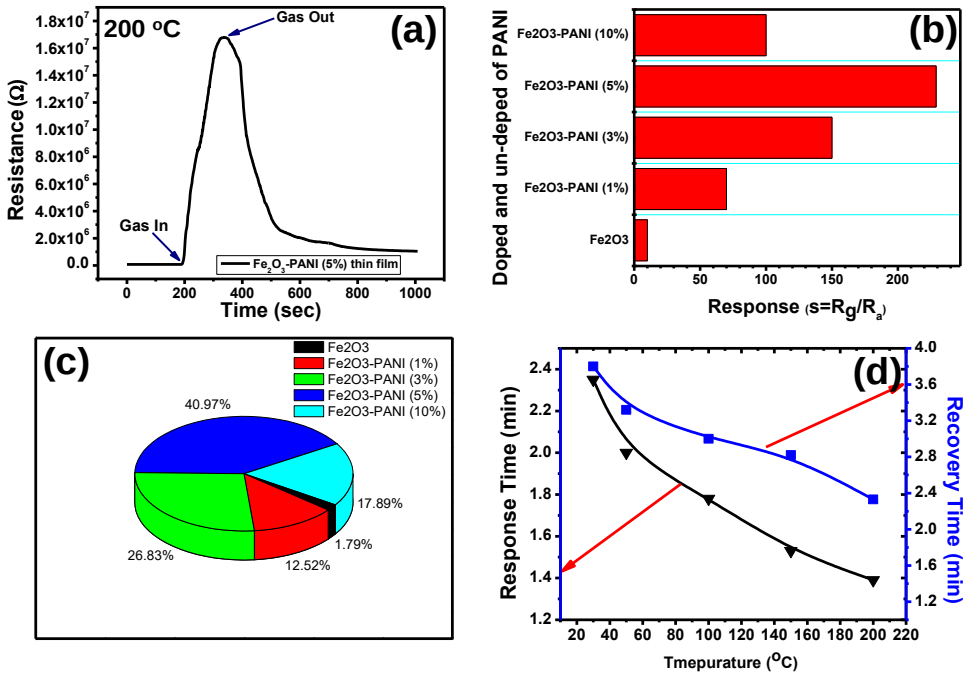

Fig. 2.6: Sensing response curve α-Fe_2O_3/PANI Thin Film (a) Dynamic response curve (b) Different wt.% doping of PANI in α-Fe_2O_3 (c) Pi-chart of sensor and (d) Response and Recovery Time sensor

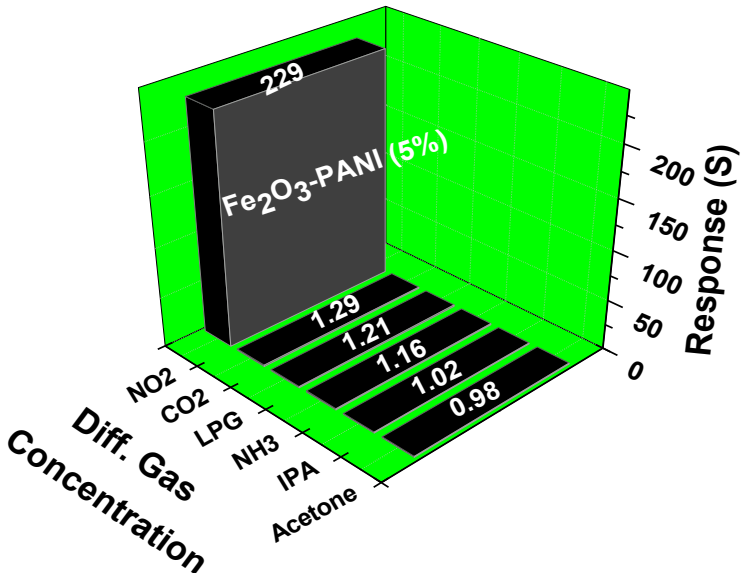

Fig. 2.7: Sensor Response of ferric oxide thin film deposited by spin coating technique towards various target gases for different concentrations at room temperature

Chapter 3

Fabrication of NO_2 gas sensor using nanostructured Zinc oxide

In the present chapter zinc oxide has been prepared by using two different methods and their characterizations were carried out using SEM, AFM, XRD, UV-vis and FTIR. Sensing performances of each samples were investigated and found that hexagonal ZnO nanocrystals were more sensitive than ZnO nanopetal structure.

3.1 Introduction

ZnO is one of the n-type semiconducting oxide materials utilized widely in the fields of transparent conducting electrodes, varistors, sensors and optoelectronic devices [1-2]. Especially, this oxide material has been extensively studied for its potential use in semiconductor type gas and UV sensors, since it has considerable sensitivity to CO or NO_x gases [3-5]. Oxidizing gas molecules adsorbed on the surfaces of oxide materials and creates electron-depleted layers, which increase the sensor resistance. There are two different types of contact between the particles of sensing materials [6]: the two-dimensional (2-D) contact between necked particles and point-to-point contact between ordinary particles. When the particles are necked together significantly and the sizes of the necked part become comparable to the thickness of the resistive electron depleted layer, the conductive channel through the neck determines the total resistivity (neck model). When the particle sizes are significantly larger than the thickness of the electron depleted layer, the conductive channel through the neck becomes too wide for the channel to control the electrical resistivity of the particles chain. In this condition, the point-to-point contacts between the grain boundaries dominate the total resistivity, giving rise to gas sensitivity independent of the particle size. Metal-oxide semiconductors such as SnO_2, TiO_2 and ZnO have high sensitivity, good chemical stability and are easy to synthesize; therefore, these semiconductors have been extensively studied to determine their suitability for use as NO_2 gas sensors [7-8].

In the present chapter, we have investigated the synthesis and characterization of ZnO in order to develop a highly responsive sensor which is robust, compact, having long life and operable at low temperature with sufficient sensitivity for the detection of nitrogen dioxide in low concentrations.

3.2 Experimental

3.2.1 Synthesis of ZnO hexagonal nanocrystals

0.01 M of zinc acetate dihydrate was dissolved in 75 ml of boiling ethanol (75 ºC) in a round bottom flask fitted with a condenser at atmospheric pressure. The solution is refluxed at 75 ºC for about 30 minutes and subsequently allowed to cool at room

temperature to give a transparent and stable Zn based precursor. In another beaker, 0.014 M of lithium hydroxide monohydrate was ultrasonically dissolved in 50 ml of ethanol to accelerate the reaction at room temperature. A clear solution was obtained after sonication for 30 min. The hydroxide containing solution was added drop by drop to the acetate containing solution at room temperature under vigorous magnetic stirring, and finally a transparent ZnO sol was obtained after hydrolyzing the precursor. Fig. 3.1(a) shows the flow chart of the growth of ZnO nanocrystals and deposition of ZnO thin-film.

3.2.2 Synthesis of ZnO nanopetals

2.62 g zinc nitrate hexahydrate was dissolved into 100 ml of distilled water. In order to make the gel of the zinc oxide 100 ml of diluted ammonia solution (3% concentration, labelled as A) was added to zinc nitrate precursor under continuous stirring. This gel was used for the fabrication of thin film. Later for increasing the pH value, concentrated ammonia solution (25% concentration, labelled as B) was added to it that results in the precipitation of the material. The obtained precipitate was separated by centrifugation at 5000 rpm for 10 min and then dispersed in 50 ml of 1,4-butanediol. The solution with the dispersed $Zn(OH)_2$ was heated at 150 °C for 36 h in a closed glass bottle.

3.2.3 Experimental Techniques

The morphology and size distribution of as-prepared ZnO nanostructures were observed by scanning electron microscope (SEM, TESCAM MiraIII). The crystallinity and structure were investigated by X-ray diffractometer (X-Pert PRO PANalytical). Optical characterization was carried out by the UV-vis Spectrophotometer. For studying the gas sensing properties, the home-made gas dilution system was utilized [9].

3.2.4 Sensing Test Chamber

The total amount of gas flow rate of the diluted NO_2 gas by dry air is 5000 ml/min and the volume of chamber is 5000 ml. The ZnO nanopetal (NP) array sensor was inserted between the two electrodes and the diluted NO_2 gas was injected into the test chamber. Variations in the electrical resistance of the sensor were measured with a

Keithley (6517B) electrometer interfaced with a personal computer. The sensing response of prepared sensor structure towards oxidizing NO_2 gas is given as under [10]:

$$S = \frac{R_g - R_a}{R_a} \quad (1)$$

where R_a and R_g are the values of resistance of the sensor in the presence of atmospheric air and target gas, respectively. The response time was measured as the time taken by the sensor to acquire the 90% of its maximum resistance value in the presence of oxidizing gas [11]. Once the maximum resistance value is attained, the target gas was flushed out from the test chamber and sensor was allowed to regain its initial resistance value in atmospheric air keeping it at the same temperature. Time taken by the sensor to reacquire about 10% higher value of its initial resistance in the presence of atmospheric air is considered as the recovery time [12].

3.2.5 Humidity sensing mechanism

Humidity sensing theory depends upon changing in the electrical resistance of sensing materials kept in a humid environment. The depiction of the water adsorption process on the ZnO surface is illustrated in Fig. 3.1(b). The hydroxyl groups, generated by the self ionization of water molecules adsorbed on the activated surface of crystalline grain covers the surface area of ZnO through the chemisorption of water in moist surroundings. The process of chemisorption occurs at very low humidity level and remains unaltered by further changes in humidity. Nevertheless, because of hydrogen bonding the water molecules are physisorbed onto this hydroxyl layer with increase in humidity level. This is because of the increase in the number of physisorbed layers at higher levels which prompts the bonding of water molecules to hydroxyl group. Porous structure of ZnO film and specific surface area of nanosized grains play the key roles in the interaction and physisorption of water vapors. Humidity gets adsorbed throughout the open porosities leading to condensation within the capillary pores that are distributed between the grains [13]. A larger surface area for the sensing material ensures higher absorption of water molecules leading to a greater density of charge carriers, usually protons.

3.3 Results and Discussion

3.3.1 Hexagonal nanocrystals based NO_2 gas sensor

XRD analysis carried out in order to investigate crystal structure of the synthesized ZnO. X-Ray diffraction shows an extent of crystallization of the material. The average crystallite size (*D*) of the sensing material was calculated by the Debye-Scherrer's formula [14], given by

$$D = \frac{K\lambda}{\beta \cos\theta} \quad (2)$$

where K= 0.94 is Scherrer's coefficient, which depends on the shape of the crystallite and the type of defects present, λ is the wavelength of X-ray radiation, β is the full width at half maximum (FWHM) of the diffraction peak and θ is the angle of diffraction. The XRD pattern of ZnO thin film is shown in Fig. 3.2(a). In this pattern, the two peaks were found at angle 34.5º and 63º corresponding to plane (002) and (103) with lattice parameters a = 3.236 Å and c = 5.203 Å with highest intensity at (002) plane. As a result, the ZnO nanoparticles grow more rapidly along facets, and the (002) direction is along the c-axis of the nanoparticles while (103) direction is the short axis [15]. The strong peak (002) implies highly oriented ZnO nanoparticles along c-axis [16-17] and the structure of ZnO is hexagonal wurtzite, which is consistent with the SEM observation. The average crystallite size of ZnO was calculated using Scherer's formula as ~ 71 nm.

Fig. 3.2(b) shows the AFM image of ZnO thin film deposited by spin coating method. The surface morphology of the thin film was examined over an area 500 × 500 nm^2 in non-contact mode. The surface morphology of the film was found to be uniform having homogeneously distributed grains with high surface roughness. The average grain size of ZnO film was found ~ 70 nm.

The scanning electron micrograph of ZnO thin film annealed at 450 ºC for 2 h at 19 kx magnification is shown in Fig. 3.3. This micrograph exhibits the surface morphology of the ZnO NC film, in which hexagonal particles are uniformly and beautifully distributed. Film is quite porous with varying pore size from 80 nm to 100 nm. These pores are responsible for the adsorption of the target gases. The inset Fig. 3.3

reveals the magnified image of single regular hexagonal ZnO nanoparticle with average edge of about 100 nm and thickness about 90 nm. The edges and corners of the hexagonal small nanoparticles may be seen more clearly. The growth of the small nanoparticles with a definite face is to minimize their interface energy. It is well known that the synthesis of NCs includes two main steps; nucleation and growth. At the nucleation stage, the intrinsic crystal properties dominated the shape of the initial precursor. Subsequently, in the next step, the precursors are absorbed in each plane and the ZnO grows with different rates along different planes. In the present case the favorable plane for the growth is (002). Average particle size was found as 120 nm with the average length of one side of hexagonal structure as 100 nm. The specific surface area (SSA) was determined using equation [18-19]:

$$A = \frac{6}{d \times D_m} \tag{3}$$

where d is the bulk density of ZnO pellet and D_m is the average crystallite size. The number 6 is the shape factor. The calculated value of SSA of the synthesized material was 272.6 m^2/g. This high value of active surface area is another significant feature for gas sensing.

FTIR spectrum of ZnO-NPs (Fig. 3.4) exhibits the peak at 475 cm^{-1} which is due to the stretching mode of ZnO-NPs and addition peak at 1572 cm^{-1} is due to leading vibration of C–H in the methyl and 2356 cm^{-1} attributed to the leading vibration molecule [20].

Fig. 3.5(a) shows that resistance decreases sharply up to 20 %RH and then linearly up to 50 %RH and further slow decrement was observed. The sensitivity of a humidity sensor can be defined as the change in resistance (*R*) of sensing element per unit change in relative humidity (%RH) i.e.,

$$S = \frac{\Delta R}{\Delta\ \%RH}\ \mathrm{M\Omega/\%RH} \tag{4}$$

The average sensitivity is calculated by taking the average of all sensitivities ranging from 10 to 90 %RH. Average sensitivity of the thin film at room temperature was

found 3.82 MΩ/%RH. Hysteresis curve for the sensing thin film annealed at 450 ºC is shown in Fig. 3.5(b) and its value was calculated as 48% for ZnO thin film.

Fig. 3.6 shows the dynamic response of pure ZnO thin film sensor at room temperature towards 20 ppm NO_2 gas. As it is evident from Fig. 3.6(a) that the exposure of NO_2 gas to the sensing film surface, results in the increase of resistance from 14.695 kΩ to 1323.178 kΩ (S = 90). The response time and recovery times of the sensor were observed to be 2.45 min and 1.76 min, respectively at room temperature (RT). The enhanced response (S = 90), and least response and recovery times are promising parameters for devising a sensor.

Fig. 3.6(b) shows the variation in the sensing response of pure ZnO thin film sensor as a function of operating temperature towards 20 ppm of NO_2 gas. It was observed that the sensing response of pure ZnO thin film decreased with the increase in temperature. The decrease in sensing response at high temperature could be due to higher rate of adsorption and desorption of gas molecule at the sensing surface. The pure ZnO thin film shows the maximum sensing response as 1.50×10^2 at room temperature. When the NO_2 gas interacts with the sensing surface of ZnO, it traps free electrons from the surface and decreases the conductivity of the sensor. Therefore, the resistance R_g for the sensor increases on exposure to NO_2 gas.

The response time is defined as the time required by sensor to attain 90% of the stabilized value of resistance after the sensing gas comes into contact with the sensing surface and recovery time as the time required by sensor to regain 10% higher value than its original resistance, after removal of the sensing gas. The variation of response and recovery time of ZnO thin film as a function of temperature towards 20 ppm of NO_2 gas is represented in Fig. 3.6(c). It is observed that the response time and recovery time vary inversely with respect to the increase in temperature. The response time decreases from 2.45 min to 1.91 min while the recovery time increases from 1.76 min to 2.38 min with increasing of temperature in the range 30 to 200 ºC towards 20 ppm of NO_2 gas. The decrease in response time is due to the large availability of vacant sites on the thin film for adsorption of the gas as evident from SEM/AFM images. Also the increase in

recovery time may be due to the gases left behind after gas interaction, resulting in decrease in desorption rate.

The selectivity is one of the most important gas sensing properties for the gas sensors. The cross sensing response between NO_2 and reducing gases such as NH_3, CO_2 and LPG were also investigated. Fig. 3.6(d) shows the selectivity of NO_2 gas to NH_3, CO_2 and LPG in the different gas concentration for ZnO sensor. The maximum sensor responses at room temperature (30 ºC) towards NH_3, CO_2 and LPG are 3.2, 2.7 and 1.5, respectively. It is indicated that the ZnO based sensor not only has high response to NO_2 but also exhibits high selectivity to reducing gas such as NH_3, CO_2 and LPG.

The sensing mechanism is based on the fact that the oxygen species were adsorbed on the surface of NCs in the air and then ionized into O_{ads}^{-} or O_{ads}^{2-} by capturing the free electrons from the conduction band; there by causing decreases in conductivity. After exposure of NO_2 to the zinc oxide sensing thin film, the NO_2 is adsorbed on the surface of sensing film and acts as an electron acceptor in the reaction, resulting in an increase in the resistance of the sensor [21].

3.3.2 Nanopetal based NO_2 gas sensor

The annealed thin film was found to be smooth, transparent and strongly adherent to the substrate. Fig. 3.7 (a, b) shows the top view of the SEM image of the ZnO thin film after annealing at 500 ºC for 4 h in air at two different magnifications. The SEM image clearly shows that the ZnO NPs were horizontal and well-aligned over the surface of the film substrate with a high density ~$1.3\times10^{10}/cm^2$. Film is porous and petals are distributed with varied agglomerations. The average thickness of each petal is 70 nm and its diameter is 400 nm. The average pore size was found 119 nm. The sensing performance of such porous film can also be controlled within a certain limit by measuring the pore sizes and inclusion of NO_2 within the pores. X-ray diffraction pattern of ZnO thin film annealed at 500 ºC for 4 h in air shown by Fig. 3.7(c) reveals the well-defined diffraction peaks corresponding to (100), (002), (101) (102) and (110) planes of ZnO observed at 31.70º, 34.34º, 36.27º, 47.63º and 56.56º, respectively and are in good agreement to the corresponding values reported for hexagonal wurtzite structure of ZnO.

The lattice constants calculated from the XRD data for (101) phase (strong reflection) are a = 3.265 Å and c = 5.214 Å, respectively. The average crystallite size was calculated as 29.70 nm.

The optical transmission spectra of the ZnO thin film deposited separately on corning glass substrate was measured in the wavelength range 190 to 1100 nm, and is shown in Fig. 3.7(d). ZnO thin film exhibits a high transmission (>80%) in the visible region and shows a sharp fundamental absorption edge in UV region at 360 nm. Band gap of the ZnO thin film deposited on corning glass substrate was calculated from the intercept on energy axis obtained by extrapolating the linear portion of the Tauc plot [$(\alpha hv)^2$ *vs* photon energy (*hv)*] as shown in inset of Fig. 3.7(d). Estimated value of band gap for as-grown ZnO thin film is found to be 3.5 eV which is close to the reported value [21].

For the sensing measurements, NO_2 gas was injected in a controlled gas chamber by different volumes for various times and variations in resistance were recorded by Keithley Electrometer. Corresponding data were plotted in Fig. 3.8(a) which shows the response of the gas sensor modulated by the repeated injection and cutting off the NO_2 gas with a concentration of 20 ppm. The maximum response was ~ 169 which is the highest as per open literature survey. During the three repeated injections of gas, its maximum response did not change and is shown by Fig. 3.8(b). The gas sensor showed excellent response and recovery characteristics, i.e. 1.42 and 1.71 min, for 90% of its full response and recovery, respectively.

The sensing mechanism is based on the fact that the oxygen species were adsorbed on the surface of NPs in the air, and then were ionized into O_{ads}^{-} or O_{ads}^{2-} by capturing the free electron from the particles; thus decreased the conductivity and increased the resistance. After exposure of NO_2 on the zinc oxide sensing thin film, then NO_2 is adsorbed by the sensing film and NO_2 acts as an electron acceptor in the reaction, resulting an increase in the resistance of sensor [22]. The chemical reactions that occur on the sensing surface are given as:

$$O_2 + e^- \leftrightarrow O_{ads}^{-} \quad (5)$$

$$NO_{2(gas)} + e^- \rightarrow NO^-_{2(ads)} \quad (6)$$

The above reactions result in the decrease of concentration of electron on the surface of ZnO which results in an increase in resistance of the material. In addition, following reaction is happened between $NO^-_{2(ads)}$ and O^-_{ads}:

$$NO^-_{2(ads)} + O^-_{ads} \rightarrow 2O^{2-}_{ads} + NO_2 \quad (7)$$

Thus the cycling reaction continued:

$$NO_{2(g)} + e^- \rightarrow NO^-_{2(ads)} \quad (8)$$

The desorption of NO^-_2 (ads) is limiting at the decomposition of the NO_2 at the zinc oxide, which is determined by the fast recovery time after the exposure to the sensor.

3.4 Conclusion

Comparative studies of ZnO Hexagonal and Nanopetals have been presented in Table 3.1.

Sensing Parameters	**ZnO hexagonal nanocrystals**	**ZnO Nanopetals**
Crystallite Size (nm)	71	29
Specific surface area (m^2/gm)	272	766
Sensing Response	90	169
Response Time (min)	2.45	1.42
Recovery Time (min)	1.76	1.71

From table we conclude that ZnO nanopetals based sensor has high sensing response 169, with lowest response time 1.42 min and fast recovery time 1.71 min whereas the sensor based on ZnO hexagonal nanocrystals show lower sensing response with enhanced response and recovery times due to bigger crystallite size (71 nm) and lower specific surface area (272 m^2/gm). Thus ZnO nanopetals based sensor may be commercialized for the detection of low level of NO_2 gas for both indoor and outdoor systems.

References:

[1] Y.K. Mishra, S. Kaps, A. Schuchardt, I. Paulowicz, Xin. Jin Xin et al., Fabrication of Macroscopically Flexible and Highly Porous 3D Semiconductor Networks from Interpenetrating Nanostructures by a Simple Flame Transport Approach, Part. Part. Syst. Charact., 30 (2013) 775-783.

[2] A. Singh, S. Singh, P. Tandon, B.C. Yadav, R.R. Yadav, Synthesis, characterization and performance of zinc ferrite nanorods for room temperature sensing applications; J. Alloy. Comp. 618 (2015) 475-483.

[3] C.M. Ghimbeu, J. Schoonman, M. Lumbreras, M. Siadat, Electrostatic spray deposited zinc oxide films for gas sensor applications, Appl. Surf. Sci. 253 (2007) 7483-7489.

[4] H.J. Lim, D.Y. Lee, Y.J. Oh, Gas sensing properties of ZnO thin films prepared by microcontact printing, Sens. Actuators A: Phys. 125 (2006) 405-410.

[5] D. Gedamu, I. Paulowicz, S. Kaps, O. Lupan, S. Wille, et al., Rapid Fabrication Technique for Interpenetrated ZnO Nanotetrapod Networks for Fast UV Sensors, Adv. Mater. 26 (2014) 1541-1550.

[6] N. Yamazoe, N. Miura, Yamauchi (Ed.) S. Chemical Sensor Technology, vol. 4, Elsevier, Amsterdam 4 (1992) 27-30.

[7] A.Z. Sadek, S. Choopun, W. Wlodarski, S.J. Ippolito, K. Kalantar-zadeh, Characterization of ZnO nanobelt-based gas sensor for H_2, NO_2, and hydrocarbon sensing, IEEE Sens. J. 7 (2007) 919-924.

[8] V. Saxena, D.K. Aswal, M. Kaur, S.P. Koiry, S.K. Gupta, J.V. Yakhmi, R.J. Kshirsagar, S.K. Deshpande, Enhanced NO_2 selectivity of hybrid poly(3-hexylthiophene): ZnO-nanowire thin films, Appl. Phys. Lett. 90 (2007) 043516-19.

[9] R. Srivastava, B.C. Yadav, Nanostructured $ZnFe_2O_4$ thick film as room temperature liquefied petroleum gas sensor, J. Exp. Nanosci., 02/2014; http://dx.doi.org/10.1080/17458080.2013.880001

[10] R.K. Sonker, A. Sharma, M. Tomar, V. Gupta, B.C. Yadav, Low Temperature Operated NO_2 Gas Sensor Based on SnO_2-ZnO Nanocomposite Thin Film, Adv. Sci. Lett. 20 (2014) 911-916.

[11] R.K. Sonker, A. Sharma, Md. Shahabuddin, M. Tomar, V. Gupta, Low temperature sensing of NO_2 gas using SnO_2-ZnO nanocomposite sensor, Adv. Mat. Lett. 4 (2013) 196-201.

[12] R.K. Sonker, B.C. Yadav, Chemical Route Deposited SnO_2, SnO_2-Pt and SnO_2-Pd Thin Films for LPG Detection, Adv. Sci. Lett. 20 (2014) 1023-1027.

[13] M. Singh, B.C. Yadav, Physics and Technology of Humidity Sensing Through a Solid State Pellet of Cerium Oxide, Sensors & Transducers, 186 (2015) 140-147.

[14] S. Gupta, B.C. Yadav, P.K. Dwivedi, B. Das, Microstructural, optical and electrical investigations of Sb-SnO_2 thin films deposited by spray pyrolysis, Materials Research Bulletin. 48 (2013) 3315-3322.

[15] C.O. Chey, O. Nur, M. Willander, Low temperature aqueous chemical growth, structural, and optical properties of Mn-doped ZnO nanowires, Journal of Crystal Growth. 375 (2013) 125-130.

[16] S. Ozturk, N. Kılınc, N. Tasaltin, Z.Z. Ozturk, A comparative study on the NO_2 gas sensing properties of ZnO thin films, nanowires and nanorods, Thin Solid Films, 520 (2011) 932-938.

[17] D.F. Wang, S.Y. Park, Y.P. Lee, Magnetic Properties of Mn-Doped ZnO Nanorods, *J*. Korean Physical Society, 53 (2008) 2257-2260.

[18] N. Rezlescu, E. Rezlescu, F. Tudorache, P.D. Popa, Gas Sensing Properties of Porous Cu-Cd and Zn-Ferrites, Roman Rep. Phys. 61 (2009) 223-234.

[19] S. Singh, B.C. Yadav, V.D. Gupta, P.K. Dwivedi, Investigation on effects of surface morphologies on response of LPG sensor based on nanostructured copper ferrite system, Materials Research Bulletin, 47 (2012) 3538-3547.

[20] R.F. Silva, M.E.D. Zaniquelli, Morphology of nanometric size particulate aluminium-doped zinc oxide films, Colliod Surf Physicochem Eng-Aspect, 198 (2002) 551-558.

[21] S. Ilican, Y. Caglar, M. Caglar, Preparation and characterization of ZnO thin films deposited by sol-gel spin coating method, J. of Opto. & Advanced Materials 10 (2008) 2578-2583.

[22] R. Ferro, J.A. Rodríguez, P. Bertrand, Peculiarities of nitrogen dioxide detection with sprayed undoped and indium-doped zinc oxide thin films, Thin Solid Films 516 (2008) 2225-2230.

Figures:

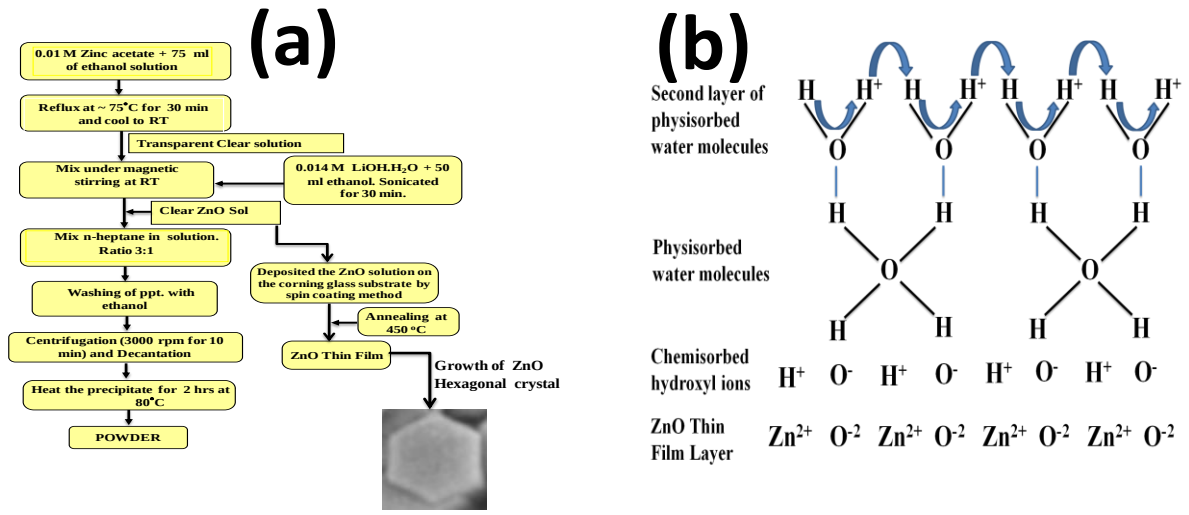

Fig. 3.1: (a) Flow chart of the growth of ZnO nanocrystals and deposition of ZnO thin film and **(b)** Grotthuss chain reaction

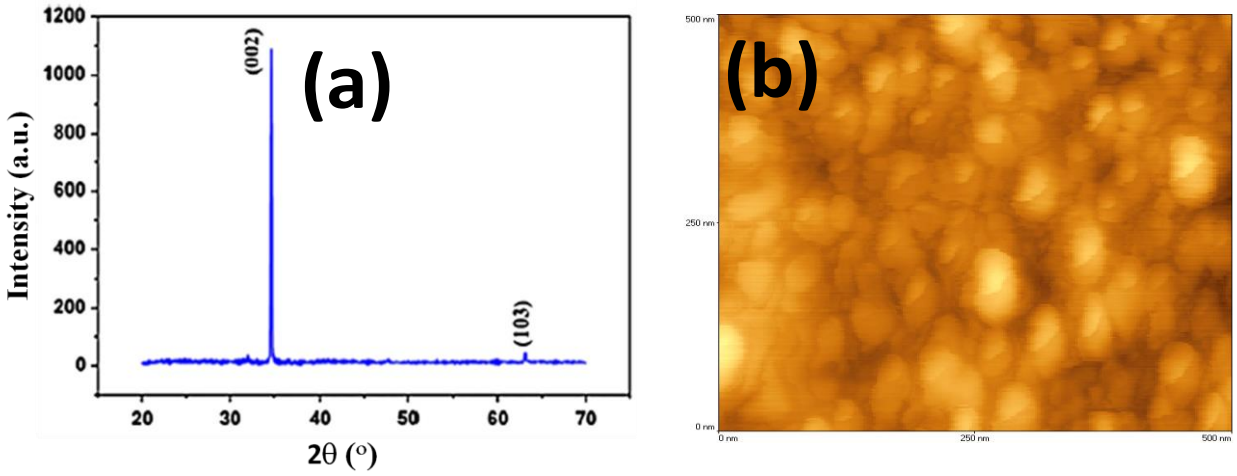

Fig. 3.2: (a) The XRD pattern of ZnO thin film and **(b)** AFM image of ZnO thin film

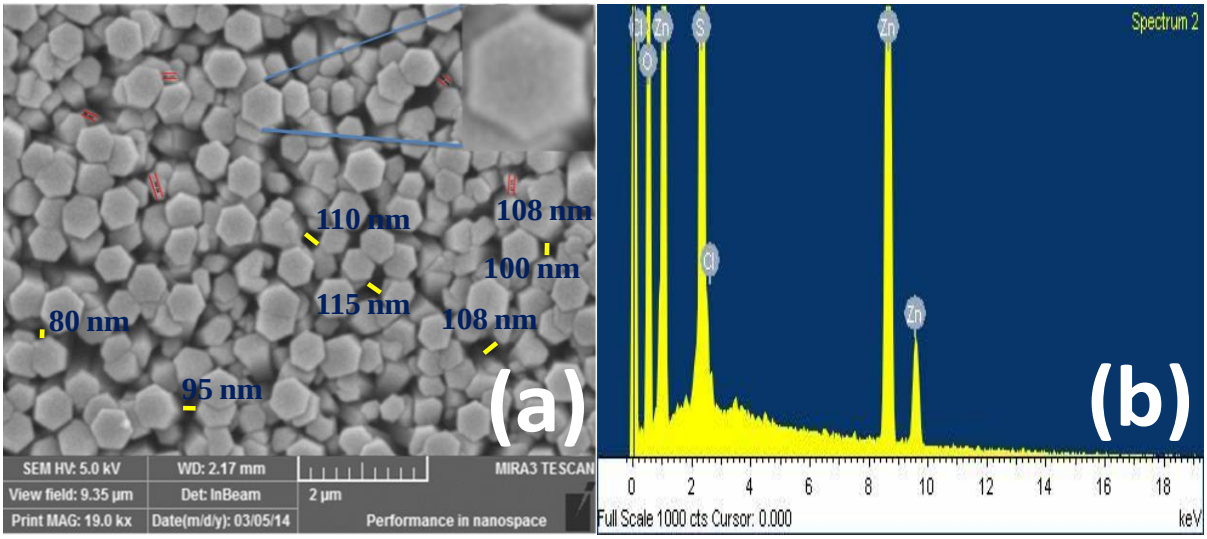

Fig. 3.3: (a) SEM image of ZnO thin film and **(b)** EDX of ZnO film

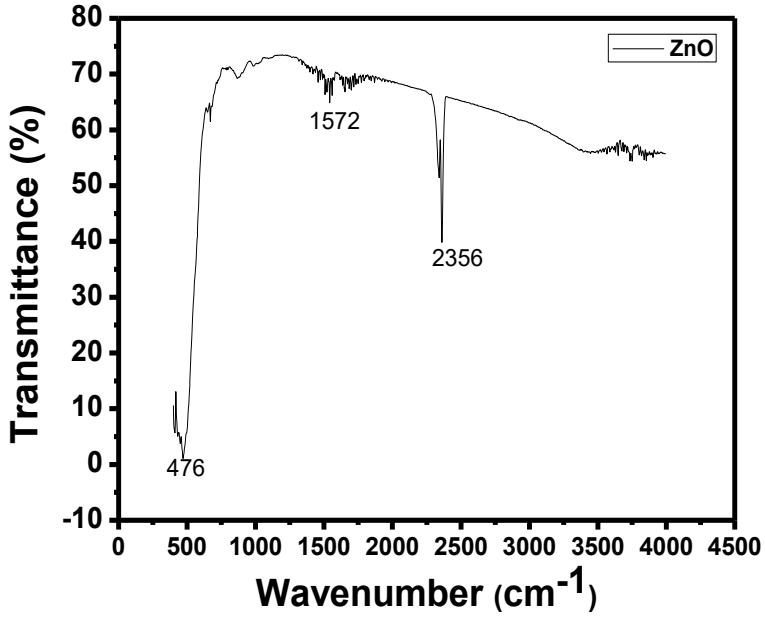

Fig. 3.4: FTIR spectra obtained of ZnO-NPs

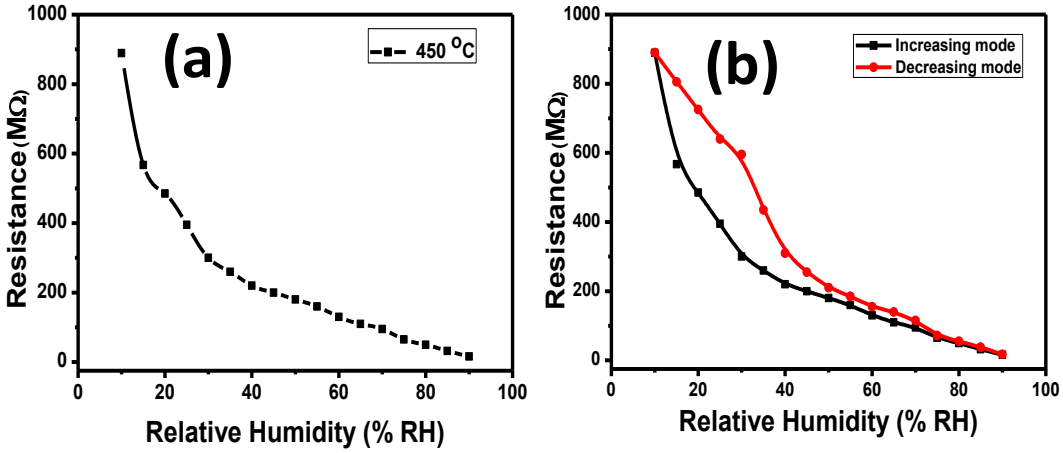

Fig. 3.5: (a) Variation in resistance of film with relative humidity and **(b)** Hysteresis curve of ZnO thin film annealed at 450 ºC

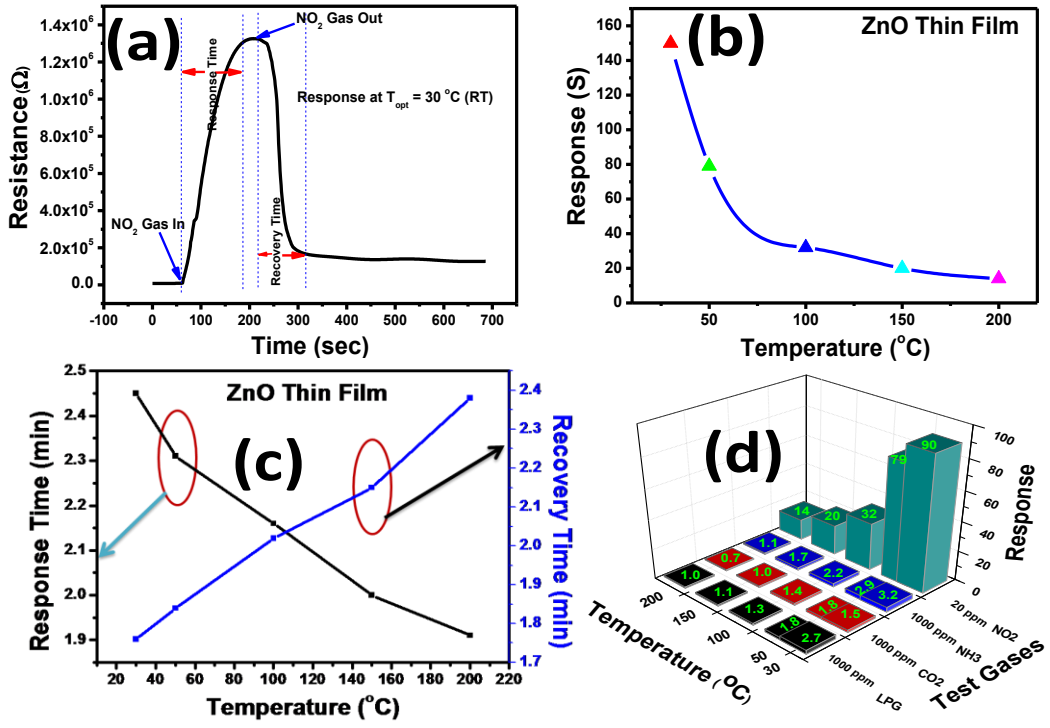

Fig. 3.6: (a) Dynamic Response ZnO thin film, **(b)** Variation of sensing response of pure ZnO thin film as a function of temperature towards 20 ppm of NO_2 gas, **(c)** Response and Recovery time of ZnO thin film as a function of temperature towards 20 ppm of NO_2 gas and **(d)** Cross selectivity of ZnO sensor at different temperature

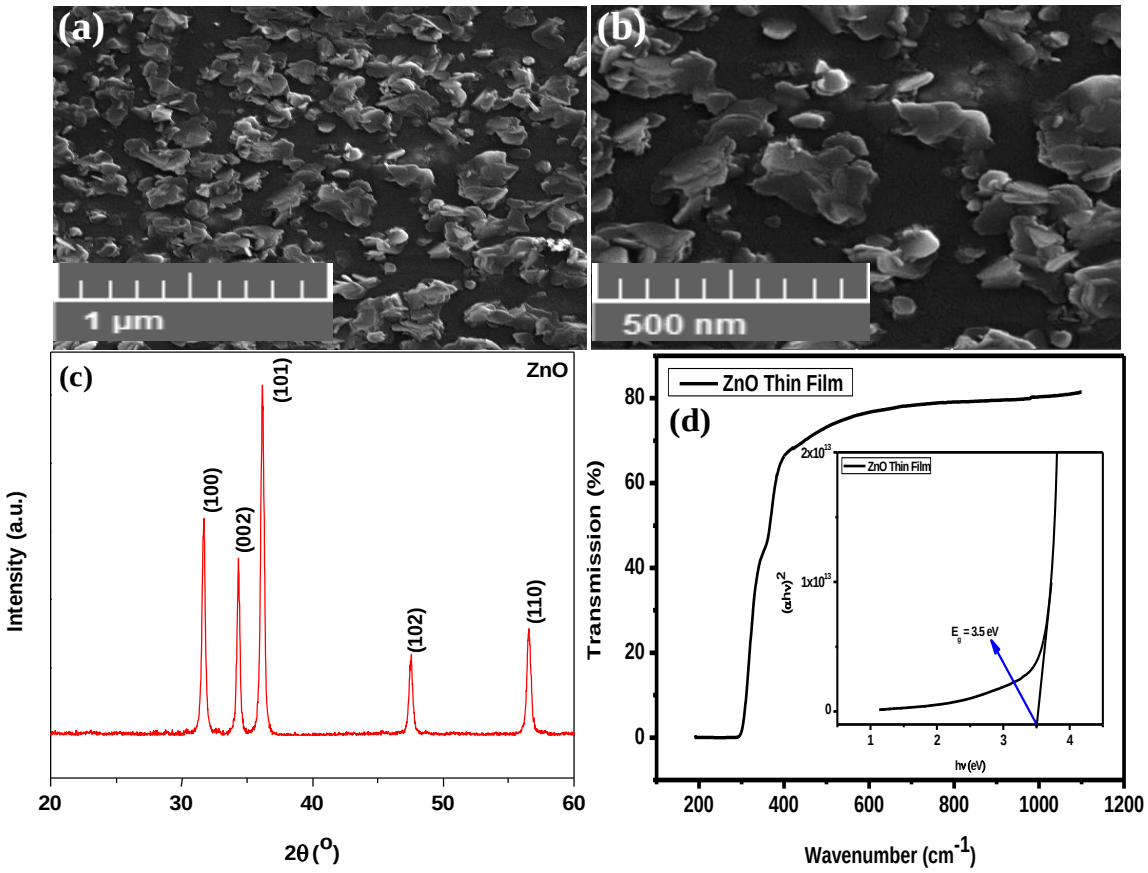

Fig. 3.7: (a, b) SEM images of ZnO nanopetal at two different magnifications, **(c)** X-Ray diffraction of the ZnO thin film, **(d)** Optical transmittance spectra of ZnO thin film (inset shows the Tauc plot.)

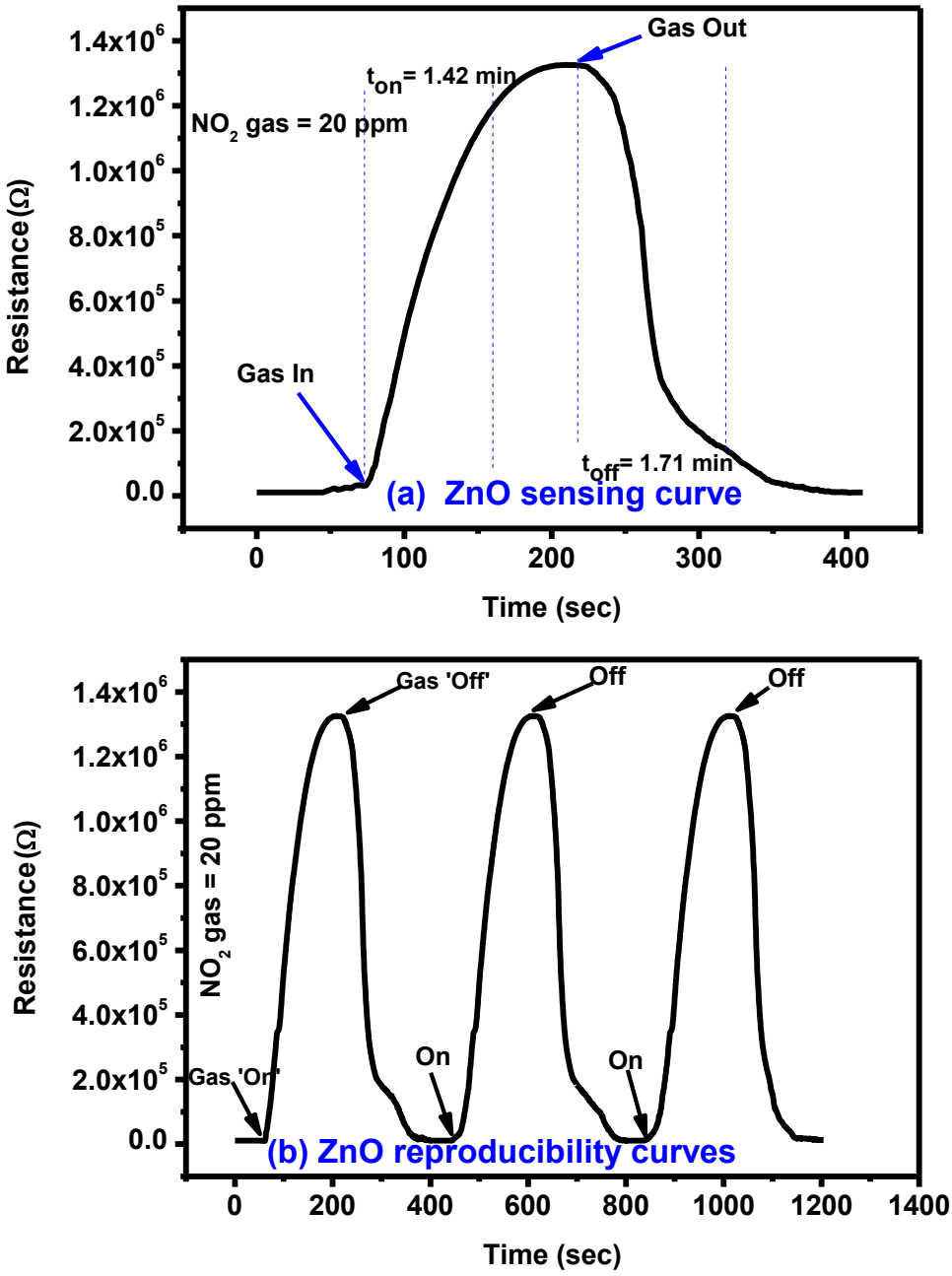

Fig. 3.8: (a) The dynamic response curve for the gas sensor with 20 ppm concentration, **(b)** ZnO reproducibility curves

Chapter 4

Experimental Investigations on NO_2 sensing of Pure ZnO and PANI-ZnO composite thin films

In the present work, the comparative investigations on NO_2 gas sensing properties of the hybrid nanocomposite thin films of Polyaniline (PANI), ZnO and PANI-ZnO towards NO_2 gas at room temperature have been reported. Effect of concentrations of PANI in the composite thin films on the NO_2 gas sensing has been investigated. Structural and surface morphological characterizations have been carried out by using X-ray diffraction (XRD) and scanning electron microscope (SEM) respectively. The presence of 5% PANI in composite film was found to give maximum sensing response of ~ 6.11×10^2 towards 20 ppm NO_2 gas having fast response and recovery time of about 2.16 min and 3.5 min respectively.

4.1 Introduction

The emission of Nitrogen dioxide (NO_2) creates bad effect on public health and the environment as well. Therefore the detection of NO_2 is quite necessary even at very low concentration. The use of conducting polymers as sensing elements in chemical sensors is a center of attraction due to their high sensitivity with the change of the electrical and optical properties when exposed to different types of gases or liquids [1]. Polyaniline (PANI) is one of the most prominent materials among the variety of conducting polymers due to its unique electrical property, environmental stability, easy fabrication process and intrinsic redox reaction [1-4]. PANI has also been used in different applications such as gas sensor [5], rechargeable batteries [6] and photovoltaic cells [7]. However, the problems with these conducting polymers regarding the yield is their mechanical strength [8]. The fabrication of hybrid composite of conducting polymers with metal oxides seems to be attractive to resolve these issues and concerns. However, no much efforts have been made towards development of a hybrid composite of PANI and ZnO especially for detection of NO_2 gas at room temperature [9]. Alternatively, the metal oxides are useful in this regard but demands low operating temperatures [10-12]. Among the inorganic materials, nanocrystalline ZnO is one of the most attractive and extensively used materials for detection of the LPG, NH_3, NO_2 and UV [13-16]. In the present work, nanoparticles of PANI and ZnO were synthesized and their hybrid composites were prepared for the detection of NO_2 gas. Also the variations of concentration of PANI in ZnO composite thin film with exposure of different concentration of NO_2 gas have been investigated.

4.2 Experimental

4.2.1 Fabrication of ZnO-PANI nanocomposite thin film sensor

PANI was prepared by polymerization of aniline. For this process HCl was used which acts as dopant for PANI molecules and bound with the central N atom of aniline molecule like [17]. Nanostructured ZnO was prepared using chemical route as prescribed in earlier work as chapter 3 also published as [18]. The prepared PANI was added to ZnO nanoparticles (NPs) sol. in different concentrations (0%, 1%, 5% and 10%). The PANI

incorporated ZnO nanoparticles suspension was sintered at 100 ºC in air for 2 h for producing powder form. Thin films of pure PANI, ZnO NPs and ZnO-PANI composites were prepared on corning glass substrates by spin coating technique at 2200 rpm for 30 s and dried on hot plate at 100 ºC for 10 min [19-22]. The thickness of the pure PANI film, pure ZnO film and PANI-ZnO film were measured by using Dektak profile meter (Veeco Dektak 150 surface profiler) and was found to be 210 nm, 290 nm and 320 nm respectively. For the gas sensing application, films were deposited on inter digital electrode (IDEs) patterned corning glass substrates by spin coating of the respective solutions.

4.2.2 Gas sensing properties measurements

NO_2 gas sensor was designed and fabricated which is based on the variations of electrical resistance with exposure of gas. Pt sputtered inter digital electrode was fabricated on a 1×1cm^2 corning glass substrate to form a transducer, which were used directly to measure the change in resistance of the sensitive PANI-ZnO composite thin film layer with exposure of NO_2 gas of various concentrations. The device was placed inside a steel box having volume 11 L, then allow to a certain amount of NO_2 gas to inject into the test chamber, the resistance was reached to a steady value in open air as shown in Fig.4.1 (a). A Keithley 2700 digital multi-meter interfaced with a computer data acquisition system was used to measure the variations in resistance of the sensor. The measurements were performed at room temperature. The sensor response towards an oxidizing gas such as NO_2 is defined as [11]:

$$S = \frac{R_g - R_a}{R_a} \quad (1)$$

If $R_g >> R_a$, then $S = \frac{R_g}{R_a}$

Where, R_a and R_g are the resistances of the sensor structure in the presence of atmospheric air and target gas respectively. The response time was measured as the time taken by the sensor to acquire the 90% of its maximum resistance value in the presence of target oxidizing gas. Once the maximum resistance value was attained, the target gas was

flushed out from the test chamber and sensor was allowed to regain its initial resistance value in atmospheric air while keeping the sensor at the same temperature. The time taken by the sensor to reacquire about 10% higher value compared to its initial resistance in the presence of atmospheric air is considered as the recovery time.

4.2.3 Formation mechanism

ZnO is formed according to the following equation:

$$Zn(CH_3COO)_2 + 2CH_3CH_2OH \rightarrow (CH_3CH_2O^-)_2Zn^{2+} + 2CH_3COOH \quad (2)$$

$$LiOH + CH_3CH_2OH \leftrightarrow CH_3CH_2O^-Li^+ + H_2O \quad (3)$$

$$(CH_3CH_2O^-)_2Zn^{2+} + 2LiOH \rightarrow Zn(OH)_2 + 2CH_3CH_2OLi \quad (4)$$

$$Zn(OH)_2 \rightarrow ZnO\downarrow + H_2O \quad (5)$$

The zinc acetate dihydrate was dissolved in the boiling ethanol at atmospheric pressure and subsequently allowed to cool at room temperature to give a transparent and stable Zn based precursor $CH_3CH_2O^-Zn^+$. When LiOH was added to precursor $(CH_3CH_2O^-)_2Zn^{2+}$, $Zn(OH)_2$ was obtained after the chemical reaction and CH_3CH_2OLi evaporated. Calcinations of corresponding reaction precursors yielded the ZnO nanocrystals. We have proposed a plausible mechanism for the formation of ZnO/PANI heterojunction microstructures, as schematically illustrated in Fig. 4.1 (b).

4.3 Results and Discussion

4.3.1 Structural Studies

Figs. 4.2(a), 4.2(b) and 4.2(c) represent the X-ray diffraction (XRD) patterns of the pure PANI, pure ZnO and ZnO-PANI composite thin films respectively. The XRD pattern of pure PANI (Fig. 5.2a) shows the reflection peaks occur at $2\theta = 24.61°$ and 20.60^o which corresponds to (110) and (100) plane of PANI respectively [15]. An additional peak at $2\theta \approx 15.06^o$ is also observed and is in agreement with the reported value [15]. Fig. 5.2(b) shows the XRD pattern with the peaks corresponding to reflection planes (100), (002), (101), (102) and (110) of the wurtzite polycrystalline structure of

ZnO [22]. X-Ray diffraction pattern of composite ZnO-PANI as shown in Fig. 4.2(c) revealed the amorphous character prominently with weak reflections corresponding to ZnO [22-23]. It appears that the molecular chains of PANI are stretched leading to decrease in crystallinty of hybrid composite film. The average crystallite size was calculated by Debye-Scherer's formula as 5 nm.

4.3.2 Scanning Electron Microscope (SEM)

Figs. 4.3(a), 4.3(b) and 4.3(c) show the SEM images of pure PANI, ZnO nanoparticles and ZnO-PANI composite thin films respectively. The SEM image of the pure PANI film (Fig. 4.3a) exhibits a fibrous structure with many pores. Fig. 5.3(b) shows the flower shaped surface morphology of the ZnO thin film annealed at 400 °C for 2 h. The SEM image of the composite thin film (Fig. 4.3c) shows the agglomeration free and uniform distribution of the PANI in ZnO thin film matrix. It can be seen that the PANI chains are closely surrounded with the mesh like structure built by ZnO nanoparticles. The average pore size was found 900 nm. Thus the fabricated porous film is preferred for gas sensing applications. The obtained rough and porous morphology of prepared thin film as shown in Fig. 4.3(c) provided the high surface to volume ratio which enhanced the sensing response.

4.3.3 Optical Properties

The optical transmission spectra of ZnO and ZnO-PANI with 1%, 5% and 10% thin films having thickness 300 nm each deposited separately on corning glass substrate were measured in the wavelength range of 190 to 1100 nm, and the variation is shown in Fig. 4.4. ZnO and ZnO-PANI thin films exhibit a high transmission (90 to 20%) in the visible region and show a sharp fundamental absorption edge at ~ 340 nm.

Optical band gap of the ZnO and ZnO-PANI thin films deposited on corning glass substrate, were calculated from the intercept on energy axis obtained by extrapolating the linear portion of the Tauc plot of $(\alpha h\nu)^2$ *vs* photon energy ($h\nu$) as shown inset Fig. 4.4. Estimated value of band gap for as-grown ZnO thin film is found to be 3.38 eV which is close to the actual values for ZnO thin films (3.3eV) grown by various techniques [14-15]. The variation in band gap shows the electronic interaction between ZnO and PANI

confining the formation of ZnO-PANI composite thin film.

4.3.4 FTIR spectra

FTIR spectrum is the feature of a particular compound that gives the information about its functional groups, molecular geometry and molecular interactions. Fig. 4.5 shows the FTIR spectra of pure PANI, ZnO NPs and PANI/ZnO hybrid nanocomposites. Fig. 4.5(a) shows that the characteristic peaks of pure PANI appeared at 1631, 1471, 1292 and 1121 cm^{-1}. FTIR spectrum of ZnO-NPs (Fig. 4.5b) exhibits the peak at 475 cm^{-1} which is due to the stretching mode of ZnO-NPs and addition peak at 1380 cm^{-1} is due to leading vibration of C–H in the methyl and 1640 cm^{-1} attributed to the leading vibration molecule [24]. Fig. 4.5(c) shows that the absorption peaks for PANI/ZnO nanocomposites appear at 1572 cm^{-1} is due to C=C stretching mode of the quinoid rings, 1465 cm^{-1} is due to C=C stretching mode of benzenoid rings, 1234 cm^{-1} is attributed to C–N stretching mode and 1148 cm^{-1} can be attributed to the in-plane and out-of plane C–H bending [25], indicating the formation of PANI in the composites. Comparing to the corresponding peaks of pure PANI, the peaks of PANI/ZnO shifted towards higher and lower wavenumber. This shifting of absorption bands may be due to the action of hydrogen bonding between the hydroxyl groups on the surface of ZnO nanoparticles and the amine groups in the PANI molecular chains [26].

4.3.5 Sensing Behaviour

Fig. 4.6(a) shows the variation in sensing response of thin film sensors of Pure ZnO and ZnO with different concentrations of PANI as 1%, 5% and 10% as a function of temperature towards 20 ppm of NO_2 gas. It can be observed that the sensing response of all sensor structures decreases with increase in operating temperature up to 120 ºC. Due to certain limitations, experiments could not be performed for higher operating temperatures. The decrease in sensing response at high temperature could be due to the higher rate of sorption of gas at the sensor surface. Pure ZnO thin film sensor shows the sensing response of 1.7×10^2 at room temperature towards 20 ppm of NO_2 gas. The ZnO-PANI (1%) doped and ZnO-PANI (10%) based sensors show the sensing response of 2.5×10^2 and 1.2×10^2 at room temperature respectively. The enhancement in sensing

response of order of 6.11×10^2 has been observed for ZnO-PANI (5%) sensor structure at room temperature. It was supposed that because of maximum adsorption sites developed and the electrons coming out from valance band to conduction band were trapped and no electrons were found in conduction band. As a result maximum increase in the resistance was observed on increasing the concentration of PANI beyond this limit and sensor response goes down up to minimum (120) for ZnO-PANI (10%).

Figs. 4.7(a) and 4.7(b) show the transient response of pure ZnO and ZnO-PANI (5%) composite thin film sensor at room temperature towards 20 ppm NO_2 gas respectively. It can be observed from Fig. 4.7(a), that with the exposure of NO_2 gas to the sensing film surface, the sensor resistance increases from 1.83 kΩ to 311 kΩ (S=170) and 196.86 kΩ to 120.58 MΩ (S = 611). The response time and recovery time of the sensor made of pure ZnO and ZnO-PANI (5%) were observed to be 300 s, 350 s and 130 s, 170 s respectively.

From Fig. 4.7 it is visualized that at room temperature, the pure ZnO thin film sensor gave response in 6 min while ZnO-PANI (1%), ZnO-PANI (5%) and ZnO-PANI (10%) doped thin film sensor showed the response time of 3, 2.16 and 3.5 min towards 20 ppm NO_2 gas respectively. Fig. 4.8 shows the variation of response time of pure ZnO, ZnO-PANI (1%), ZnO-PANI (5%) and ZnO-PANI (10%) thin film sensors. Fig. 4.9 indicates the recovery time of ZnO-PANI (1%), ZnO-PANI (5%) and ZnO-PANI (10%) thin film sensors, when NO_2 gas was flushed out from the gas test chamber. From Fig. 4.8 it is clear that at room temperature, the recovery time of pure ZnO thin film is 5.33 min whereas ZnO-PANI (1%), ZnO-PANI (5%) and ZnO-PANI (10%) thin films have the recovery times as 3.5, 2.5 and 3.8 min respectively. Furthermore, response and recovery times are seen to be reducing with temperature. This may be attributed to the fact that at room temperatures the rate of adsorption and desorption of gases increases. So, ZnO-PANI (5%) doped thin film sensor is seen to be exhibiting better sensing properties compared to the other fabricated sensor structures.

Figs. 4.10(a) and 4.10(b) show the reproducibility response of pure ZnO and ZnO-PANI (5%) sensor structures, when continuously exposed to 20 ppm of NO_2 gas and air for four consecutive cycles at room temperature. The sensor structures show the

similar sensing response (R_a to R_g and R_g to R_a) repeatedly for four consecutive cycles towards 20 ppm NO_2 gas and air which confirms the good reproducibility of the prepared sensor structure. The observed results show the good stability of the fabricated sensor in comparison to earlier reported sensor.

4.3.6 Selectivity of gas

The selectivity of sensing device made of ZnO, ZnO-PANI (1 %), ZnO-PANI (5 %), and ZnO-PANI (10 %) were investigated at room temperature by injecting 20 ppm NO_2 and 1000 ppm concentration of other tested gases (LPG, C_2H_5OH, NH_3, isopropyl alcohol and acetone). It was found that ZnO-PANI hybrid nanocomposite thin-film sensors with different PANI weight ratio could exhibit high response to NO_2 but very low response to LPG, C_2H_5OH, NH_3, IPA and acetone. Among all the above mentioned ZnO-PANI (1-5 %) hybrid nanocomposite thin film sensors, the sensor made of ZnO-PANI (5%) exhibited the highest response of 611 to 20 ppm of NO_2.

The selectivity of ZnO and ZnO-PANI (5%) hybrid nanocomposite thin-film sensor is shown in bar diagram of Fig. 4.11. In order to study selectivity, 20 ppm of the test gases as NO_2, LPG, C_2H_5OH, NH_3, IPA and acetone were introduced in the test chamber and exposed to ZnO and ZnO-PANI (5%) hybrid nanocomposite thin-film sensors. The responses of ZnO and ZnO-PANI (5%) hybrid nanocomposite thin-film sensors to the NO_2 gas (20 ppm) were 120 and 611, respectively, and least responses were observed for the other test gases.

4.3.7 Gas sensing mechanism

Gas sensing of semiconductor sensors is based on the resistance change of the material due to the chemical and electronic interaction between the gas and sensing matrix. The chemical interaction involves the adsorption of the target gas molecules on the surface of ZnO thin film, where subsequent reaction with oxygen species adsorbed on the ZnO surface, results in the detection for the target gas [27-28].

The adsorption and reaction process can be described as follows: when ZnO sensor is exposed to air, oxygen molecules adsorb on the surface of the materials to form

chemisorbed oxygen anions ($O_{2(\overline{ads})}$) by capturing electrons from the conductance band, resulting in the formation of a depletion layer, known as the space charge layer, on the surface of the sensor material which results in an increase in resistance of the material.

$$O_2 + e^- \leftrightarrow O_{2(\overline{ads})} \quad (6)$$

when the ZnO thin film is exposed to NO_2 gas, it is adsorbed directly on the surface of ZnO thin film. Therefore, the concentration of electrons on the surface of ZnO thin film decreases and, correspondingly, the resistance of ZnO layer increases. The process of the reaction can be described as follows:

$$NO_{2(g)} + e^- \leftrightarrow NO^-_{2(ads)} \quad (7)$$

The above reactions result in the decrease of concentration of electron on the surface of ZnO which results in an increase in resistance of the material. In addition, following reaction is happened between $NO^-_{2(ads)}$ and $O_{(\overline{ads})}$:

$$NO_{2(gas)} + O_{2(\overline{ads})} + 2e^- \leftrightarrow NO^-_{2(ads)} + 2O^-_{(ads)} \quad (8)$$

Thus the cyclic reaction continues as in equation (7).

With the incorporation of p-type PANI [29] into n-type ZnO [17], the sensing response towards NO_2 gas was found to increase. This may be due to the formation of p-n junctions in the hybrid composite films and PANI chains are surrounded with mesh like structures made by ZnO nanoparticles. Here we have proposed a corresponding model of sensing mechanism of NO_2 through the ZnO-PANI heterojunction microstructures. The schematic of mechanism is shown by Fig. 4.12.

During the formation of pn junction minority carrier in PANI are lesser in number and they require lesser energy to move to conduction band as a result in beginning a small variation will be observed but as the ZnO in n-type and excess in amount in the sample as result n-type a nature of film will be dominating. Only the role of PANI will be to enhance the rate of reaction with oxidizing gas like NO_2.

The first oxygen species were adsorbed on the surface of particles in the air, and then ionized into O^-_{ads} capturing free electron from the particles, thus leading to the formation of thin space charge layer and increasing of surface band bending. The doped PANI has a lower band gap and work function (E_g = 2.8 eV, $\emptyset = 4.14$ eV) than that of ZnO (E_g =3.37 eV, $\emptyset = 5.2$ eV), the electrons are transfered towards the PANI, leading to the formation of an accumulation layer at the ZnO-PANI interface. After getting stabilized the film was exposed to NO_2 and it was adsorbed by the heterojunctions between ZnO and PANI, NO_2 acts as an electron acceptor in the reaction, and an acceptor surface state was occurred. As the surface state energy level is close to the valence band edge then to bring the Fermi level close to the surface state, the surface Fermi energy must be close to the valence band. In such a situation the acceptor surface state is so low in the band diagram that it extracts electrons from the valence band leaving a substantial hole concentration. As a result the lesser number of electrons are transferred from ZnO to PANI causing increase in the resistance [30]. On the other hand, the trapped electrons are released to heterojunctions between ZnO and PANI by NO_2 after stopping the supply of NO_2, leading to a decrease of the resistance.

4.4 Conclusion

The maximum sensing response ~ 611 at room temperature towards 20 ppm of NO_2 gas was obtained for ZnO-PANI (5%) hybrid composite sensor with a fast response and recovery times of about 2.16 min and 2.83 min respectively. However, the sensing responses as 170, 250 and 120 were obtained for pure ZnO, ZnO-PANI (1%) and ZnO-PANI (10%) sensor structures respectively towards the same amount of NO_2 gas showing the importance of optimum concentration of PANI (5%) in the sensing layer of nanocomposite ZnO-PANI. Thus this sensor structure can be reliably used for the detection of NO_2 gas at room temperature at commercial level.

References:

[1] H.S. Hwang and J.T. Song, Characteristic of a NO_x gas sensor based on a Low Temperature Co-Fired Ceramic and Ga- Doped ZnO, J. Korean Phys. Soc., 53 (2008) 1384-1387.

[2] R.L.N. Chandrakanthi, M.A. Careem, Preparation and characterization of CdS and Cu_2S nanoparticle/polyaniline composite films, Thin Solid Films, 417 (2002) 51-56.

[3] P.R. Somani, R. Marimuthu, U.P. Mulik, S.R. Mulik, S.R. Sanikar, D.P. Amalnerkar, High piezorestivity and its origin in conducting polyaniline/ZnO composites, Synth. Met., 106 (1999) 45-52.

[4] Y. He, Synthesis of polyaniline/nano-CeO_2 composite microspheres via a solid – stabilized emulsion route, Mater. Chem. Phys., 92 (2005) 134-137.

[5] O. Lupan, V. Cretu, M. Deng, D. Gedamu, I. Paulowicz, S. Kaps, Y.K. Mishra, Versatile Growth of Freestanding Orthorhombic Alpha-Molybdenum Trioxide Nano-and Microstructures by Rapid Thermal Processing for Gas Nanosensors, J. of Physical Chemistry C, 118 (2014) 15068-15078.

[6] A.G. MacDiarmid, L.S. Yang, W.S. Huang, B.D. Humphrey, Polyaniline: electrochemistry and application to rechargeable batteries, Synth. Met., 18 (1987) 393-398.

[7] D. Verma, V. Datta, Role of novel microstructure of polyaniline-CSA thin film in ammonia sensing at room temperature, Sens. Actuator B: Chem.,134 (2008) 373-376.

[8] I. Paulowicz, V. Hrkac, S. Kaps, V. Cretu, O. Lupan, T. Braniste, V. Duppel, Y.K. Mishra, Three-Dimensional SnO_2 Nanowire Networks for Multifunctional Applications: From High-Temperature Stretchable Ceramics to Ultraresponsive Sensors, Advanced Electronic Materials, 2015 (doi: 10.1002/aelm.201500081).

[9] R.K. Sonker, B.C. Yadav, Growth mechanism of hexagonal ZnO nanocrystals and their sensing application, Materials Letters, 160 (2015) 581-584.

[10] R.K. Sonker, B.C. Yadav, Chemical Route Deposited SnO_2, SnO_2-Pt and SnO_2-Pd Thin Films for LPG Detection, Adv. Sci. Lett. 20 (2014) 1023-1027.

[11] R.K. Sonker, A. Sharma, M. Tomar, V. Gupta, B.C. Yadav, Nanocatalyst (Pt, Ag and CuO) Doped SnO_2 Thin Film Based Sensors for Low Temperature Detection of NO_2 Gas, Adv. Sci. Lett. 20 (2014)1374-1377.

[12] B.C. Yadav, R. Srivastava, C.D. Dwivedi and P. Pramanik, Moisture sensor based ZnO nanomaterial synthesized through oxalate route, Sens. Actuat. B: Chem., 131 (2008) 216-222.

[13] M. Enachi, O. Lupan, T. Braniste, A. Sarua, L. Chow, Y.K. Mishra, D. Gedamu, Integration of individual TiO_2 nanotube on the chip: Nanodevice for hydrogen sensing, Physica Status Solidi-RRL, 9 (2015) 171-174.

[14] G.S. Devi, V.B. Subrahmanyam, S.C. Gadkari, S.K. Gupta, NH_3 gas sensing properties of nanocrystalline ZnO based thick films, Analytica Chimica Acta, 30 (2006) 102-105.

[15] H. Xu, X. Chen, J. Zhang, J. Wang, B. Cao, D. Cui; NO_2 gas sensing with SnO_2-ZnO/PANI composite thick film fabricated from porous nanosolid; Sens. Actuators B:Chem., 176 (2013) 166-173.

[16] D. Gedamu, I. Paulowicz, S. Kaps, O. Lupan, S. Wille, G. Haidarschin, Rapid Fabrication Technique for Interpenetrated ZnO Nanotetrapod Networks for Fast UV Sensors, Advanced Mater., 26 (2014) 1541-1550.

[17] X.B. Yan, Z.J. Han, Y. Yang, B.K. Tay, NO_2 gas sensing with polyaniline nanofibers synthesized by a facile aqueous/organic interfacial polymerization, Sens. Actuators B: Chem., 123 (2007) 107-113.

[18] R.K. Sonker, A. Sharma, Md. Shahabuddin, M. Tomar, V. Gupta Low temperature sensing of NO_2 gas using SnO_2-ZnO nanocomposite sensor, Adv. Mat. Lett. 4 (2013) 196-201.

[19] S.L. Patil, S.G. Pawar, A.T. Mane, M.A. Chougule, V.B. Patil, Nanocrystalline ZnO thin films: optoelectronic and gas sensing properties, Journal of Materials Science: Materials in Electronics, 21 (2010) 1332-1336.

[20] G. Sarala Devi, V.B. Subrahmanyam, S.C. Gadkari, S.K. Gupta, NH_3 gas sensing properties of nanocrystalline ZnO based thick films, Analytica Chimica Acta, 30 (2006) 102-105.

[21] S.G. Pawar, S.L. Patil, M.A. Chougule, A.T. Mane, D. M. Jundale, V.B. Patil, Synthesis and Characterization of Polyaniline: TiO_2 Nanocomposites, International Journal of Polymeric Material, 59 (2010) 777-789.

[22] R.K. Sonker, S.R. Sabhajeet, Satyendra Singh, B.C. Yadav, Synthesis of ZnO nanopetals and its application as NO_2 gas sensor, Materials Letters, 152 (2015) 189-191.

[23] S.K. Shukla, N.B. Singh, R.P. Rastogi; Efficient ammonia sensing over zinc oxide/polyaniline nanocomposite, I. J. of Eng. & Mater. Sci., 20 (2013) 319-324

[24] R.F. Silva, M.E.D. Zaniquelli, Morphology of nanometric size particulate aluminium-doped zinc oxide films, Colliod Surf Physicochem Eng-Aspect, 198 (2002) 551-558.

[25] F. Ahmed, S. Kumar, N. Arshi, M.S. Anwar, L.S.Yeon, G.S. Kil, D.W. Park, B.H. Koo, C.G. Lee, Preparation and characterizations of polyaniline (PANI)/ZnO nanocomposites film using solution casting method, Thin Solid Films, 519 (2011) 8375-8378.

[26] Y. He, A novel emulsion route to sub-micrometer polyaniline/nano-ZnO composite fibers, Appl. Surf. Sci. 249 (2005) 1-6.

[27] S.L. Bai, L.Y. Chen, D.Q. Li, W.H. Yang, P.C. Yang, Z.Y. Liu, A.F. Chen, C.L. Chung, Different morphologies of ZnO nanorods and their sensing property, Sens. Actuator B: Chem., 146 (2010) 129-137.

[28] P. Rai, Y.S. Kim, H.M. Song, M.K. Song, Y.T. Yu; The role of gold catalyst on the sensing behavior of ZnO nanorods for CO and NO_2 gases; Sens. Actuator B: Chem., 165 (2012) 133-142.

[29] X.B. Yan, Z.J. Han, Y. Yang, B.K. Tay, NO_2 gas sensing with polyaniline nanofibers synthesized by a facile aqueous/organic interfacial polymerization, Sens. Actuators B: Chem., 123 (2007) 107-113.

[30] S. Singh, B.C. Yadav, M. Singh and R. Kothari, A Review Report on Nanostructured Ferrites as Liquefied Petroleum Gas Sensor, International Journal of Science, Technology & Society, 1 (2015) 4-21.

Figures:

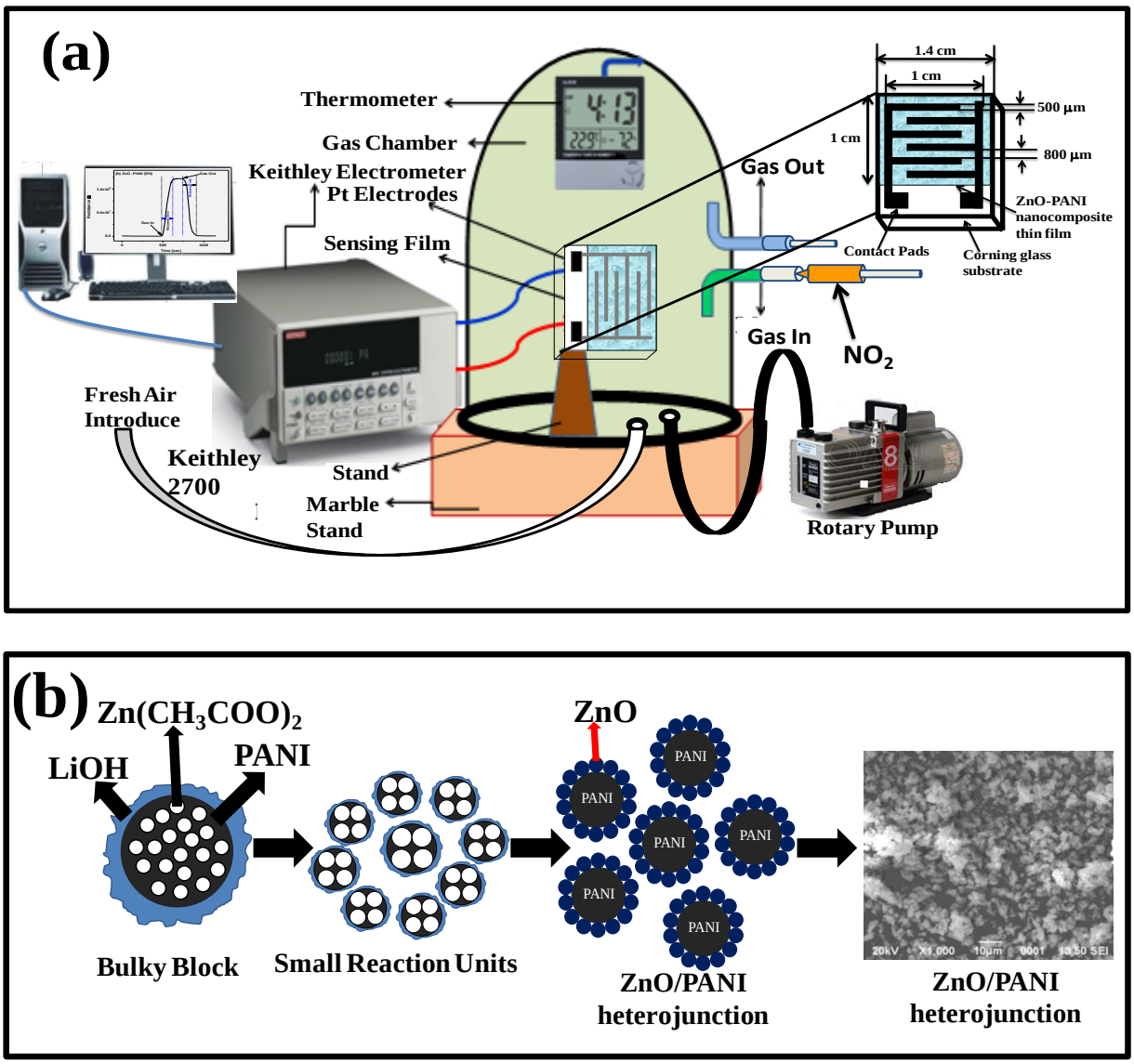

Fig. 4.1: (a) Schematic diagram of sensing device and (b) Schematic illustrating the mechanism of formation of ZnO/PANI heterojunction microstructures

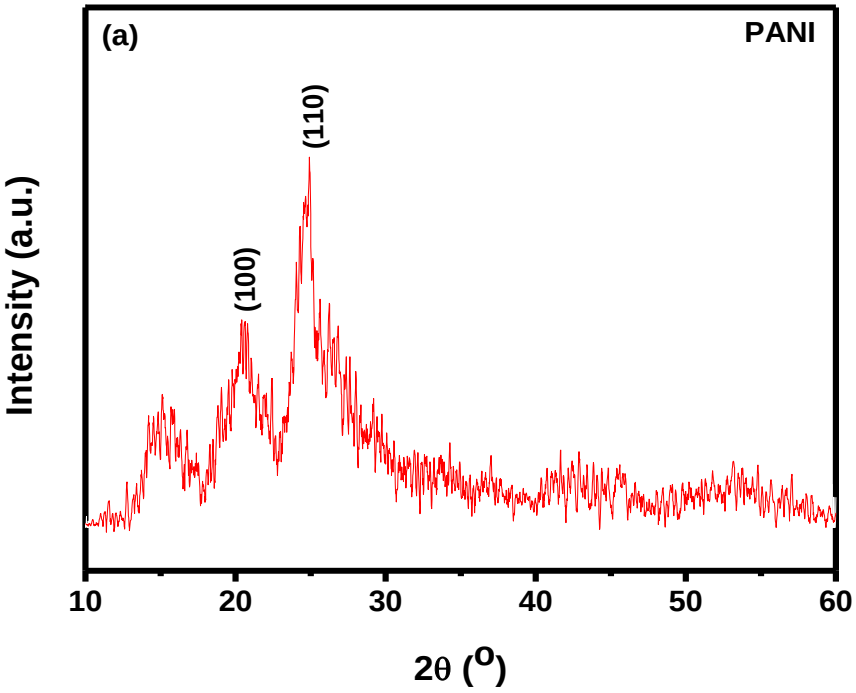
(a)
PANI
(110)
(100)
Intensity (a.u.)
10
20
30
40
50
60
2θ (O)

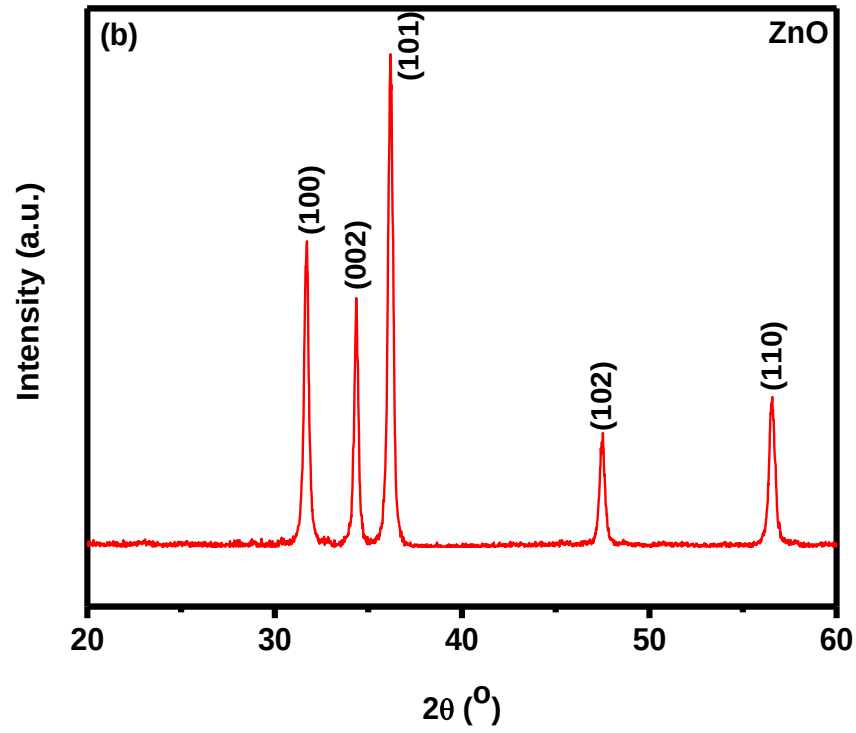
(b)
ZnO
(101)
(100)
(002)
(102)
(110)
Intensity (a.u.)
20
30
40
50
60
2θ (O)

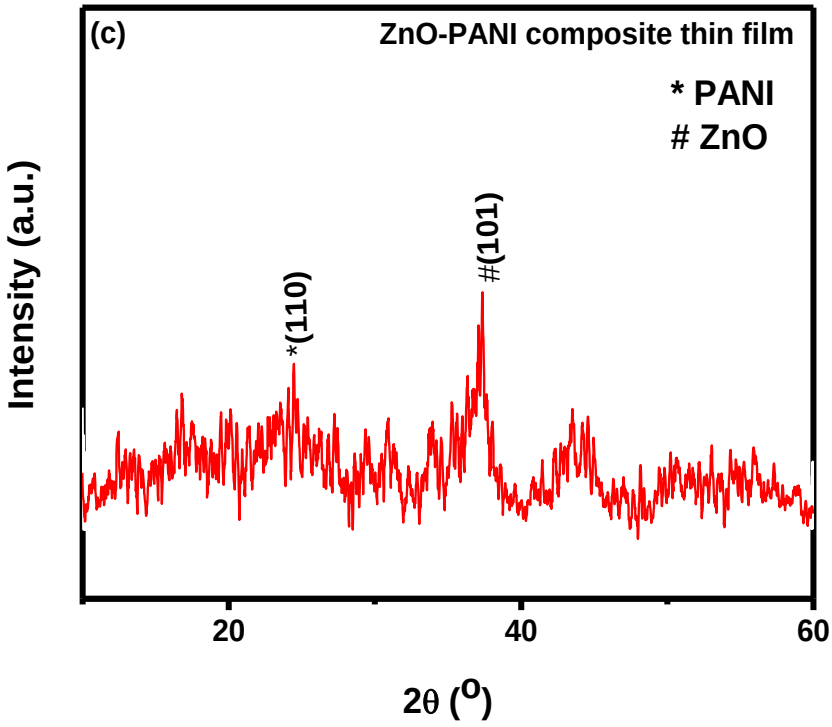

Fig. 4.2: X-ray diffraction patterns of (a) pure PANI, (b) ZnO and (c) ZnO-PANI

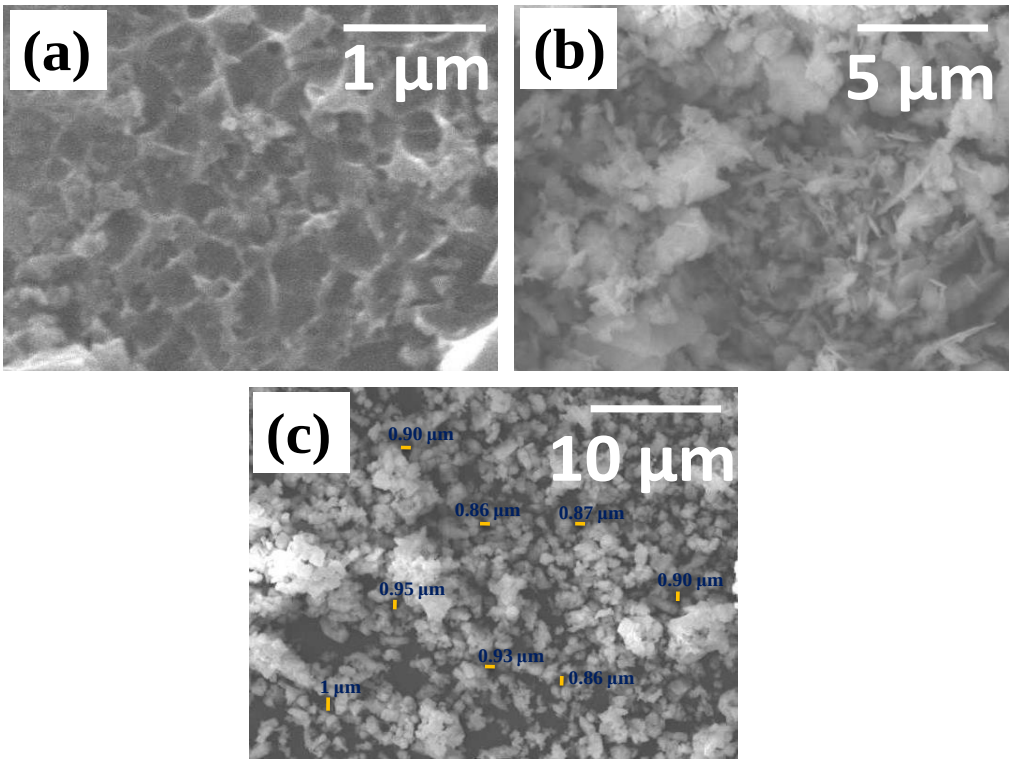

Fig. 4.3: Scanning electron micrographs of (a) PANI, (b) ZnO and (c) PANI-ZnO composites thin film

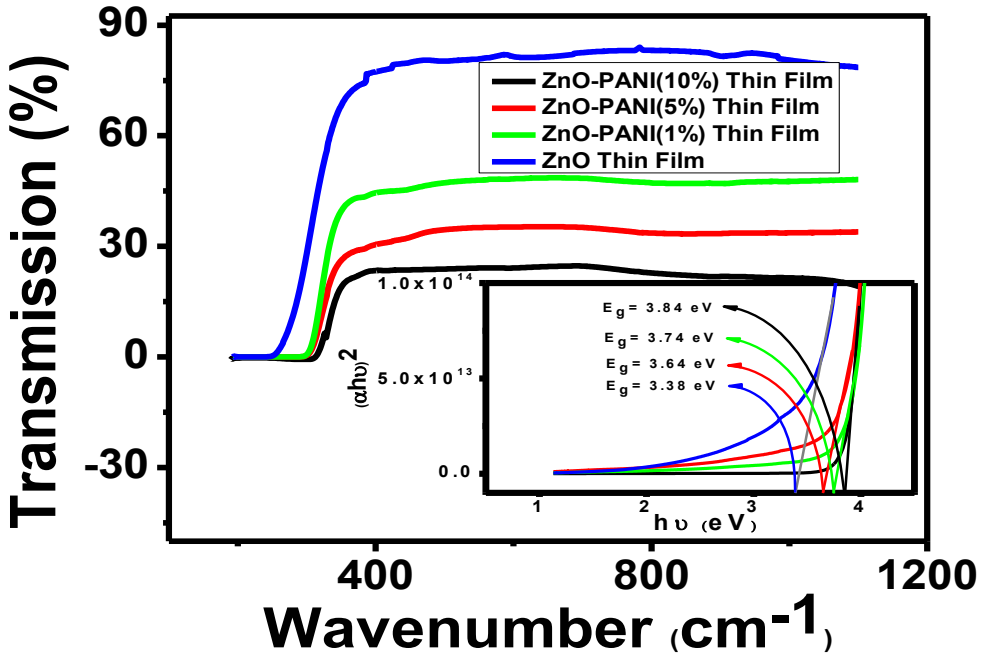

Fig. 4.4: Transmission spectra of ZnO, ZnO-PANI(3%), ZnO-PANI(5%) and ZnO-PANI(10%) composite thin films and inset Tauc plot $(\alpha h\nu)^2$ vs. $h\nu$ of ZnO, ZnO-PANI(3%), ZnO-PANI(5%) and ZnO-PANI(10%) composite thin films

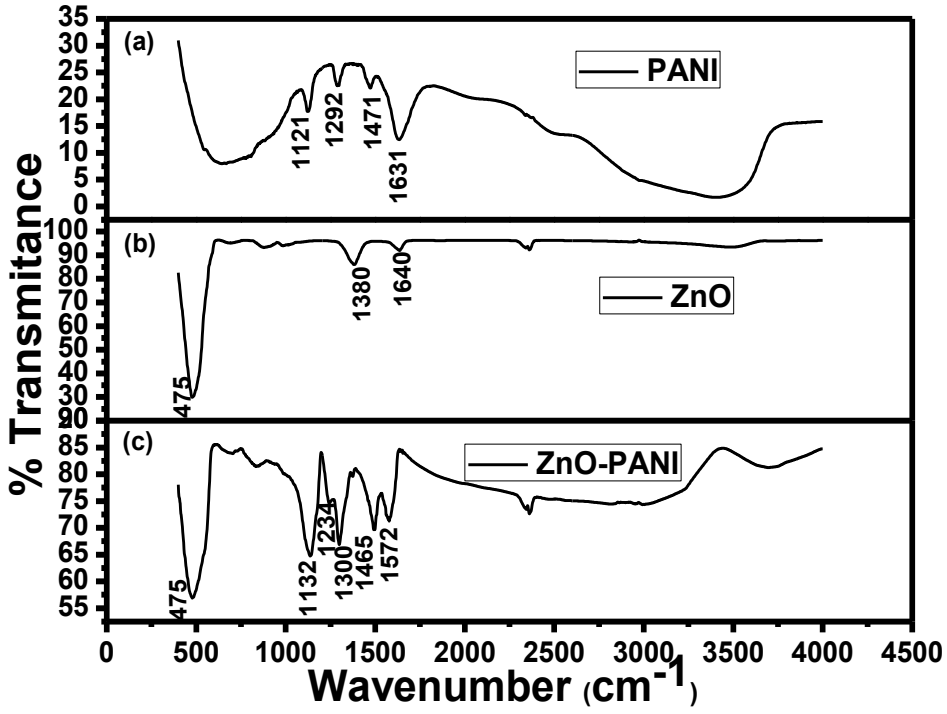

Fig. 4.5: FTIR spectra obtained for (a) PANI (b) ZnO-NPs (c) ZnO-PANI composite

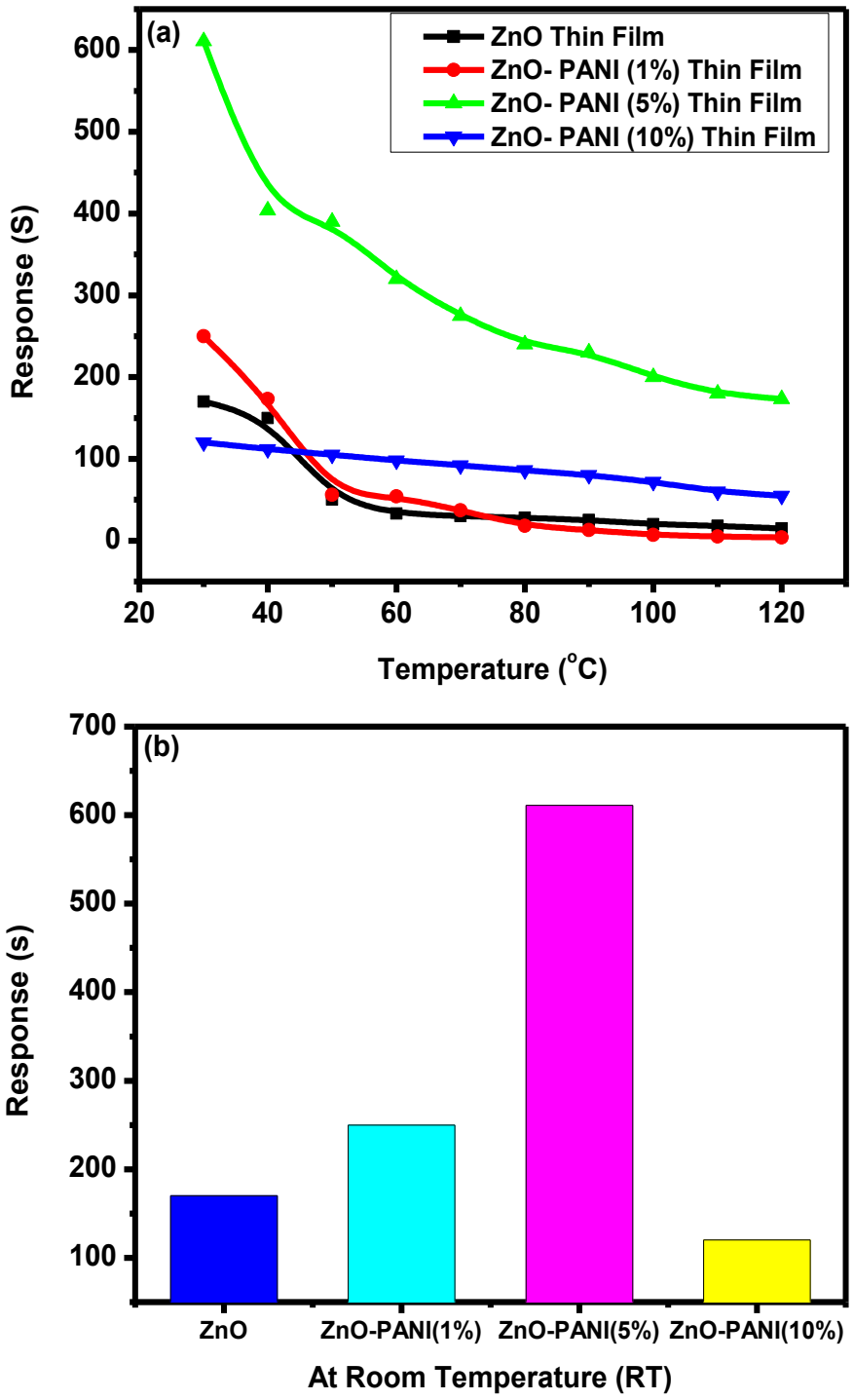

Fig. 4.6: Variation in sensing response (a) pure ZnO (b) ZnO-PANI (1%), ZnO-PANI (5%) and ZnO-PANI (10%) thin film sensors as a function of temperature towards 20 ppm of NO_2 gas

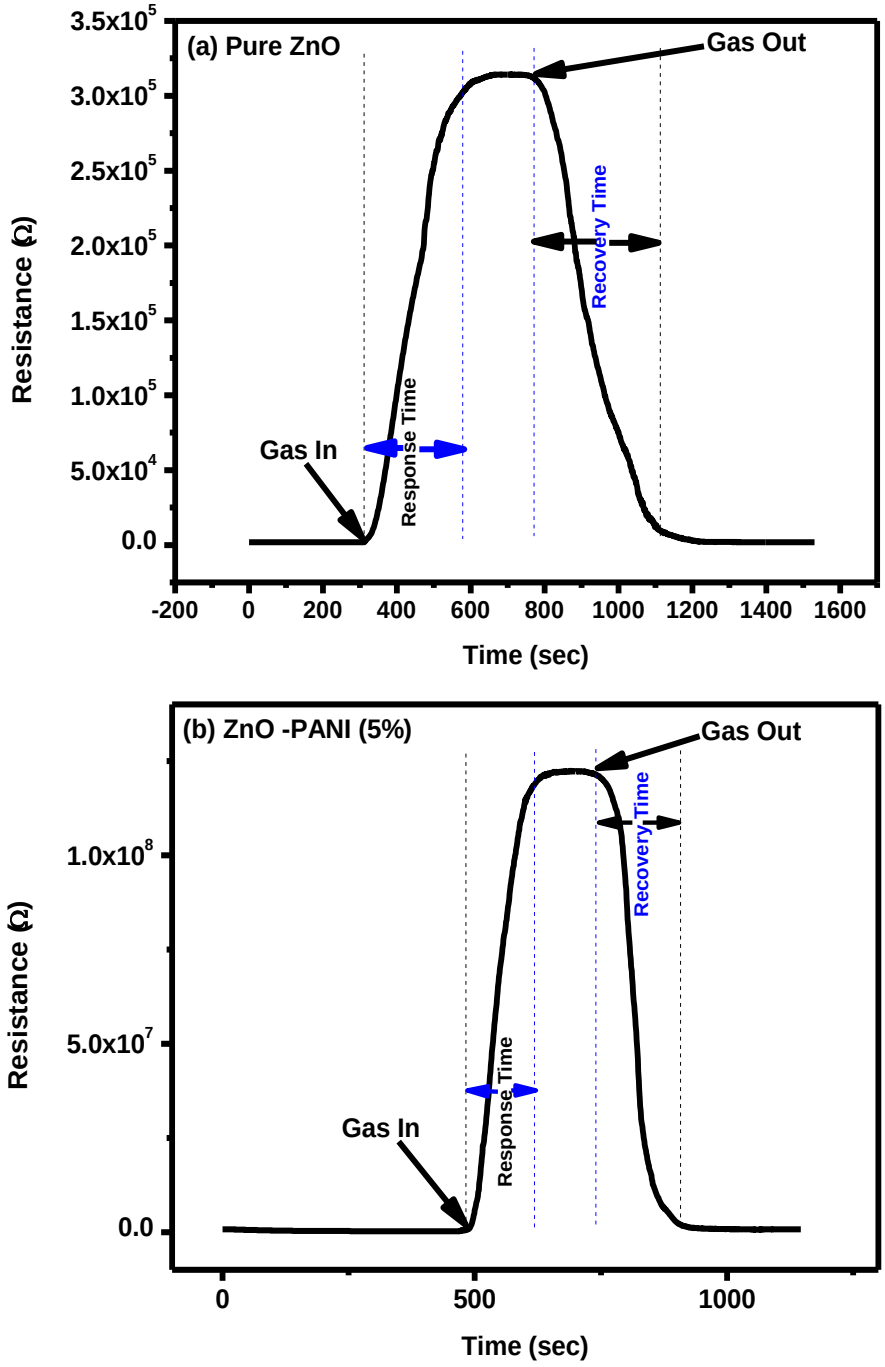

Fig. 4.7: Transient response of (a) pure ZnO and (b) ZnO-PANI (5%) sensor towards 20 ppm of NO_2 gas at room temperature

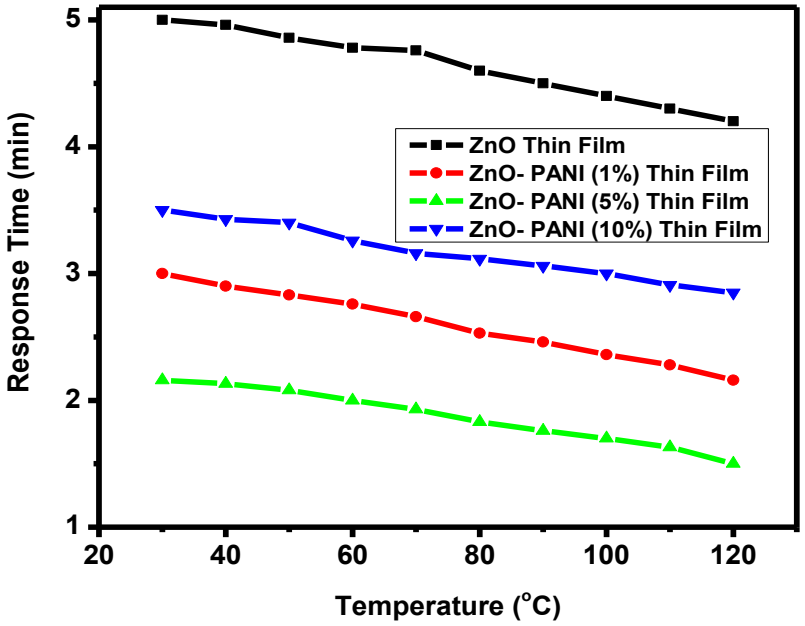

Fig. 4.8: Variation in response time of the pure ZnO, ZnO-PANI (1%), ZnO-PANI (5%) and ZnO-PANI (10%) thin film sensors

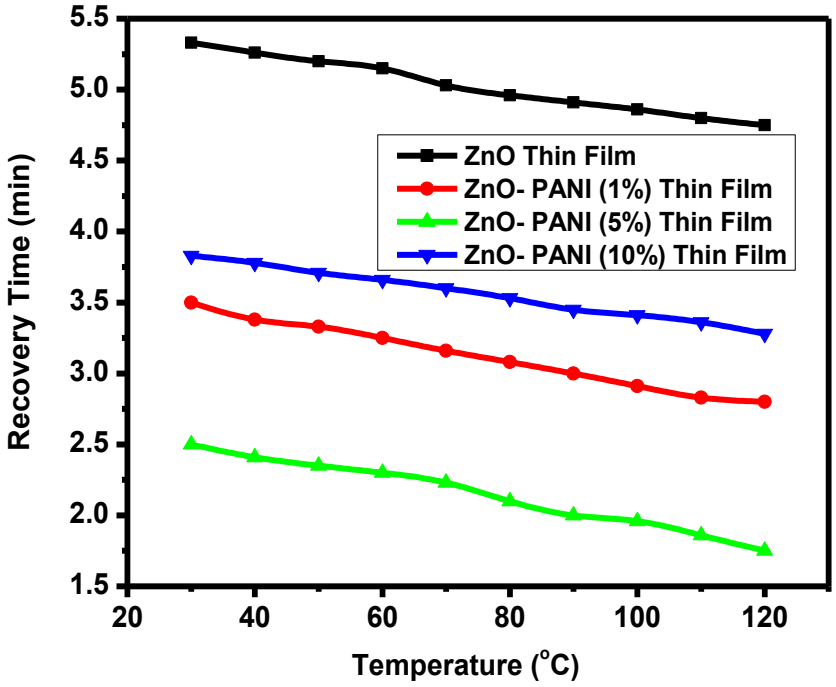

Fig. 4.9: Variation in recovery time of the pure ZnO, ZnO-PANI (1%), ZnO-PANI (5%) and ZnO-PANI (10%) thin film sensors

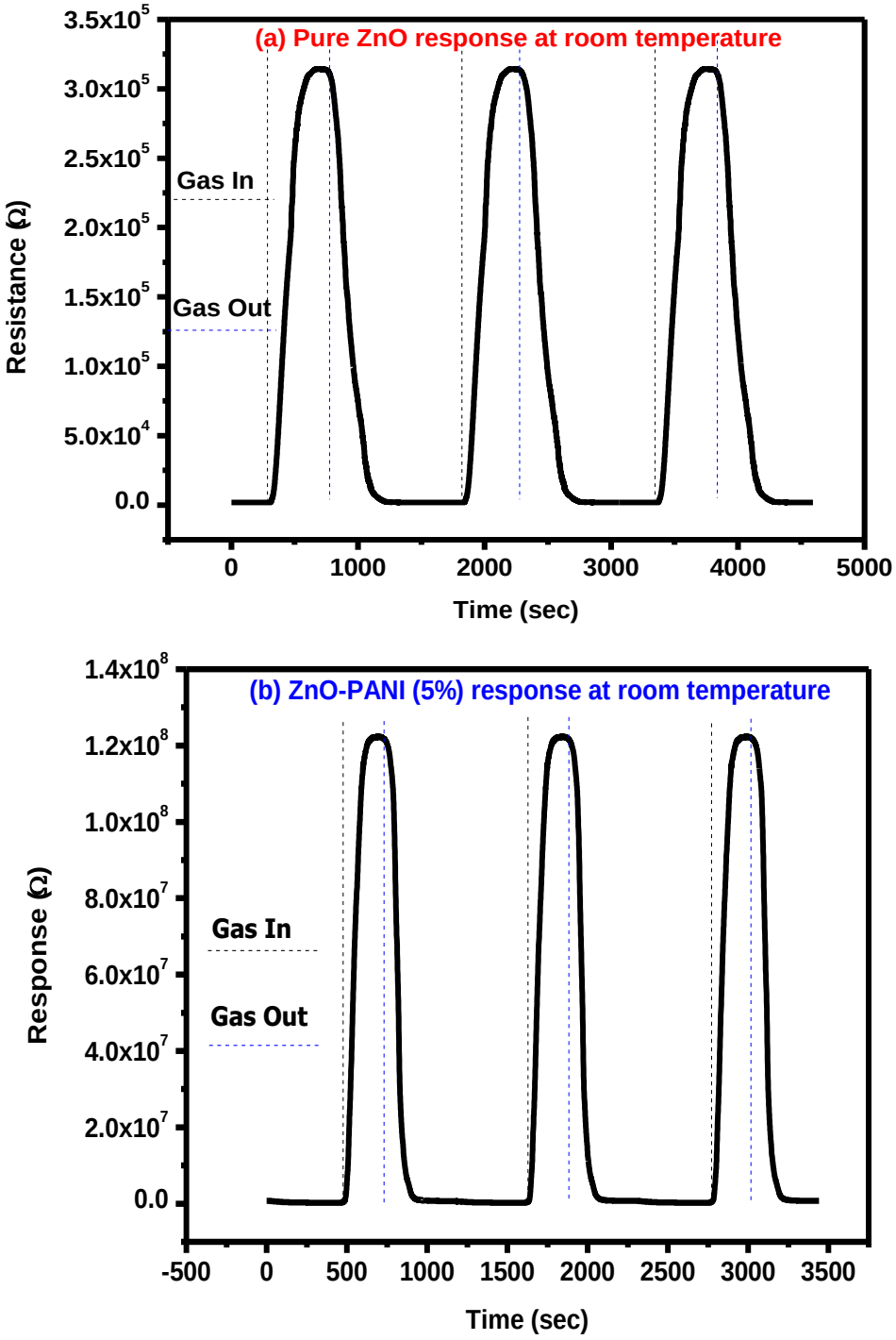

Fig. 4.10: Transient Response curve of repeated cycle towards 20 ppm of NO_2 gas for (a) pure ZnO and (b) ZnO-PANI Thin Film Sensor at room temperature

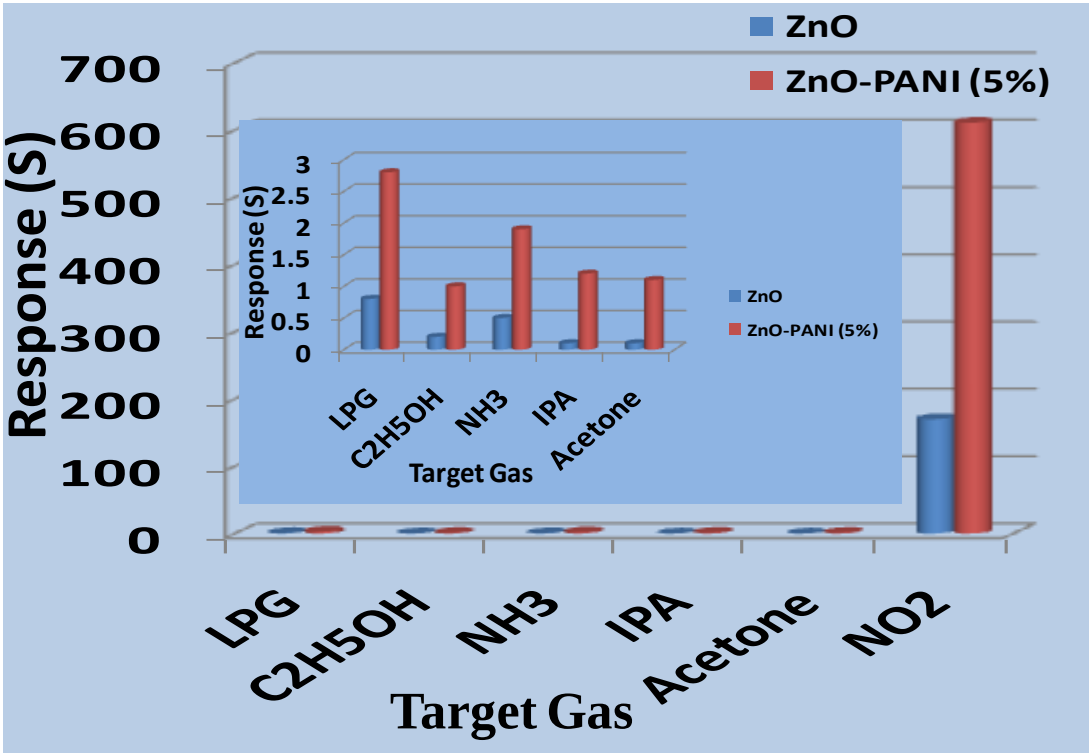

Fig. 4.11: Selectivity of ZnO and ZnO-PANI(5%) for different tested gases as NO_2, LPG, C_2H_5OH, NH_3, IPA and acetone

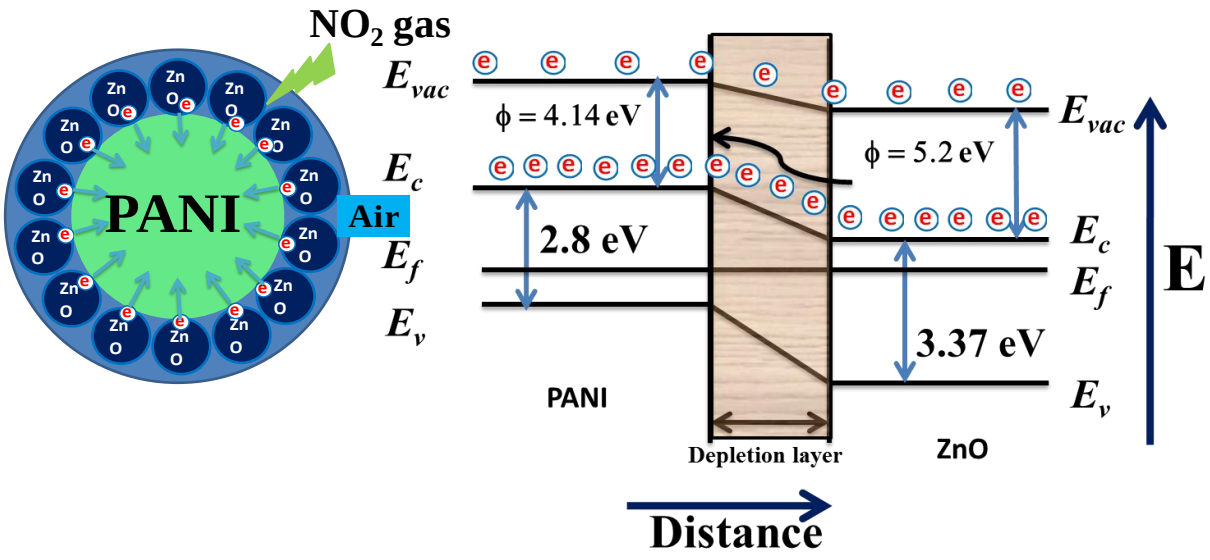

Fig. 4.12: Schematic diagram of the proposed mechanism of NO_2 sensing of ZnO/PANI heterojunctions

Chapter 5

Nanocatalyst (Pt, Ag and CuO) doped SnO_2 thin film based sensors for low temperature detection of NO_2 gas

The highly sensitive low temperature operated nitrogen dioxide (NO_2) gas sensor has been fabricated using SnO_2 thin film doped with different catalysts (Pt, Ag and CuO) using chemical route. Amongst all the prepared sensor structures, Pt-doped SnO_2 thin film based sensor (SnO_2-Pt) was found to give maximum sensing response of about 1.83 $\times 10^2$ towards low concentration of (20 ppm) of NO_2 gas at a lower operating temperature of 90 °C with fast response (~ 6 sec) and recovery (~ 13 sec) time. The structural, microstructural and optical properties of the prepared sensor have been studied using X-ray diffraction (XRD), Scanning electron microscope (SEM) and UV-Visible spectroscopy and the results have also been correlated with the observed gas sensing properties.

5.1 Introduction

Persistent progress in metal oxide-based nanomaterials, such as nanowires [1], nanofibers [2], nanorods [3], nanobelts [4], and hollow structures [5] has led to the major development of gas sensing devices [6–8]. SnO_2 is an n-type semiconductor with a wide band gap (3.6 eV), which has been extensively used in the fabrication of NO_2 gas sensor because of its natural non-stoichiometry, low cost and high chemical stability. In recent years, many methods have been employed in preparing SnO_2 thin-film gas sensors, including chemical vapor deposition (CVD) [9], sol-gel [10], sputtering [11] and spray pyrolysis [12]. In addition, many nanostructures are also used in preparing SnO_2 thin-film NO_2 sensors, like nanoparticles [13], nanosheets [14], nanotubes [15], nanowires [16], hollow spheres [17] and quantum dots [18] etc. However, the fabrication of thin/thick film sensors usually requires either complicated preparation process or sophisticated equipments. Thus in the present work a simple chemical route to prepare the SnO_2 thin film based gas sensor has been proposed [19]. High operating temperatures and poor response and recovery characteristics are also the major concerns which require further studies on NO_2 gas sensors. To overcome these problems various dopants like WO_3, ZnO, Pt, Ag etc. have been exploited in literature but the reported results still lack the enhanced sensing response along with faster response and recovery times which hinders the practical application of these sensors [20-22]. An effort has been made in this report to develop sensor structure based on, SnO_2 nanostructures doped with different catalysts (Pt, Ag and CuO) using chemical route to detect 20 ppm of NO_2 gas. The sensors have been fabricated by spin coating of nanoparticles colloidal solution onto corning substrate having Pt electrodes. The fabricated sensors have been exploited for the detection of NO_2 gas.

5.2 Experimental Details

SnO_2 doped with Pt, Ag and CuO catalysts were prepared by chemical route using $SnCl_4.5H_2O$, propanol and deionized water as precursors for SnO_2 fabrication. The preparation of Pt, Ag, CuO and SnO_2 nanoparticles have been mentioned elsewhere [23-26]. The prepared nanoparticles (Pt, Ag and CuO) were doped into SnO_2 nanoparticle

colloidal solution in the ratio of 3:0.3 (SnO_2:catalysts) and respective sols were prepared (SnO_2-Pt; SnO_2-Ag; SnO_2-CuO). SnO_2-Pt, SnO_2-Ag and SnO_2-CuO sol were used to deposit respective thin films on corning glass and Pt inter digital electrode (IDEs) patterned corning glass substrates by spin coating. For comparison, pure SnO_2 sol was also used to deposit pure SnO_2 thin film. The prepared samples were annealed at 500 ºC for 3 h in atmospheric air in order to stabilize the sensors. All the prepared samples were of same thickness (400 nm). Thickness of all the prepared films was measured using a surface profiler (Veeco dektak 150). Crystalline structure and surface morphology of the sensing layer were studied using Bragg–Brentano (θ–2θ) scan of a X-ray Diffractometer (Bruker D8 Discover) using the CuKα1 source (λ = 0.154 nm) and Scanning Electron Microscope (TESCAM MiraIII) respectively.

Optical properties of the prepared thin films were studied using Perkim Elmer UV-Visible spectrophotometer (Lambda 35). Pt, Ag, CuO doped and undoped SnO_2 thin film based sensor structures were named as SnO_2-Pt, SnO_2-Ag, SnO_2-CuO and Pure SnO_2 respectively. Gas sensing properties of all the prepared sensor structures were studied in a laboratory made gas sensing test ring set-up [11]. The change in sensor resistance was observed in the presence of 20 ppm of NO_2 gas and the data was obtained from Keithley 2002 digital multimerter which was interfaced with computer. The sensing response of prepared sensor structures towards oxidizing NO_2 gas is reported in Chapter 4, subheading 4.2.2.

5.3 Results and Discussions

5.3.1 Structural Studies

The X-Ray diffraction analysis of samples SnO_2, SnO_2-Pt, SnO_2-Ag and SnO_2-CuO were performed by using X-Ray Diffractometer (Bruker D8 Discover). Fig. 5.1(a-d) shows the XRD pattern of SnO_2, SnO_2-Pt, SnO_2-Ag and SnO_2-CuO thin film. Fig. 5.1(a) reveals the broad and well defined reflections corresponding to (110), (101), (200) and (211) planes of SnO_2 as observed at 26.62º, 33.97º, 37.95º and 51.57º respectively for the deposited SnO_2 thin film and are in good agreement (JCPDF-win 411445) to the corresponding values reported for the rutile structure of SnO_2. The values of lattice

constants (‘a’ and ‘c’) estimated from XRD data for the SnO_2 thin films were found to be about 4.81 Å and 3.14 Å respectively which are close to the reported value [11]. The crystallite size was estimated using well known Debye-Scherer formula and is found to be about 5.34 nm corresponding to the FWHM of dominant peak of (110) reflecting plane. However, Fig. 5.1(b) shows that the Pt doped SnO_2 thin film peak corresponding to Pt as observed at 39.4°, which can be ascribed to the Pt (111) diffraction [27]. X-ray diffraction patterns for the SnO_2-Ag and SnO_2-CuO films show that only peaks 35.7° (002) and 38.8° (111) correspond to the presence of Ag and CuO in the respective films due to low concentration of dopants in SnO_2 thin films [28-29].

5.3.2 Optical Properties

The optical transmission spectra of the as grown SnO_2 thin films (400 nm thin) deposited on corning glass substrate was measured in the wavelength range of 190 to 1100 nm, and is shown in Fig. 5.2. It can be observed that SnO_2 thin film exhibits a high transmission (>90%) in the visible region and show a sharp fundamental absorption edge in UV region at 350 nm. However, with the incorporation of 0.01 wt% Pt, 0.01wt% Ag and 0.01wt% CuO, transmission reduces to about 90%, 86% and 82% respectively in the visible region. Optical band gap of SnO_2 thin films deposited on corning glass substrate, was calculated from the intercept on energy axis obtained by extrapolating the linear portion of the Tauc plot of $(\alpha h\nu)^2$ *vs* photon energy ($h\nu$) as shown Fig. 5.3. Estimated value of band gap for pure SnO_2 thin film is found to be 4.27 eV. The values of energy band gaps were found to be decreased slightly to 3.73 eV, 3.94 eV and 4.00 eV after the incorporation of Pt, Ag and CuO nanoparticles into SnO_2 thin film respectively. The decrease in the band gap with the incorporation of Pt, Ag and CuO into SnO_2 thin film may be due to electronic transition between dopants and SnO_2 thin film.

5.3.3 Scanning Electron Microscope (SEM)

The 2D surface morphology of SnO_2, SnO_2-Pt, SnO_2-Ag and SnO_2-CuO nanocomposite thin films were shown in Fig. 5.4(a-d). The microstructure of a SnO_2 thin film is randomly distributed forming clusters of molecules shown by Fig. 5.4(a). SEM image of SnO_2-Pt thin film shown by Fig. 5.4(b) exhibits more porous surface

morphology. Average pore size of each material has been depicted in Table 5.1. From table it may be seen that average pore size of SnO_2-Pt is largest and distribution of pores is also uniform. Such morphology helps to absorb NO_2 gas due to more exposed area which improves gas sensing properties.

5.3.4 Sensing Behaviour

Fig. 5.5 shows the variation in sensing response of pure SnO_2, SnO_2-Pt, SnO_2-Ag and SnO_2-CuO thin film sensors as a function of temperature towards 20 ppm of NO_2 gas. It was observed that the sensing response of all sensor structures increases with increase in temperature till 90 ºC (operating temperature) and on further increasing the temperature, it reduces. Pure SnO_2 thin film sensor shows the sensing response of 67 at an operating temperature of 90 ºC towers 20 ppm of NO_2 gas. The SnO_2-Ag doped and SnO_2-CuO based sensors show the sensing response of 52 and 95 at an operating temperature of 90 ºC respectively. The enhancement in sensing response to 1.8×10^2 has been observed for SnO_2-Pt sensor structure at an operating temperature of about ~ 90 ºC. When NO_2 gas interacts with the (Pt, Ag and CuO) doped SnO_2 thin films, it traps free electrons from the sensor surface and decreases the conductivity. Thus the resistance R_g for all the sensors increases on exposure to NO_2 gas. At higher operating temperatures (~ 90 ºC), the predominant oxygen species on the SnO_2 surface are still O_2^- but NO_2 gas molecules interact directly with tin ionic sites instead of reacting with O_2^- species.

$$O_2^- \rightarrow 2O^- + e^-$$

Physisorbed nitrogen dioxide molecules forms new surface acceptor levels deeper than surface oxygen ions. Therefore, bound electron is transferred from O_2^- ion to physisorbed NO_2 molecule [30].

$$NO_2 + e^- \rightarrow NO_2^- \text{ (ad)}$$

$$NO_2 + Sn^{2+} \xrightarrow{\text{adsorption}} (Sn^{3+} - NO_2^-) \xrightarrow{\text{desorption}} (Sn^{3+} - O^-) + NO$$

$$2(Sn^{3+} - O^-) \xrightarrow{\text{desorption}} 2Sn^{2+} + O_2$$

During adsorption, NO_2 gas molecules attack the available free Sn sites on the sensor surface and take away electrons from the conduction band of SnO_2 forming NO_2^- species. The reduction in the concentration of charge carriers in the conduction band of SnO_2 results in an increase in sensor resistance (R_g) as observed in the present study. With the incorporation of Pt, Ag and CuO, the numbers of atmospheric adsorbed species increases which leads to enhancement in sensing response. The maximum sensing response has been obtained for SnO_2-Pt sensor structure and this may be attributed to the fact that the work function of Pt (6.35 eV) is higher than SnO_2 (4.35 eV), Ag (4.73 eV) and CuO (5.2 eV). Thus, because of higher work function space charge reason is higher at SnO_2-Pt interface. The larger space charge region may lead to absorption of more oxygen species from atmosphere which participates in reaction when NO_2 gas interacts with sensor surface. Regarding the low response of Ag doped SnO_2 thin film it may be attributed that as Ag has higher conductivity with respect to Cu and Pt [31], therefore its doping in SnO_2, decreases the resistance and as a result response after exposing to oxidizing gas is also decreased.

Fig. 5.6 shows the variation of response time of pure SnO_2, SnO_2-Pt, SnO_2-Ag and SnO_2-CuO thin film sensors with operating temperatures. From figure it may be seen that at a temperature of 90 ºC, the pure SnO_2 thin film sensor responses in 250 sec while SnO_2-Pt, SnO_2-Ag and SnO_2-CuO doped thin film sensor show their responses in 10, 89 and 26 sec towards 20 ppm NO_2 gas respectively. Fig. 5.7 indicates the recovery time of SnO_2, SnO_2-Pt, SnO_2-Ag and SnO_2-CuO thin film sensors, when NO_2 gas is flushed out from gas test chamber. From Fig. 5.7 it is clear that at a temperature of 90 ºC, the recovery time of pure SnO_2 thin film is 355 sec whereas SnO_2-Pt, SnO_2-Ag and SnO_2-CuO thin films have the recovery times as 15, 186 and 50 sec respectively. Furthermore, response and recovery times are seen to be reducing with increasing operating temperature. This may be attributed to the fact that at higher temperatures, the rate of adsorption and desorption of gases increases.

5.4 Conclusion

NO_2 gas sensors operating at a low operating temperature of 90 ºC were fabricated by doping Pt, Ag and CuO into SnO_2 thin film using chemical route. The maximum sensing response of about 183 at a low operating temperature of 90º C towards 20 ppm of NO_2 gas was obtained for SnO_2-Pt sensor structure with a fast response and recovery times of 5 sec and 13 sec respectively. However, the sensing responses of 52 and 95 were observed for SnO_2-Ag and SnO_2-CuO sensor structures respectively towards 20 ppm of NO_2 gas at the same operating temperature with response and recovery times of about 85 sec and 186 sec; 25 sec and 50 sec respectively. The enhanced sensing response obtained by incorporation of Pt in SnO_2 has been attributed to the better surface morphology of film and lowest band gap of material as compared to others.

References:

[1] J.Y. Kim, J.W. Cho, S. H. Kim, The characteristic of the ZnO nanowire morphology grown by the hydrothermal method on various surface-treated seed layers, Materials Letters 65 (2011) 1161-1164.

[2] S.W. Choi, J.Y. Park, S.S. Kim, Growth Behavior and Sensing Properties of Nanograins in CuO Nanofibers, Chemical Engineering Journal 172 (2011) 550-556.

[3] J.Y. Park, D.E. Song, S.S. Kim, An approach to fabricating chemical sensors based on ZnO nanorod arrays, Nanotechnology 19 (2008) 105503.

[4] A. Kolmakov, D.O. Klenov, Y. Lilach, S. Stemmer, M. Moskovits, Enhanced Gas Sensing by Individual SnO_2 Nanowires and Nanobelts Functionalized with Pd Catalyst Particles**,** Nano Letters 5 (2005) 667-637.

[5] J.Y. Park, S.W. Choi, S.S. Kim, A synthesis and sensing application of hollow ZnO nanofibers with uniform wall thicknesses grown using polymer templates, Nanotechnology 21 (2010) 475601.

[6] C.W. Na, H.S. Woo, I.D. Kim, J. H. Lee, Selective detection of NO_2 and C_2H_5OH using a Co_3O_4-decorated ZnO nanowire network sensor, Chemical Communications 47 (2011) 5148-5150.

[7] S.W. Choi, S.H. Jung, J.Y. Park, S.S. Kim, Improvement in Sensing Properties of SnO_2 Nanowires by Functionalizing with Pt Nanodots Synthesized by γ-Ray Radiolysis, J. Nanoscience and Nanotechnology 12 (2012) 1526-1529.

[8] H.Y. Lai, C.H. Chen, Highly sensitive room-temperature CO gas sensors: Pt and Pd nanoparticle-decorated In_2O_3 flower-like nanobundles, Journal of Materials Chemistry 22 (2012) 13204-13208.

[9] A. Rosental, A. Tarre, A. Gerst, T. Uustare, V. Sammelselg, Atomic-layer chemical vapor deposition of SnO_2 for gas-sensing applications, Sens. Actuator B: Chem.,77 (2001) 297-300.

[10] A.Z. Adamyan, Z.N. Adamyan, V.M. Aroutiounian, A.H. Arakelyan, K.J. Touryan, J.A. Turner, Sol-gel derived thin-film semiconductor hydrogen gas sensor, International Journal of Hydrogen Energy 32 (2007) 4101-4108.

[11] A. Sharma, M. Tomar, V. Gupta, SnO_2 thin film sensor with enhanced response for NO_2 gas at lower temperatures, Sens. Actuator B: Chem.,156 (2011) 743-752.

[12] G. Korotcenkov, V. Brinzari, J. Schwank, M. DiBattista, A. Vasiliev, Peculiarities of SnO_2 thin film deposition by spray pyrolysis for gas sensor application, Sens. Actuator B: Chem., 77 (2001) 244-252.

[13] S. Habibzadeh, A.A. Khodadadi, Y. Mortazavi, CO and ethanol dual selective sensor of Sm_2O_3-doped SnO_2 nanoparticles synthesized by microwave-induced combustion, Sens. Actuator B: Chem., 144 (2010) 131-138.

[14] P. Sun, W. Zhao, Y. Cao, Y. Guan, Y. Sun, G. Lu, Porous SnO_2 hierarchical nanosheets: hydrothermal preparation, growth mechanism, and gas sensing properties, Cryst Eng Comm 13 (2011) 3718-3724.

[15] W.S. Kim, B.S. Lee, D.H. Kim, H.C. Kim, W.R. Yu, S. H. Hong, SnO_2 nanotubes fabricated using electrospinning and atomic layer deposition and their gas sensing performance, Nanotechnology 21 (2010) 245605-245611.

[16] A. Kock, A. Tischner, T. Maier, M. Kast, C. Edtmaier, C. Gspan, G. Kothleitner, Atmospheric pressure fabrication of SnO_2-nanowires for highly sensitive CO and CH_4 detection, Sens. Actuator B: Chem.,138 (2009) 160-167.

[17] J. Zhang, S. Wang, Y. Wang, Y. Wang, B. Zhu, H. Xia, X. Guo, S. Zhang, W. Huang, S. Wu, NO_2 sensing performance of SnO_2 hollow-sphere sensor, Sens. Actuator B: Chem., 135 (2009) 610-617.

[18] S. Mosadegh Sedghi, Y. Mortazavi, A. Khodadadi, Low temperature CO and CH_4 dual selective gas sensor using SnO_2 quantum dots prepared by sonochemical method, Sens. Actuator B: Chem.,145 (2010) 7-12.

[19] R.K. Sonker, A. Sharma, Md. Shahabuddin, M. Tomar, V. Gupta, Low temperature sensing of NO_2 gas using SnO_2-ZnO nanocomposite sensor, Adv. Mat. Lett. 4 (2013) 196-201.

[20] S.W. Choi, S. S. Kim, Platinum nanoparticle-functionalized tin dioxide nanowires via radiolysis and their sensing capability, Journal of Materials Research 27 (2012) 1688-1694.

[21] Q. Xiang, G. Meng, Y. Zhang, J. Xu, P. Xu, Q. Pan, W. Yu, Ag nanoparticle embedded-ZnO nanorods synthesized via a photochemical method and its gas-sensing properties, Sens. Actuator B: Chem.,143 (2010) 635-640.

[22] A. Chowdhuri, V. Gupta, K. Sreenivas, R. Kumar, S. Mozumdar, P.K. Patanjali, Response speed of SnO_2-based H_2S gas sensors with CuO nanoparticles, Appl. Phys. Lett. 84 (2004) 1180-1182.

[23] R. Rella, A. Serra, P. Siciliano, L. Vasanelli, G. De, A. Licciulli, A. Quirini, Tin oxide-based gas sensors prepared by the sol-gel process, Sens. Actuator B: Chem., 44 (1997) 462-467.

[24] T. Herricks, J. Chen, Y. Xia, Polyol synthesis of platinum nanoparticles: control of morphology with sodium nitrate, Nano Lett. 4 (2004) 2367-2371.

[25] F.N. Meng, Xin-P. Di, H.W. Dong, Y. Zhang, Chun-Ling Zhu, C. Li, Yu-Jin Chen, ppb H_2S gas sensing characteristics of Cu_2O/CuO sub-microspheres at low-temperature, Sens. Actuator B: Chem.,182 (2013) 197-204.

[26] J.I. Hussain, S. Kumar, A.A. Hashmi, Z. Khan, Silver nanoparticles: preparation, characterization, and kinetics, Adv. Mat. Lett. 2 (2011) 188-194.

[27] I. Kocemba, J. Rynkowski, The influence of catalytic activity on the response of Pt/SnO_2 gas sensors to carbon monoxide and hydrogen, Sens. Actuators B: Chem., 155(2011) 659-666.

[28] Y.Y. Choi, K.H. Choi, H. Lee, H. Lee, J.W. Kang, H.K. Kim, Nano-sized Ag-inserted amorphous $ZnSnO_3$ multilayer electrodes for cost-efficient inverted organic solar cells, Solar Energy Materials and Solar Cells, 95 (2011) 1615-1623.

[29] W. Zhou, M. Tan, Synthesis and optical properties of SnO_2-CuO nanocomposite, Optik, 123 (2012) 2171-2173.

[30] S.T. Shishiyanu , T.S. Shishiyanu, O.I. Lupan, Novel NO_2 gas sensor based on cuprous oxide thin films, Sens. Actuator B: Chem., 113 (2006) 468-476.

[31] http://eddy-current.com/conductivity-of-metals-sorted-by-resistivity/

Figures:

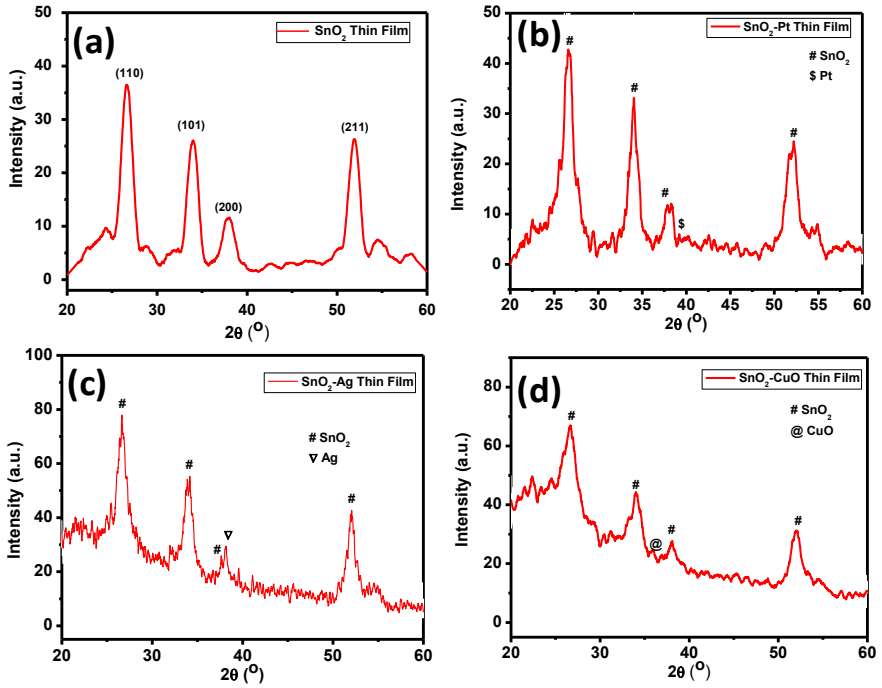

Fig. 5.1: XRD Pattern of SnO_2, SnO_2-Pt, SnO_2-Ag and SnO_2-CuO thin film

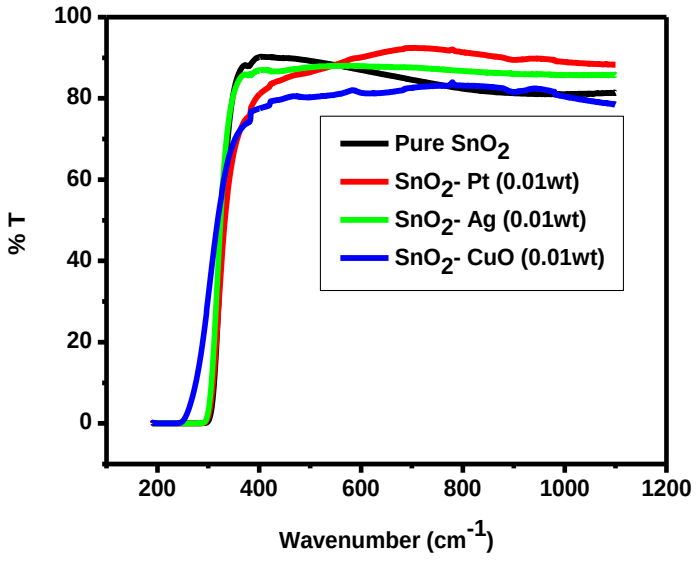

Fig. 5.2: UV-Visible Transmittance spectra of pure SnO_2, SnO_2-Pt, SnO_2-Ag and SnO_2-CuO thin films

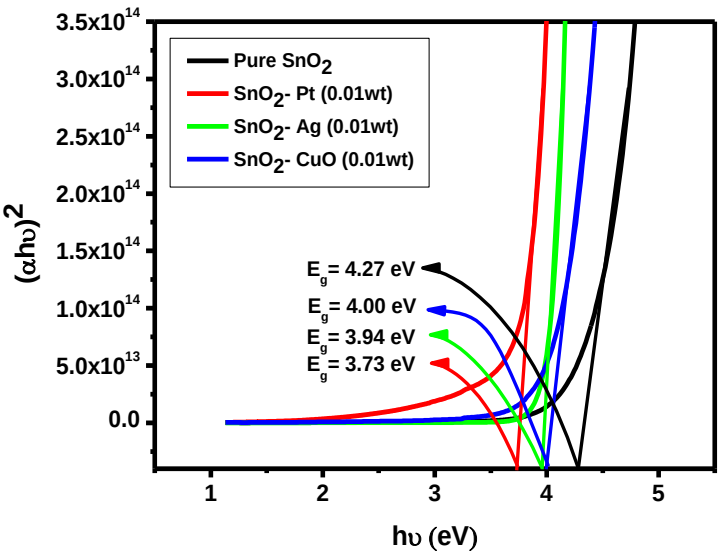

Fig. 5.3: Tauc plot of $[(\alpha h\upsilon)^2$ vs. $h\upsilon]$ of pure SnO_2, $SnO\upsilon_2$-Pt, SnO_2-Ag and SnO_2-CuO thin films

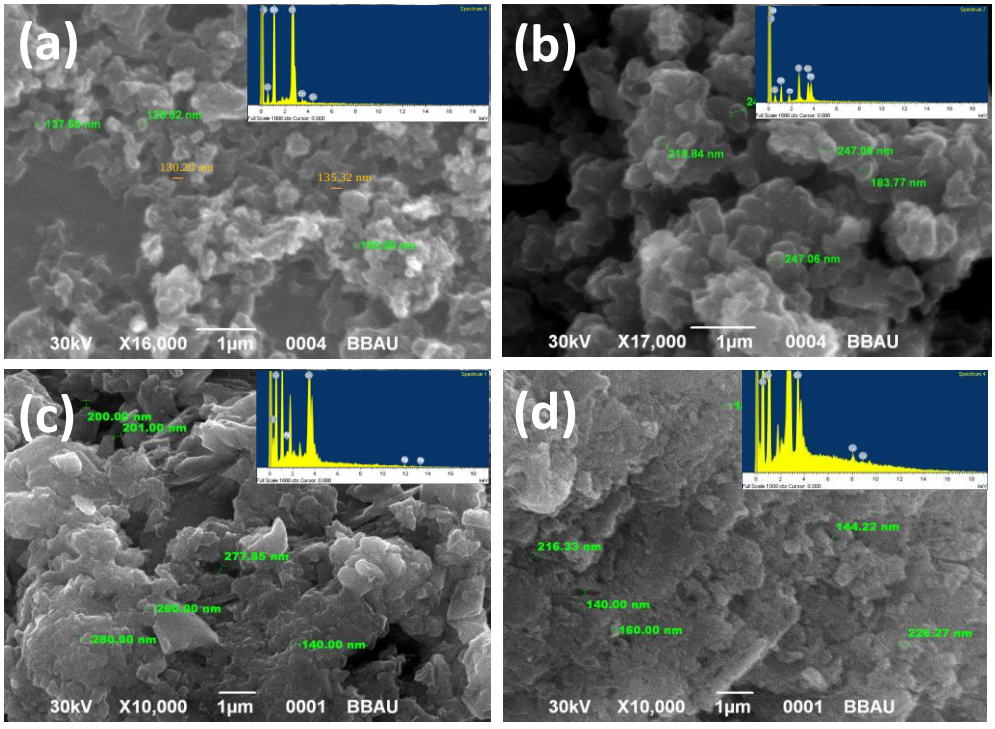

Fig. 5.4: SEM image of the surface SnO_2, SnO_2- Pt, SnO_2- Ag and SnO_2- CuO thin films sensor

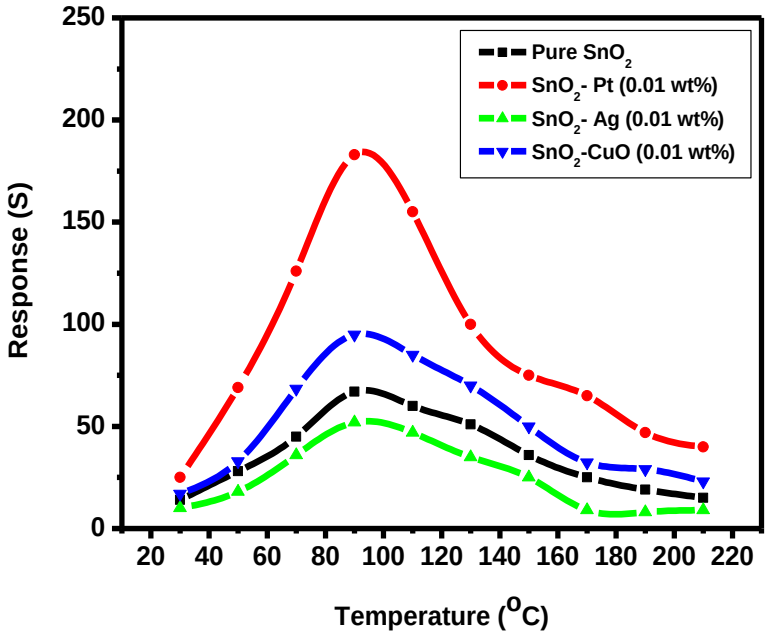

Fig. 5.5: Variation in sensing response of pure SnO_2, SnO_2-Pt, SnO_2-Ag and SnO_2-CuO thin film sensors as a function of temperature towards 20 ppm of NO_2 gas

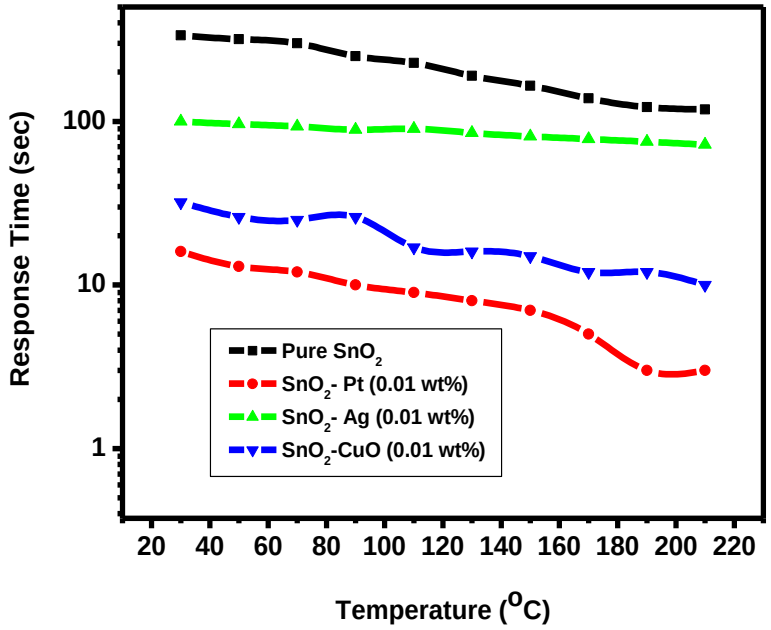

Fig. 5.6: Variation in response time of the pure SnO_2, SnO_2-Pt, SnO_2-Ag and SnO_2-CuO thin film sensors

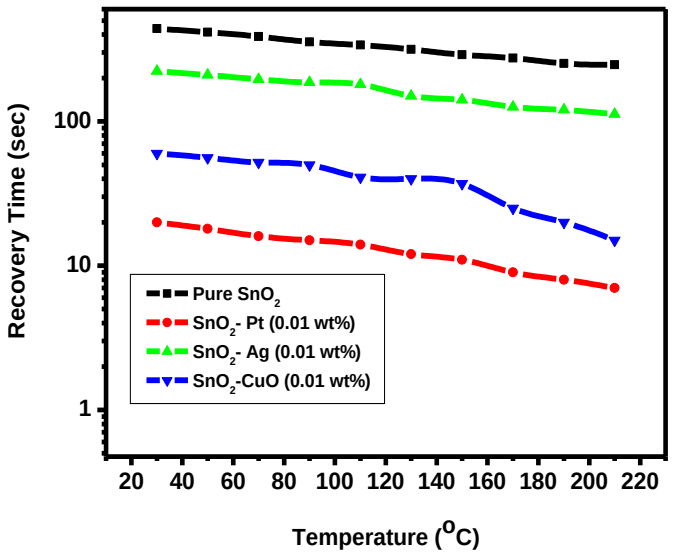

Fig. 5.7: Variation in recovery time of the pure SnO_2, SnO_2-Pt, SnO_2-Ag and SnO_2-CuO thin film sensors

Table 5.1: Average pore sizes of materials

S. No.	**Material**	**Pore Size (nm)**	**Average Pore Size (nm)**
1	SnO_2	137, 125, 100, 130, 135	125
2	SnO_2-Pt	218, 247, 247, 183, 240	227
3	SnO_2-Ag	200, 201, 277, 260, 140	215
4	SnO_2-CuO	216, 140, 160, 144, 266	177

Chapter 6

Design and fabrication of tin oxide-polyaniline nanocomposite thin films and their employment as nitrogen oxide gas sensor

A novel sensor structure has been fabricated by incorporating polyaniline (PANI) into SnO_2 sensing film using chemical route and exploited for room temperature detection of NO_2 gas. Amongst different concentration of PANI incorporated into SnO_2 thin film, 1% PANI was found to give maximum sensing response (~ 2.58×10^2) at room temperature towards 20 ppm of NO_2 gas with modulated response and recovery time of about 5.8 min and 4.55 min respectively. The structural, morphological and optical properties of the prepared sensor structures have been revealed by X-ray diffraction (XRD), Scanning Electron Microscope (SEM), Transmission Electron Microscope (TEM), Fourier transform infrared spectroscopy (FTIR) and UV-Visible spectroscopy.

6.1 Introduction

Nitrogen dioxide (NO_2) is important to be detected because it is flammable, toxic and dangerous, even in very low concentration (~20 ppm). NO_2 can be produced by many of the processes like automobile exhaust fumes, production of nitric acid, the combustion of coal and fuel, etc. [1]. Nowadays, NO_2 is one of the most hazardous polluting gases to the atmosphere in urban areas. Moreover, the chemical reaction of NO_2 gas with water vapor would cause acid rain [2]. Therefore, the development of a NO_2 gas sensor for environmental monitoring has become a very important task. Semiconducting tin oxide (SnO_2) has been proven to be one of the most attractive sensing materials for gas sensor applications, owing to its suitable physical–chemical properties, and possibility to detect many reducing and oxidizing gases with high response [3-8]. However, most of the NO_2 gas sensors based on SnO_2 thin film and nanostructures lack high sensitivity and operate at high temperature (300-500˚C). Thus, SnO_2 nanostructures doped with metal/metal oxides could improve the sensing response characteristics with high specificity at low operating temperature [9].

Recently, several organic semiconductors, such as polyaniline(PANI), polypyrrole (PPy), polythiophene (PTh) and metal substituted phthalocyanines (MSPs) have been explored for detecting toxic gases (such as NO_2, SO_2, O_3 etc.) [10-15]. As one kind of conducting polymers, PANI and its derivatives, have received considerable attention for their low operating temperature, low cost, easy preparation, and very good thermal stability [16-17]. However, PANI still exhibits some shortcomings as gas sensitive materials, including low sensitivity, irreversible response, unsatisfying long-time stability and poor selectivity [18]. In order to overcome these disadvantages, hybrid composite of organic-inorganic materials as sensing element are intensively investigated worldwide [18-21]. Wu et al. have fabricated PANI/SnO_2 hybrid material by hydrothermal route and exploited for the detection of ethanol and acetone gas. It was observed that the PANI/SnO_2 hybrid material could overcome the shortcomings of slow response time of PANI and the high operating temperature of SnO_2 [18]. Jiang et al. reported that PANI/titanium nanocomposite thin film revealed higher sensor response, least response and recover rates to NH_3 than those of a pure PANI film [21]. Thus, in the present work,

an effort has been made to develop SnO_2-PANI nanocomposite thin film based sensor for efficient detection of NO_2 gas at room temperature. For comparison, pure SnO_2 based sensor has also been investigated.

6.2 Experimental

6.2.1 Sensor Preparation

Tin (IV) chloride pentahydrate ($SnCl_4.5H_2O$), isopropanol, propanol, aniline, HCl, ammonium persulphate and ammonium hydroxide used for the sensor preparation were purchased from Sigma Aldrich Chemical Co. with 99.99% purity. A mixture of 12.37 g tin tetrachloride ($SnCl_4.5H_2O$) with 15 g isopropanol was prepared. As this was an exothermic reaction, hence the solution was cooled down to room temperature and 3.42 g water in 10 g propanol mixture was added for hydrolysis reaction forming the sol of SnO_2 nanoparticles [22].

50 ml of conc. HCl was added to 500 ml of distilled water in a beaker marked as A. 331 ml of distilled water was taken into it and 18.924 g of Ammonium persulphate was added with stirring in another beaker marked as B. To beaker A, 8.33 ml of aniline was added and stirred for 20 min in ice bath. Ammonium persulphate solution was then added drop wise (15 s between 2 drops) to the above solution with continuous stirring. After complete addition, the solution was left overnight and then filtered. The precipitate was washed with water repeatedly till the filtrate became colorless and after washing, it was left overnight. The precipitate was then dried at 40-50 ºC and made into fine powder. The fine powder was then washed with methanol, refluxed for 4-5 h at 40-50 ºC. It was again dried at 40-50 ºC to obtain Emeraldine salt of PANI. To un-doped Emeraldine salt, it was washed with ammonium hydroxide solution, filtered and dried to obtain Emeraldine base of PANI [23].

PANI was prepared by polymerization of aniline. For this process acids (HCl) was used which acts as dopant for PANI molecules and bound with the central N atom of aniline molecule like $H^+ - N - Cl^-$. At room temperature in equilibrium, the positive charge of bonded hydrogen shifts on N atom making the structure looks like $H - N^+ - Cl^-$. While the negative charge on Cl^- is retained with it and remains localized, the

positive charge on N atom becomes mobile charge in PANI matrix via its other bonds making the PANI as a p-type semiconductor.

6.2.2 Preparation of SnO_2-PANI composite thin film

The prepared PANI (0.061 g) was added to SnO_2 colloidal in 1% and 3% concentration solution. The SnO_2-PANI composite solution was sintered at 80 ºC in air for 2 h. SnO_2 colloidal solution and SnO_2-PANI composite solution were used to deposit respective thin films on corning glass and platinum (Pt) inter digital electrode (IDEs) patterned corning glass substrates by spin coating technique. The Pt IDEs were patterned over the corning glass substrates using conventional photolithography technique prior to deposition of sensing layers [24]. After every coating, the samples were pyrolized at 80 ºC to evaporate the precursor. Thickness of all films was kept 600 nm. In the present work thin film prepared using SnO_2 colloidal solution and PANI doped SnO_2 solutions were named as pure SnO_2 and PANI-SnO_2 respectively.

Thickness of deposited thin films was measured using a VeecoDektak 150 surface profiler. Crystalline structure and surface morphology of SnO_2-PANI composite thin films were studied using Bragg-Brentano (θ-2θ) scan of a X-ray Diffractometer (Bruker D8 Discover) with the CuKα1 source (λ = 0.154 nm) and transmission electron microscopy (TEM: Tecnai G2, at 300 kV) respectively. FT-IR spectrum was recorded on a Frontier 88277 FT-IR spectrophotometer to identify one bond formation and the presence of impurities. A Double Beam UV–visible Spectrophotometer (Perkin Elmer, Lambda 35) was used to study the optical properties of pure SnO_2 and SnO_2-PANI composite thin films.

6.2.3 Gas sensing characteristics measurement

The sensing response characteristics of pure SnO_2 and SnO_2-PANI composite thin films were studied using Pt IDEs as shown in Fig. 6.1(a) and interaction of NO_2 gas molecules on the film surface is as shown in Fig. 6.1(b). NO_2 gas sensing characteristics of the sensors were studied in a specially designed “gas sensor test rig (GSTR)” having a glass test chamber. Commercially procured NO_2 gas of defined concentration was introduced into the glass test chamber using calibrated leaks through needle valves.

Volume of the test chamber was taken to be 11.0 L and target NO_2 gas was injected in the test chamber through a syringe of 0.2 ml at the time of taking response for 20 ppm of NO_2 gas. A pirani gauge with a rotary pump was used to control the flow of target gas in the test chamber. Vacuum of the order of $\sim 10^{-3}$ Torr was first created in the test chamber and subsequently a mixture of the known concentration of target gas and clean (dry synthetic) air was introduced till the test chamber acquired the atmospheric pressure to ensure that the target gas was free from any other disturbing gas. Gas sensing characteristics of prepared sensor structures were measured as a function of temperature (30-120 ºC) towards 20 ppm of analyte gas (NO_2). At each temperature the sensor was first stabilized in air to obtain a stable resistance value. NO_2 gas (20 ppm) was introduced into the glass bell jar and changes in the sensor resistance were recorded every second using a data acquisition system consisting of a digital multi-meter (DMM model: Keithley 2700) interfaced with a computer. While doing the sensing response experiment, humidity in the test chamber was maintained at 30 %RH. Target gas (NO_2) of specific concentration (20 ppm) was introduced into the test chamber and changes in the sensor resistance were recorded after every second. Sensor Response, Response and Recovery time, hysteresis, selectivity and other parameters were observed and respective data were plotted.

6.3 Results and Discussion

6.3.1 Crystal structural of SnO_2 nanoparticles and PANI

Fig. 6.2 (a) & (b) shows the XRD patterns of pure SnO_2 and SnO_2-PANI (1%) composite thin film. It can be seen from Fig. 6.2(a) that the peaks observed at 2θ = 26.39º, 33.74º, 37.78º and 51.72º correspond to reflection plane (110), (101), (200) and (211) of rutile structure of SnO_2 respectively [25], whereas, the peaks observed at 2θ = 26.74º, 33.72º, 37.89º and 51.55º in Fig. 6.2 (b) correspond to (110), (101), (200) and (211) reflection planes of SnO_2 respectively and reflection peak observed at 2θ = 17.59º corresponds to (100) plane of PANI confirming the presence of PANI and SnO_2 in SnO_2-PANI composite thin film [26]. Furthermore, degradation of film crystallinity on incorporating PANI into the composite thin film may also be seen from the XRD shown in Fig. 6.2(b). Crystallite size of pure SnO_2 and SnO_2-PANI (1%) composite thin films

were estimated using well known Scherer's formula along the dominant (110) reflection plane. The crystallite size of pure SnO_2 thin film was found to be ~ 7.05 nm. With the incorporation of PANI into SnO_2 the crystallite size was found to decrease to ~ 5.64 nm for SnO_2-PANI composite thin film. The decrease in crystallite size with incorporation of PANI may be attributed to the generation of stress which can also be observed from the shift in the XRD peak positions of SnO_2 on incorporating PANI into the composite thin films.

6.3.2 Thermo Gravimetric Analysis (TGA)

Fig. 6.3 shows the TGA curves of SnO_2 and PANI-SnO_2 composites. It is clearly observed that all the volatile precursors were completely removed below 300 ^oC, which resulted in the formation of SnO_2 and SnO_2-PANI composite. The presence of PANI in SnO_2-PANI composite shows an increase in the degradation temperature of SnO_2. The TG analysis showed that the isopropanol and the water start evaporating at 110 °C while the remaining organic compounds are removed up to 280 °C. Loss of precursor becomes prominent at a temperature of 300 °C. It can be observed from the TG analysis that after the annealing of SnO_2 and SnO_2-PANI composite samples at 300 ^oC, the difference between the weight percentages remains 1% which clearly indicates the presence of 1% PANI in SnO_2-PANI composite sample. Thus the PANI-SnO_2 composite is more thermally stable compared to SnO_2.

6.3.3 FT-IR spectroscopy of SnO_2-PANI composite thin film

To find out the nature of bonding in the thin film material of SnO_2-PANI, FT-IR spectra of the sample (SnO_2-PANI having 1% PANI doping) was obtained in the transmission range of 500 to 4000 cm^{-1} and is shown in Fig. 6.4. The absorption peaks at 1460, 1300, 1130 and 1048 cm^{-1} corresponds to PANI confirming its presence in the composite thin film. The peak at 1460 cm^{-1} is attributed to C=C stretching mode for the benzenoid ring while peak at 1300 cm^{-1} correspond to N–H bending vibrations. The peaks at 1130 and 1048 cm^{-1}can be attributed to the in-plane and out-of-plane C–H bending, respectively. However, the absorption peaks at 1630, 811 and 559 cm^{-1} corresponds to N–H vibration, Sn–OH and Sn–O–Sn bands respectively [27-28]. Thus,

after incorporation of PANI into SnO_2 thin film, some electronic interaction is taking place between PANI and SnO_2.

6.3.4 Optical characterization of composite thin film

The optical transmission spectra of the pure SnO_2, SnO_2-PANI (1%) and SnO_2-PANI (3%) thin films deposited separately on corning glass substrates were measured in the wavelength range of 190 to 1100 nm, and is shown in Fig. 6.5. It can be observed that pure SnO_2 thin film exhibits a high transmission (>85%) in the visible region and show a sharp fundamental absorption edge in UV region at 380 nm. However, with the incorporation of 1% PANI and 3% PANI, transmission reduces to about 40% and 53% respectively in the visible region.

Optical band gap of SnO_2 thin film deposited on corning glass substrate, was calculated from the intercept on energy axis obtained by extrapolating the linear portion of the Tauc plot of $(\alpha h\nu)^2$ *vs* photon energy ($h\nu$). Estimated value of band gap for as-grown SnO_2 thin film is found to be 3.95 eV and is close to the reported values for SnO_2 thin films (3.6 eV) grown by various techniques [24]. The value of band-gap was found to increase slightly for SnO_2-PANI composite thin film with the incorporation of PANI in range 4.0 eV to 4.03 eV as tabulated in the table shown in the inset of Fig. 6.5. Thus with increasing the concentration of PANI from 1% to 3%, the band-gap of SnO_2 thin film increases slightly which may be correlated with electronic transition between conduction band of SnO_2 and PANI.

6.3.5 TEM and SEM analysis

Fig. 6.6 (a) & (b) shows the TEM images of SnO_2 nano-particles and SnO_2-PANI nano-composite loaded over carbon coated copper grids. Fig. 6.6(a) shows the SnO_2 nano-particles of diameter ~100 nm found in the colloidal solution whereas Fig. 6.6(b) shows a homogeneous, porous composite structure that is uniformly distributed. The dark region in Fig. 6.6(b) indicates the PANI region whereas the lighter spherical regions indicate the SnO_2 particles. The spherical particles with blurry boundaries are SnO_2 enwrapped by PANI [28]. Fig. 6.7 shows the SEM image of the SnO_2-PANI composite

film indicating that the composite thin films possess a regular porous surface. The average pore size was found as 152 nm.

6.3.6 Gas sensing characteristics

Fig. 6.8 shows the variation in sensing response of pure $SnO_2$and SnO_2-PANI (1 % and 3 %) sensing elements towards 20 ppm NO_2 gas as a function of temperature. Sensing response of all sensor structures have been optimized with temperature. From Fig. 6.8, it can be seen that the pure SnO_2 thin film sensor structure shows the maximum sensing response of 130 at an operating temperature of 70 °C towards 20 ppm of NO_2 gas, whereas, with the incorporation of 1% PANI into SnO_2 thin film, the sensor structure shows the maximum sensing response of ~258 at an operating temperature of 30 °C. When the concentration of PANI is further increased to 3%, the sensing response reduces to ~ 80 at a comparatively higher operating temperature of 90 °C. Thus, the appropriate amount of PANI plays a crucial role in reducing the operating temperature. This may be attributed to the fact that PANI is very well known to exhibit p-type and SnO_2 the n-type conductivity [29], so there is a possibility of the formation of p-n junction at the interface of PANI and SnO_2 nano-particles. When exposed to NO_2 gas, PANI/SnO_2 sensor shows an enhancement in the resistance. A space charge region is formed at the p-n junction of SnO_2 with PANI which increases in the presence of NO_2 gas enhancing the sensor resistance as NO_2 gas molecules trap free electrons from SnO_2 surface, thereby increasing the resistance of sensor structure as exposure to NO_2 gas. However, when PANI is incorporated in higher concentration (i.e. 3%) in SnO_2 thin film, the PANI nano-particles block the interaction of NO_2 gas molecules with the SnO_2 nano-particle surface with trap free electrons, which hinders the modulation of space charge region, thereby, giving lesser change in resistance of SnO_2-PANI (3%) sensor structure leads to poor sensing response. From Fig. 6.8, it is also observed that the SnO_2-PANI (1%) composite thin film sensor shows the sensing response of ~258 at room temperature whereas the pure SnO_2 thin film and SnO_2-PANI (3 %) composite thin film sensors show the poor response of about 40 and 16 at room temperature towards NO_2 gas. The humidity effect on sensor structure based on SnO_2-PANI (1%) composite thin film was studied by exposing the

sensor to different humidity environment (20 %RH to 70 %RH) and found that the sensor showed negligible effect towards humidity.

Fig. 6.9 (a) & (b) shows the transient response of SnO_2-PANI (1%) composite thin film sensor at room temperature and 50 ^oC towards 20 ppm NO_2 gas respectively. It can be observed from Fig. 6.9 that with the exposure of NO_2 gas to the sensing film surface the sensor resistance increases from 2.51 MΩ to 649 MΩ (sensing response = 258). The response time and recovery time of the sensor were observed to be 5.8 and 4.55 min respectively at room temperature, whereas, from Fig. 6.9(b) it can be observed that at slightly higher temperature of 50 °C the sensing response has been reduced to 130 but the reduced response and recovery times of 3.73 min and 2.81 min have been obtained respectively.

Fig. 6.10 shows the variation of response time of pure SnO_2 thin film and SnO_2-PANI (1 % and 3 %) composite film with substrate temperature. From Fig.10 it is visualized that at room temperature the SnO_2-PANI (1%) composite thin film gave response in 5.8 min while SnO_2-PANI (3%) composite thin film and pure SnO_2 film showed the response time of 8 and 13.7 min towards 20 ppm NO_2 gas respectively. Fig. 6.11 indicates the recovery time of pure SnO_2 film and SnO_2-PANI (1% and 3%) composite thin film sensors, when NO_2 gas is flushed out from gas test chamber. From Fig. 6.10 it is clear that at room temperature the recovery time of SnO_2-PANI (1%) film is 4.55 min, whereas SnO_2-PANI (3%) composite thin film and pure SnO_2 thin films have the recovery times as 4.03 and 22.13 min respectively. Furthermore, response and recovery times are found to be reducing with temperature. This may be attributed to the fact that at higher temperatures the rate of adsorption and desorption of gases increases. So, SnO_2-PANI (1%) composite thin film sensor is seen to be exhibiting better sensing properties compared to the other two structures.

The issue of slow response and recovery time can be overcome if the sensor works at higher operating temperature because at higher temperatures the rate of adsorbtion and desorption of gases at sensor surface becomes fast which reduces the response and recovery times. As observed in SnO_2-PANI (1%) composite thin film, the response time (5.8 min) and recovery time (4.55 min) have been improved at higher

operating temperatures (≥ 60 °C). The room temperature operation with high response (258) is attractive for the sensor developed in the present case. The observed response (5.8 min) and recovery (4.55 min) times are much better than those reported by many workers [27, 30-42]. Table 1 summarizes few reports available in literature on the detection of NO_2 gas. Jimenez et al. have reported the sensing response of SnO_2 thin film of about 4 towards 2 ppm of NO_2 gas at an operating temperature of 250 °C with poor response and recovery times of about 16 and 25 min respectively [30]. Hyodo et al. have the sensing response characteristics of macroporous SnO_2 thick film and reported the response of 500 towards 100 ppm NO_2 gas with slow response and recovery times of 20 and 40 min respectively at an operating temperature of 225 °C [32]. Leghrib et al. reported the room temperature detection of NO_2 gas, sensor response of 8 with poor response time of 10 min. towards 0.5 ppm of NO_2 gas [36]. Qin et al. (2011) have observed that the $W_{18}O_{49}$ nanowire bundles were giving the sensing response of about 648 towards 1ppm of NO_2 gas with response and recovery times of about 1.5 and 3 min respectively [43]. However, the operating temperature was observed to be 150 °C. Cho et al. (2011) also reported the high sensing response of SnO_2 hollow spheres of about 81 with fast response time of ~ 51 s at an operating temperature of ≥ 300 °C [44]. Thus the problem of fast response and recovery time could be easily overcome by increasing the operating temperatures.

Fig. 6.12 shows the selectivity of SnO_2-PANI (1%) composite thin film towards NO_2 gas. The gas sensing of SnO_2-PANI (1%) composite film was carried out by monitoring the change in electrical resistance towards different interfering gases in very high concentration (2000 ppm) including CH_4, LPG, NH_3, CO and SO_2 at room temperature. The prepared sensor was found to be highly selective towards NO_2 gas (Fig. 6.10) giving much higher increase in the sensor resistance after interaction with NO_2 gas molecules at room temperature.

SnO_2-PANI (1%) sensor structure was tested repeatedly for consecutively 2 months and was found to give almost similar response within the error of ±5%. Fig. 6.13 shows the repeatability response of SnO_2-PANI (1%) sensor structures, when continuously exposed to 20 ppm of NO_2 gas and air for four consecutive cycles at room

temperature. The sensor structures show the similar sensing response (R_a to R_g and R_g to R_a) repeatedly for four consecutive cycles towards 20 ppm NO_2 gas and air which confirms the good reproducibility of the prepared sensor structure. The observed results show the good stability of the prepared sensor in comparison to earlier reported sensor [28].

6.4 Conclusion

In the present chapter, an effort has been made to develop a SnO_2-PANI composite thin film gas sensor which responds efficiently towards NO_2 gas at room temperature. The variation of PANI concentration in SnO_2 thin film has been studied and found that 1% of PANI gives the enhanced sensing response of about 258 at room temperature (30 ºC) towards 20 ppm of NO_2 gas with moderate response and recovery time of 5.8 and 4.55 min. respectively. The possible enhancement is related to the formation of p-n junction at interface of PANI (p-type) and SnO_2 (n-type) nano-particles. The surface morphology having nanocrystalline grains are found to be important for obtaining enhanced response characteristics. Also the fabricated SnO_2-PANI (1%) sensor structure was found to be highly selective towards NO_2 gas at room temperature with enhanced sensor characteristics.

References:

[1] B.T. Marquis, J.F. Vetelino, A semiconducting metal oxide sensor array for the detection of NO_x and NH_3, Sens. Actuators B: Chem., 77 (2001) 100-110.

[2] J. Brunet, V.P. Gracia, A. Pauly, C. Varenne, B. Lauron, An optimised gas sensor microsystem for accurate and real-time measurement of nitrogen dioxide at ppb level, Sens. Actuators B: Chem., 134 (2008) 632-639.

[3] Z. Ling, C. Leach, The effect of relative humidity on the NO_2 sensitivity of a SnO_2/WO_3 heterojunction gas sensor, Sens. Actuators B: Chem., 102 (2004) 102-106.

[4] A.A. Firooz, T. Hyodo, A.R. Mahjoub, A.A. Khodadadi, Y. Shimizu, Synthesis and gas-sensing properties of nano- and meso-porous MoO_3-doped SnO_2, Sens. Actuators B: Chem., 147 (2010) 554-560.

[5] R.K. Sonker, B. C. Yadav, Chemical Route Deposited SnO_2, SnO_2-Pt and SnO_2-Pd Thin Films for LPG Detection, Adv. Sci. Lett. 20 (2014) 1023-1027.

[6] R.K. Sonker, A. Sharma, Md. Shahabuddin, M. Tomar, V. Gupta, Low temperature sensing of NO_2 gas using SnO_2:ZnO nanocomposite sensor, Adv. Mat. Lett. 4 (2013) 196-201.

[7] I. Paulowicz, V. Hrkac, S. Kaps, V. Cretu, O. Lupan, T. Braniste, V. Duppel, I. Tiginyanu, L. Kienle, R. Adelung, Y. K. Mishra, Three-Dimensional SnO_2 Nanowire Networks for Multifunctional Applications: From High-Temperature Stretchable Ceramics to Ultraresponsive Sensors, Adv. Electron. Mater. 2015, 1500081

[8] B.C. Yadav, N. Verma, S. Singh, Nanocrystalline SnO_2-TiO_2 thin film deposited on base of equilateral prism as an opto-electronic humidity sensor, Optics & Laser Technology 44 (2012) 1681-1688.

[9] B.C. Yadav, R. Singh, S. Singh, P.K. Dwivedi, Humidity sensing investigations on nanostructured zinc stannate synthesized via chemical precipitation method, Int. J. of Green Nanotechnology: Mat. Sci. Eng. 4 (2012) 1-9.

[10] D.W. Hatechett, M. Josowicz, Composites of intrinsically conducting polymers as sensing nanomaterials, Chemical Reviews 108 (2008) 746-769.

[11] U. Lange, N.V. Roznyatovskaya ,V.M. Mirsky, Conducting polymers in chemical sensors and arrays, Analytica Chimica Acta 614 (2008) 1-26.

[12] H. Bai, G.Q. Shi, Gas sensors based on conducting polymers, Sensors, 7 (2007) 267-307.

[13] M.I. Newton, T.K.H. Starke, M.R. Willis, G. McHale, NO_2 detection at room temperature with copper phthalocyanine thin film devices, Sens. Actuators B: Chem., 67 (2000) 307-311.

[14] Y.L. Lee, C.H. Chang, NO_2 sensing characteristics of copper phthalocyanine films : effects of low temperature annealing and doping time, Sens. Actuators B: Chem., 119 (2006) 174-179.

[15] C. Park, D.H. Yun, S.T. Kim, Y.W. Park, Enhancement of the NO_2-sensing capability of copper phthalocyanine by measuring the relative resistance change, Sens. Actuators B: Chem., 30 (1996) 23-27.

[16] N.G. Deshpande, Y.G. Gudage, R. Sharma, J.C. Vyas, J.B. Kim, Y.P. Lee, Studies on tin oxide-intercalated polyaniline nanocomposite for ammonia gas sensing applications, Sens. Actuators B: Chem., 138 (2009) 76-84.

[17] A.A. Athawale, S.V. Bhagwat, P.P. Katre, Nanocomposite of Pd-polyaniline as a selective methanol sensor, Sens. Actuators B: Chem., 114 (2006) 263-267.

[18] L.N. Geng, ZY.Q. hao, X.L. Huang, S.R. Wang, S.M. Zhang, S.H. Wu, Characterization and gas sensitivity study of polyaniline/SnO_2 hybrid material prepared by hydrothermal route, Sens. Actuators B: Chem., 120 (2007) 568-572.

[19] A. Choudhury, Polyaniline/silver nanocomposites: dielectric properties and ethanol vapour sensitivity, Sens. Actuators B: Chem., 138 (2009) 318-325.

[20] M.L. Singla, S. Awasthi, A. Srivastava, Humidity sensing using polyaniline/Mn_3O_4 composite doped with organic/inorganic acids, Sens. Actuators B: Chem., 127 (2007) 580-585.

[21] H.L. Tai, Y.D. Jiang, G.Z. Xie, J.S. Yu, X. Chen, Fabrication and gas sensitivity of polyaniline–titanium dioxide nanocomposite thin film, Sens. Actuators B: Chem., 125 (2007) 644-650.

[22] R.K. Sonker, A. Sharma, M. Tomar, V. Gupta, B.C. Yadav, Low Temperature Operated NO_2 Gas Sensor Based on SnO_2-ZnO Nanocomposite Thin Film, Adv. Sci. Lett. 20 (2014) 911-916.

[23] J. Stejskal, R.G. Gilbert, Preparation of a conducting polymer, Pure Appl. Chem. 74 (2002) 857-867.

[24] A. Sharma, M. Tomar, V. Gupta, SnO_2 thin film sensor with enhanced response for NO_2 gas at lower temperatures, Sens. Actuators B: Chem., 156 (2011) 743-752.

[25] R.K. Sonker, A. Sharma, M. Tomar, V. Gupta, B.C. Yadav, Nanocatalyst (Pt, Ag and CuO) Doped SnO_2 Thin Film Based Sensors for Low Temperature Detection of NO_2 Gas, Adv. Sci. Lett. 20 (2014) 1374-1377.

[26] M. Alam, A.A. Ansari, M.R. Shaik, N.M. Alandis, Optical and electrical conducting properties of Polyaniline/Tin oxide nanocomposite, Arabian Journal of Chemistry 6 (2013) 341-345.

[27] H. Xu, X. Chen, J. Zhang, J. Wang, B. Cao, D. Cui, NO_2 gas sensing with SnO_2-ZnO/PANI composite thick film fabricated from porous nanosolid, Sens. Actuators B: Chem., 176 (2013) 166-173.

[28] G. Lina, Z. Yingqiang, H. Xueliang, W. Shurong, Z. Shoumin, Wu. Shihua, Characterization and gas sensitivity study of polyaniline/SnO_2 hybrid material prepared by hydrothermal route, Sens. Actuators B: Chem., 120 (2007) 568-572.

[29] P.J. Benjamin, E. Phillip, J.E. Richard, L.H. Colin, M.R. Norman, Novel composite organic-inorganic semiconductor sensors for the quantitative detection of target organic vapours, Jour. Mater. Chem. 6 (1996) 289-294.

[30] I. Jimenez, A. Cirera, J. Folch, A. Cornet, J.R. Morante, Innovative method of pulverization caoring of prestabilized nanopowders for mass production gas sensor, Sens. Actuators B: Chem., 78 (2001) 78-77.

[31] K. Anothainart, M. Burgmair, A. Karthigeyan, M. Zimmer, I. Eisele, Light enhanced NO_2 gas sensing with tin oxide at room temperature: conductance and work function measurements, Sens. Actuators B: Chem., 93 (2003) 580-590.

[32] T. Hyodo, K. Sasahara, Y. Shimizu, M. Egashira, Preparation of macroporous SnO_2 films using PMMA microspheres and their sensing properties to NO_x and H_2, Sens. Actuators B: Chem., 106 (2005) 580-590.

[33] M.K. Ram, O. Yavuz, M. Aldissi, NO_2 gas sensing based on ordered ultrathin films of conducting polymer and its nanocomposite, Synthetic Metals 151 (2005) 77-84.

[34] X.B. Yan, Z.J. Han, Y. Yang, B.K. Tay, NO_2 gas sensing with polyaniline nanofibers synthesized by a facile aqueous/organic interfacial polymerization, Sens. Actuators B: Chem., 123 (2007) 107-113.

[35] N.M. Shaalan, T. Yamazaki, T. Kikuta, Influence of morphology and structure geometry on NO_2 gas-sensing characteristics of SnO_2 nanostructures synthesized via a thermal evaporation method, Sens. Actuators B: Chem., 153 (2011) 11-21.

[36] R. Leghrib, A. Felten, J.J. Pireaux, E. Llobet, Gas sensors based on doped-CNT/SnO_2 composites for NO_2 detectionat room temperature, Thin Solid Films 520 (2011) 966-970.

[37] D.D. Trung, N.V. Toan, P.V. Tong, N.V. Duy, N.D. Hoan, N.V. Hieun, Synthesis of single-crystal SnO_2 nanowires for NO_x gassensors application, Ceramics International 38 (2012) 6557-6563.

[38] M.A. Chougule, D.S. Dalavi, S. Mali, P.S. Patil, A.V. Moholkar, G.L. Agawane, J.H. n, V.B. Patil, Novel method for fabrication of room temperature polypyrrole-ZnO nanocomposite NO_2 sensor. Measurement 45 (2012) 1989-1996.

[39] A. Maity, S.B. Majumder, NO_2 sensing and selectivity characteristics of tungsten oxide thin films, Sens. Actuators B: Chem., 206 (2015) 423-429.

[40] N.D. Chinh, N.V. Toan, Vu Van. Quang, N. Van. Duy, N. Hoa, N. Duc, N.V. Hieu, Comparative NO_2 gas-sensing performance of the self-heated individual, multiple and networked SnO_2nanowire sensors fabricated by a simple process, Sens. Actuators B: Chem., 201 (2014) 7-12.

[41] R.K. Sonker, S.R. Sabhajeet, S. Singh, B.C. Yadav, Synthesis of ZnO nanopetals and its application as NO_2 gas sensor, Materials Letters 152 (2015) 189-191.

[42] P.H. Suman, A.A. Felix, H.L. Tuller, J.A. Varela, M.O. Orlandi, Comparative gas sensor response of SnO_2, SnO and Sn_3O_4 nanobelts to NO_2 and potential interferents, Sens. Actuators B: Chem., 208 (2015) 122-127.

[43] Y. Qin, W. Shen, X. Li, M. Hu, Effect of annealing on microstructure and NO_2-sensing properties of tungstenoxide nanowires synthesized by solvothermal method, Sens. Actuators B: Chem., 155 (2011) 646-652.

[44] N.G. Cho, D.J. Yang, M.J. Jin, H.G. Kim, H.L. Tuller, I.D. Kim, Highly sensitive SnO_2 hallow nanofiber-based NO_2 gas sensors, Sens. Actuators B: Chem., 160 (2011) 1468-1472.

Figures:

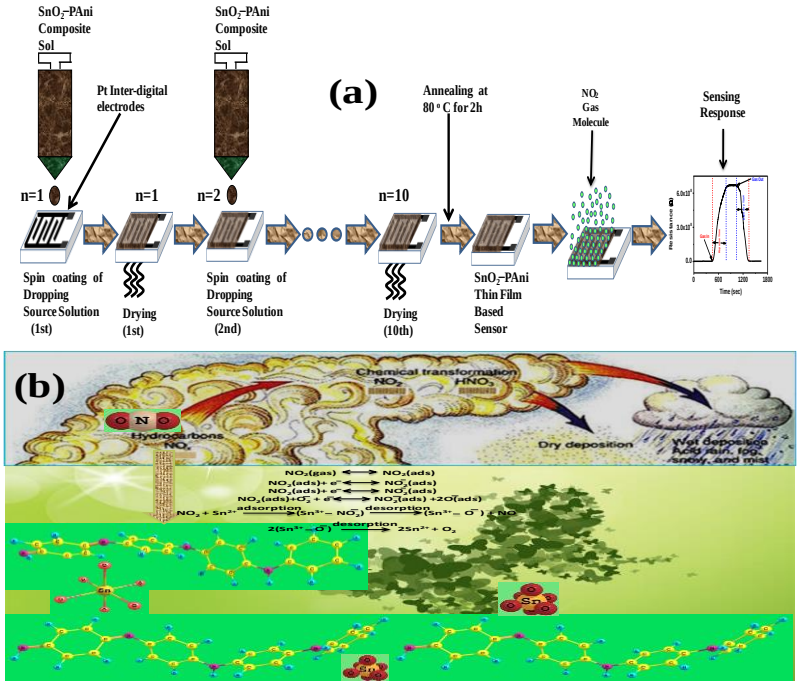

Fig. 6.1: (a) Schematic diagram of thin film deposition by spin coating and (b) Interaction of NO_2 with sensing material

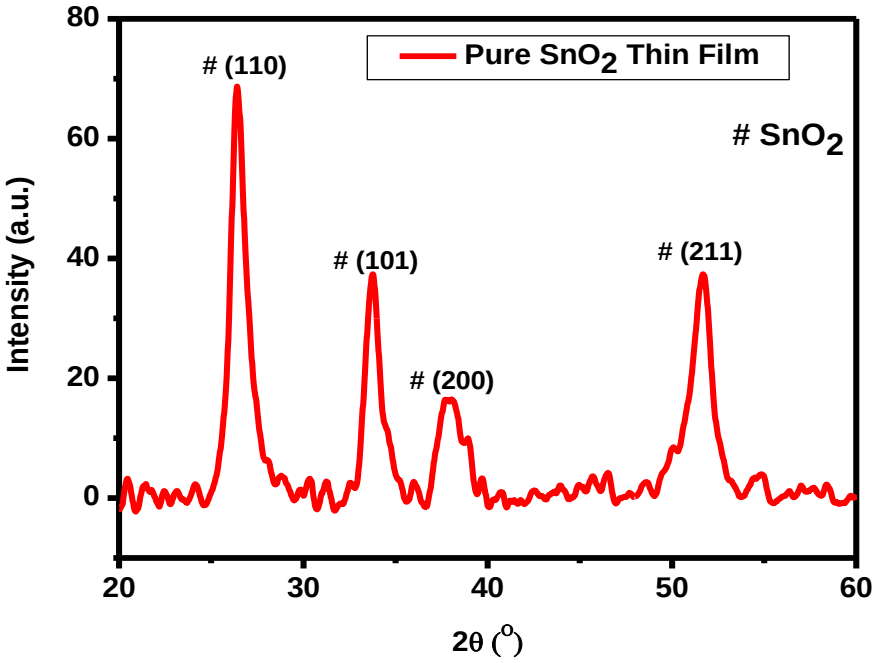

Fig. 6.2: (a) XRD patterns for SnO_2 thin film

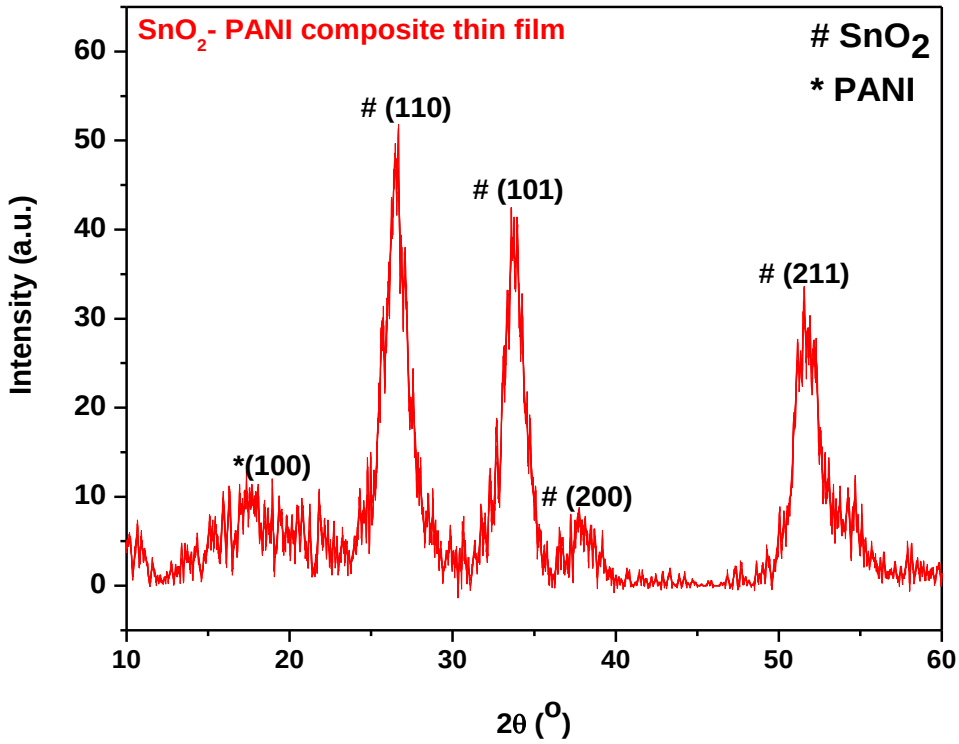

Fig. 6.2 (b): XRD patterns for SnO_2-PANI composite thin film

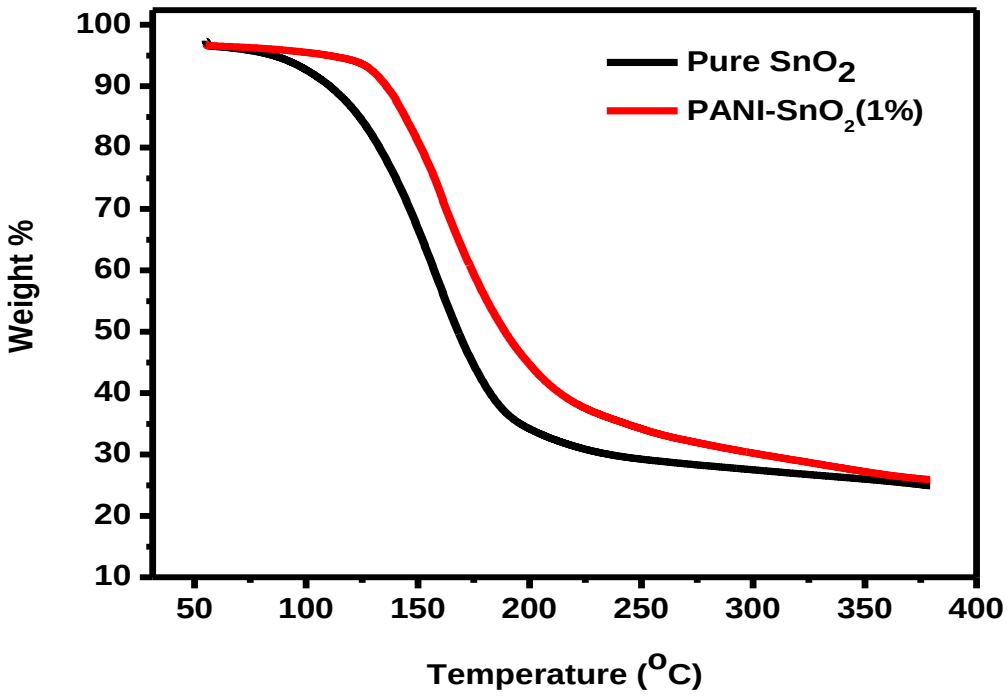

Fig. 6.3: Thermo gravimetric analysis profiles of SnO_2 and SnO_2-PANI composite

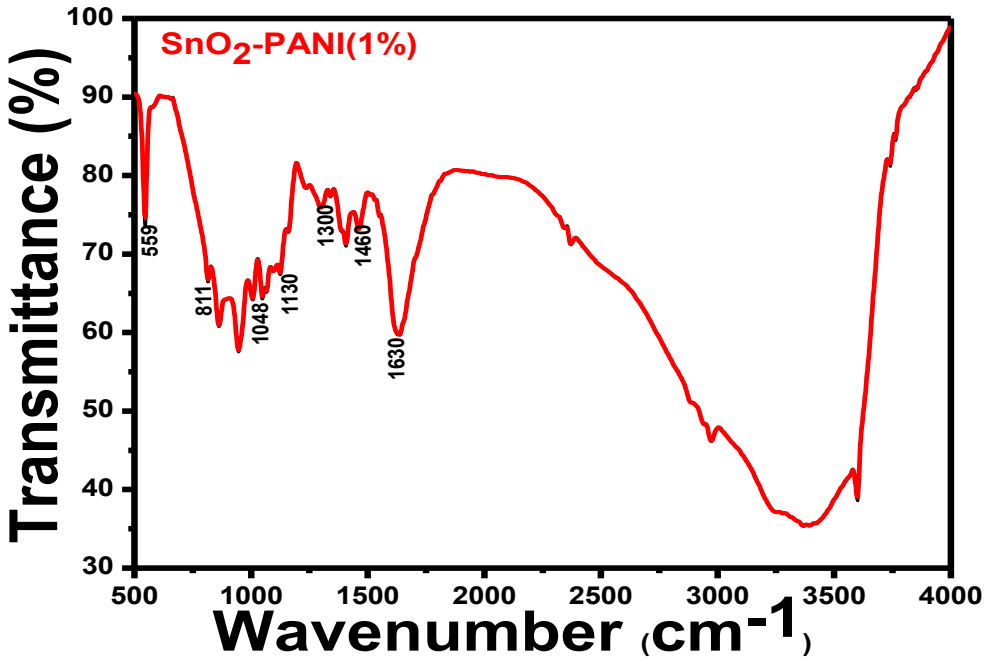

Fig.6.4: FT-IR spectra of SnO_2-PANI composite thin film

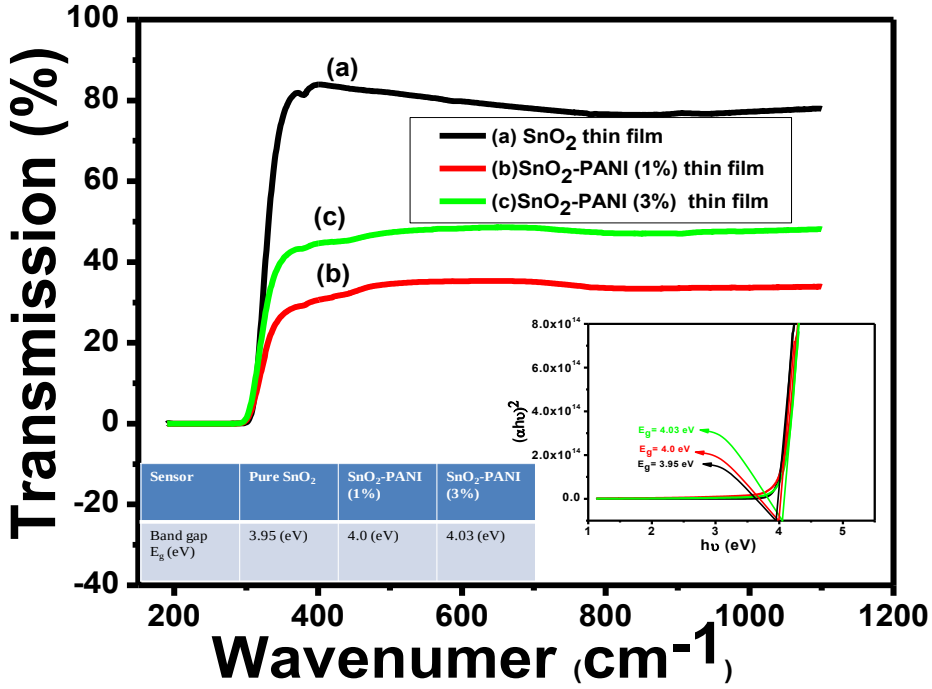

Fig. 6.5: Transmittance spectra of (a) SnO_2 (b) SnO_2-PANI (1%) and (c) SnO_2-PANI (3%) thin film. Inset shows the values of optical band gap obtained for the SnO_2 and SnO_2-PANI composite thin films

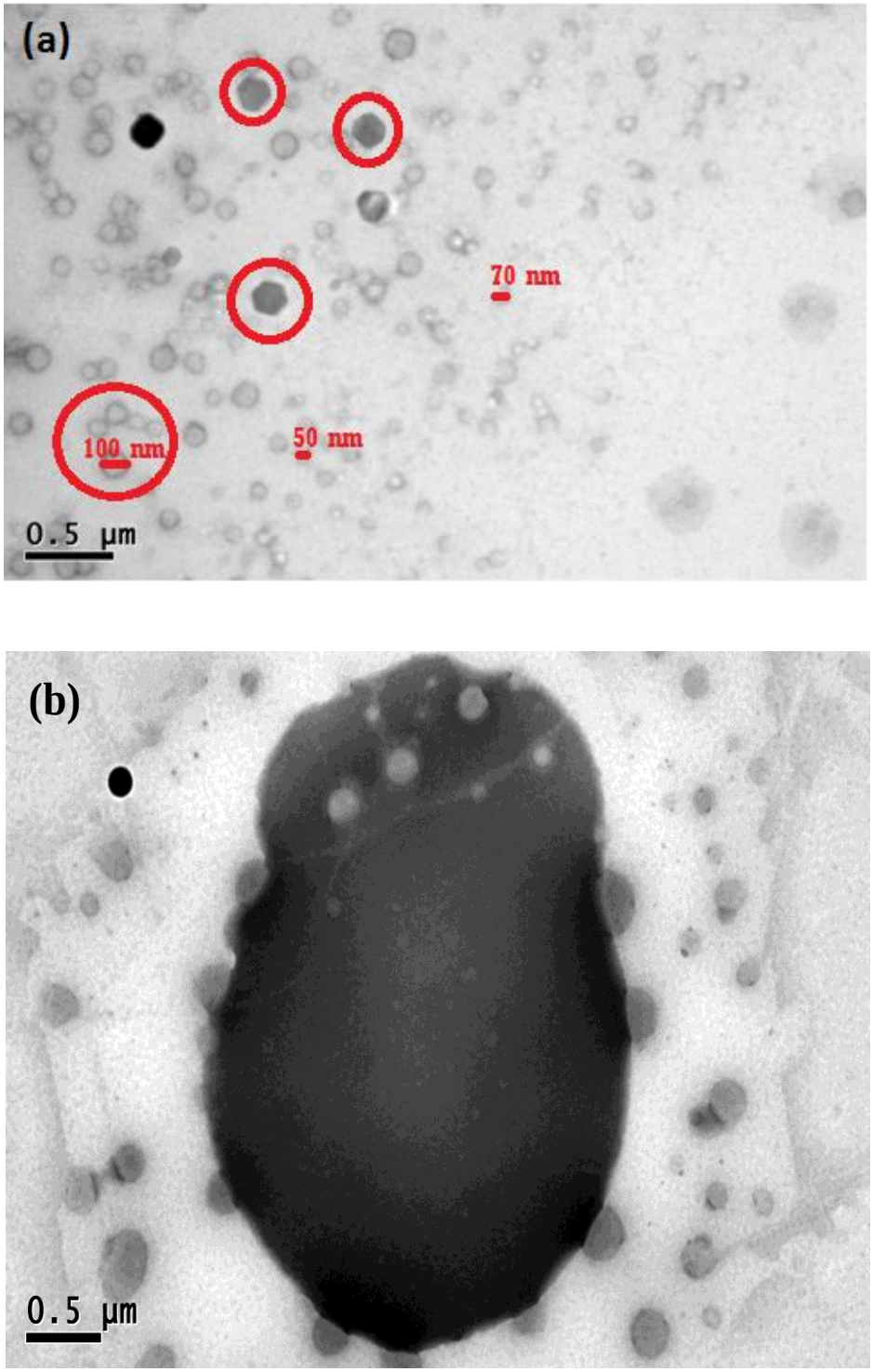

Fig. 6.6: TEM micrograph of (a) Pure SnO_2 (b) SnO_2-PANI composite thin film

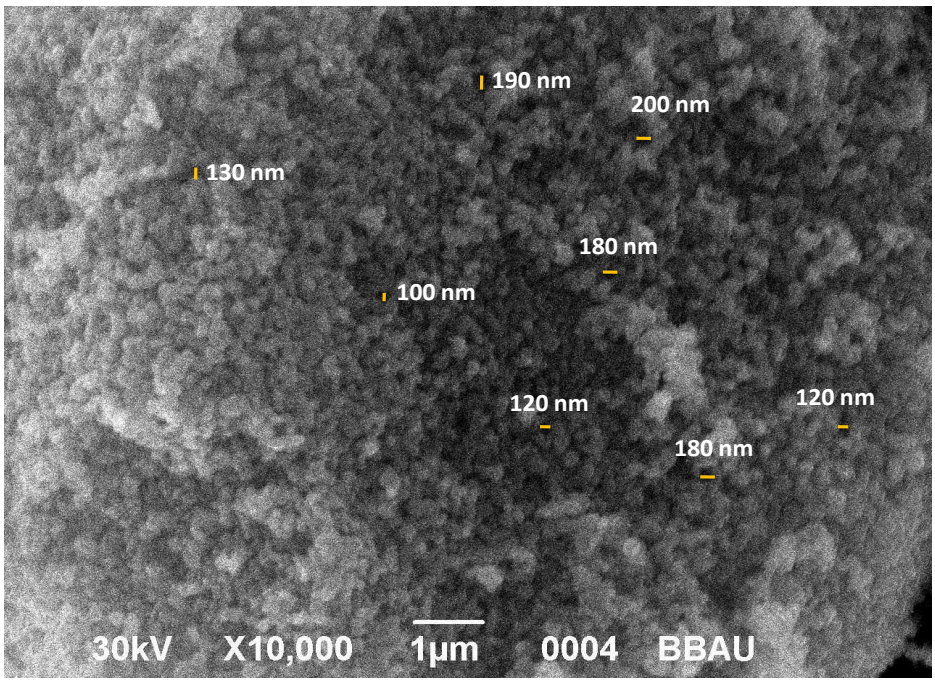

Fig. 6.7: SEM image of SnO_2-PANI composite thin film

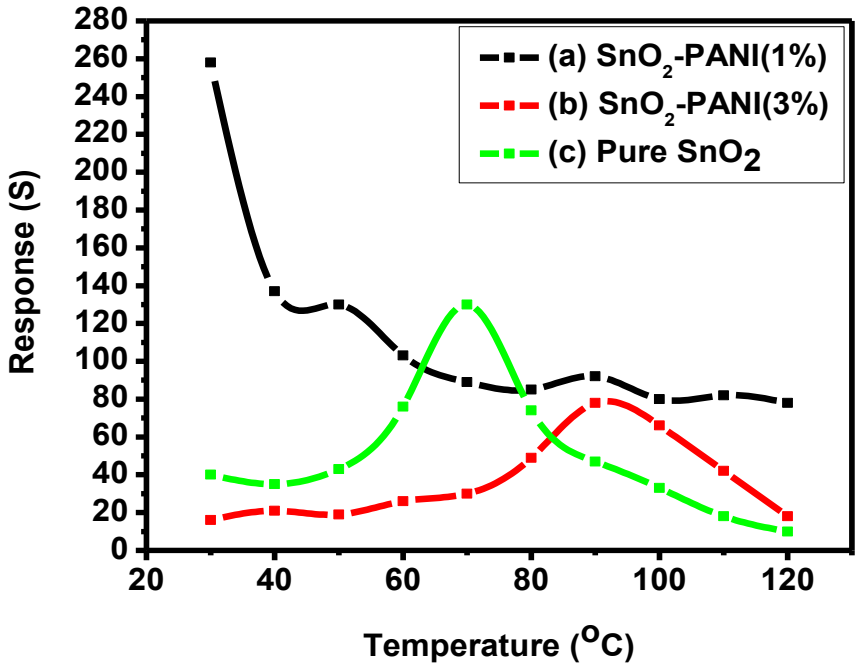

Fig.6.8: Variation in Response of the (a) SnO_2-PANI (1%) (b) SnO_2-PANI (3%) and (c) SnO_2 thin film sensors with temperature

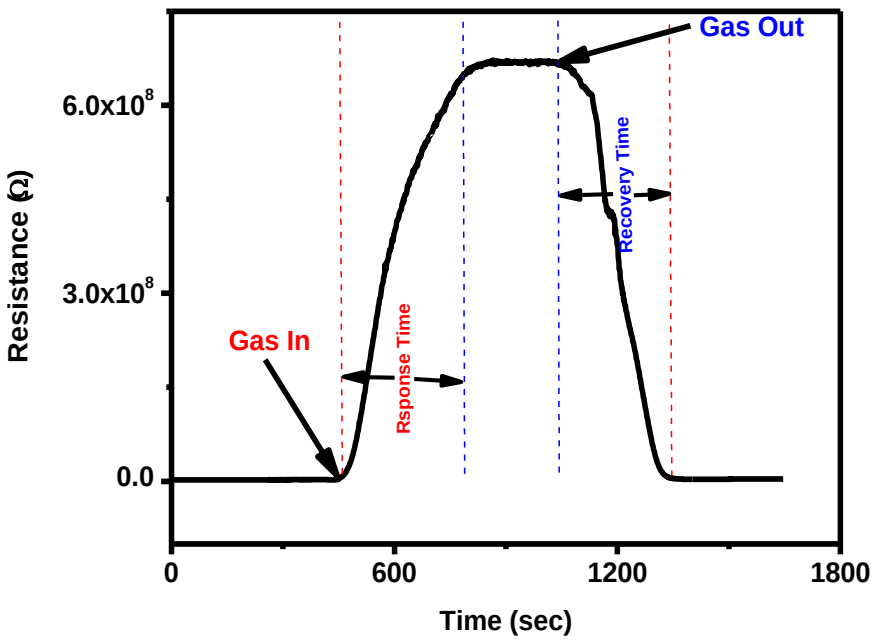

Fig. 6.9 (a): Transient response of SnO_2-PANI (1%) sensor towards 20 ppm of NO_2 gas at room temperature

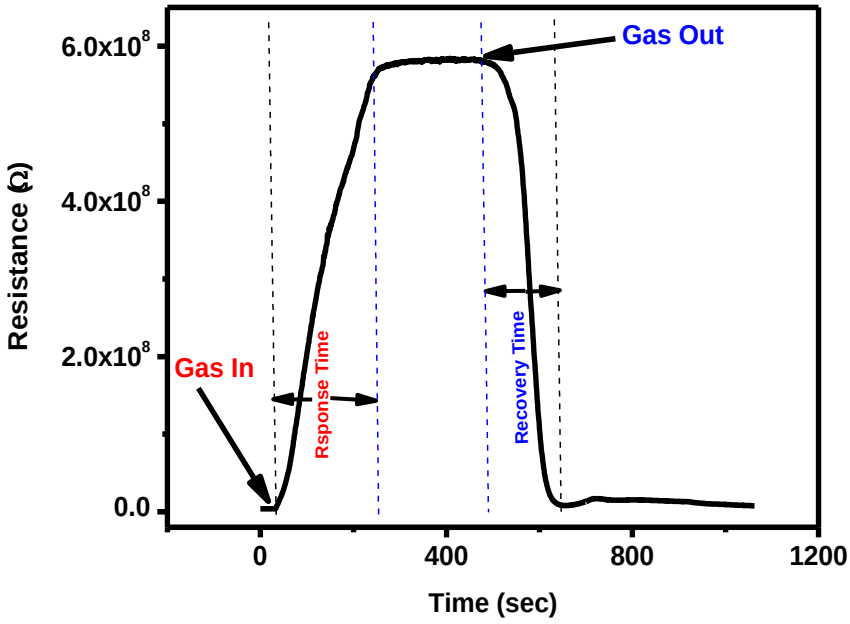

Fig. 6.9 (b): Transient response of SnO_2-PANI (1%) sensor towards 20 ppm of NO_2 gas at an operating temperature of 50 ^oC

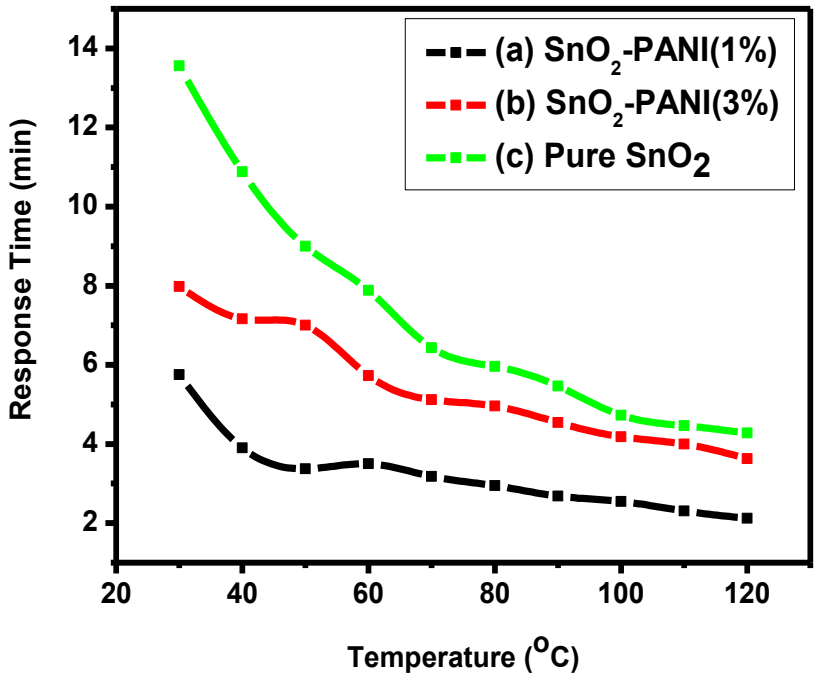

Fig. 6.10: Variation in response time of the (a) SnO_2-PANI (1%) (b) SnO_2-PANI (3%) and (c) SnO_2 thin film sensors with temperature

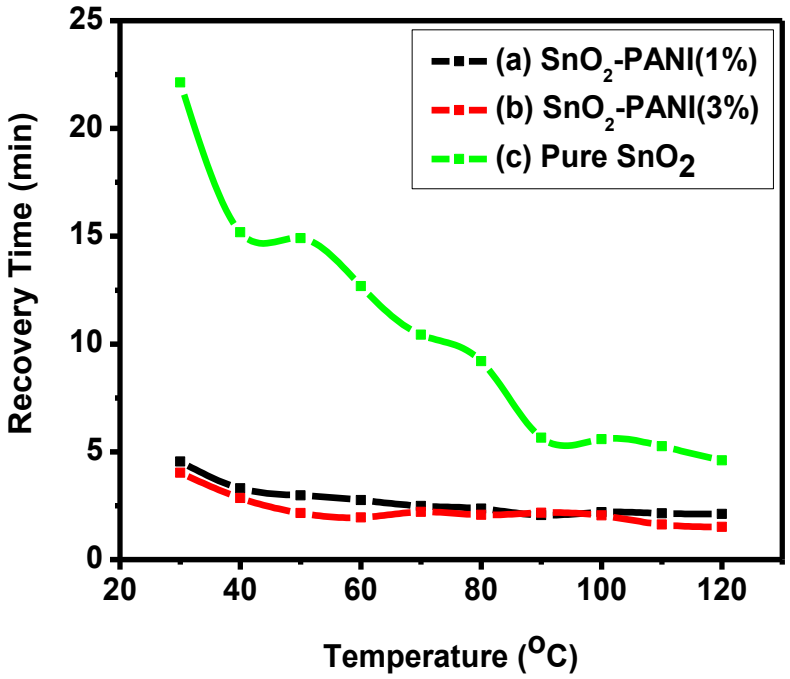

Fig. 6.11: Variation in recovery time of the (a) SnO_2-PANI (1%) (b) SnO_2-PANI (3%) (c) SnO_2 film with temperature

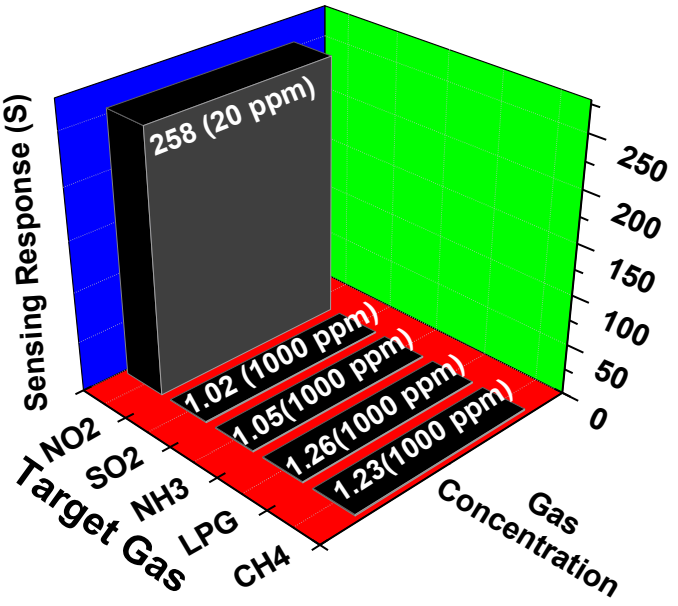

Fig. 6.12: Sensor Response of SnO_2-PANI composite thin film sensor deposited by spin coating technique towards various interfering target gases at room temperature

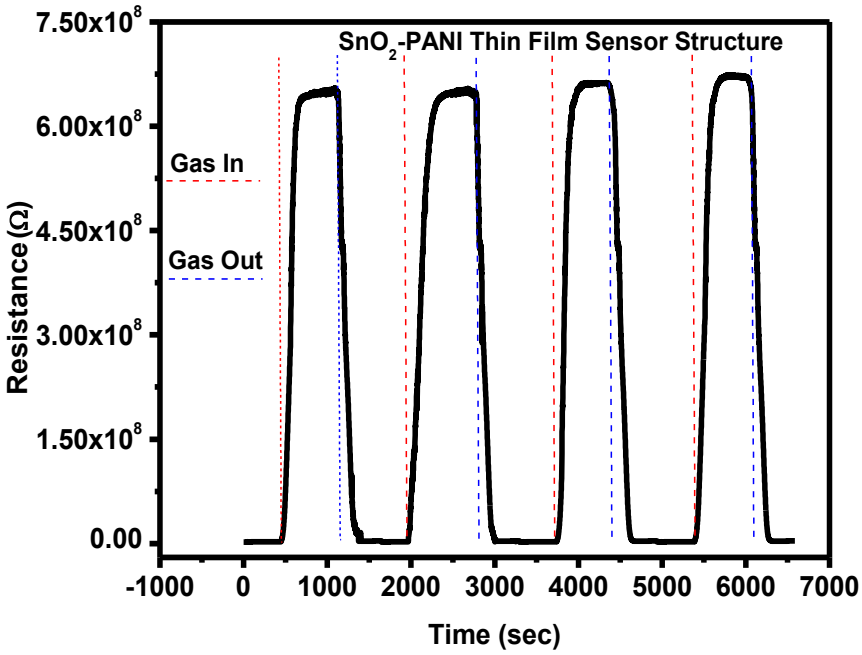

Fig. 6.13: Dynamic Response curve of SnO_2-PANI Thin Film Sensor

Chapter 7

Low temperature operated NO_2 gas sensor based on SnO_2-ZnO nanocomposite thin film

Nitrogen dioxide (NO_2) is a typical automotive air pollutant that causes many environmental and health problems. Detection of low concentrations of NO_2 is becoming very important now a day and various approaches have been used for the same. SnO_2 and ZnO are the two widely explored semiconductor materials for the detection of a number of toxic and harmful gases. Thus, in the present chapter an effort has been made to synthesize nanocrystalline composite thin films of Zinc oxide and Tin oxide (SZO) using chemical route. The structural, optical and surface morphology properties of the SZO composite thin film have been studied by X-ray diffraction (XRD), Fourier transform infrared spectroscopy (FTIR), UV-Visible spectroscopy, Scanning electron microscopy (SEM). Thin film of SnO_2-ZnO (SZO) composite was prepared onto the surface of Pt IDEs/corning glass and has been exploited for studying the gas sensing response characteristics towards NO_2 gas. The prepared SZO sensor structure showed a high sensing response of about 3×10^2 towards 20 ppm of NO_2 gas at operable room temperature with an average response and recovery time of 10.23 and 11.75 min. respectively.

7.1 Introduction

Nitrogen oxide (NO_x) is very harmful because it contributes to the formation of smog by photochemical reaction, which can have significant impact on environment and human health. The two most predominant oxides of nitrogen are nitrogen dioxide (NO_2) and nitric oxide (NO), which are significant pollutants at lower atmosphere. NO_2 is found to more dangerous and acting as a highly reactive oxidant, possessing exceedingly corrosive nature [1]. NO_2 is one of the hazardous gases polluting the atmosphere in urban areas. NO_2 gas is precursor for both ozone at ground level and acid precipitation, each of which are blamed for injury to plants [2]. Thus trace-level detection of NO_2 is almost important and hence in the present work focus has been given on the detection of NO_2 gas.

Tin oxide (SnO_2) is a wide band-gap (E_g = 3.6 eV at 300 K) n-type semiconductor material having good chemical and mechanical stability. SnO_2 is widely used as gas sensing material due to easy adsorption of atmospheric oxygen on its surface. SnO_2 is well known used for the detection of variety of hazardous gas species such as LPG, CO_2, CO, CH_4, NH_3, SO_2, NO_2, etc. The thick film based sensors have been mostly exploited for the detection of a number of toxic and harmful gases, however, a lot of research is continuing for attaining improved sensing response characteristics [3]. Since, gas sensing is primarily a surface dominating phenomena, thin films and nanostructures of SnO_2 are gaining extensive attention of research community due to a high surface to volume ratio and feasibility to alter the surface properties of the sensing layer in comparison to their bulk counterpart and are expected to give enhanced sensing response characteristics at low operating temperature. There are many reports available in Table 7.1 [4-14] on different nanostructures and thin films of SnO_2 explored for the detection of NO_2 gas. ZnO is another material which has been exploited for the fabrication of NO_2 gas sensors. Hence, a composite structure of SnO_2 with ZnO may be beneficial for enhancing the sensing response with selective detection of trace level NO_2 gas. Thus, in the present work an effort has been made to develop a gas sensor based on nanocomposite of SnO_2 and ZnO hybrid using chemical route for the efficient detection of NO_2 gas at lower operating temperature.

7.2 Experimental

7.2.1 Materials

All chemical including Tin (IV) chloride pentahydrate ($SnCl_4.5H_2O$ with 99.99% purity), isopropanol, propanol, zinc acetate, lithium hydroxide, ethanol and n-butyl acetate of high grade used for the sensor structures preparation were procured from Sigma Aldrich Chemical Co.

7.2.2 Preparation of SnO_2 solution using chemical routes

In a beaker a mixture of 12.37 g tin tetrachloride ($SnCl_4.5H_2O$) with 15 g isopropanol was prepared which is an exothermic reaction. Hence, further the solution was cooled down to room temperature and 3.42 g water and 10 g propanol mixture was added for hydrolysis reaction forming the sol. of SnO_2 nanoparticles [15].

7.2.3 Preparation of ZnO solution using chemical routes

0.01 M of zinc acetate dihydrate was dissolved in the 75 ml of boiling ethanol (75 °C) in a round bottom flask fitted with a condenser at atmospheric pressure. The solution was refluxed at 75 °C for about 30 minutes and subsequently allowed to cool at room temperature to give a transparent and stable Zn based precursor. In another beaker, 0.014 M of lithium hydroxide monohydrate was dissolved in 50 ml of ethanol ultrasonically, to accelerate the reaction at room temperature. A clear solution was obtained after sonication for 25-30 min. The hydroxide containing solution was added drop wise to the acetate containing solution at room temperature under vigorous magnetic stirring, and finally a transparent ZnO sol was obtained after hydrolyzing the precursor. The alcoholic solution of zinc acetate was heated at 75 °C to prepare an intermediate species through hydrolysis and condensation. The acetic acid produced during the heat treatment reacted with ethanol and results in the generation of additional water through an etherification process. The addition of LiOH to the transparent precursor led to the formation of ZnO nanoparticle solution [16].

7.2.4 Preparation of SnO_2 and ZnO nanocomposite hybrid solution

The prepared precursor solution for ZnO was added into colloidal solution

containing SnO_2 nanoparticles in the ratio of 40:60 (ZnO:SnO_2). Later SnO_2 and ZnO:SnO_2 solutions were used to deposit respective thin films on corning glass and inter digital electrode (IDEs) patterned on corning glass substrates by spin coating. Each coating was followed by paralyzed the sample at 150 ºC to evaporate the precursors. The samples were then annealed at 500 °C for 2 h in a programmable tubular furnace (Metrex 6400) in the presence of atmospheric air.

The sensing response characteristics of SnO_2 and ZnO:SnO_2 nanocomposite thin films were studied using the films deposited on IDE/glass substrates as shown in Fig. 7.1. The Pt IDEs were patterned over the corning glass substrates using conventional photolithography, prior to deposition of sensing layer (ZnO:SnO_2 nanocomposite thin film). The platinum thin film of 90 nm thicknesses was deposited by RF sputtering using platinum metal target in 100% Ar. In order to improve the adhesion of Pt on corning glass substrate an ultrathin (10 nm) buffer layer of Titanium was deposited prior to Pt deposition. The prepared sensor structures of SnO_2 and ZnO-SnO_2 nanocomposite hybrids were named as pure SnO_2 and ZnO respectively.

Thickness and surface roughness of the deposited thin films were measured using a Veeco Dektak 150 surface profiler. Crystalline structure and surface morphology of the sensing layer were studied using Bragg–Brentano (θ–2θ) scan of a X-ray Diffractometer (Bruker D8 Discover) using the CuKα1 source (λ = 0.154 nm), Atomic force microscope (AFM: Veeco DICP2) and Scanning Electron Microscope (SEM) respectively. A Double Beam UV–visible Spectrophotometer (Perkin Elmer, Lambda 35) was used to study the optical properties of pure SnO_2 and SZO thin films.

7.3 Results and Discussion

7.3.1 Optical behaviour of composite film

The optical transmission spectra of the SnO_2 thin films deposited separately on corning glass substrate was measured in the wavelength range of 190 to 1100 nm, and is shown in Fig. 7.2. SnO_2 thin film exhibits a high transmission (>80%-90%) in the visible region and shows a sharp fundamental absorption edge in UV region at 380 nm.

Band gap of the SnO_2 thin film deposited on corning glass substrate, was

calculated from the intercept on energy axis obtained by extrapolating the linear portion of the Tauc plot of $(\alpha h\nu)^2$ *vs* photon energy (*hν)* as shown in inset of Fig. 7.2. Estimated value of band gap for as-grown SnO_2 thin film is found to be 4.0 eV and is close to the reported value for SnO_2 thin films (4.3 eV) grown by various techniques [17]. Fig. 7.3 shows the UV visible spectra of the as deposited SZO nanocomposite hybrid thin film having high transmission (>65%) in the visible region. Inset of Fig. 7.3 shows the tauc plot of the SZO nanocomposite hybrid thin film. It can be observed that with the incorporation of ZnO and SnO_2 colloidal solution increases the band gap to 4.56 eV. This may be attributed to the electronic transition between ZnO and SnO_2 nanoparticles which confirms the nanocomposite hybrid between ZnO and SnO_2.

Fig. 7.4 shows FT-IR spectra of SZO nanocomposite thin film within 400–4000 cm^{-1}. It reveals that the peak at 3438 cm^{-1} comes from the stretching mode vibrations of OH band attached to SZO thin film, while the peak at 1632 cm^{-1} is attributed to the bending vibrations of adsorbed H_2O molecules. The small peak at 1364 cm^{-1} is due to the bending vibrations of C–H in the methyl which may be comes from the residues of preparation processes. It indicates that there may be a very small amount of organic residues in the SnO_2 and ZnO nanoparticles. The peaks observed at around 475 and 665 cm^{-1} attributed to the vibrations of Zn–O and Sn–O bonds, respectively [18-19].

7.3.2 Structural Studies

The XRD pattern of the as-grown SnO_2 and SZO nanocomposite thin films were found to be amorphous, and become nanocrystalline after a post deposition annealing treatment at 500 ^oC for 2 h in air. The annealed thin films were found to be porous, transparent and strongly adherent to the substrate. Fig. 7.5 shows the XRD pattern of SnO_2 thin film. Broad and well defined reflections corresponding to (110), (101) and (211) planes of SnO_2 were observed at 26.50^o, 33.66^o and 51.57^o respectively and are in good agreement to the corresponding values reported for rutile structure of SnO_2 [18]. The values of lattice constants (‘a’ and ‘c’) estimated from XRD data for the SnO_2 thin films were found to be about 0.46 nm and 0.31 nm respectively which are close to the reported value. The average crystallite size was calculated by Scherer’s formula as 4.50

nm. Fig. 7.6 shows the XRD pattern of the SZO nanocomposite hybrid thin film. It can be clearly observed from Fig. 7.5 that at 37.84^{o} a peak is obtained which corresponds to the (101) reflection plane of ZnO. It can also be seen from Fig. 7.6, that the peaks observed corresponding to (110), (101), (211) reflection planes of SnO_2 are shifted as compared to those obtained for the pure SnO_2 thin film. This may be attributed to the stress generation in SZO film due to the interaction and formation of nm hetrojunction at the interface between ZnO and SnO_2 nanoparticles. Thus, XRD of SZO thin film confirms the presence of ZnO in SnO_2 solution.

7.3.3 Surface Morphological Studies

Fig. 7.7 shows AFM images of the surface of SnO_2 and SZO nanocomposite thin films deposited on corning glass substrate. It can be observed from Fig. 6(a) and (b) that the performed SnO_2 and ZnO nanocomposite thin films are highly porous. The grain size is found to decrease with incorporation of ZnO nanoparticles. Thus, the SZO nanocomposite hybrid thin film provides more grain boundaries leading to the higher surface to volume ratio as compared to pure SnO_2 thin film, which is beneficial for getting, enhance sensing response. However, the surface roughness of both the prepared samples was found to be almost same.

Fig. 7.8 shows the SEM images. Typical SEM image of SZO composite thin film as-grown composite showed irregular sized and shaped agglomerated particles in the nano-scale range having high surface to volume ratio as observed in AFM images [Fig. 7.7(a) & (b)]. The average pore size was found 105 nm.

7.3.4 Sensing Behaviour

Fig. 7.9 shows the variation in sensing response of pure SnO_2 and SZO nanocomposite thin film as a function of temperature towards 20 ppm of NO_2 gas. From Fig. 7.9, it is obvious that with the increase in temperature the sensing response of pure SnO_2 and SZO thin films increases till 70 ^{o}C and on further increasing temperature, it starts decreasing. The pure SnO_2 thin film shows the maximum sensing response of 5.19

$\times 10^2$. On the other side, with incorporation of ZnO in SnO_2 enhances the sensing by one order ($\sim 1.58 \times 10^3$).

Figs. 7.10 and 7.11 show the response times of pure SnO_2 and SZO nanocomposite thin films as function of temperature. From the Fig. 7.10, it can be observed that the response and recovery times decrease with the increase in temperature. This is attributed to the fact that at higher temperatures the rate of adsorption and desorption increases. At an operating temperature of 70 ºC, the pure SnO_2 thin film shows the response and recovery time as 13 and 9 min respectively which get improved with the incorporation of ZnO.

Figs. 7.12 and 7.13 exhibit the variation of resistance of pure SnO_2 and SZO nanocomposite thin film as a function of temperature in presence of air and 20 ppm of NO_2 gas. Fig. 7.12 shows that with increase in temperature the value of resistance (R_a) in presence of air for both the sensor structure decreases, which is due to the semiconducting behavior of pure SnO_2 and SZO nanocomposite thin films. It can also be observed that the value of resistance (R_g) in presence of 20 ppm of NO_2 gas first increases till 70 ºC and then reduces with further increase in temperature which confirms the faster rate of adsorption and desorption of NO_2 gas at elevated temperatures. This is due to fact that at higher temperature, because of higher desorption rate, the less number of target gas species interact with surface of sensing thin film.

7.3.5 Sensing Mechanism

Sensing response of sensor based on SZO is function of R_a and R_g as per Eq. 1, Chapter 4. If R_g is high and R_a is low then response will be higher. As NO_2 gas is an oxidizing gas and interacts with SZO nanocomposite thin film and reduces the number of charge carriers in the conduction band. This may be observed through Fig. 7.12, in which the incorporation of ZnO in SnO_2 thin film reduces the sensor resistance from 540 kΩ to 76 kΩ at room temperature.

At lower temperatures, the predominant oxygen species on the SnO_2 surface are still O_2^- but NO_2 gas molecules interact directly with tin ionic sites instead of reacting with O_2^- species [21]. SnO_2 responds to NO_2 gas as under [22]:

$$NO_2 + Sn^{2+} \xrightarrow{\text{adsorption}} (Sn^{3+} - NO_2^-) \xrightarrow{\text{desorption}} (Sn^{3+} - O^-) + NO \quad (1)$$

$$2(Sn^{3+} - O^-) \xrightarrow{\text{desorption}} 2Sn^{2+} + O_2 \quad (2)$$

When NO_2 gas molecules adsorbed on the surface of SnO_2 sensor element attack the available Sn sites and take away electrons from the conduction band of SnO_2 forming NO_2^- species. The reduction in the number of charge carriers in the conduction band of SnO_2 results in an increase in sensor resistance (R_g) as observed in the present study. However, this is a slow phenomenon and undergoes a reversible oxidizing interaction at Sn sites available on the surface of SnO_2 film [21]. Therefore value of R_g depends upon the availability of Sn sites on the surface of SnO_2 thin films, which in turn are influenced by the physisorbed oxygen for interaction with target NO_2 gas molecules. On the other side in the case of SZO nanocomposite thin film, the value of resistance (R_g) also increases in 20 ppm of NO_2 gas interacts with sensor surface. However, the increase in R_g is not as much as it is observed in case of pure SnO_2 thin film, but the high reduction in R_a value of SZO nanocomposite with incorporation of ZnO in SnO_2 thin film as compared to pure SnO_2 thin film, result in significant variation in the value of resistance from R_a to R_g in presence of 20 ppm of NO_2 gas leading to enhanced sensing response of about 1.5×10^3 at an operating temperature of 70 ºC.

7.4 Conclusion

SnO_2 thin film and SZO nanocomposite thin films based sensor structures have been fabricated and exploited for the trace level (20 ppm) detection of NO_2 gas. SZO nanocomposite thin film based sensor was found to better in sensing response i.e. (1.578×10^3) with faster response time (7 min.) and recovery time (6 min.) at operating temperature 70 °C. Nanoporous surface morphology having nanocrystalline grains are found to be important for obtaining enhanced response characteristics.

References:

[1] B.T. Marquis, J.F. Vetelino, A semiconducting metal oxide sensor array for the detection of NO_x and NH_3, Sens. Actuator B: Chem., 77 (2001) 100-110.

[2] L. Shi, Y. Hasegawa, T. Katsube, K. Onoue, K. Nakamura, Highly sensitive NO_2 gas sensor fabricated with RF induction plasma deposition method, Sens. Actuator B: Chem., 99 (2004) 361-366.

[3] L. Chen, S. Bai, Gu. Zhou, Dia. Li, A. Chen, C. Li. Chung; Synthesis of ZnO-SnO_2 nanocomposites by microemulsion and sensing properties for NO_2, Sens. Actuator B: Chem., 134 (2008) 360-366

[4] F. Parret, Ph. Menini, A. Martinez, K. Soulantica, A. Maisonnat, B. Chaudret, Improvement of micromachined SnO_2 gas sensors selectivity by optimised dynamic temperature operating mode, Sens. Actuator B: Chem., 118 (2006) 276-282.

[5] E. Comini, L. Pandolfi, S. Kaciulis, G. Faglia, G. Sberveglieri, Correlation between atomic composition and gas sensing properties in tungsten–iron oxide thin films, Sens. Actuator B: Chem., 127 (2007) 22-28.

[6] J. Kaur, S. C. Roy, M. C. Bhatnagar, Highly sensitive SnO_2 thin film NO_2 gas sensor operating at low temperature, Sens. Actuator B: Chem., 123 (2007) 1090-1095.

[7] J. Kaur, R. Kumar, M. C. Bhatnagar, Effect of indium-doped SnO_2 nanoparticles on NO_2 gas sensing properties, Sens. Actuator B: Chem., 126 (2007) 478-484.

[8] J. Kaur, V.D. Vankar, M.C. Bhatnagar, Effect of MoO_3 addition on the NO_2 sensing properties of SnO_2 thin films, Sens. Actuator B: Chem., 133 (2008) 650-655.

[9] K.Y. Choi, J.S. Park, K.B. Park, H.J. Kim, H.D. Park, S.D. Kim, Low power micro-gas sensors using mixed SnO_2 nanoparticles and MWCNTs to detect NO_2, NH_3, and xylene gases for ubiquitous sensor network applications, Sens. Actuator B: Chem., 150 (2010) 65-72.

[10] J. A. Park, J. Moon, S. J. Lee, S. H. Kim, H. Y. Chu, T. Zyung, SnO_2-ZnO hybrid nanofibers-based highly sensitive nitrogen dioxides sensor, Sens. Actuator B: Chem., 145 (2010) 592-595.

[11] I. S. Hwang, S. J. Kim, J. K. Choi, J. Choi, H. Ji, G. T. Kim, G. Cao, J. H. Lee, Synthesis and gas sensing characteristics of highly crystalline ZnO–SnO_2 core–shell nanowires, Sens. Actuator B: Chem., 148 (2010) 595-600.

[12] L. Peng, J. Zhai, D. Wang, Y. Zhang, P. Wang, Q. Zhao, T. Xie, Size- and photoelectric characteristics-dependent formaldehyde sensitivity of ZnO irradiated with UV light, Sens. Actuator B: Chem., 148 (2010) 66-73.

[13] R. Leghrib, A. Felten, J.J. Pireaux, E. Llobet, Gas sensors based on doped-CNT/SnO_2 composites for NO_2 detection at room temperature, Thin Solid Films 520 (2011) 966-970.

[14] A. Sharma, M. Tomar, V. Gupta, WO_3 nanoclusters-SnO_2 film gas sensor heterostructure with enhanced response for NO_2, Sens. Actuator B: Chem., 176 (2013) 675-684.

[15] R. Rella, A. Serra, P. Siciliano, L. Vasanelli, G. De, A. Licciulli, A. Quirini, Tin oxide-based gas sensors prepared by the sol–gel process, Sens. Actuator B: Chem., 44 (1997) 462-467.

[16] H. K. Yadav, K. Sreenivas, V. Gupta, Effect of surface defects on the visible emission from ZnO nanoparticles, J. Mater. Res., 22 (2007) 9.

[17] G. Feng, W. F. Shu, Lu K. Meng, Che. F. Xiu, Su Wen Liu, G. J. Zhou, D. Xu, Du. R. Yuan, Luminescence of SnO_2 thin films prepared by spin-coating method, Journal of Crystal Growth 262 (2004) 182-185.

[18] M.A. Gondala, Q.A. Drmosh, T.A. Saleh, Preparation and characterization of SnO_2 nanoparticles using high power pulsed laser, Appl. Surf. Sci. 256 (2010) 7067-7070.

[19] P. Dayal, T. Kyua, Facile synthesis of SnO_2 mesoporous tubular nanostructure with high sensitivity to ethanol, J. Appl. Phys. 100 (2006) 0435121-0435126.

[20] A. Sharma, M. Tomar, V. Gupta, SnO_2 thin film sensor with enhanced response for NO_2 gas at lower temperatures, Sens. Actuator B: Chem., 156 (2011) 743-752.

[21] B. Ruhland, T. Becker, G. Muller, Gas kinetic interactions of nitrous oxides with SnO2 surfaces, Sens. Actuator B: Chem., 50 (1998) 85-94.

[22] J. Kaur, S.C. Roy, M.C. Bhatnagar, Effect of indium doped SnO_2 nanoparticles on NO_2 gas sensing properties, Sens. Actuator B: Chem., 126 (2007) 478-484.

Figures:

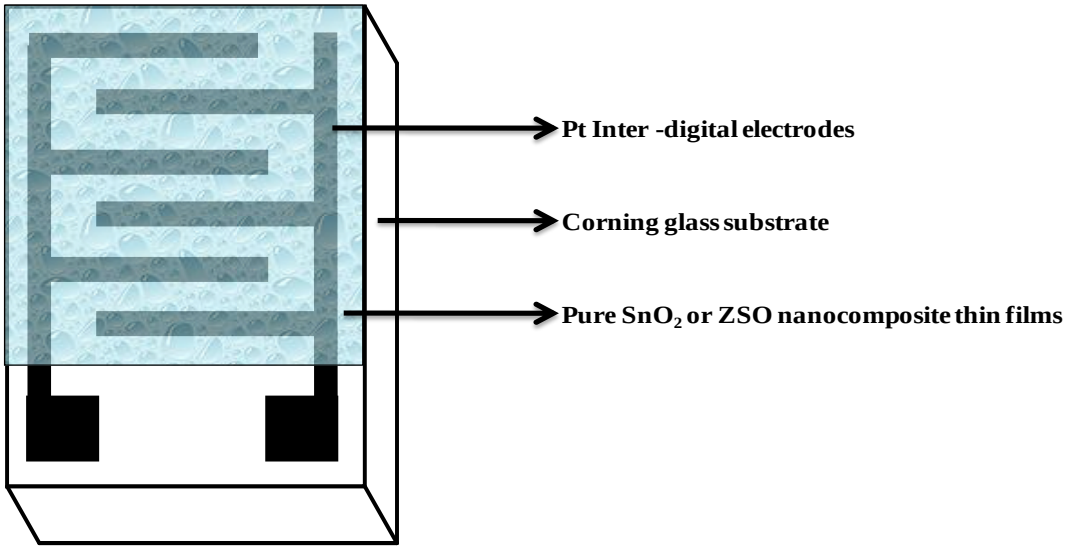

Fig. 7.1: Schematic of gas sensor structure

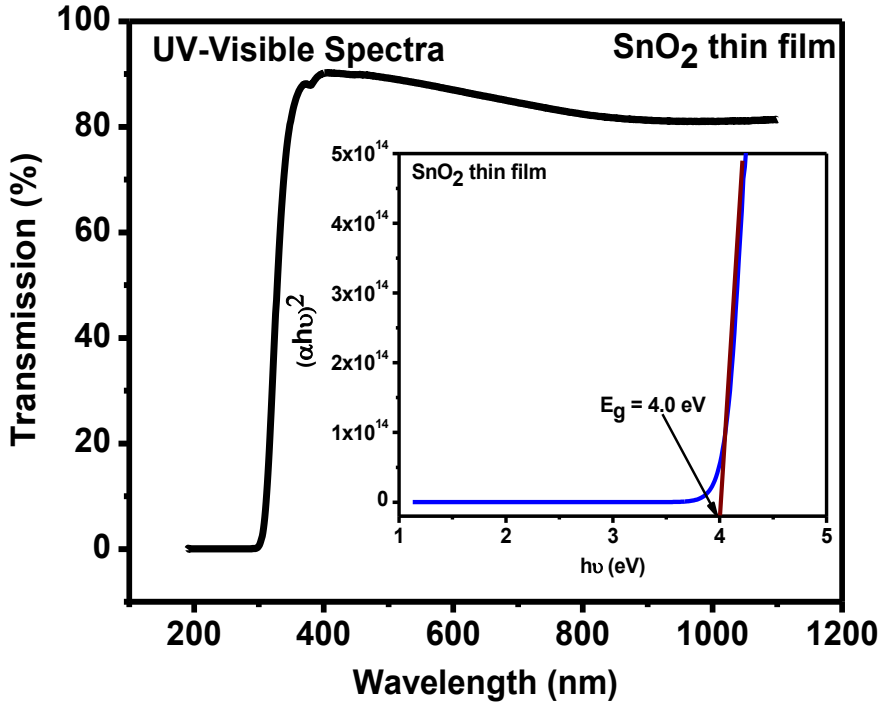

Fig. 7.2: Optical Transmittance spectra of SnO_2 thin film. Inset shows the Tauc plot of $(\alpha h\upsilon)^2$ versus $h\upsilon$ of SnO_2 thin film

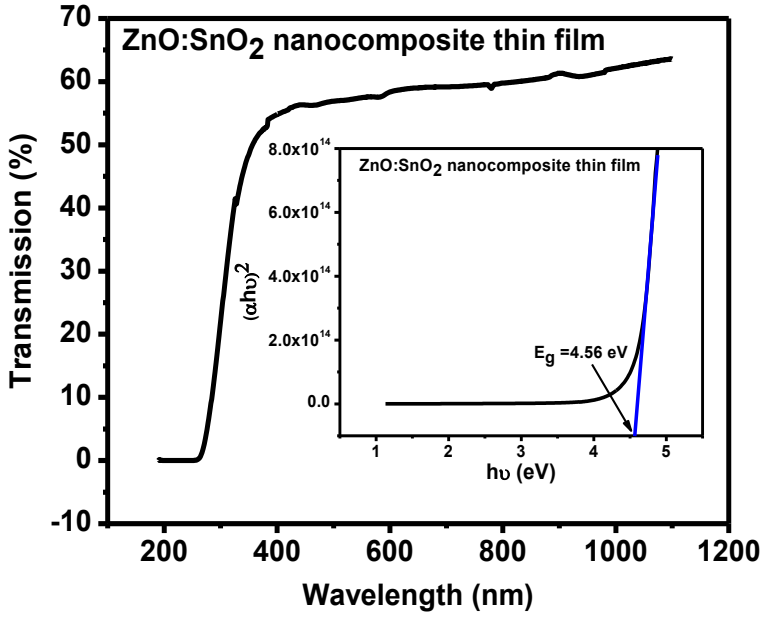

Fig. 7.3: Optical Transmittance spectra of SZO nanocomposite thin film. Inset shows the Tauc plot of $(\alpha h\upsilon)^2$ versus $h\upsilon$ of SZO nanocomposite thin film

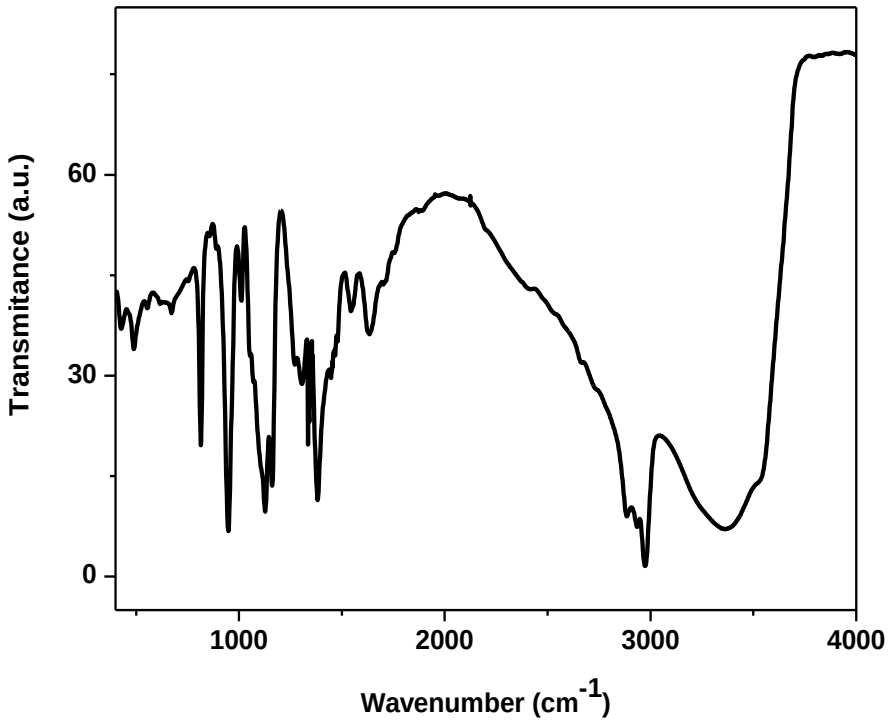

Fig. 7.4: FT-IR spectra of SZO nanocomposite thin film

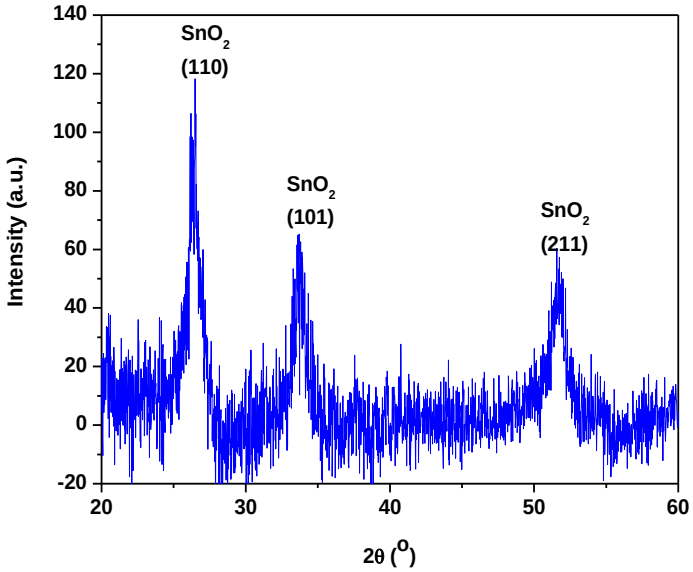

Fig. 7.5: X-Ray Diffraction of the SnO_2 thin film

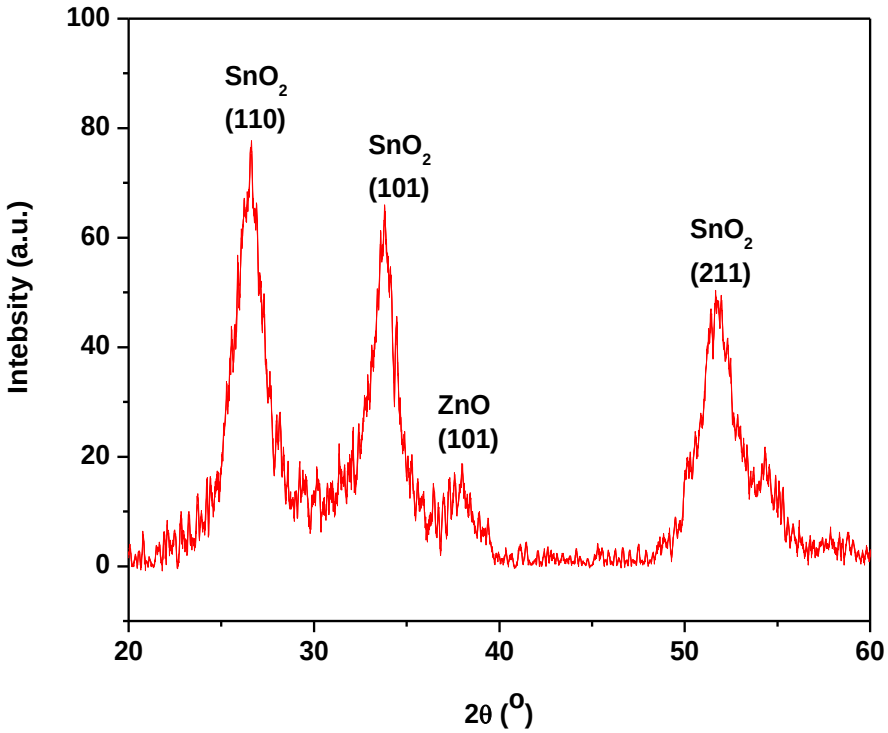

Fig. 7.6: X-Ray Diffraction of the SZO nanocomposite thin film

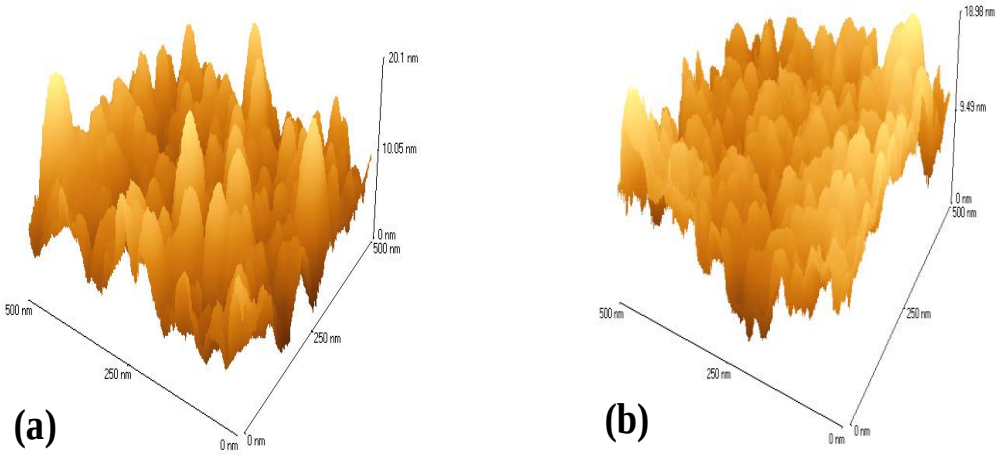

Fig. 7.7: Atomic force micrograph of (a) SnO_2 thin film (b) SZO nanocomposite thin film

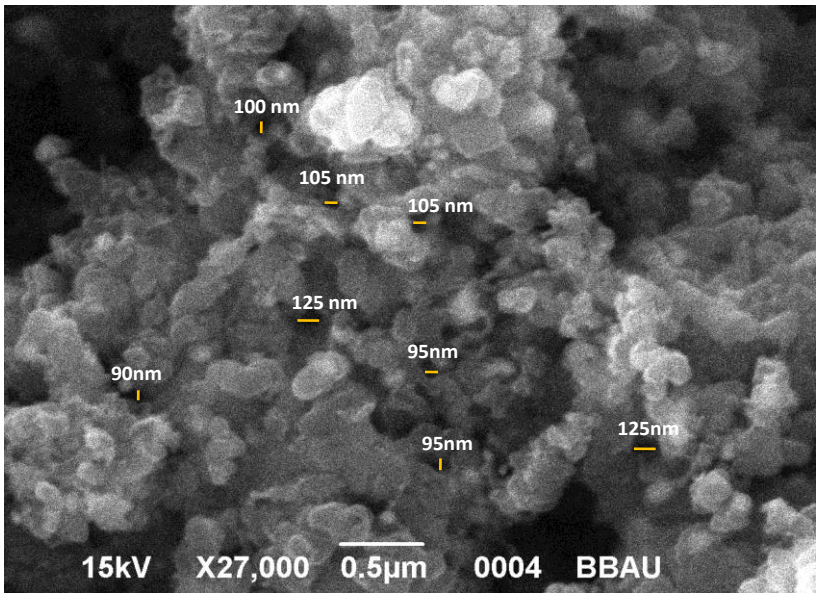

Fig. 7.8: Scanning electron microscope of SZO nanocomposite thin film

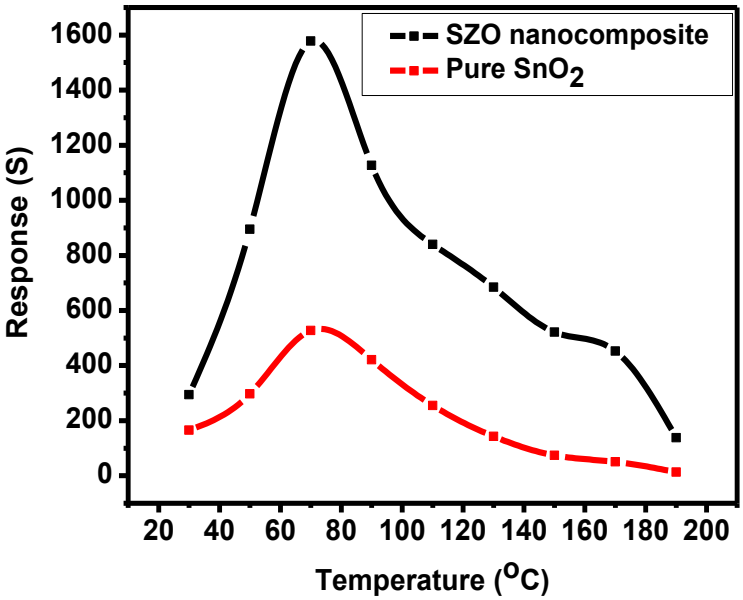

Fig. 7.9: Variation in sensing response of pure SnO_2 and SZO nanocomposite thin films as a function of temperature towards 20 ppm of NO_2 gas

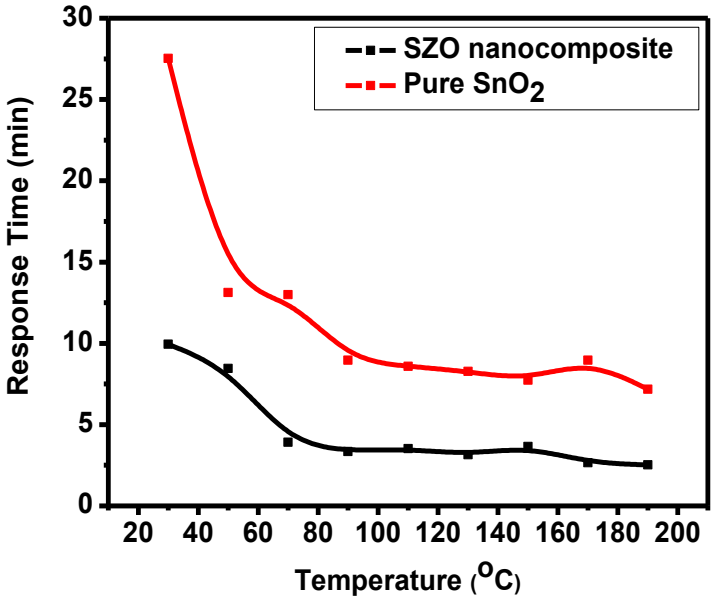

Fig. 7.10: Variation in Response time of pure SnO_2 and SZO nanocomposite thin films as a function of temperature towards 20 ppm NO_2 gas

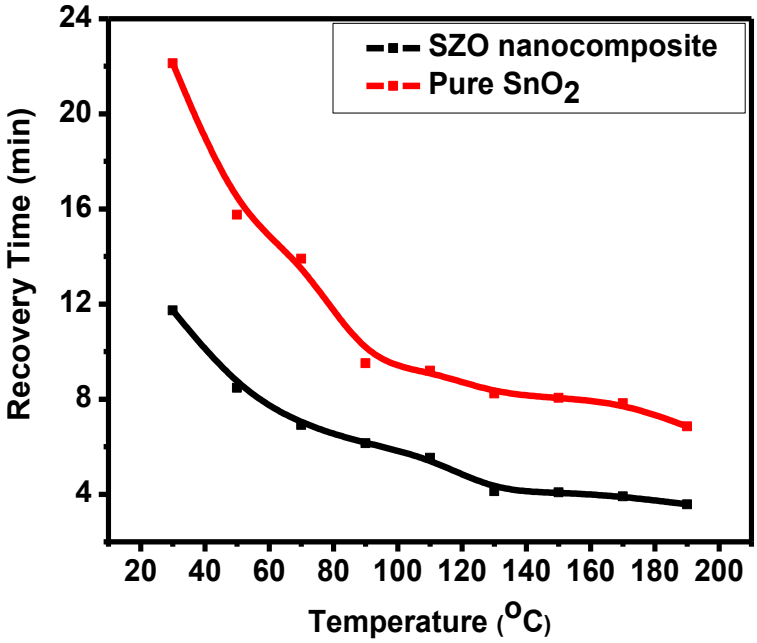

Fig. 7.11: Variation in recovery time of pure SnO_2 and SZO nanocomposite thin films as a function of temperature towards 20 ppm NO_2 gas

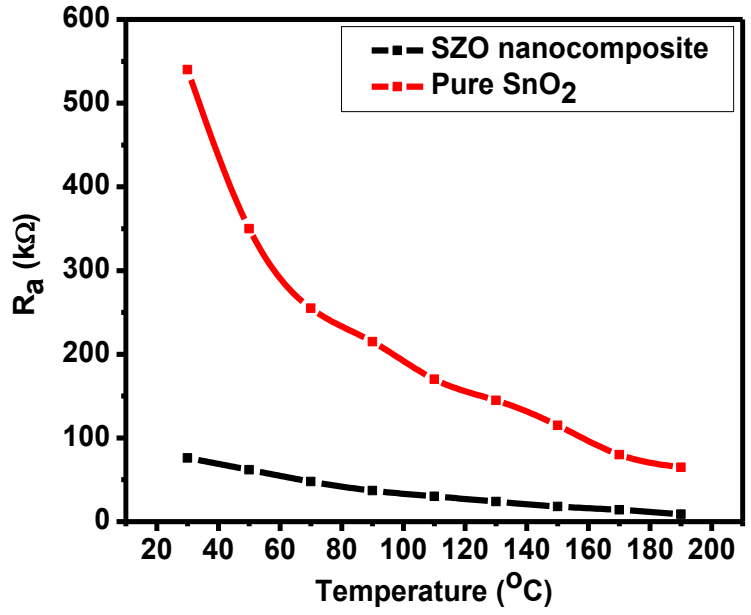

Fig. 7.12: Variation of sensor resistance in air (R_a) for pure SnO_2 and SZO nanocomposite thin films

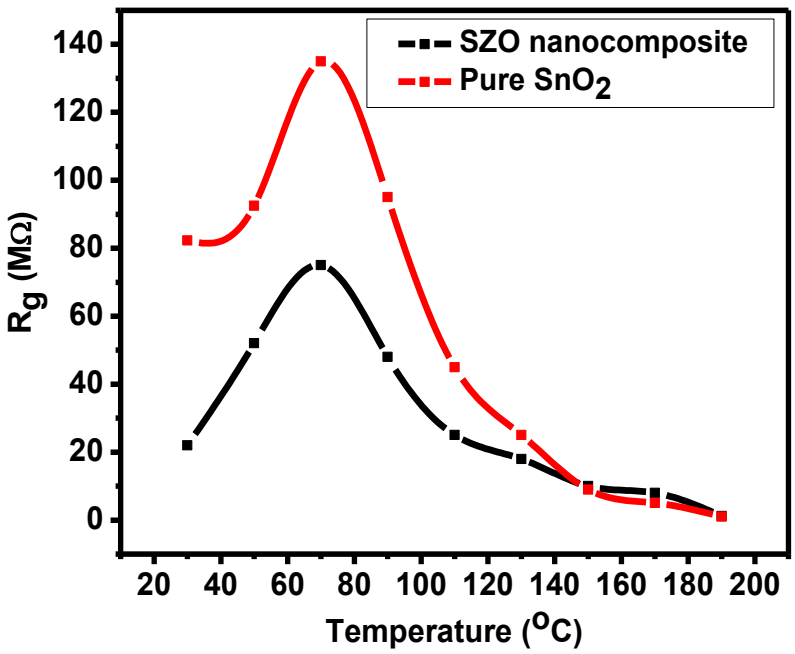

Fig.7.13: Variation of sensor resistance of pure SnO_2 and SZO nanocomposite thin films in presence of 20 ppm NO_2 gas as a function of temperature

Table 7.1: Literature survey on catalyst modified SnO_2 based NO_2 gas sensors

Material used	**Method**	**Catalyst/ doping**	**Temp (^oC)**	**Sensor Response (gas Conc.)**	**Response/ Recovery time**	**Ref. No.**
SnO_2 nano-materials	Chemical route	Pd	300	0.1 (200 ppm)	0.2 sec/ 1 sec	4
SnO_2 thin film	Sputtering	Mo	270	20 (10 ppm)	- / -	5
SnO_2 thin film	Sol gel	WO_3	150	33,359 (500 ppm)	2 sec/1.5min	6
SnO_2 thin film	Sol gel	Indium	150	72 (500 ppm)	2 sec/2 min	7
SnO_2 thin film	Sol- Gel	MoO_3	170	3.5 (500 ppm)	30 sec/100 sec	8
SnO_2 nanocrystals	Electrostatic-force-directed assembly	CNT	RT	2 (100 ppm)	5 min/20 min	9
SnO_2 nanofibres	Pulse Laser Depostion	ZnO	180	100 (3.2 ppm)	4 min/ 8 min	10
SnO_2 nanowires	Two-Step Vapor Growth	ZnO	300	12.3 (10 ppm)	5 sec/ 12 sec	11
SnO_2 nanowires	Two-Step Vapor Growth	ZnO	300	12.3 (10 ppm)	5 sec/ 12 sec	12
SnO_2 thin film	Chemical Route	CNT	RT	8 (0.5 ppm)	10 min	13
SnO_2 thin film	Sputtering	WO_3	300	5.1×10^4 (10 ppm)	67sec /17min	14

Chapter 8

Fabrication of SnO_2-Polyaniline-ZnO (SPZ) multilayer nanocomposite thin film for improved NO_2 sensing at Room Temperature

---

We report the fabrication of SnO_2-polyaniline (PANI)-ZnO composite thin film for NO_2 sensor using spin coating technique. It was found that the composite sensor has high selectivity and response to low concentration NO_2 gas. Furthermore, the composite sensor also showed high stability to NO_2 over a long period at room temperature (30 ºC). Sensor response was calculated as 995 for 20 ppm NO_2 gas at room temperature. The response and recovery times were found as about 3.8 and 2.2 min respectively. The sensor investigated here may be used for the indoor as well out door applications.

8.1 Introduction

The nanostructure-based sensors have higher sensitivity, superior spatial resolution and rapid response compared to thin film gas sensors due to the high surface-to-volume ratios of nanocomposite film. Nitrogen dioxide (NO_2) can be produced by many of processes like automobile exhaust fumes, production of nitric acid, the combustion of coal and fuel, etc. [1]. The most common NO_2 sensors are chemiresistors type based on semiconducting metal oxides such as SnO_2, WO_3, or ZnO [2-4]. Nowadays, NO_2 is one of the hazardous gases polluting the atmosphere in urban areas. Moreover, the chemical reaction of NO_2 gas with water vapor would cause acid rain [5]. Therefore, the development of a NO_2 gas sensor for environmental monitoring has become a very important task. Semiconducting tin oxide (SnO_2) has been proven to be one of the most attractive sensing materials for gas sensor applications, owing to its suitable physical-chemical properties, and possibility to detect many reducing and oxidizing gases with high response. The several organic semiconductors, such as polyaniline (PANI), polypyrrole (PPy), polythiophene (PTh) and metal substituted phthalocyanines (MSPs) have been used for detecting toxic gases (such as NO_2, O_3) [6-11]. As one kind of conducting polymers, PANI and its derivatives, have received considerable attention for their low working temperature, cheap, easy preparation, and thermal stability. However, PANI still exhibits some shortcoming as gas sensitive materials, including low sensitivity, irreversible response, unsatisfying long-time stability and poor selectivity [12]. In order to overcome these drawbacks, organic-inorganic hybrid sensors are intensively investigated [12-14]. Wu et al. fabricated PANI/SnO_2 hybrid material by a hydrothermal route and found that the PANI/SnO_2 hybrid material could overcome the shortcomings of long response time of PANI and the operating temperature of SnO_2 [12].

Earlier reported work was as the next step to others (Chapter 2-7). Sensing parameters were found to be improved, however, there were certain disadvantages, such as low sensitivity, poor selectivity, irreversible response and unsatisfying long-time stability. In view of the eradication of such issues we have proposed here a multilayered structure deposited by precursor of SnO_2, PANI and ZnO on corning glass substrate. This

sensor structure was identified SnO_2-PANI-ZnO (SPZ) composite thin film employed for NO_2 sensing.

8.2 Experimental

Fig. 8.1 shows the flow chart of the growth and deposition of SnO_2, ZnO and PANI nanocrystals deposited on corning glass substrate using spin coating method. For studying the gas sensing properties, gas dilution system developed by our group was utilized [15]. The change in sensor resistance was recorded in the presence of different concentrations of NO_2 gas with the help of Keithley electrometer interfaced with a computer. The sensing response and other parameters of prepared sensor structure towards oxidizing (NO_2) gas were calculated [16].

8.2.1 Characterization techniques

Thickness and surface roughness of the deposited thin films were measured using a Veeco Dektak 150 surface profiler. Crystalline structure and size of the synthesized material were studied using Bragg–Brentano (θ–2θ) scan of a X-ray Diffractometer (Bruker D8 Discover) using the $CuK\alpha_1$ source (λ = 0.154 nm). Surface morphologies were investigated using field emission scanning electron microscope (FE-SEM). Fourier transform infrared (FTIR) spectra were obtained in the range of 4000–400 cm^{-1} with a 4 cm^{-1} spectral resolution by using a Nicolet^{TM} 6700 spectrometer (Thermo, Scientific, USA). A Double Beam UV–visible Spectrophotometer (Thermo, Evolution 200) was used to study the optical properties of ZnO thin films.

8.3 Results and Discussion

FESEM images of SPZ thin films under different magnifications (64 kx and 289 kx) are shown separately in Fig. 8.2 (a)-(d). From Fig. 8.2(a), it has been observed that, the SPZ film is composed of closely packed nanometer sized grains. The regular shaped grains forms compact morphology that covers the entire corning substrate. The higher magnification image (129 kx) shows [Fig. 8.2(b-c)], the closely regular shaped nano sized grains having average grain size ~200 nm. From its magnified FESEM image [Fig. 8.2(d)], well-defined nanosized ZnO structure with an average diameter 18 nm has been

observed by unitary method calculation. This enables an easy passage of NO_2 at npn heterojunction interface. The dense morphology of the (SPZ) composite thin film with porous nanosized particle is allowing the NO_2 sensor at operable room temperature which adsorbs and de-adsorbs gas molecules easily to the interface. The rough surface morphology facilitates room temperature sensing and faster gas response and recovery times.

8.3.1 Structural characterizations

X-ray diffraction pattern of the SPZ thin films on corning glass substrate is shown by Fig. 8.3. It can be observed that at $2\theta = 26.41^{o}$ and 51.86^{o} correspond to reflection plane (110) and (211) of rutile structure of SnO_2 respectively. Whereas, reflection peak observed at $2\theta = 16.67^{o}$ corresponds to (100) plane confirming the presence of PANI [26]. XRD pattern shows several sharp peaks corresponding to (100), (002), (101), (102) and (110) planes of single ZnO phase polycrystalline nature. This characteristic supports presence of pure ZnO phase without any secondary phases [24]. The diffraction peaks in the XRD pattern are identified as wurtzite structured ZnO with lattice parameter a = 3.25Å; c = 5.21Å. The intensity of the peak assigned to the (002) plane of wurtzite ZnO is higher in comparison to the other planes, i.e. (100) and (101). This result indicates growth of ZnO on top of the SnO_2 and PANI.

8.3.2 Optical Analysis

The FTIR spectra of before and after gas exposure of SnO_2/PANI/ZnO nanocomposites are shown in Fig. 8.4. When no gas was exposed the peak at 3450 cm^{-1} comes from the stretching mode of vibration of –OH, while the peak at 1630 cm^{-1} is attributed to the bending vibrations of adsorbed H_2O molecules. The peak at 1576 and 1487 cm^{-1} are attributed to C–N and C–C stretching mode for quinoid and benzenoid rings [16-17], while 1380 cm^{-1} is due to the bending vibration of C–H in the methyl which may be come from the increase of preparation process, the peak at 1241 and 1158 cm^{-1} is due to the C–N stretching mode of vibration, the peak at 808 and 1006 cm^{-1} correspond to C–H out of plane bonding in benzenoid ring [18]. The small peak at 615 cm^{-1} can be attributed to the vibration of Sn–O bond in SnO_2 [19] and peak 511 cm^{-1} can

be attributed to vibration of Zn–O bind in ZnO [20]. When NO_2 gas molecules interact with the film, the bond shifted towards low wave number and resistance of film increases.

8.3.3 Sensing Analysis

Fig. 8.5 shows the dynamic response of SPZ thin film sensor at room temperature towards 20 ppm NO_2 gas. As is evident from the figure that the exposure of NO_2 gas to the sensing film surface, results in the increase of resistance from 1.25 to 1244 MΩ (S = 995). The response and recovery times of the sensor were observed to be 3.8 and 2.2 min, respectively at room temperature (30 ºC). It was found that the sensor exhibit high response to NO_2 even at room temperature. The comparison between the sensing performance of the sensor and literature reports [21-26] is summarized in Table 8.1. The advantage of our SPZ sensor is relatively higher response to NO_2, so it can be expected to serve as a promising functional material in NO_2 gas sensor. The response and recovery characteristics to 20 ppm of NO_2 at operating temperature 30 ºC were investigated, and corresponding curve is shown in Fig. 8.5. The four reversible cycles of the response curve indicated that the sensor had good repeatability and stability as shown in the inset of Fig. 8.5.

Variation of the sensing response of SPZ thin film as a function of temperature towards 20 ppm of NO_2 gas is shown in Fig. 8.6. It was found that as temperature increases sensor response has been decreased. This decrease in sensing response at high temperature could be due to higher rate of adsorption and desorption of gas molecules at the sensing surface. The SPZ thin film shows the maximum sensing response as 9.95×10^2 at room temperature. When the NO_2 gas interacts with the sensing surface of SPZ, it traps free electrons from the surface and decreases the conductivity of the sensor. The inset of Fig. 8.6 shows the sensing response of SPZ sensor at operating temperature 30 ºC after the exposure of 20 ppm of NO_2 gas.

The response/recovery time is an important parameter used for characterizing a sensor. It is defined as the time required to reach 90% of the final change in resistance, when the gas is turned on and off, respectively. Fig. 8.7 shows the response and recovery time of SPZ nanocomposite thin film sensor for different temperature variation at 20 ppm

of NO_2 gas. From Fig. 8.7, it is observed that the response time has increased from 3.8 to 2 min, while the recovery time has increased from 2.2 to 3.6 min with increasing of temperature in the range 30 to 200 ºC towards 20 ppm of NO_2 gas. The decrease in response time is due to the large availability of vacant sites on the thin film for adsorption of the gas as evident from SEM images. Also the increase in recovery time may be due to the gases left behind after gas interaction, resulting in decrease in desorption rate.

The selectivity is one of the most important gas sensing properties for the gas sensors. The cross sensing response between NO_2 and other reducing gases such as NH_3, CO_2 and LPG were also investigated. Fig. 8.8 shows the selectivity of NO_2 gas over to NH_3, CO_2 and LPG in the different gas concentration. The maximum sensor responses at room temperature (30 ºC) towards NH_3, CO_2 and LPG are found as 3.2, 2.7 and 1.5, respectively.

8.3.4 Sensing mechanism

ZnO and SnO_2 are n-type semiconductors in which adsorbed oxygen reacts with the target gas, the electron in the conduction band by which the conductivity decreases and increased the film resistance. PANI is normally a p-type semiconductor. This is due to the fact that during the polymerization process aniline, acids (such as HCl) are used, which acts, as dopants of PANI molecule. Due to the reversible reaction; $O_2 + e^- \leftrightarrow O^-_{(ads)}$; $NO_{2(gas)} + e^- \leftrightarrow NO^-_{(ads)}$; $H^+ - PANI - Cl^- \leftrightarrow H - PANI^+ - Cl^-$; $PANI^+ + e^- + NO_2 \leftrightarrow PANI^+ + NO_2^-$; the protons on $-NH-$ groups were transferred to NO_2 to from NO_2^- while PANI turned into its base. When NO_2 was removed, the nitronium oxide ion could be decomposed to NO_2 gas and electron.

In our experiments, when NO_2 gas was exposed to SPZ nanocomposite thin film, the gas molecules were adsorbed through ZnO film which is an n-type semiconducting material. Therefore the film resistance increases. The sensing mechanism of SPZ nanocomposite is governed by the charge carriers/electrons in the conduction band of ZnO. SnO_2 is base material on which a PANI was deposited. As PANI is a p-type material but here it only increases the porosity of the film and decreases the activation energy along with the band gap near the interface of ZnO-PANI. Hence the resistance of

nanocomposite increases significantly with the exposure of NO_2 gas. As a result of the response of the SPZ nanocomposite film is much higher than sensor reported in previous Chapters.

8.4 Conclusion

We have prepared the SnO_2-PANI-ZnO (SPZ) nanocomposite thin film by a simple method using spin coating and investigated the NO_2 sensing properties. The XRD pattern confirmed that the formation of SPZ nanoparticles having polycrystalline nature with a c-axis orientation perpendicular to the substrate surface. The gas sensing tests indicated the SPZ nanocomposite thin film sensor exhibited good gas sensing performances to NO_2 gas, including high response value, fast response and recovery characteristics, great stability, good repeatability, good selectivity and low operating temperature (30 °C) due to high specific area, spatial structure and morphological properties. The SPZ thin film exhibited highest response of 995 and fast response and recovery time of 3.8 and 2.2 min respectively.

References:

[1] B.T. Marquis, J.F. Vetelino, A semiconducting metal oxide sensor array for the detection of NOx and NH_3, Sens. Actuators B: Chem., 77 (2001) 100-110.

[2] N. Barsan, D. Koziej, U. Weimar, Metal oxide-based gas sensor research: how to? Sens. Actuators B: Chem., 121 (2007) 18-35.

[3] N. Barsan, U. Weimar, Conduction model of metal oxide gas sensors, Journal of Electroceramics 7 (2001) 143-167.

[4] T. Inoue, K. Ohtsuka, Y. Yoshida, Y. Matsuura, Y. Kajiyama, Metal oxide semiconductor NO_2 sensor, Sens. Actuators B: Chem., 25 (1995) 388-391

[5] J. Brunet, V.P. Gracia, A. Pauly, C. Varenne, B. Lauron, An optimised gas sensor microsystem for accurate and real-time measurement of nitrogen dioxide at ppb level, Sens. Actuators B: Chem., 134 (2008) 632-639.

[6] D.W. Hatechett, M. Josowicz, Composites of intrinsically conducting polymers as sensing nanomaterials, Chemical Reviews 108 (2008) 746-769.

[7] U. Lange, N.V. Roznyatovskaya, V.M. Mirsky, Conducting polymers in chemical sensors and arrays, Analytica Chimica Acta 614 (2008) 1-26.

[8] H. Bai, G.Q. Shi, Gas sensors based on conducting polymers, Sensors 7 (2007) 267-307.

[9] M.I. Newton, T.K.H. Starke, M.R. Willis, G. McHale, NO_2 detection at room temperature with copper phthalocyanine thin film devices, Sens. Actuators B: Chem., 67 (2000) 307-311.

[10] Y.L. Lee, C.H. Chang, NO_2 sensing characteristics of copper phthalocyanine films: effects of low temperature annealing and doping time, Sens. Actuators B: Chem., 119 (2006) 174-179.

[11] C. Park, D.H. Yun, S.T. Kim, Y.W. Park, Enhancement of the NO_2-sensing capability of copper phthalocyanine by measuring the relative resistance change, Sens. Actuators B: Chem., 30 (1996) 23-27.

[12] L.N. Geng, Y.Q. Zhao, X.L. Huang, S.R. Wang, S.M. Zhang, S.H. Wu, Characterization and gas sensitivity study of polyaniline/SnO_2 hybrid material prepared by hydrothermal route, Sens. Actuators B: Chem., 120 (2007) 568-572.

[13] A. Choudhury, Polyaniline/silver nanocomposites: dielectric properties and ethanol vapour sensitivity, Sens. Actuators B: Chem., 138 (2009) 318-325.

[14] R.K. Sonker, S.R. Sabhajeet, S. Singh, B.C. Yadav, Synthesis of ZnO nanopetals and its application as NO_2 gas sensor, Mat. Lett. 152 (2015) 189-191.

[15] R.K. Sonker, A. Sharma, M. Tomar, V. Gupta, B.C. Yadav, Low Temperature Operated NO_2 Gas Sensor Based on SnO_2-ZnO Nanocomposite Thin Film, Adv. Sci. Lett. 20 (2014) 911-916.

[16] C.Q. Bian, Y.J. Yu, G. Xue, Synthesis of conducting polyaniline/TiO_2 composite nanofibres by one-step in situ polymerization method, Journal of Applied Polymer Science 104 (2007) 21-26.

[17] H. Liu, J.Y. Wang, X.B. Hu, R. Boughton, S.R. Zhao, Q. Li, M.H. Jiang, Structure electronic transport properties of polyaniline/$NaFe_4P_{12}$ composite, Chemical Physics Letters 352 (2002) 185-190.

[18] H. Xu, X. Chenc, J. Zhang, J. Wang, B. Cao, D. Cui, NO_2 gas sensing with SnO_2-ZnO/PANI composite thick film fabricated from porous nanosolid, Sens. Actuators B: Chem., 176 (2013) 166-173.

[19] K. Dutta, S.K. De, Optical and nonlinear electrical properties of SnO_2–polyaniline nanocomposites, Materials Letters 61 (2007) 4967-4971.

[20] G.N. Dar, A. Umar, S.A. Zaidi, Ahmed A. Ibrahim, M. Abaker, S. Baskoutas, M.S. Al-Assiri, Ce-doped ZnO nanorods for the detection of hazardous chemical, Sens. Actuators B: Chem., 173 (2012) 72-78.

[21] J. Elizalde-Torres, H. Hu, A. García-Valenzuela, NO_2-induced optical absorbance changes in semiconductor polyaniline thin films, Sens. Actuators B: Chem., 98 (2004) 218-226.

[22] C. Wongchoosuk, A. Wisitsoraat, D. Phokharatkul, M. Horprathum, A. Tuantranont, T. Kerdcharoen, Carbon doped tungsten oxide nanorods NO_2

sensor prepared by glancing angle RF sputtering, Sens. Actuators B: Chem., 181 (2013) 388-394.

[23] M.A. Chougule, D.S. Dalavi, S. Mali, P.S. Patil, A.V. Moholkar, G.L. Agawane, et al., Novel method for fabrication of room temperature polypyrrole–ZnO nanocomposite NO_2 sensor, Measurement, 45 (2012) 1989-1996.

[24] H. Xu, X. Chen, J. Zhang, J. Wang, B. Cao, D. Cui, NO_2 gas sensing with SnO_2–ZnO/PANI composite thick film fabricated from porous nanosolid, Sens. Actuators B: Chem., 176 (2013) 166-173.

[25] C.A. Betty, S. Choudhury, S. Arora, Tin oxide-polyaniline heterostructure sensors for highly sensitive and selective detection of toxic gases at room temperature, Sens. Actuators B: Chem., 220 (2015) 288-294.

[26] H. Xu, D. Ju, W. Li, H. Gong, J. Zhang, J. Wang, et al., Low-working-temperature, fast-response-speed NO_2 sensor with nanoporous-SnO_2/polyaniline double-layered film, Sens. Actuators B: Chem., 224 (2016) 654-660.

Figures:

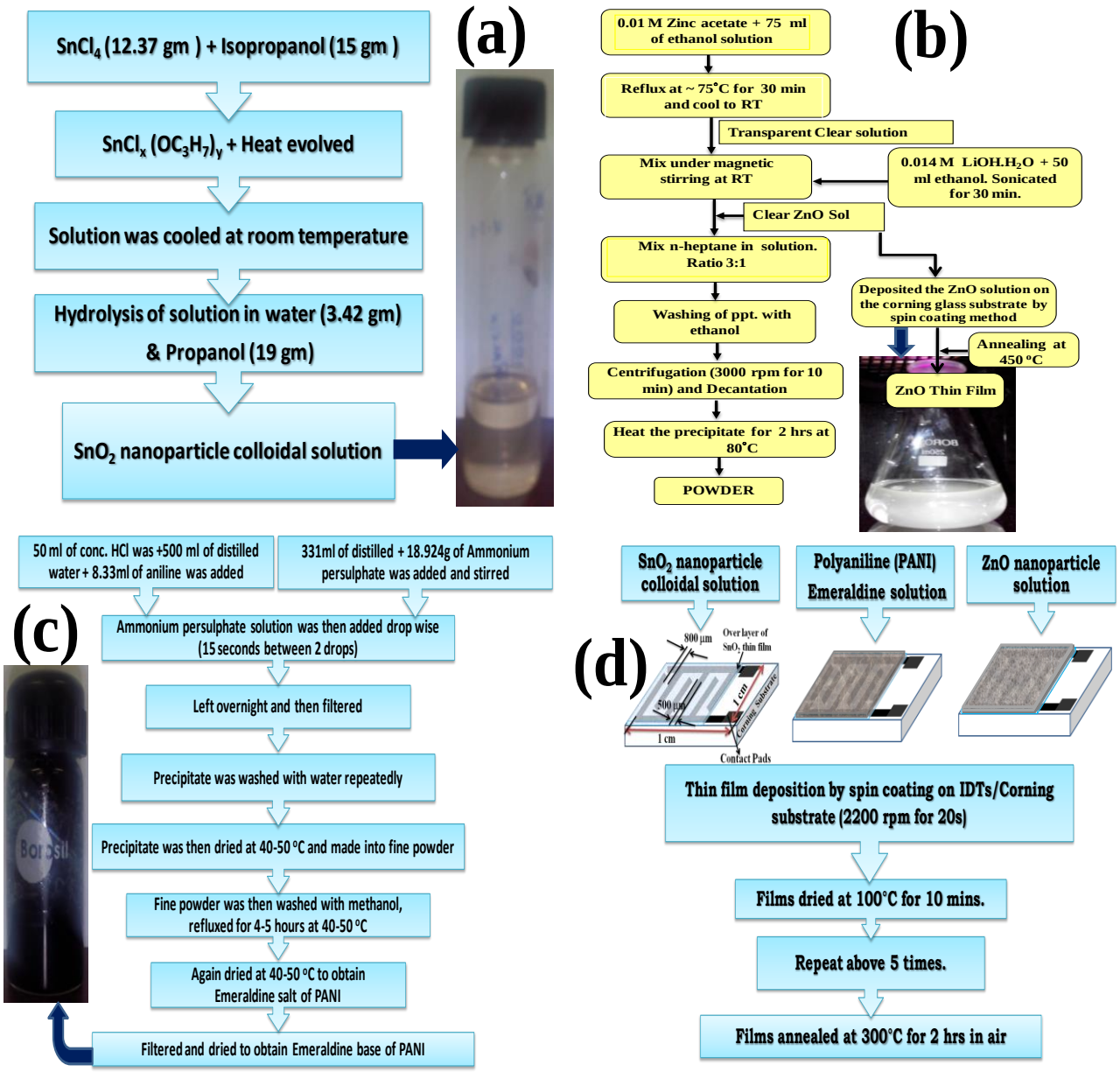

Fig. 8.1: Flow chart of the growth of (a) SnO_2 nanoparticle, (b) ZnO nanoparticle, (c) Emeraldine base PANI nanoparticle and (d) Fabrication of SPZ Sensor

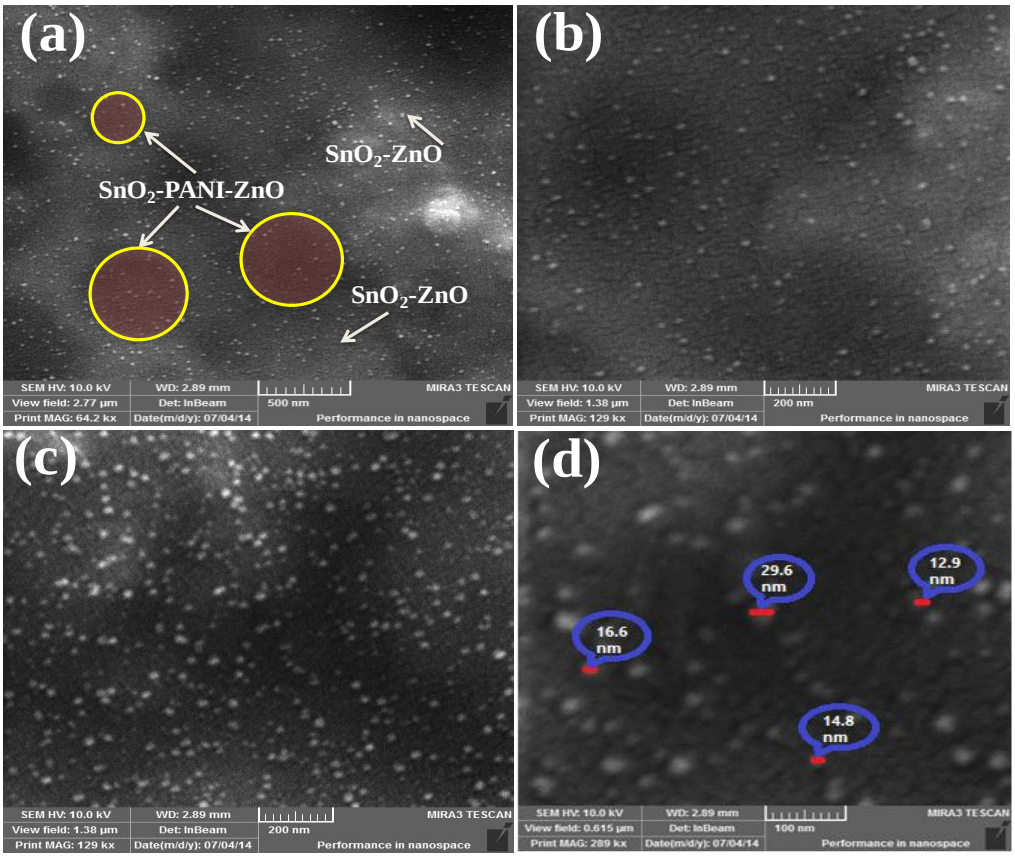

Fig. 8.2: The scanning electron micrographs of composite thin film

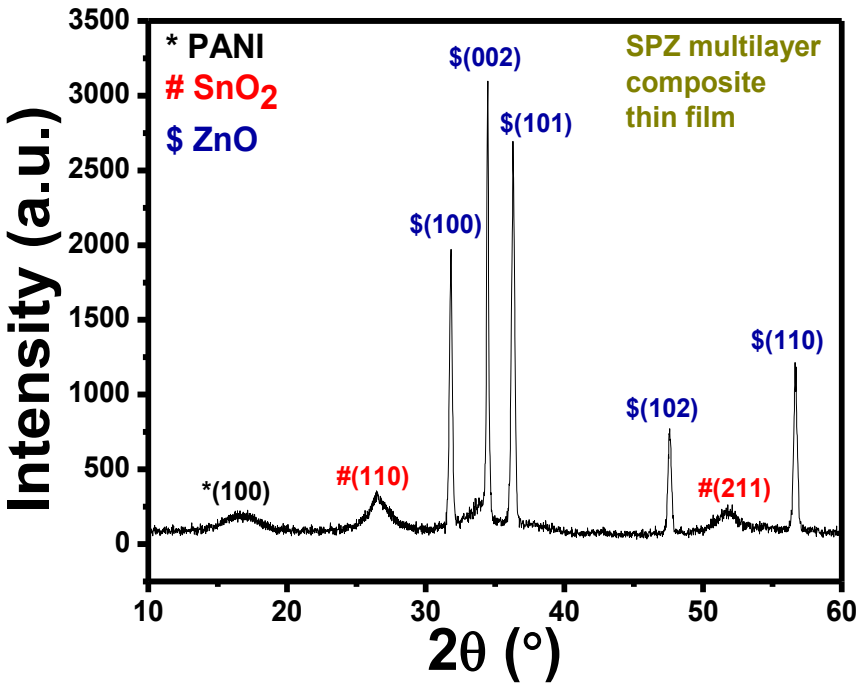

Fig. 8.3: SPZ nanocomposite thin film

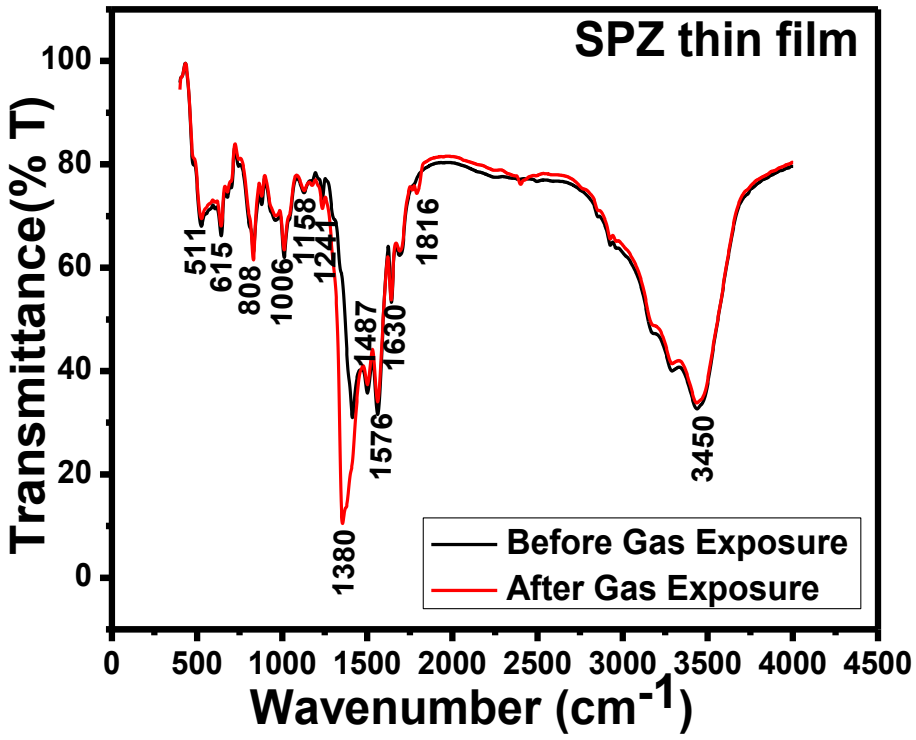

Fig. 8.4: FTIR spectra of SPZ film

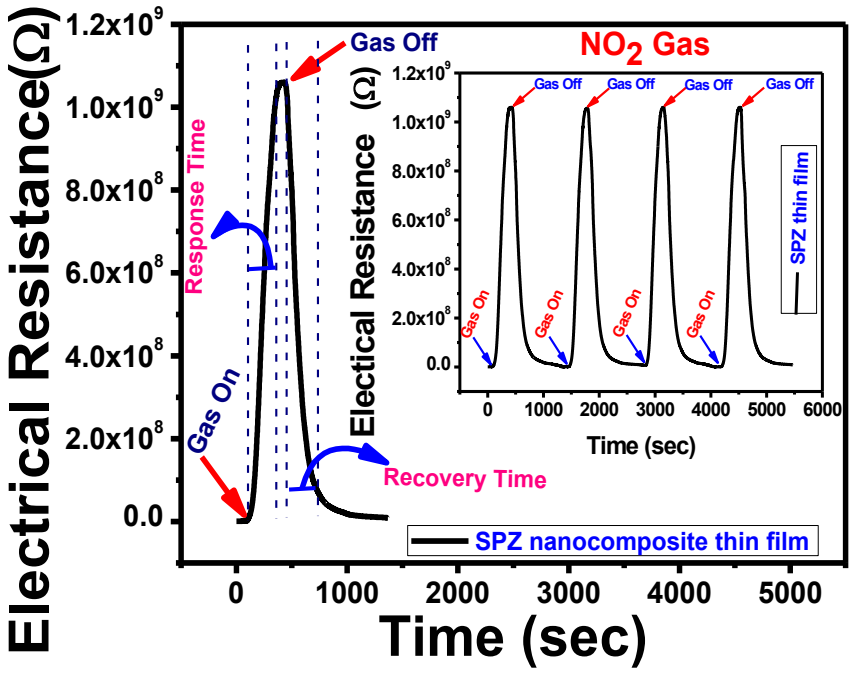

Fig. 8.5: Dynamic Response of the sensor to 20 ppm operable at room temperature, the inset displaying four periods of response curve

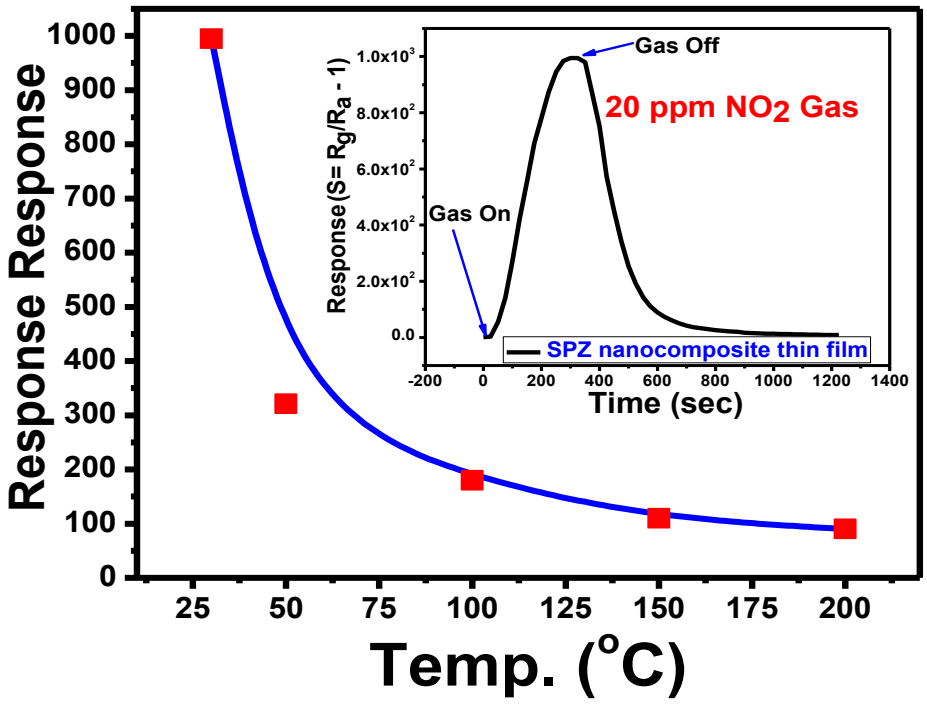

Fig. 8.6: Variation of sensing response of SPZ thin film as a function of temperature towards 20 ppm of NO_2 gas, the inset shown sensing response curve

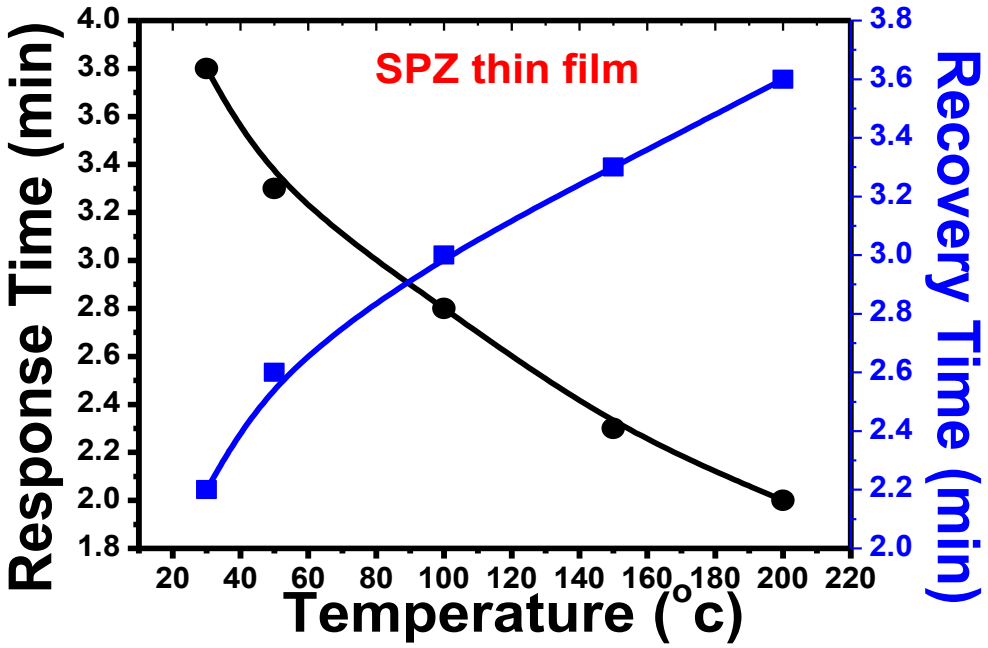

Fig. 8.7: Response and Recovery time of SPZ thin film as a function of temperature towards 20 ppm of NO_2 gas

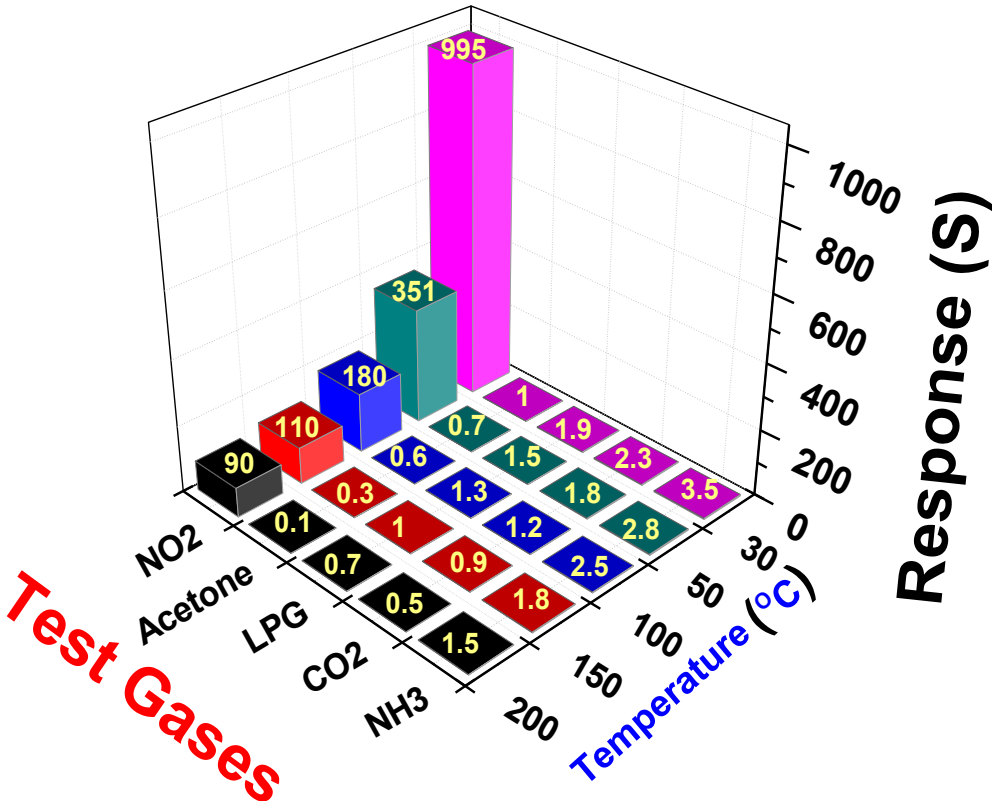

Fig. 8.8: Cross selectivity of SPZ sensor at different temperature

Table 8.1: Literature survey on catalyst modified/polymer doped metal oxide based NO_2 gas sensors

Materials Used	**Modifiers/ Catalyst**	**Methods**	**Opera-ting Temp. (^oC)**	**Gas Conc. (ppm)**	**Response**	**Res./Rec. Time**	**Ref.**
PANI	PAMPS	Sol-Gel	RT	10	50%	-/-	[21]
WO_3	Carbon	Sputtering	150	5	325	17 s/21s	[22]
ZnO	PPy	Hydrother mal	RT	10	57%	4 min/15 min	[23]
SnO_2-ZnO	PANI	Sol-Gel	180	35	376	9 s/ 27 s	[24]
SnO_2	PANI	Sol-Gel	RT	1	1.21	5 min/15 min	[25]
SnO_2	PANI	Sol-Gel	140	37	8.3	17 s/25 s	[26]
SnO_2	PANI/ZnO	Sol-Gel	RT	20	995	3.8 min/2.2 min	Present Work

Chapter 9

Concluding Remarks and Scope of Further Research

A study of synthesis, characterization and NO_2 sensing properties of polyaniline, iron oxide, zinc oxide and tin oxide is summarised in the present chapter. This chapter also gives the guidelines for further research work in the field of nanosized materials and their composites as NO_2 sensor.

9.1 Conclusion

Use of nanotechnology in engineering materials for sensor applications may improve the working detection limit of gas sensors to lower temperatures. This will be achieved predominantly by alterations of the space charge layers for each grain and enhancing other electronic properties of the material. The large surface to volume ratio of nanomaterials can be used as an advantage to contribute in gas sensor development. The surface reaction on the gas sensor is improved when the number of defect sites for reaction is increased. The large surface area to volume ratio of nanocrystalline structures increases the opportunity for this surface reaction to occur. This in turn will increase the sensitivity of the gas sensor. The surface of nanomaterials can comprise much of the actual material making them ideal for gas sensors. Chapter-1 includes the introduction of recent development in sensor and its limitations. The sensing principle and extensive survey of literature on the development of NO_2 sensor and its present status have been discussed. The orientation of work, aims and objectives of the present research investigation are well described at the end of the Chapter. It also deals with the description of synthesis and characterization techniques used in the present research work. The advantage of sol-gel technique over other synthesis methods has been described. Chapter-2 describes the synthesis of nanostructured Fe_2O_3 and Fe_2O_3-PANI thin films and their applications as NO_2 gas sensor working at room temperature. Various chemical pollutants have been released in high quantities into the atmosphere as a result of human activities and have generated environmental risks. In order to monitor the air pollution on a large scale, inexpensive, reliable and easy to use gas sensors are needed. In the Chapter-3 an effort has been made to fabricate nanopetal structured thin film of zinc oxide using chemical route for the efficient and fast detection of NO_2 gas at lower operating temperature. A study of synthesis, characterization and NO_2 sensing properties of ZnO and ZnO-PANI is summarized in Chapter 4. Chapter 5 describes the fabrication of Nanocatalyst (Pt/Ag/Cu) doped SnO_2 thin films and its applications as NO_2 sensors operable at low temperature. In Chapter 6 describes the synthesis of SnO_2-PANI nanocomposite using sol-gel method fabrication of same material deposited on the corning glass substrate IDEs using spin coating technique. Also this material was

exploited for room temperature detection of NO_2 gas. In Chapter 7 the preparation of SnO_2-ZnO nanocomposite thin film and its applications as NO_2 gas sensor is described in details. Chapter 8 describes the synthesis of SnO_2-polyaniline (PANI)-ZnO nanocomposite thin film for NO_2 sensor operable at room temperature. Chapter 9 deals with summary of the work done and the concluding remarks drawn from the present research work. Future scope for further research work in the field of nanosized materials and their composite as NO_2 gas sensor has been depicted at the end of this thesis.

A study of synthesis, characterization and sensing properties of polymer doped metal oxide is summarized as below:

9.2 Low temperature study of nanostructured Fe_2O_3 and Fe_2O_3-PANI thin films as NO_2 sensor

Nanostructured ferric oxides of different surface morphologies were synthesized via sol-gel method as shown in Fig. 9.1. The employed sol-gel method of synthesis was simple and high yielding without incorporation of any organic material. This method can be used for scale-up industrial production of ferric oxide. The structural analysis confirmed the formation of Fe_2O_3 with α-phase and rhombohedral structure. We have investigated the NO_2 sensing properties of PANI doped ferric oxides having different surface morphologies. Variations in resistance of the thin film as prepared, annealed at 200 °C and 500 °C with time after exposure of 20 ppm of NO_2 gas were recorded at room temperature (30 °C). Ferric oxide-polyaniline composite thin film sensor structure has been designed for the trace level (20 ppm) detection of NO_2 gas at room temperature with sensor response ~2.29×10^2, moderate response time ~2.35 min and recovery time as 3.80 min. Nanoporous spherical surface morphology having nanocrystalline grains were found of much importance for obtaining the enhanced response characteristics.

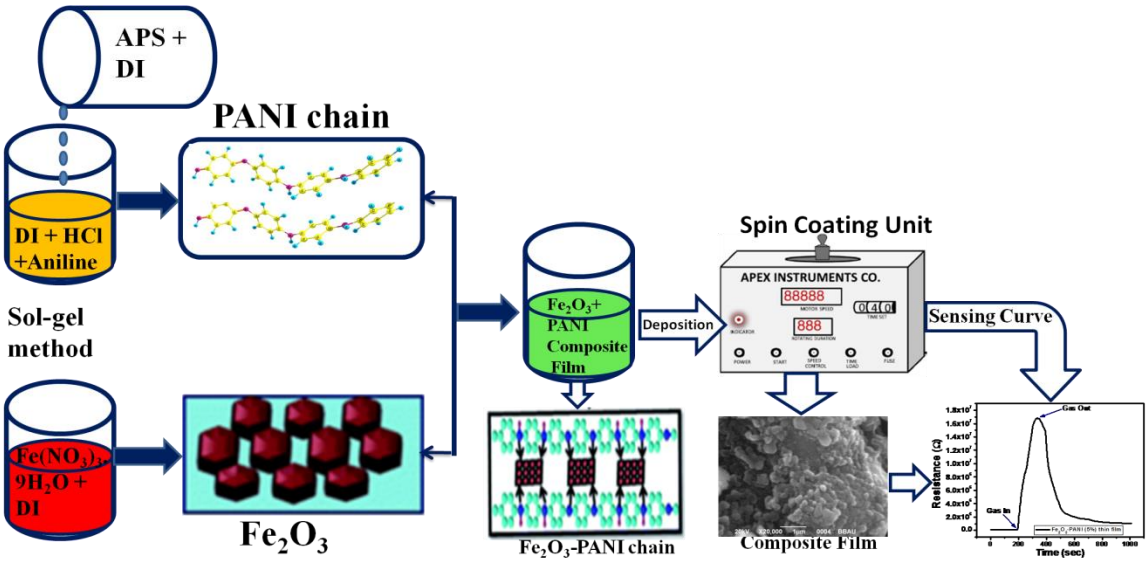

Fig. 9.1: Flow chart of iron oxide-PANI composite thin film

9.3 Fabrication of NO_2 gas sensor using nanostructure Zinc oxide

We have described the synthesis of nanopetals shaped and hexagonal zinc oxide nanoparticles and characterized for their structural, optical and surface morphological properties.

The mechanism of the NO_2 gas sensing of ZnO thin film has been explained on the basis of surface adsorbed oxygen on the sensor surface (shown in Fig. 9.2). we conclude that ZnO nanopetals based sensor has high sensing response 169, with lowest response time 1.42 min and fast recovery time 1.71 min whereas the sensor based on ZnO hexagonal nanocrystals show lower sensing response with enhanced response and recovery times due to bigger crystallite size (71 nm) and lower specific surface area (272 m^2/gm). Thus this study explored the relevancy and possibility of ZnO nanopetals based sensor for the detection of low level of NO_2 gas at room temperature.

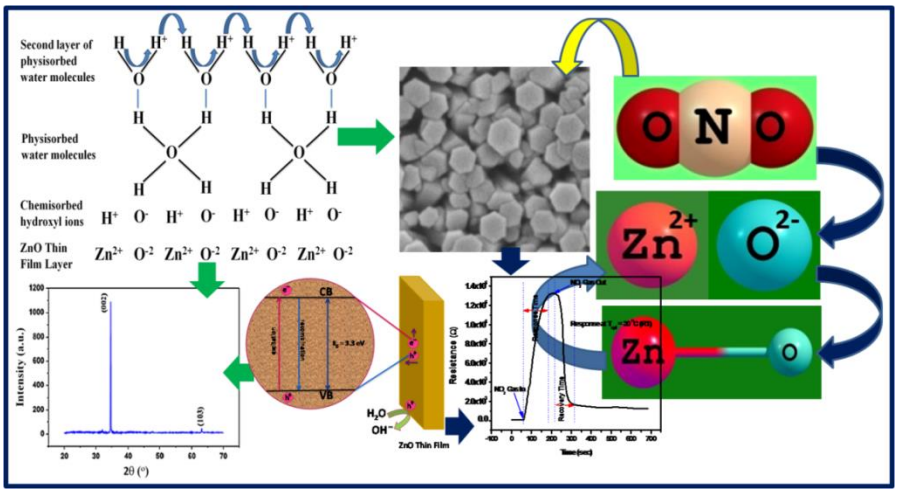

Fig. 9.2: The adsorption of NO_2 gas molecule and corresponding phenomenon

9.4 Experimental Investigations on NO_2 sensing of Pure ZnO and PANI-ZnO composite thin films

ZnO and PANI-ZnO composite film was prepared by sol-gel method on IDEs/corning glass substrate and their NO_2 sensing properties as variations in conductivity of sensor were investigated. The sol-gel method has certain advantages such as low cost, simple in construction and having excellent sensing properties. SEM images show nails type of the surface morphology throughout the surface. XRD analysis shows all the peaks correspond to wurtzite of ZnO. The values of energy band gaps of as prepared ZnO and ZnO-PANI composite were found as 3.38 and 3.74 eV from the UV-visible transmittance spectrum.

The NO_2 sensing properties of the ZnO and PANI-ZnO composite films were investigated at different operating temperature towards 20 ppm NO_2 gas. The variations in electrical resistance of the film were measured with the exposure of NO_2 as a function of time. The maximum sensing response ~ 611 at room temperature towards 20 ppm of NO_2 gas was obtained for ZnO-PANI (5%) hybrid composite sensor with a fast response and recovery times of about 2.16 min and 2.83 min respectively. However, the sensing responses as 170, 250 and 120 were obtained for bare ZnO, ZnO-PANI (1%) and ZnO-PANI (10%) sensor structures respectively towards 20 ppm of NO_2 gas showing the importance of optimum concentration of PANI (5%) in the sensing layer of

nanocomposite ZnO-PANI. Thus this sensor structure can be reliably used for the detection of NO_2 gas at commercial level at room temperature. The schematic of the reaction of NO_2 sensing is shown in Fig. 9.3.

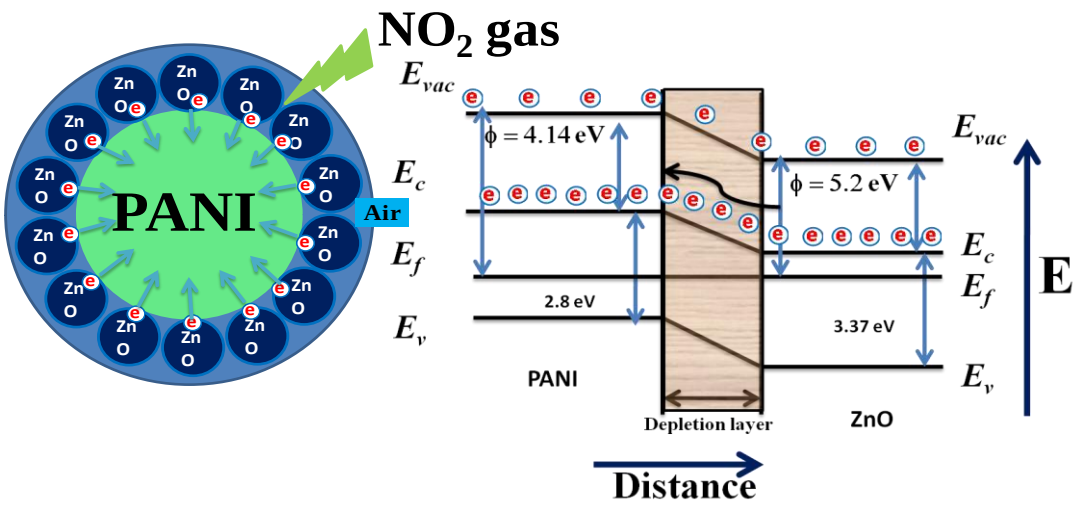

Fig. 9.3: Schematic of the sensing mechanism of NO_2 through ZnO-PANI with Energy Band Diagram

9.5 Nanocatalyst (Pt, Ag and CuO) doped SnO_2 thin film based sensors for low temperature detection of NO_2 gas

Sol-gel method has been used for the synthesis of porous tin oxide nanoparticles which were applied as NO_2 sensing material and has been demonstrated as an evidence of hollow structure effects on the sensing characteristics. X-ray diffraction analysis revealed the formation of SnO_2 having rutile structure. The minimum crystallite size was found 5.34 nm. Surface morphological investigations showed the uniform and bead structured surface morphology.

Other NO_2 gas sensors operating at a low operating temperature of 90 ºC were fabricated by doping Pt, Ag and CuO into SnO_2 thin film using chemical route. The maximum sensing response of about 183 towards 20 ppm of NO_2 gas was obtained for SnO_2-Pt sensor structure with a fast response and recovery times of 5 sec and 13 sec respectively. However, the sensing responses of 52 and 95 were obtained for SnO_2-Ag and SnO_2-CuO sensor structures respectively towards 20 ppm of NO_2 gas with fast

response and recovery times of about 85 and 186 sec; 25 and 50 sec respectively. The enhanced sensing response obtained by incorporation of Pt in SnO_2 has been attributed to the higher work function of Pt as compared to other dopants.

9.6 Design and fabrication of tin oxide-polyaniline nanocomposite thin films and their employment as nitrogen oxide gas sensor

Tin oxide-polyaniline was successfully synthesized and thin film was fabricated using sol-gel spin coating technique as shown in Fig. 9.4. This material exhibits a new strategy to produce NO_2 sensor by combining readily gas-accessible sensing layers and catalytic surface additives. X-ray diffraction analysis reveals the formation of SnO_2 having rutile structure. The estimated value of average crystallite size of SnO_2 and SnO_2-PANI was found 7.05 and 5.64 nm. The XRD pattern clearly identifies that only tetragonal SnO_2 phase was formed after annealing at 550 °C.

In the present work, an effort has been made to develop SnO_2-PANI composite thin film gas sensor which responds efficiently towards NO_2 gas at room temperature. The variation of PANI concentration in SnO_2 thin film has been studied and found that 1% of PANI gives the enhanced sensing response of about 258 at room temperature (30 ^oC) towards 20 ppm of NO_2 gas with moderate response and recovery time of 5.8 and 4.55 min. respectively. The possible enhancement is related to the formation of p-n junction at interface of PANI (p-type) and SnO_2 (n-type) nano-particles. The surface morphology having nanocrystalline grains are found to be important for obtaining enhanced response characteristics. Also SnO_2-PANI (1%) sensor structure was found to be highly selective towards NO_2 gas at room temperature with enhanced sensor characteristics.

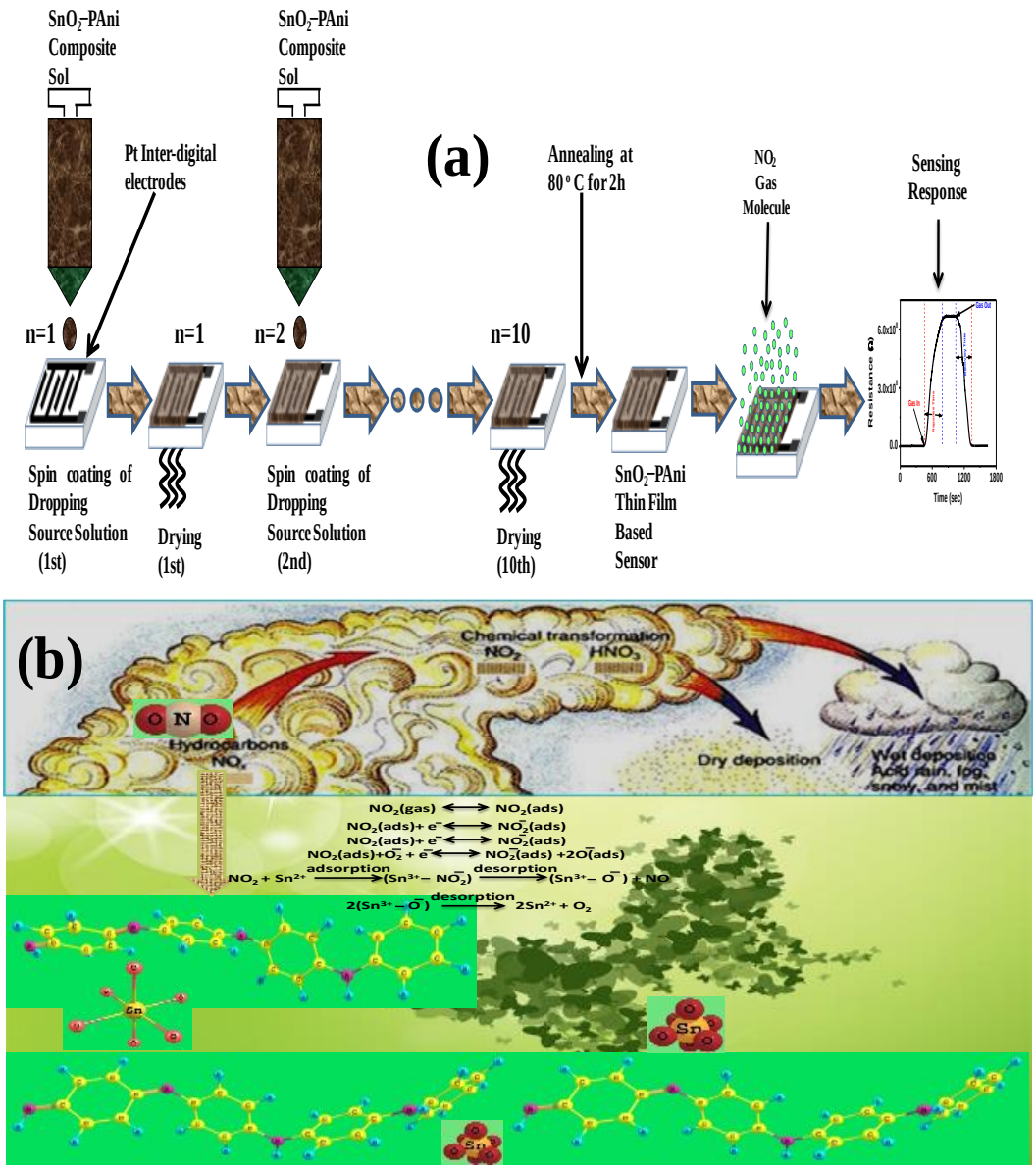

Fig. 9.4: (a) Spin coating technique for fabrication of thin film and (b) Effect of NO_2 on environment

9.7 Low temperature operated NO_2 gas sensor based on SnO_2-ZnO nanocomposite thin film

SnO_2-ZnO (SZO) nanocomposites of different surface morphologies were synthesized via sol-gel method shown in Fig. 5. This method can be used for scale-up industrial production of SnO_2 and ZnO. The structural analysis confirmed the formation

of SZO nanocomposite and tetragonal structure. SnO_2 thin film and SZO nanocomposite thin films based sensor structure have been fabricated and exploited for the trace level (20 ppm) detection of NO_2 gas at low operating temperatures (<100 °C). This sensor exhibited the enhanced sensing response as 1.578 $\times 10^3$ with faster response time (7 min.) and recovery times (6 min.) at operating temperature of 70 °C in comparison to previously reported sensor. Mesoporous surface morphology having nanocrystalline grains were found to be important for obtaining the enhanced response characteristics.

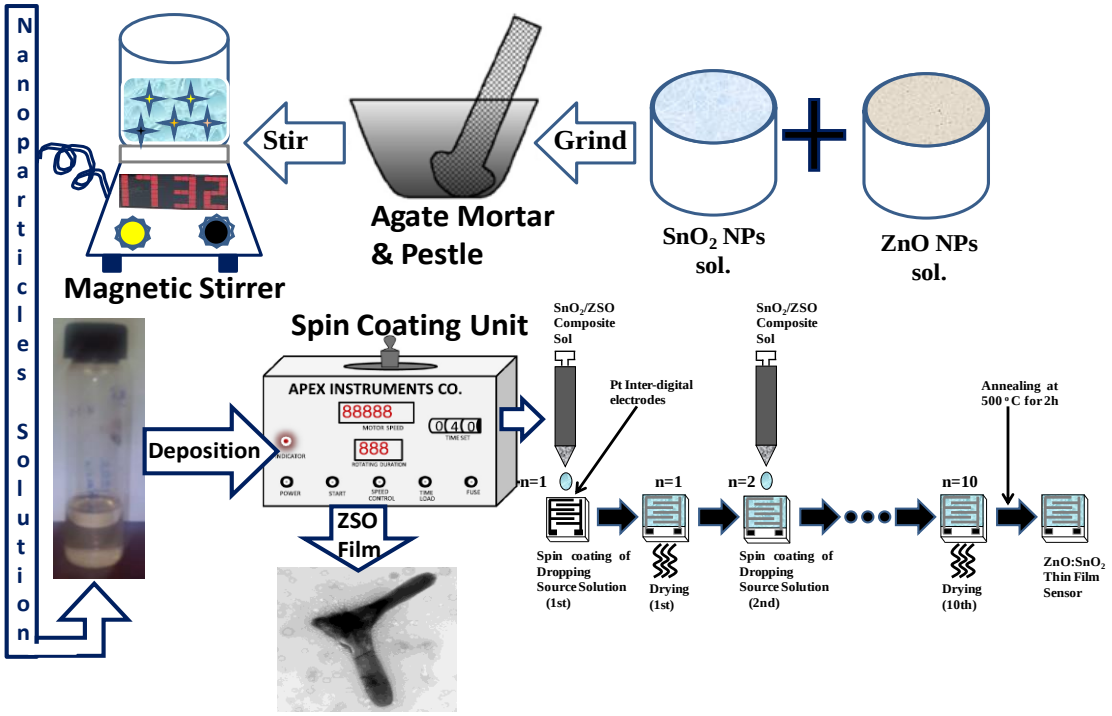

Fig. 9.5: Synthesis of SnO_2 and SZO nanocomposite material and thin film deposition

9.8 SnO_2-Polyaniline-ZnO (SPZ) multilayered nanocomposite thin film as NO_2 gas sensor

We have prepared the SnO_2-PANI-ZnO (SPZ) nanocomposite thin film by a simple method using spin coating and investigated the NO_2 sensing properties. The XRD pattern confirmed that the SPZ nanoparticle have polycrystalline nature with a c-axis orientation perpendicular to the substrate surface. The gas sensing tests indicated the SPZ nanocomposite thin film sensor exhibited good gas sensing performances to NO_2 gas,

including high response value, fast response and recovery characteristics, good stability, repeatability, high selectivity and low operating temperature (room temperature) due to high specific area, spatial structure and morphological properties. The SPZ thin film exhibits the highest response of 995 and fast response and recovery times as 3.8 and 2.2 min respectively. The graphical abstract of entire work carried out is shown in Fig. 9.6.

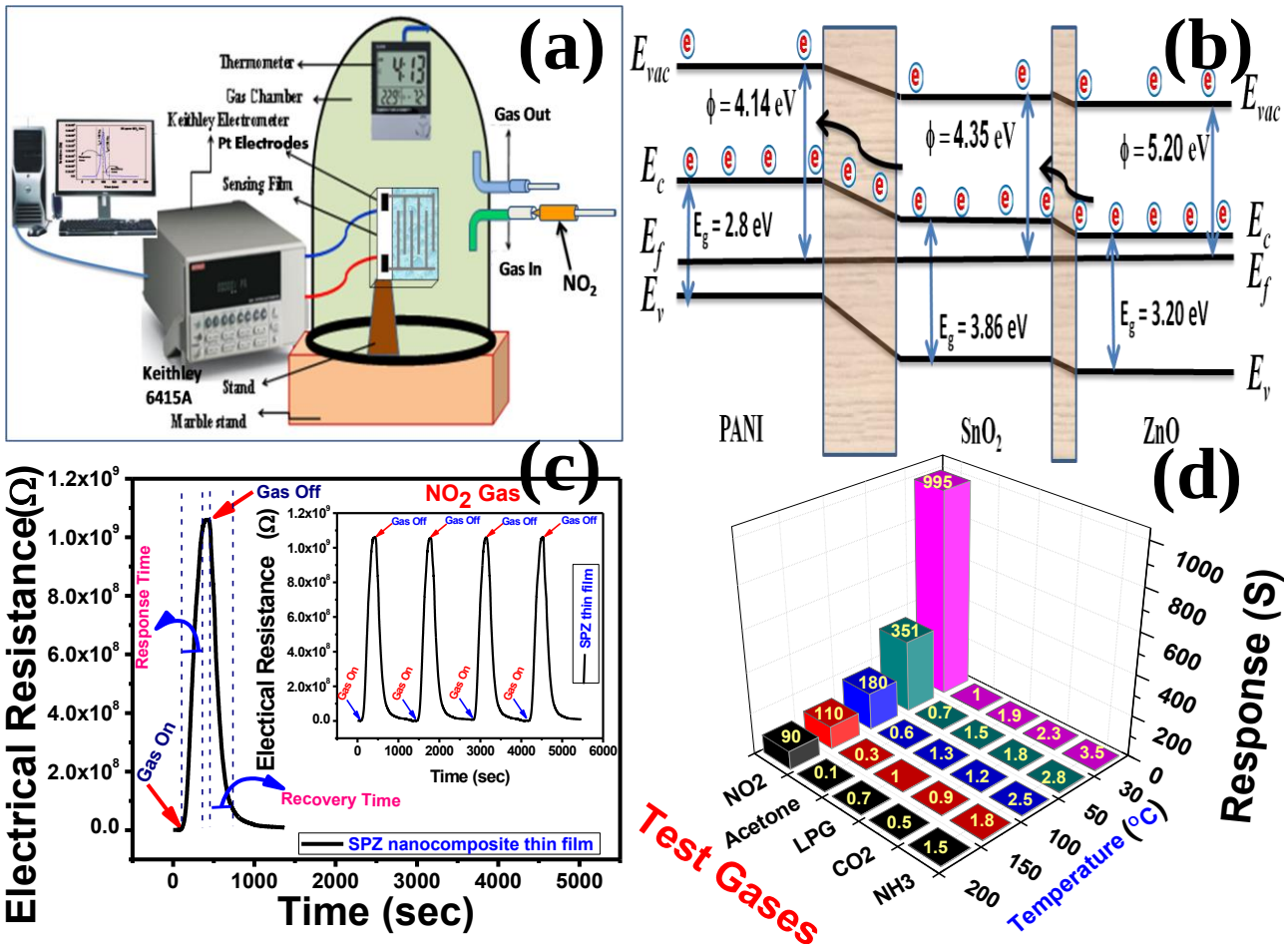

Fig. 9.6: Graphical Abstract

A chapter wise sketch of the thesis including the materials, dopants, percentage sensor response, response and recovery time, crystallite size and pore size is depicted in Table 9.1. The main goal of our research work carried out was to design and fabricate a NO_2 gas sensor which would be robust, cost effective and highly responsive than previously reported sensors.

Table 9.1: A chapter wise sketch of the Thesis

Chapter No.	**Sensing Material**	**Doping**	**Max. Response at 20 ppm of NO_2 gas**	**Min. Response Time (min)**	**Min. Recovery Time (min)**	**Crystallite Size (nm)**	**Pore Size (nm)**
Chapter 1	Introduction						
Chapter 2	Fe_2O_3 thin film Fe_2O_3-PANI thin film	-----	114 229	7.13 2.35	7.66 3.80	34 27	125 258
Chapter 3	hexagonal nanocrystals ZnO nanopetals ZnO	---- ----	90 169	2.42 1.42	1.76 1.71	71.0 29.1	80 119
Chapter 4	ZnO nanoparticle	PANI	611	2.16	3.50	5	900
Chapter 5	SnO_2 thin film	Pt	183	0.10	0.25	5.3	38
Chapter 6	SnO_2 thin film	PANI	258	5.80	4.55	5.4	152
Chapter 7	SnO_2 thin film	ZnO	300	10.23	11.75	4.5	105
Chapter 8	SnO_2-ZnO composite thin film	PANI	995	3.80	2.20	--	--
Chapter 9	Conclusion						

9.9 Scope and Further Research

1. In the present work, only the Polyaniline (PANI) doped metal oxide thin film has been optimized, however, the diameter and distribution of the modifiers may also affect the response characteristics. Hence, an effort may be made to use different type of masks to optimize the diameter and distribution of PANI/modifiers doped metal oxide.

2. An effort may also be made to integrate the reduced grapheme oxide (rGO) doped nanostructured ZnO and SnO_2 by CVD/chemical route for NO_2 sensing application.

3. ZnO and SnO_2 thin film based NO_2 gas sensors have been prepared using sol-gel technique. To improve the sensing response parameters, there is scope for integration of best identified modifiers like WO_3, TeO_2 and Al_2O_3 for the fast detection of NO_2 gas for the outdoor applications.

4. Theoretical modelling on sensing mechanism of NO_2 and other oxidising gases with the metal oxides may be under taken for further investigations.

APPENDIX

Experimental Methods and Characterization Techniques

The experimental facilities used throughout the whole thesis work have been presented in this chapter. The synthesis part shows the chemical route of the synthesis of conducting polymer, metal oxides whereas the characterization part shows the experimental techniques used such as TEM, SEM, Raman, AFM, TGA, FTIR,UV-visible, dielectric spectroscopy etc.

A.1 Introduction

The experimental part of research work plays very critical role in the outcome of any research work. This Chapter describes the methodology and various experimental techniques used in the preparation and modification of nanostructured polyaniline (PANI) doped Tin oxide (SnO_2-PANI), polyaniline (PANI) doped zinc oxide (ZnO-PANI), PANI doped iron oxide (Fe_2O_3-PANI), zinc oxide doped tin oxide (SnO_2-ZnO) and PANI doped zinc oxide doped tin oxide (SnO_2-ZnO-PANI) composite thin films. These films were characterized using Fourier transform infrared (FT-IR), Raman, UV-Vis spectroscopy, AFM, SEM, TEM, and TGA. These techniques have been described in detail in this chapter.

A.2 Methodology of present work

The methodology adopted in the present thesis is summarized as following:

- Synthesis of conducting PANI doped ZnO as thin film and bulk composite by sol-gel techniques.
- Synthesis of conducting PANI doped SnO_2 as thin film and bulk composite by sol-gel techniques.
- Synthesis of conducting ZnO doped SnO_2 as thin film and bulk composite by sol-gel techniques.
- Sensing characteristics of the optimized Fe_2O_3, Fe_2O_3-PANI, ZnO, ZnO-PANI, SnO_2-PANI, SnO_2-ZnO and SnO_2-ZnO-PANI composite thin films towards NO_2 sensing.

A.2.1 Methods

A.2.1.1 Sol-gel Techniques

A solution (sol) is a dispersion of the solid particles (~ 0.1-1 μm) in a liquid where only the Brownian motions suspend the particles. A gelation (gel) is a state where both liquid and solid are dispersed in each other, which forms a solid network containing liquid components. The schematic flow chart of sol-gel process is shown in Fig. 1.1. The sol-gel coating process usually consists of 4 steps [1-2].

1. The desired colloidal particles are dispersed in a liquid to form a sol.
2. The deposition of sol produces the coatings on the substrate by spraying, dipping or spinning.
3. The particles in sol are polymerized through the removal of the stabilizing components and produce a gel in a state of a continuous network.
4. The final heat treatment pyrolyze the remaining organic or inorganic components and form an amorphous or crystalline coating.

The increasing demand for multifunctional materials requires a stronger multidisciplinary approach as well as the merging of the traditional scientific disciplines (chemistry, physics, and biology) into new cross-boundary technologies. Moreover, these novel technologies have to be able to bridge the gap between polymers, ceramics or metals, between organic and inorganic materials, or between the mineral and biological world. Sol-gel technology might offer a solution. The first experiment on sol-gel was performed in the fifties of the previous century. By their inorganic nature, sol-gel layers are extremely strong and wear resistant. Therefore, very thin 'nanometric' layers surface to obtain the desired effects. Since several years, there is an increasing demand of sol-gel technology in the application of device fabrication. However, the formula and methods used in other industrial branches have to be adopted to the raw materials and specific properties [3-4]. In the present work, sol-gel technique will be exploited for the synthesis and deposition of ZnO-PANI, SnO_2-PANI and SnO_2-ZnO thin films.

A.2.2 Fabrication Techniques for Thin Film

A.2.2.1 Sputtering

In an alternating electric field, electrons oscillate to and fro and during their motion they collide with other atoms. The ordered motion changes to random motion due to the collisions. The energy of electrons increases sufficiently to produce ionization collision, which further releases more electrons. The high voltage, essential in dc-sputtering for the generation of secondary electrons to sustain the discharge is not

required in rf sputtering. The electrons in the plasma will have sufficient energy to directly ionize gas atoms, reducing the dependence on the secondary generation of electrons at the cathode. At an operating frequency of 13.56 MHz, the ions in the plasma can no longer move quickly enough to offset the changing field, due to which only a little accumulation of positive ions occur during the portion of the cycle in which the target electrode is acting as a cathode. However, due to the high mobility of electrons, the electron current in the target surface is initially much higher than the ion current. This results in a fixed negative dc bias on the target with respect to the plasma. The value of the bias potential is close to half of the peak-to-peak rf voltage on the target surface. The positive ions from the plasma are accelerated towards the target essentially by the bias potential (V_b) rather than the rf potential, and bombard the target surface with energy of the order of V_b electron volts to sputter out the atoms. The rf diode sputtering unit were use for preparation of Pt Interdigited electrods (IDTs) shown in Fig. 1.2 and a platinum IDTs shown in Fig. 1.3.

A.2.2.2 Spin coating unit

Preparation of a highly cross-linked solid thin film, onto substrates can be achieved by mean of hydrolysis and condensation of the molecular precursor using the spin coating technique. The substrate is placed on the chunk table and holded by vacuum (~10^{-2} mTorr), so as to keep it stable while providing rotation. Once the substrate is fixed on the chuck, the filtered precursor solution is drop casted on the substrate using the pipette in measured quantity and allowed to spin at a particular rpm in spin coater (Fig. 1.4). Typical spinning speed is ranging from 500 to 6000 rpm, depending on the properties of the fluid as well as the substrate. To achieve a required thickness of film along with uniformity the combination of spin speed and time are selected and optimized. In the spin-up stage, the liquid flows radially outwards by means of centrifugal force acting outwards giving rise to the formation of uniform thin film.

A.3 Thin Film Characterization techniques

Synthesis of ZnO-PANI, SnO_2-PANI and SnO_2-ZnO composite thin films were characterized by various characterization techniques to study the optical properties,

surface morphology and electrical and dielectric properties using XRD, FTIR, UV-Visible, Raman Spectroscopy, Scanning Electron Microscopy (SEM), TEM, AFM and TGA.

A.3.1 Structural Characterization

A.3.1.1 X-ray diffraction

X-ray diffraction (XRD) is an indispensable characterization tool for the study of crystallographic structure of matter and has been extensively used for the investigation of the orientation of deposited material, determination of grain size, estimation of stress etc. The periodic and regular arrangement of atoms in the crystal acts as scattering centers, because the interplanar spacing is of the order of the wavelength of X-rays. In a typical powder XRD system monochromatic X-ray radiation is incident on the powder specimen at an angle θ, called the Bragg's angle, and the intensity of the diffracted beam is measured simultaneously. For a given angle of incidence (θ), only those reflections from a crystal plane will be detected in the scattered beam which satisfies the Bragg's diffraction condition:

$$n\lambda = 2d \sin\theta \qquad (1.1)$$

where, n is the order of diffraction, 'λ' is the wavelength of X-rays (λ = 1.54056 Å for Cu K_α radiation), and 'd' is the inter-planar spacing.

In the present work, a Bruker D 80 X Ray diffractometer is used to study the crystallographic structure of the metal oxide (SnO_2) and polymer doped metal oxide thin films shown in Fig. 1.B.5. The specimen is mounted at the center of the diffractometer and is rotated continuously around an axis parallel to the film surface. The X-ray beam after passing through the collimator strikes the specimen. The diffracted radiations are detected by the detector which converts it into a corresponding electrical signal. The various reflections obtained in the XRD spectra of a sample corresponding to the crystal planes (*hkl*) could be indexed after matching with the standard data available for same material composition. Subsequently, the value of interplanar spacing distance (d_{hkl}) corresponding to a particular plane (*hkl*) can be estimated using equation 1.1.

A.3.1.2 Lattice parameter and crystallite size calculation

The lattice constants (*a, b* and *c*) of the unit cell of a sample can be determined from the values of interplanar distance (d_{hkl}) for a particular crystal plane (*hkl*). SnO_2 possess a rutile structure with a unit cell having '$a = b \neq c$', wherein the tin atom has six coordinates and the oxygen atom has three coordinates [5]. For a tetragonal lattice, the interplanar distance (d_{hkl}) is given by [6]:

$$\frac{1}{d_{hkl}} = \frac{h^2}{a^2} + \frac{k^2}{b^2} + \frac{l^2}{c^2} \tag{1.2}$$

For SnO_2 unit cell 'a = b', therefore Eq.(1.2) reduces to

$$\frac{1}{d_{hkl}} = \frac{h^2 + k^2}{a^2} + \frac{l^2}{c^2} \tag{1.3}$$

ZnO possess a hexagonal wurtzite structure with a unit cell having 'a = b ≠ c'. For a hexagonal lattice, the interplanar distance (d_{hkl}) is given by [6]:

$$\frac{1}{d_{hkl}^2} = \frac{h^2 + hk + k^2}{a^2} + \frac{l^2}{c^2} \tag{1.4}$$

Linear equations corresponding to each reflection in the XRD spectra could be obtained after substituting the respective value of *d* for (*hkl*) plane in equations (1.3) and (1.4) respectively for SnO_2 and ZnO samples, and the values of lattices parameters can be calculated. For (002) reflection of ZnO, substituting $h = k = 0$ and $l = 2$ in equation (1.4) the lattice parameter 'c' can be calculated as:

$$c = 2d_{hkl} \tag{1.5}$$

The average crystallite size (*X*) of the synthesized material (in thin film, ceramic or powder form) can be calculated from the full width at half maximum (FWHM) of the dominant peak in the XRD spectra using the well known Scherrer's formula given by

$$X = 0.94\,\lambda/(\beta\, cos\theta) \tag{1.6}$$

Where β is the full width at half maximum FWHM (in radians) of the dominant XRD peak and λ is the wavelength of X-rays (1.5406 Å for Cu $K\alpha_1$ radiation).

Stress induced in ZnO thin films can also be determined using XRD data as [7]:

$$\sigma = \left[2c_{13} - c_{33}\frac{(c_{11}+c_{12})}{c_{13}}\right]\frac{c_0 - c}{c_0} \quad (1.7)$$

where, c_0 is the lattice constant of bulk and c is the lattice constant of the film and C_{ij} are the elastic stiffness constants for ZnO.

A.3.2 Optical characterization

A.3.2.1 Fourier Transform Infrared (FTIR) Spectroscopy

Fourier transform infrared spectroscopy is a useful method for the characterization of conducting polymers because it does not require polymers to be soluble in any other solvent. It is primarily used for the detection of functional groups but analysis of spectra in the lower frequency finger print region can give evidence of degree of polymerization. The absorption versus frequency characteristics of light transmitted through a specimen irradiated with a beam of infrared radiation provide a detail of molecular structure. The infrared radiation is absorbed when a dipole vibrates naturally at the same frequency in the absorbing material. The pattern of vibrations is unique for a given molecular structure. The intensity of absorption is related to the quantity of absorber. Fig. 1.6 (a) shows the Schematic for Michelson interferometer and Fig. 1.6 (b) shows the Perkin Elmer GX 2000 FTIR spectrometer. Therefore, infrared spectroscopy allows the determination of components or groups of atoms/molecules that absorb the radiation in the infrared frequency range, permitting identification of the molecular structure [8-13].

Crystalline and molecular strain can also be measured with instruments of high spectral resolution. Copolymer dispersions can be determined as block copolymers absorb additively and alternating copolymers which deviate from this addictively due to interaction of neighboring groups. In general, the spectrometer with a dispersive prism or grating has been largely superseded by a moving mirror is used in an interferometer to produce an optical transform of the infrared signal. Numerical Fourier analysis is able to give the relation of intensity and frequency, i.e., the IR spectrum. FTIR technique can be

used to analyze gases, liquids and solids with minimal preparation of sample. FTIR technique has been applied to study many such systems which include adsorption on polymer surfaces, chemical modification and irradiation of polymers and oxidation of rubbers [14]. Moreover, the application of infrared spectroscopy to the study of polymers has been reviewed by Bower and Maddams [10].

In particular, π-conjugated delocalized electron system shows an interesting class of long molecules (macromolecules/polymer) where the extent of delocalization of π-electron cloud affects position of bands for a particular bond and helps in distinguishing two different types of bonds even for polymeric chains having same type of constituents. By knowing the absorption position (cm^{-1}) of a particular bond attached to π–conjugated chain, an idea about extent of effective π–electron delocalization can be known which ultimately shows the quality of electronic polymer. In the present thesis work, FTIR spectra have been recorded on the instrument name as Frontier 88277 FT-IR spectrophotometer mode in the wave number range 400–4000 cm^{-1} (figure 1.6). The spectroscopic grade KBr disks have been used for collecting the spectra with a resolution of 4 cm^{-1} and performing 32 scans. It gives idea about different functional groups and their arrangements (symmetrical or asymmetrical) present in the polymeric chain and shows very sharp changes when the nature and conformation of inherent polymeric chains change.

A.3.2.2 Raman spectroscopy

The Raman spectroscopy technique is a powerful and non-destructive technique named after Sir C. V. Raman, for the evaluation of vibrational, rotational and other low frequency modes in the materials. It provides the information about molecules which is complementary to infrared spectroscopy. For a vibrational mode in a molecule to be Raman active, it must be associated with changes in the polarization and is sensitive to symmetrical molecules too. The process is based on the inelastic scattering of the radiation. This can detect a change in vibrational, rotational or electronic energy of a molecule. It is very useful for analysis of vibrational modes in single crystals due to their anisotropic nature. The molecular vibrations and phonons of the system interact inelastically with incident radiation that leads to the shift in its energy known as Raman

(stokes or anti-stokes) scattering. This shift in the energy is equal to the energy of vibration of the scattering molecule and is called Raman shift. The electric field '*E*' of the incident electromagnetic radiation distorts the electron cloud of molecule and induces dipole moment '*P*' via relation $P = \alpha E$, but the molecular vibration changes the polarizability (α) and thereby the energy of the scattered electromagnetic radiation get changed. The Raman shift (ν wavenumber) in cm^{-1} is given by the relation;

$$\nu = \frac{1}{\lambda_{incident}} - \frac{1}{\lambda_{scattered}} \quad (1.8)$$

Where, $\lambda_{\text{incident}}$ and $\lambda_{\text{scattered}}$ are wavelengths of incident and Raman scattered photons in cm. The plot of intensity of scattered light *vs.* energy difference/Raman shift in cm^{-1} gives the Raman spectrum. The features like peak position, intensity, width *etc.* of spectra of the materials are very sensitive to the chemical composition, functional groups, structural phase, defects and impurities. The selection rules of information are very sensitive to the local and global symmetries. In crystalline solids, the Raman Effect deals with phonons instead of molecular vibrations. The fundamental requirement of a phonon to become Raman active is that the first derivative of the polarizability with respect to the vibrational normal coordinate should be a non-zero value.

The Raman spectra of particular material consists the specific characteristic features and variations in these features depict the changes in the molecular/structural symmetry of materials. A Renishaw in Via Micro-Raman equipped was employed for the characterization of pure and doped crystals for their compositional and structural analysis. The schematic for optics and photograph of the spectrometer is shown in Fig. 1.7.

This spectrometer is facilitated with two laser sources: one near infrared diode laser (HP-NIR) source (300 mW) for excitation at 785 nm and another Argon ion laser source (25 mW) for excitation at 514 nm. The laser beam was focused on the crystal surface in the form of spot of 1 μm radius and the exposure time was kept 10 s. The spectra were recorded in backscattering geometry in wavenumber range of 50-4000 cm^{-1}.

A.3.2.3 UV-VIS Spectroscopy

As mentioned in the previous sections, UV-Vis spectroscopy is a useful technique for characterization of polyaniline due to presence of various dopants and different oxidation states of PANI. The sensitivity of polyaniline to the pH of a medium is also reflected by the color change and can record optical absorption spectra of electrochemically deposited film of PANI or PANI dissolved in suitable organic solvent which gives qualitative information about the level of doping, extent of conjugation and the presence of radical cations in the PANI. In case of conducting polymer, conductor to-insulator transition arising from the change in pH of the medium can be clearly monitored.

A molecule or macromolecule leads to transitions between the electronic energy levels of the molecule or macromolecule in the spectra range ultraviolet (200-400 nm)/visible (400-800 nm) radiation [15-16] and shows the absorption of radiation in the range. The excited state so formed is in a very short time (~10-15 s) resulting that the atoms of the molecule do not move following the Franck-Condon principle. There are many factors such as, solvents, substituents, position/conformation of substituents, etc. which influence the relative energies of molecular orbitals. The knowledge of these factors is the essence of electronic spectroscopy. The strength of electronic spectroscopy lies in its ability to measure the extent of multiple bond or aromatic conjugation within molecules or macromolecules.

The longer the conjugation, longer will be the maximum wavelength of the absorption spectrum. Non-bonding electrons in oxygen, nitrogen and sulfur atoms may also be involved in extending π-conjugation of multiple-bond systems. The progression in electronic spectra of a π-conjugated polymer continues with increased conjugation to a limit of 550-600 nm (more than 20 double bonds in conjugation). Addition for each substituent –R alkyl (5 nm), –Cl, –Br (5 nm), –CH=CH– additional π-conjugation (30 nm), etc., is in accordance with Woodward's rules. These rules are empirically based on similar model compounds and will only hold good for other compounds whose structures are close to those of the models. Photograph of Shimadzu UV-1601 Spectrphoto meter

shown in Fig. 1.8 (a) and Fig. 1.8 (b) Schematic of the optical system indicating: D2: Deuterium lamp, WI: Halogen lamp, M1-M5: Mirrors (M3 is half-mirror), S1: Entrance slit, G: Diffraction grating, S2: Exit slit, F: Filter, W: Window plate, Reference cell, Sample cell, Lens 1, Lens 2P.D.: Photodiodes.

Application of electronic spectroscopy is of importance in the exploration of electronic property of semiconducting polymers [17-18]. The intensity and λ_{max} values increase with increasing π–conjugation and electron donating substituents which is regularly attached to main π–conjugated backbone of polymer. It can also be shown that the angular strain or steric overcrowding (caused by bulky and irregularly attached side groups) can disturb the planar geometry and distribution of the chromophore. For example, π-conjugation is reduced by lowering π-orbital overlap. Electronic spectroscopy is so sensitive to the distribution of the chromophore that one can turn this to an advantage in demonstrating that the distortion present in the molecule is caused by the influence of steric inhibition of resonance in the π-conjugation.

In the present work, UV-visible spectra of polyaniline doped with ZnO and SnO_2 have been recorded on Perkin Elmer, Lambda 35 PC spectrophotometer. In order to prepare a sample for measurement, the known amounts of samples have been dissolved in chloroform and measurements have been performed in a single quartz curette with 1 cm path length.

A.3.3 Surface morphological characterization

A.3.3.1 Transmission electron microscopy (TEM)

Transmission electron microscopy (TEM) has been used to study size, shape and distribution of materials at nanoscale [19]. The schematic diagram of a typical transmission electron microscope has been represented by Fig 1.9 [20]. A thin solid specimen (< 200 nm) is bombarded in vacuum with a highly focused, mono energetic beam of electrons in TEM. The smaller de Broglie wavelength associated with high energy electron beam is responsible for high resolution and its ability to focus the electron beam. As an example, the electrons having energy of 100 keV corresponds to de Broglie wavelength of 3.7×10^{-3} nm. In general, TEM is expected with the electron beams

having energy in the range of 20-200 keV. The spatial resolution is large enough for higher energy electron beam. In the energy range, the beam has enough high energy to propagate through the specimen. A series of electromagnetic lenses are used to magnify the transmitted electron signals [19].

There are two modes of TEM which are employed to study a desired specimen they are: image and diffraction. The image mode contrast must be induced in order to produce image for analysis of materials. There are many contrast forming mechanisms. The interpretation of images is complicated due to the interplay of the different mechanisms. The most commonly used imaging techniques in TEM are mass thickness imaging, diffraction imaging and phase contrast imaging. In diffraction imaging mode, the pattern of the diffracted electrons is obtained from the electron illuminated sample.

When the electron beam is incident on the sample, the scattering events occur because all the illuminated parts of the sample act as scattering sources. Interference between scattering beam causes coherently scattered beams when Bragg's law is fulfilled. The scattered beams are recorded in the form of a "*spot*". This spot pattern of diffracted electron beam from the selected sample area is called the selected area electron diffraction (SAED) pattern and provides the information about the crystalline and crystal orientation. The dependence of electron transpiring lies as the sample thickness, as a thick sample would cause too many interactions leaving no intensity in the transmitted beam. On the other hand a thick sample also increases the risk that an electron is scattered on multiple occasions and the resulting image would be difficult to interpret. In the work presented in this thesis the samples for TEM imaging have been prepared by dispersing powder sample in isopropanol using sonication and a small drop of that solution was casted onto the carbon coated copper grid. In the present thesis work, TEM has been used to analyze the shape, size and particle size distribution of PANI-ZnO nanoparticles.

- **High resolution transmission electron microscopy (HRTEM)**

If a scattered electron beam is a sharp spot diffracted from a single crystal, the phase contrast image that forms only when it is recombined with the unscattered beam is

an image of the crystal lattice planes that produce the scattering by Bragg diffraction. The resulting image of the crystal lattice can be obtained when several beams are recombined.

This specialized phase contrast technique has been utilized for the study of atomic scale structure in many types of crystalline metals and ceramics. It is called high resolution electron microscopy (HREM) which allows the direct imaging of defects and interfaces at the atomic scale [21-23]. However, this technique is difficult to apply for the study of polymeric materials due of their instability in the electron beam as the high resolution images require high beam intensities.

High-resolution electron microscopy can provide information that is difficult to obtain in any other way but it needs skill and experience. In case of polymers, lattice fringe images have been obtained from a wide range of polymers. In the present thesis, the particle size, the morphology of ZnO-PANI, SnO_2-PANI and SnO_2-ZnO nanocomposites have been examined using a high-resolution transmission electron microscope (HRTEM, Tecnai G2 F30 S-Twin) operating at an accelerating voltage of 300 kV, having a point resolution of 0.2 nm and a lattice resolution of 0.14 nm (Fig. 1.10).

A.3.3.2 Scanning electron microscopy (SEM)

Scanning Electron Microscopy (SEM) is a very useful technique and widely accepted to study the surface morphology, surface topography, composition and other properties such as electrical conductivity of the samples. It offers a better resolution than that of optical microscope. It can have resolution of a few nanometers and provides high magnification [24]. The schematic of scanning electron micrograph is shown in Fig. 1.11 [25].

In a typical SEM instrument, Tungsten or LaB_6 is used to emit monochromatic electrons with the energy range of 10-30 keV. These electrons are focused by magnetic field which acts as condenser lenses to form a beam with a very fine spot size ~ 1 to 5 nm. Then beam passes through a pair of scanning coils in the objective lenses, which deflects the beam in a raster fashion over the sample surface. This beam of primary electrons interacts with sample volume, the thickness of which ranging from less than

100 nm to 5 μm. The signals secondary electrons, internal currents, photon emission etc. so generated are detected by appropriate detectors. The cathode ray is used to generate the final image on the screen. In addition, SEM can provide information about the sample composition near the surface. This is known as Energy Dispersive Spectroscopy [26-27].

In the present work, SEM has been used to study the morphology of nanostructured polyaniline (PANI) doped zinc oxide (ZnO) and polyaniline (PANI) doped tin oxide (SnO_2) composite fabricated onto glass substrate.

A.3.3.3 Atomic force microscopy (AFM)

Atomic force microscope (VECCO DI multimode SPM), was used to study the surface morphology of zinc oxide (ZnO) doped tin oxide (SnO_2) nanocomposite thin film fabricated onto corning glass substrate (Fig. 1.12). The surface morphology of the films was examined over an area of 5.5×5.5 μm^2 in the non contact mode. The AFM images of as-grown and post-deposition zinc oxide (ZnO) doped tin oxide (SnO_2) nanocomposite fabricated onto corning glass substrate are shown in Fig. 1.13.

AFM images of the as-grown SnO_2-ZnO nanocomposite fabricated onto glass substrate thin film reveals the formation of a rough surface morphology (Fig. 1.12). Fig. 1.12 show, the 3D AFM images of the surface of SnO_2-ZnO thin film. The growth of sensing layer with rough and porous morphology is advantageous for gas sensing application, due to increased surface area which facilitates the large interfacial contact between the target gas molecule (NO_2) and ZnO of the sensing layer and expected to give enhanced response characteristics.

A.4 Thermal characterization

A.4.1Thermo-gravimetric Analysis (TGA)

TGA (Mettler Toledo TGA/SDTA 851e) was used to investigate the thermal stability of polymers in nitrogen atmosphere with a flow rate of 60 mL/min. A heating rate of 10 ^oC/min and a sample size (in the form of fine powder) of 10 ± 2 mg was used in each experiment. Thermo-gravimetric analyzer determines the change in weight of a

material as a function of temperature [28]. TGA was used to investigate not only the thermal stability of polymers but also to determine absorbed moisture contents in materials, presence of additives, solvents, degradation temperatures and kinetics. Thermo gravimetric analyzer operates on a null balancing principle with a sensitive balance maintaining a reference position for comparison with the weight of the sample. A current flow is produced to balance variations in weight between the reference and the sample and this current is proportional to the change in sample weight. The relative thermal stability of polymers is quite important in end use properties. In case of conducting polymers, it is a useful technique to study the thermal stability of the polymer and the quantitative estimation of different substituents present in the polymer.

A.4.2 Differential Scanning Calorimetry (DSC)

Differential Scanning Calorimetric studies on conducting copolymers and film of different blends were carried out using Mettler Toledo 822e . DSC was recorded from 25 ºC to 450 ºC for conducting copolymers and their blends, The heating/cooling rate was kept constant at 10 ºC per minute. A sample mass of 5 ±2 mg was used. DSC gives an idea about the primary and secondary transition with change in temperature. It gives the exothermic and endothermic changes occurring over a particular temperature range. DSC was recorded for both heating and cooling cycles. Endothermic changes like melting were recorded during heating cycle, and exothermic changes like crystallization were recorded during cooling. The melting point (T_m) as well as temperature of crystallization (T_c) and corresponding endothermic (ΔH_m) and exothermic (ΔH_c) changes in heat capacity were recorded.

A.5 Electrical studies

A.5.1 Electrical Characterization

The gas sensing characteristic properties of prepared sensors were studied in a specially designed “gas calibrator and test system (GCTS)” having a glass test chamber. Different concentrations of NO_2 gas (20 ppm) were introduced into the glass test chamber using calibrated leaks through fine needle valves.

The test chamber volume was taken to be 11.0 L and target NO_2 gas was injected in the test chamber through a syringe of 0.2 ml at the time of taking sensing response. A pirani gauge with a rotary pump was used to control the flow of target gas in the test chamber. The testing of sensor in present work is carried out using following procedure. Initially the test chamber was evacuated for a pressure of ~ 10^{-3} Torr to avoid any kind of interference from the residual gases present in atmosphere. Subsequently the sensitivity in relative response of sensor was recorded after incorporating the desired concentration of nitrogen dioxide (target) gas along with clean air (dry synthetic) at atmospheric pressure. The sensing measurement we carried out at room temperature in the presence of 30% humidity in the test chamber to obtain the real field situation. The gas sensing measurements were carried out in a static mode. At the time of recovery of the sensor, target gas was flushed out of the test chamber (by creating vacuum again) and the clean dry air was introduced. Target gas (NO_2) of specific concentration was introduced into the test chamber and changes in the sensor resistance were recorded after every second using a data acquisition system consisting of a precision digital multi-meter (model: Keithley 2700) interfaced with a computer (Fig. 1.15).

A.5.2 Gas injection and calibration of sensor for different gas concentration

The gas for which the sensing parameter of the sensor element is to be studied is injected into the glass chamber, through the gas inlet from ppm level in the air ambient, by using medical practitioners syringe. The required gas concentration inside the system is achieved by injection a predefined known volume of the test gas. The volume of chamber is 5 liters. The gas concentration in ppm can be determined as:

$$concentration\ of\ gas\ (ppm) = \frac{volume\ of\ ejected\ gas\ (ml)}{volume\ of\ chamber\ (L)} \times 10^6$$

The gas calibration chart based on the above equation is given in Table No.1.

Table No. 1 Conversion chart of ml to ppm level of the gas

Quantity of gas ejected in chamber (ml)	0.05	0.1	0.2	0.3	0.4	0.5
Concentration of gas in chamber (ppm)	5	10	20	30	40	50

A.5.3 Gas Sensing Parameters

It is very much important to understand the sensing parameters of a good sensor. These are defined as:

- Sensing response,
- Operating temperature,
- Response time and
- Recovery time

There are some of the salient parameters that are associated with measurement of response characteristics of a gas sensor.

(a) Sensing Response:

The response (*S)* of a gas sensor to a target gas at a given temperature T is determined from the measured value of resistance of the sensing element (ZnO, PANI, SnO_2 thin film) in the absence (R_a) and presence of the sensing gas (R_g). The sensor response *S* is defined as:

$$S = \frac{R_g - R_a}{R_a}$$

where $R_g >> R_a$ for oxidizing gases, and therefore to a good approximation

$$S \approx \frac{R_g}{R_a}$$

(b) Response Time (T_{res}):

The response time is defined as the time taken by the sensor to acquire 90% of its maximum resistance value in the presence of target oxidizing gas.

(c) Recovery time (T_{rec}):

The recovery time is defined as time taken by the sensor to reacquire about 10% higher value of its initial resistance in the presence of atmospheric air.

The typical variation in the response (S) of a gas sensor with temperature for a specific concentration of target gas is shown in Fig. 1.B.16. The maximum in the response (S_{max}) at a certain critical temperature (T_{opt}) is referred to as the operating temperature of the sensor.

Response (t_{res}) and recovery (t_{rec}) time characterization of a typical sensor are shown in Fig. 1.17 which gives a clear picture about the increase in resistance value as soon as any oxidizing gas comes in contact with n-type semiconducting sensing layer. The sample regains its original resistance value (R_a) as soon as the sensing gas is expelled out from its vicinity.

References:

[1] C.J. Brinker and G.W. Sherer, Sol-Gel Science, The Physics and Chemistry of Sol-Gel Processing, Academic Press, San Diego, 1990.

[2] C.J. Brinker, A.J. Hurd, P. R. Schunk, C.S. Ashely, R.A. Cairncross, J. Samuel, K. S. Chen, C. Scotto and R. A. Schwartz, "Sol-Gel Derived Ceramic Films--Fundamentals and Applications", in: K. Stern (Ed.), Metallurgical and Ceramic Protective Coatings, Chapman & Hall, London, 1996, pp. 112.

[3] T. Troczynski and Q. Yang, Process for Making Chemically Bonded Sol-Gel Ceramics, U.S. Pat. No. 6,284,682, May, 2001.

[4] T. Olding, M. Sayer and D. Barrow, Ceramic sol-gel composite coatings for electrical insulation, Thin Solid Films 398 (2001) 581-586.

[5] K. Ihokura, J. Watson, The Stannic Oxide Gas Sensor, Principles and Applications, CRC press, Boca Raton, FL, 1994.

[6] B.D. Cullity, S.R. Stock, Elements of x-ray diffraction, Prentice Hall, Inc. New Jersy (2001).

[7] V. Gupta, A. Mansingh, Influence of postdeposition annealing on the structural and optical properties of sputtered zinc oxide film, Journal of Applied Physics 80 (1996) 1063-1073.

[8] H.W. Siesler, K.H. Moritz, Infrared and Raman Spectroscopy of Polymers (Marcel Dekker, New York, 1980).

[9] P.C. Painter, M.M. Coleman, J.L. Koenig, The Theory of Vibrational Spectroscopy and its Application to Polymers (John Wiley, New York, 1982, pp. 530).

[10] D.L. Bower, W.F. Maddams, The Vibrational Spectroscopy of Polymers (Cambridge University Press, Cambridge, 1989).

[11] E.C. Faulques, D.L. Perry and A.V. Yeremenko, Eds. Spectroscopy of Emerging Materials (Springer, Sudak, Crimea , Ukraine , 2004, pp. 414).

[12] J.L. Koenig, Infrared and Raman Spectroscopy of Polymers (Rapra Technology, Shropshire UK, 2001, pp. 154).

[13] P.R. Griffith, Chemical Infrared Fourier Transform Spectroscopy (Wiley, New York, 1975).

[14] L.H. Lee, Ed. Characterization of Metal and Polymer Surfaces: Polymer Surfaces (Academic Press, New York, 1977).

[15] P. Atkins, J. de Paula, Physical Chemistry, (Oxford University Press), 7th Edition, 2002, 291.

[16] C.N. Banwell, E.M. McCash, Fundamentals of Molecular Spectroscopy, (Tata McGraw-Hill Publishing Company Limited, New Delhi), 4th Edition, (1994).

[17] K. Kaeriyama, "Handbook of Organic Conducting Molecules and Polymers", (John Wiley & Sons, Chichester), H. S. Nalwa (Ed.), 2 (1997) 271.

[18] E.J. Samuelsen, J. Mårdalen, "Handbook of Organic Conducting Molecules and Polymers", (John Wiley & Sons, Chichester), Nalwa H.S. (Ed.) 3 (1997) 81.

[19] D.B. Williams, Transmission electron microscopy, A textbook for material science, Plenum Press. New York and London, 1996.

[20] http:/www.steve.gb.com/image/science/transmission_electron_mocroscope.png.

[21] P. Buseck, J. Cowley, L. Eyring, Eds. High-Resolution Transmission Electron Microscopy and Associated Techniques (Oxford University Press, Oxford, 1988).

[22] J.C.H. Spence, High-Resolution Electron Microscopy, 3rd ed. (Oxford University Press, Oxford, 2003).

[23] F. Ernst, M. Ruhle, Eds. High-Resolution Imaging and Spectrometry of Materials (Springer, New York, 2003).

[24] G. Lawes, Scanning electron microscopy and X-ray microanalysis: Analysis chemistry by open learning, John Willey and Sons, 1987.

[25] www.purdue.edu/REM/rs/sem.htm

[26] C. Juan, C.M. Lino, A. Pena, J.C. Molto, J. Manes, I. Silveira, Determination of ochretoxin A in maize bread samples by LC with fluorescence detection, Talanta 73, 2007, 246-250.

[27] N. Axelrod, E. Axelrod, A. Gutina, A. Puzenko, P. Ben Ishai, and Yu Feldman, Dielectric spectroscopy data treatment: I. Frequency domain, Meas. Sci. Tech. 15, 2004, 755-764.

[28] Elton N. Kaufmann, (ed) Characterization Of Materials Vol.1, John Wiley & Sons Inc., Hoboken, New Jersey, 2003.

Figures:

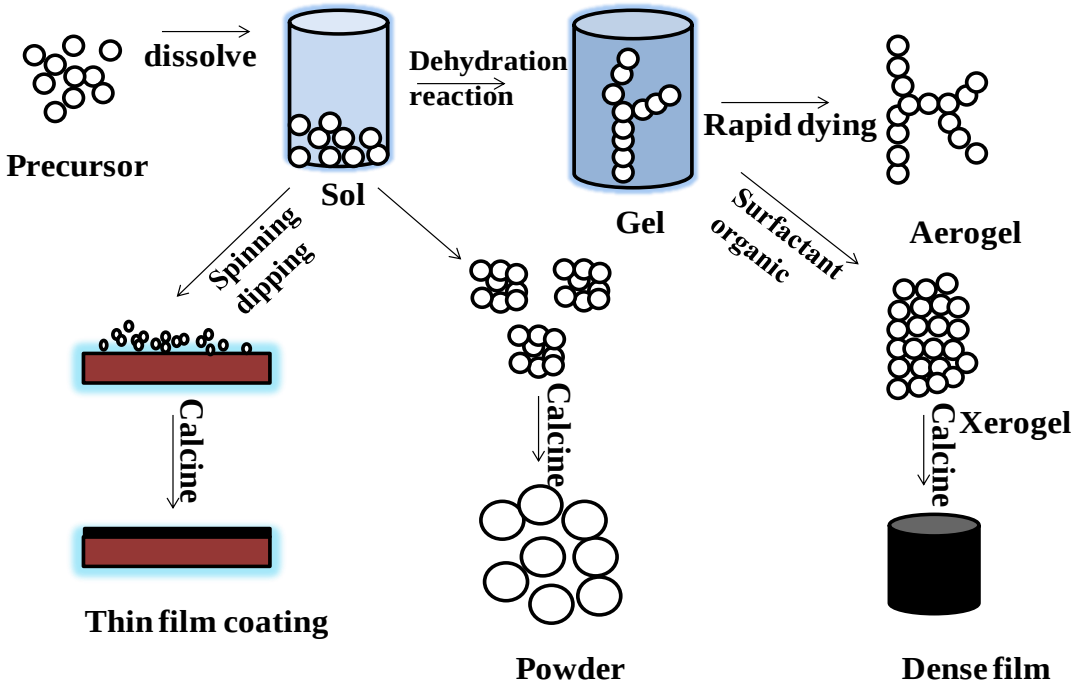

Fig. 1.1: Sol- Gel Process

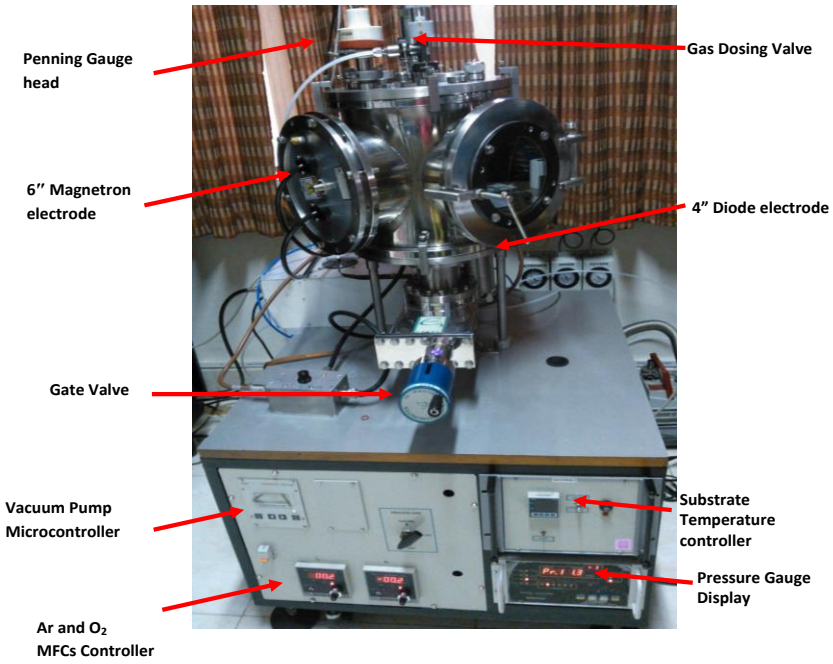

(a)

Parameters	Platinum	Titanium
Target	Platinum foil	Titanium
Gas composition	100% Ar	100% Ar
Sputtering pressure	10 m Torr	10 m Torr
TS distance	7.5 cm	7.5 cm
RF Power	100 W	150 W
Substrate Temperature	No heating	No heating

(b)

Fig. 1.2: (a) Photograph of the rf diode sputtering unit and (b) Platinum & Titanium thin film deposition parameters

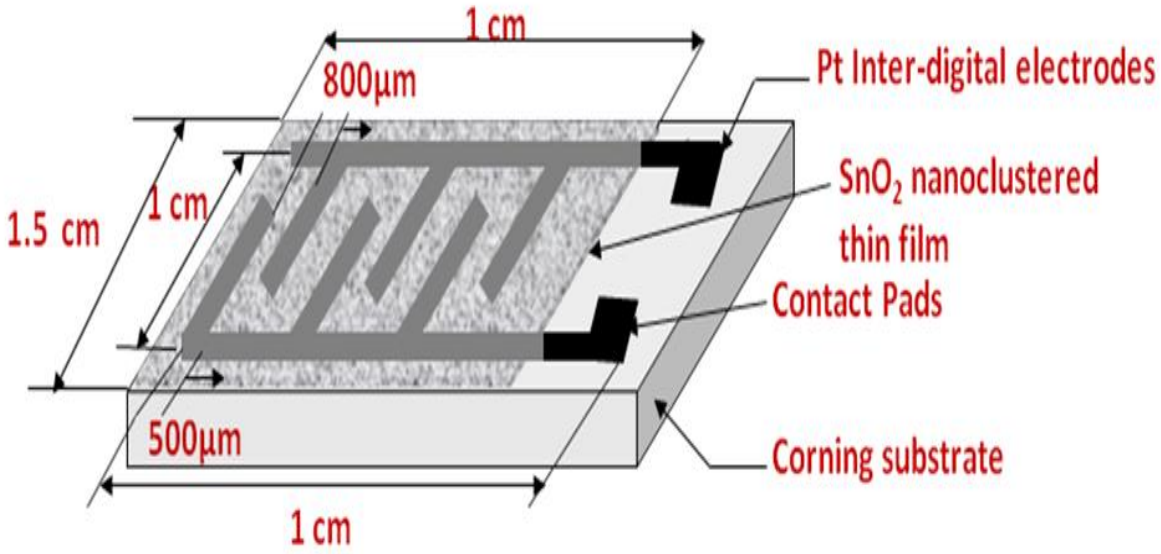

Fig. 1.3: Platinum IDTs on glass substrate

Fig. 1.4: Photograph of spin coater used in the preparation of thin film

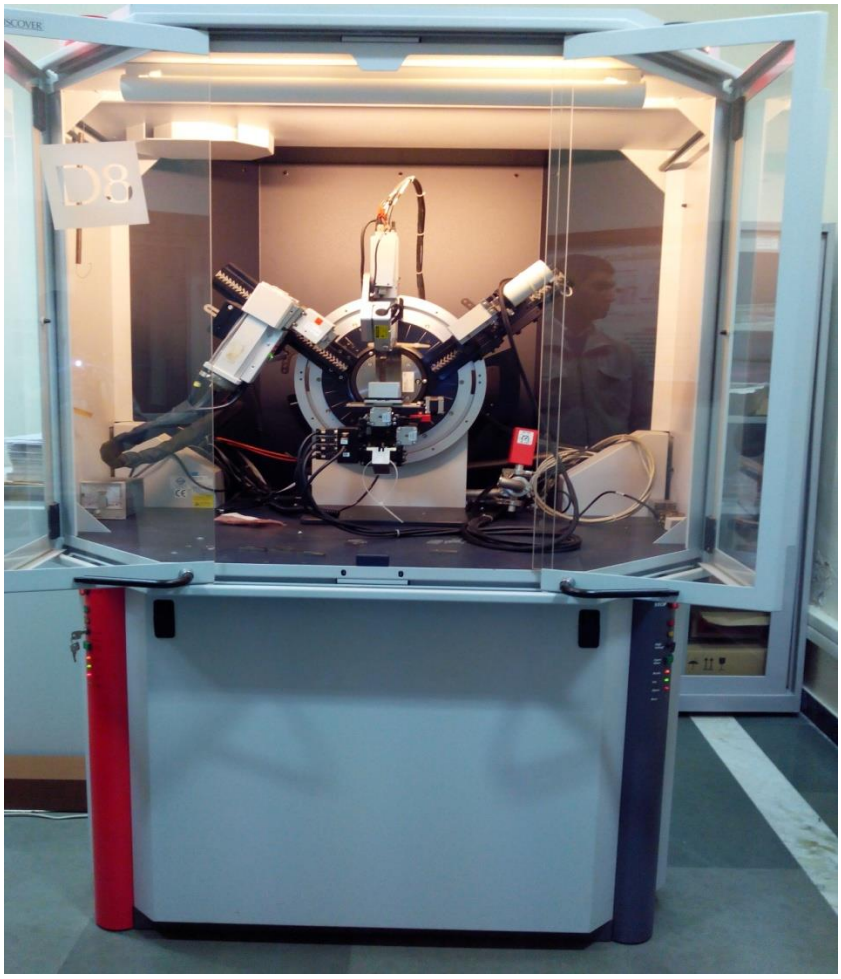

Fig. 1.5: Photograph of Bruker D 80 X-Ray diffractometer

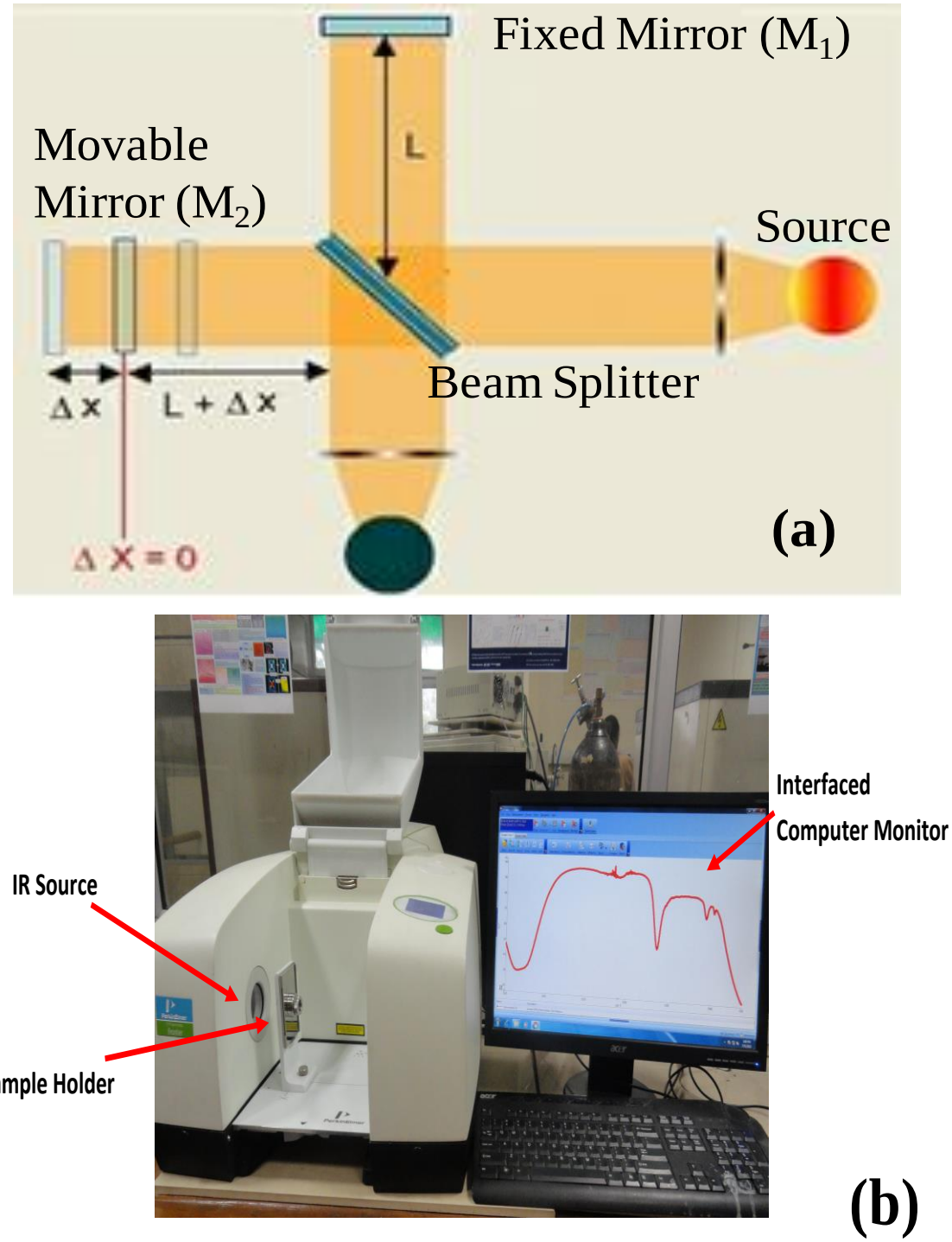

Fig. 1.6: (a) Schematic for Michelson interferrometer and (b) FTIR spectrometer

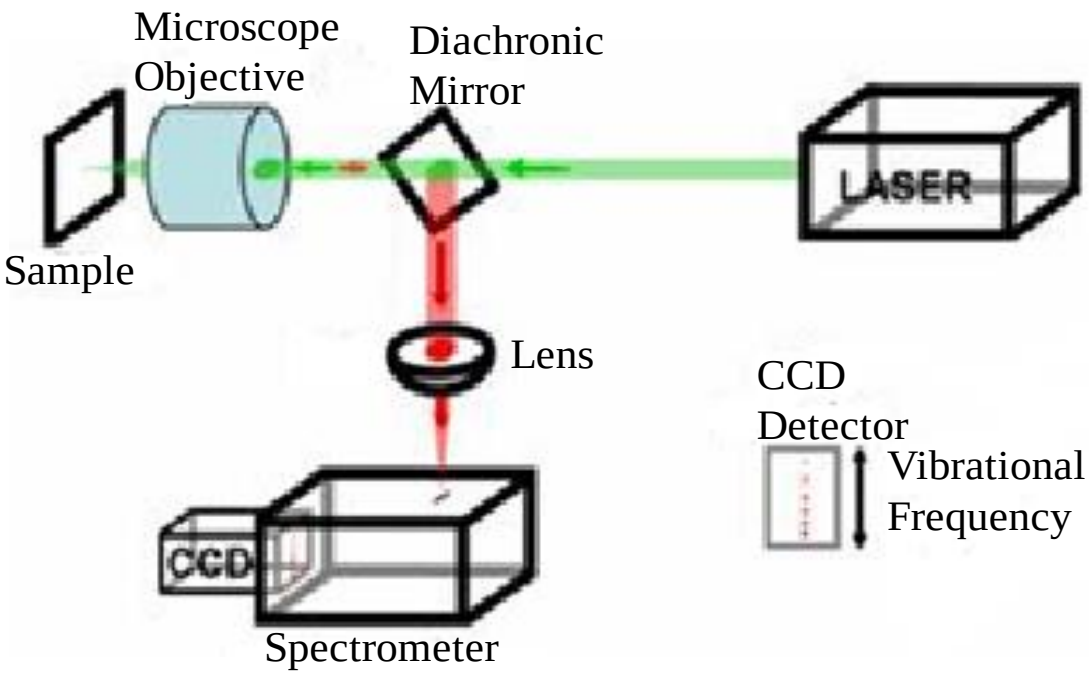

Fig. 1.7: Renishaw via Raman spectrometer

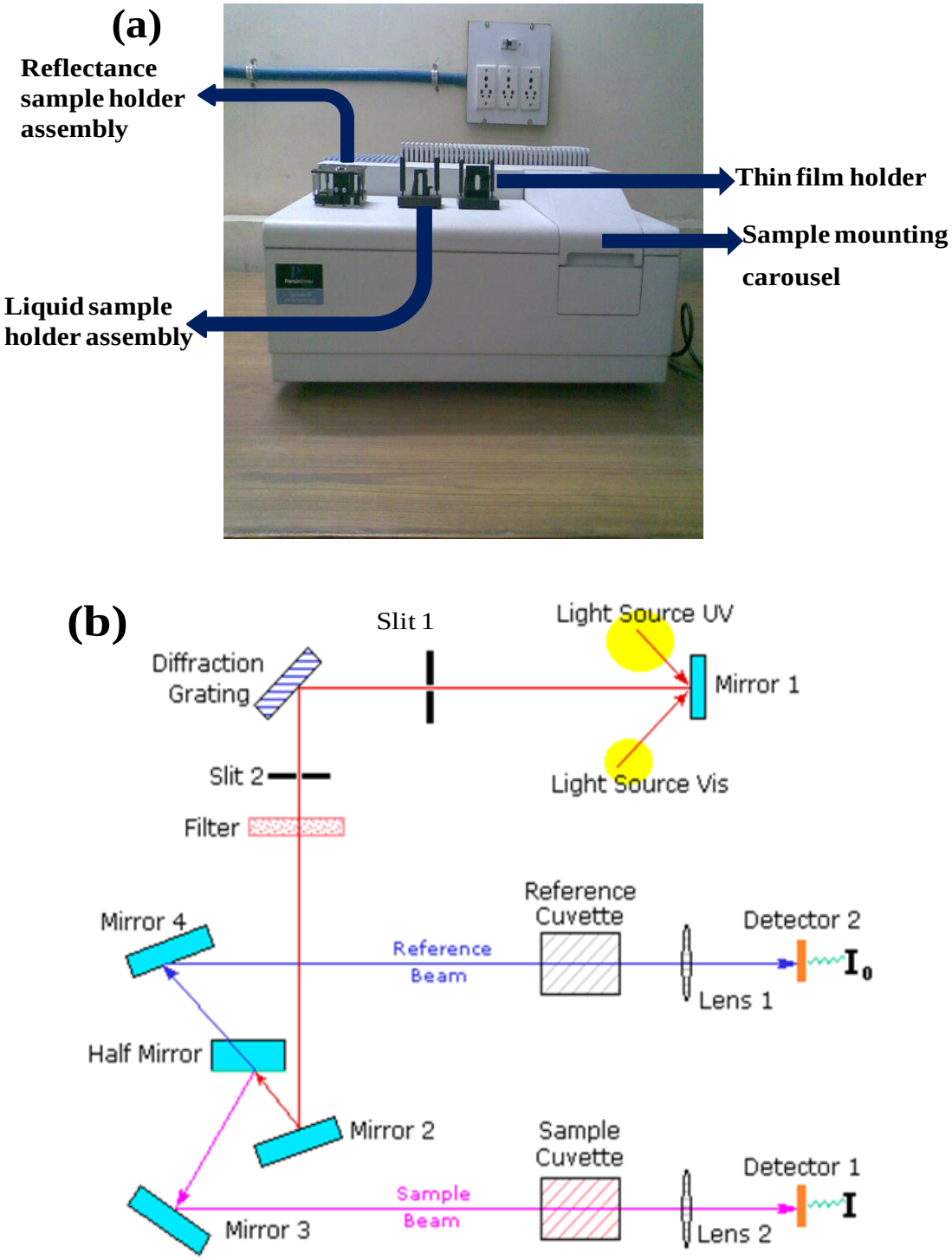

Fig. 1.8: (a) UV-Visible spectrophotometer (Perkin Elmer, Lambda 35) and (b) Schematic of the optical system

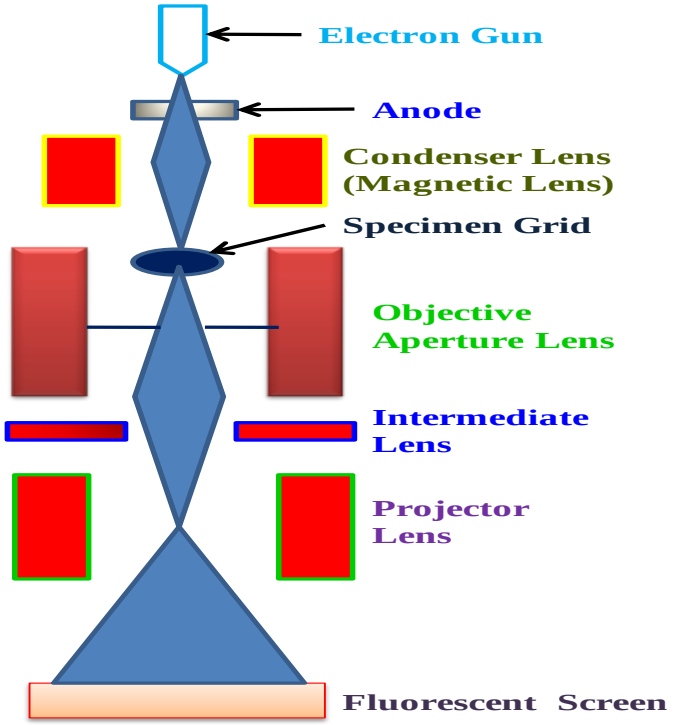

Fig. 1.9: Schematics diagram of Transmission Electron Microscope (TEM)

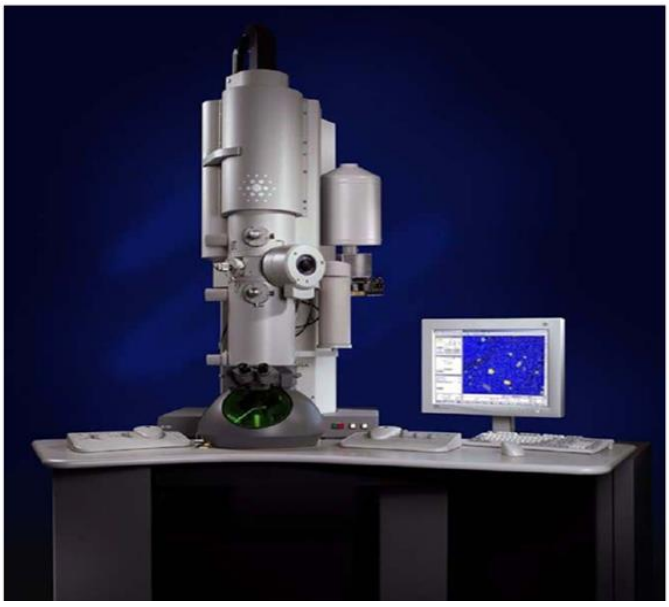

Fig. 1.10: Photograph of High-Resolution Transmission Electron Microscope (Philips T20ST, operated at 200 kV)

Fig. 1.11: (a) Photograph of Scanning Electron Microscopes (JEOL, JSM-6490LV)

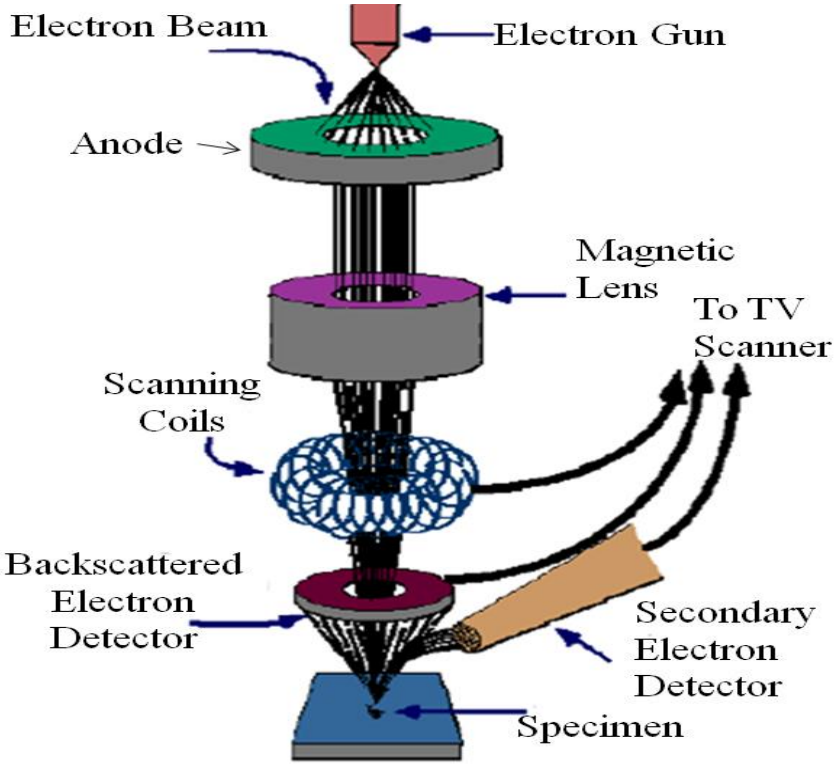

Fig. 1.11: (b) Schematics of Scanning Electron Microscope (SEM)

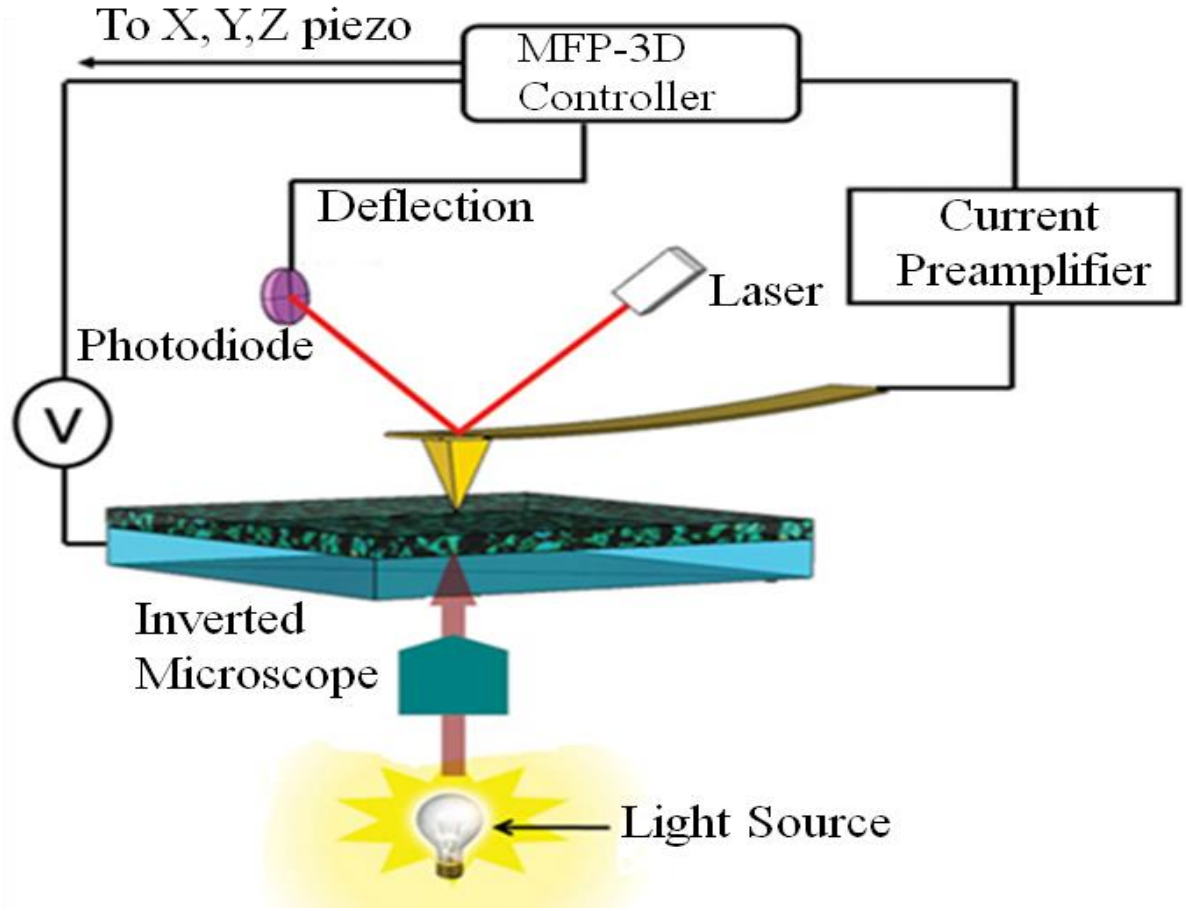

Fig. 1.12: Schematic of Atomic force microscope (AFM)

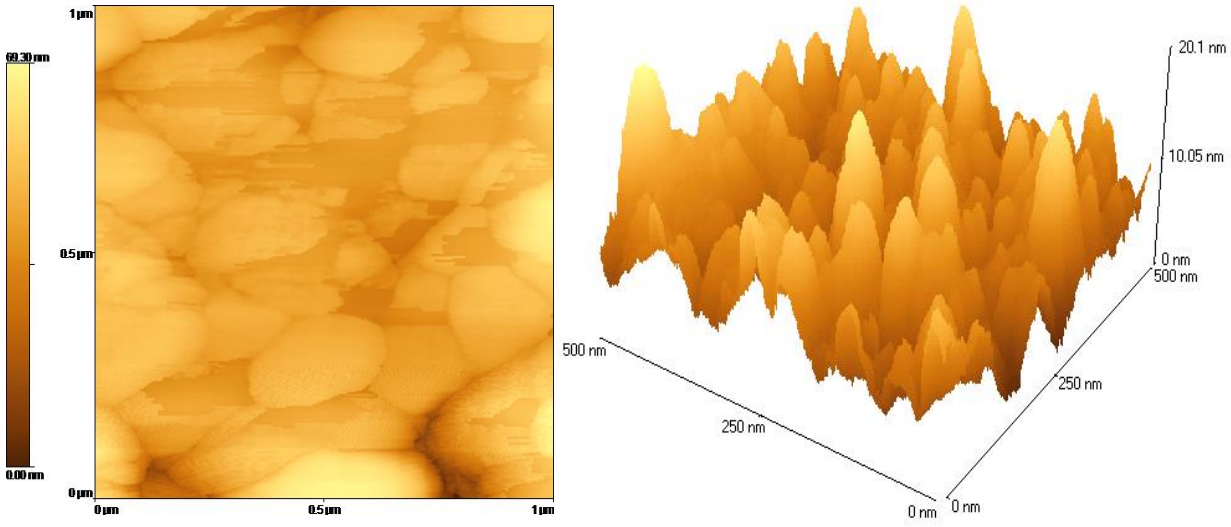

Fig. 1.13: AFM images (3D) of ZnO doped SnO_2

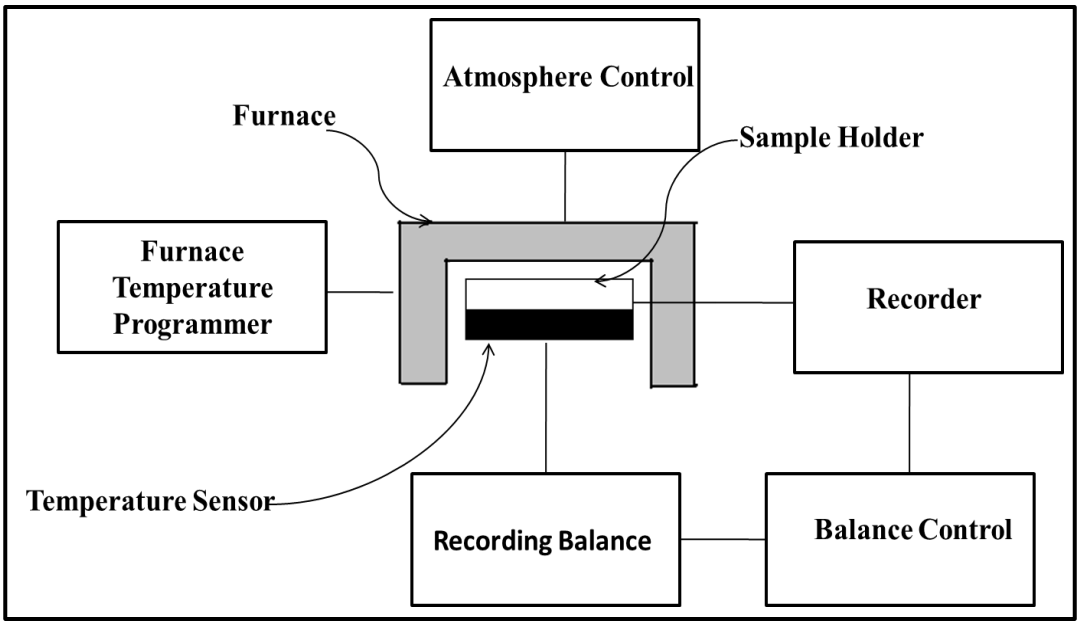

Fig. 1.14: Block diagram of a Thermobalance

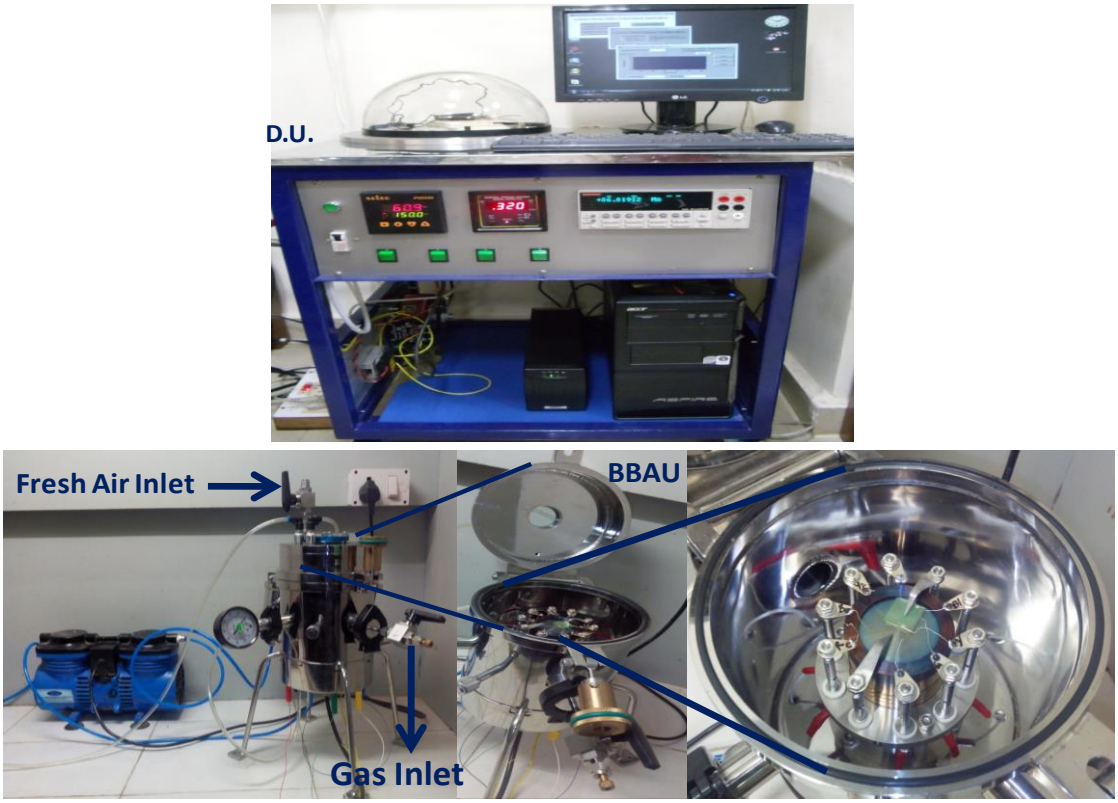

Fig. 1.15: Photograph of actual gas sensing unit

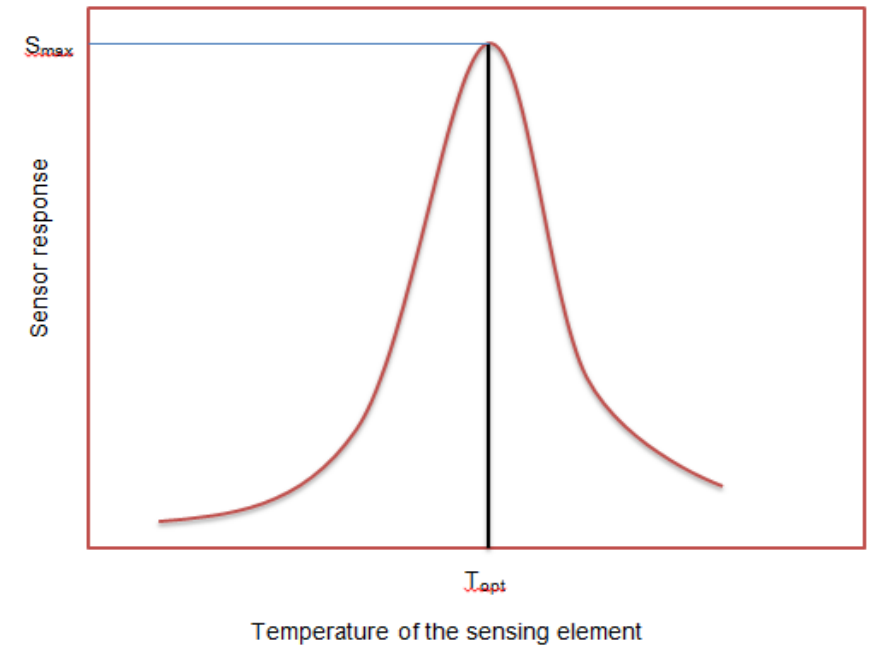

Fig. 1.16: Variation of sensor response with temperature for a typical sensor

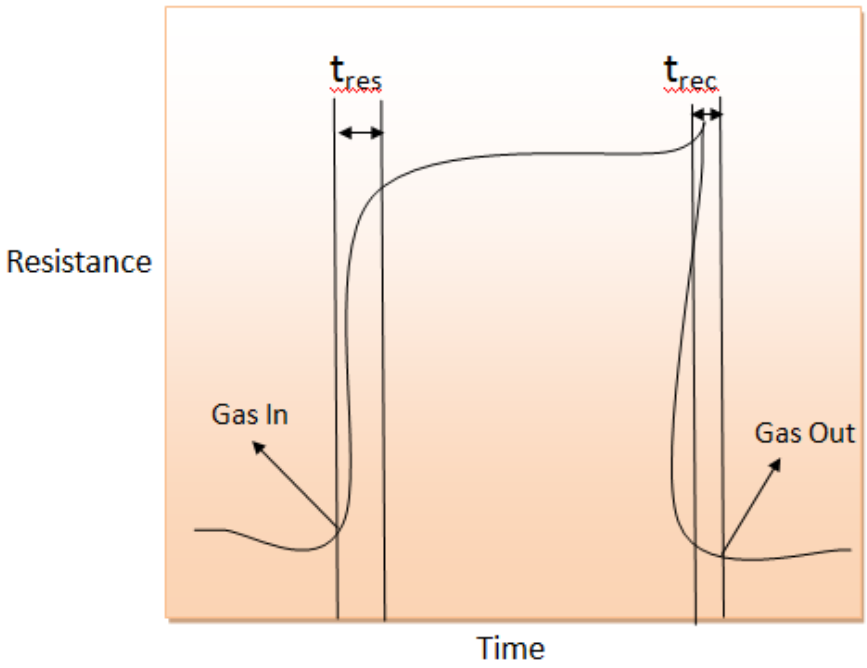

Fig. 1.17: Sensor response as a function of time, defining response time and recovery time of a typical sensor in response to an oxidizing gas